Engineered polysaccharide, Alpha-1,3 Glucan, as a Functional Filler of Rubber Composites

by

Azin Adibi

A thesis

presented to the University of Waterloo

in fulfillment of the

thesis requirement for the degree of

Doctor of Philosophy

in

Chemical Engineering

Waterloo, Ontario, Canada, 2023

Examining Committee Membership

The following served on the examining committee for this thesis. The decision of the examination committee is by majority vote.

External Examiner:	Robert Pelton Professor, Department of Chemical Engineering, McMaster University
Supervisors:	Tizazu H. Mekonnen Associate Professor, Department of Chemical Engineering University of Waterloo
	Leonardo Simon Professor, Department of Chemical Engineering, University of Waterloo
Internal Examiner:	Michael K.C. Tam Professor, Department of Chemical Engineering, University of Waterloo
	Boxin Zhao Professor, Department of Chemical Engineering, University of Waterloo
Internal-External Examiner:	Sushanta Mitra Professor, Department of Mechanical and Mechatronics Engineering, University of Waterloo

Author's Declaration

I hereby declare that I am the sole author of this thesis. This is a true copy of the thesis, including any required final revisions, as accepted by my examiners. I understand that my thesis may be made electronically available to the public.

Abstract

Rubber products represent an essential and highly functional class of performance materials required in many daily applications. However, the increasing interest in enhancing the overall material sustainability of rubber products has accelerated the focus on compatible, lightweight, and environmentally sustainable fillers. As part of the effort to design sustainable rubber composites, enzymatic polymerization derived polysaccharide fillers, alpha-1,3 glucan, with designed fibrids, platelet and spherical morphology and high crystallinity was employed as a novel sustainable filler system in natural rubber (NR) films. The alpha-1,3 glucan is supplied by International Fragrances and Flavors (IFF), former E.I. DuPont Industrial Biosciences. Initially, lightly crosslinked NR films reinforced with 0 – 10 phr MCG were fabricated using dipping and casting processes. The effect of MCG on the physicochemical properties, chemical stability, and thermo-mechanical properties of the composite films was investigated. In the subsequent project, colloidal alpha-1,3 glucan with spherical morphology was employed as a functional filler of NR coating films. Coating formulations containing NR latex and 10 – 100 phr colloidal alpha-1,3 glucan were prepared and applied to paper substrates at three different thicknesses. The effect of various coating formulations on the barrier properties against water vapor, oxygen, oil as well as on dry and wet mechanical properties were investigated. In order to study the impact of alpha,1-3 glucan's morphology on the barrier properties of the paper coating, the following studies were conducted. This study employed enzymatically polymerized microcrystalline glucan (MCG) as a functional additive in natural rubber (NR)-based coating formulations. Typically, NR coating formulations containing 0–50

wt. % MCG were fabricated at a constant coating thickness with a constant solid content. The influence of MCG on the wet and dry strength, rheology, adhesion strength, and barrier properties such as moisture, oxygen, and grease barrier of the formulated coatings was investigated. Also, further study on the effect of solid content and low crosslinking on the barrier properties was conducted.

The last stage of the study involved a solvent-free, batch mixer-based reactive process to carry out the reaction of ENR with glucan. In order to enhance the degree of dispersion and bonding of polar filler in a nonpolar natural rubber matrix, *in situ* melt grafting of epoxidized natural rubber (ENR) onto the polysaccharide was employed to achieve enhanced material properties. The process of temperature and shear-mediated melt grafting, in the presence of two catalysts (sodium hydroxide (NaOH) and dicumyl peroxide (DCP)), was investigated. Analytical characterization techniques, including Fourier transform infrared spectroscopy, X-ray photoelectron spectroscopy, and solvent swelling, were employed to confirm the formation of covalent bonds between alpha1,3-glucan and ENR. The selected ENR-glucan masterbatch samples were then subjected to melt-mixing with NR formulations to produce NR composites. Overall, this study aimed to develop a sustainable rubber composite with the incorporation of alpha-1,3 glucan as a functional filler targeting dipped rubber, packaging, and footwear applications and indicating the potential of this study in alleviating the environmental pollution induced by traditional polymers.

Acknowledgements

I am deeply grateful to my supervisor, Professor Tizazu Mekonnen, for his unwavering support, inspiration, positive outlook, and guidance throughout my doctoral program. His encouragement to constantly push forward and his patient responses to my countless questions have been invaluable. I extend my sincere appreciation to my co-supervisor, Professor Leonardo Simon, whose resourceful expertise and vast knowledge have made my PhD journey a highly productive and enriching experience. I am truly fortunate to have had such exceptional supervisors, and I am immensely grateful for their continual guidance and mentorship.

I would like to express my gratitude to the members of my supervisory committee and the external examiners, Dr. Michael K.C Tam, Dr. Boxin Zhao, Dr. Sushanta Mitra, and Dr. Robert Pelton, for their invaluable time and effort in reviewing my thesis and providing insightful feedback. Their expertise and constructive input have immensely contributed to the quality and rigor of my research.

Furthermore, I would like to acknowledge the research group at the International Flavors and Fragrances Inc. (IFF Inc.), namely Dr. Christian Lenges, Dr. Natnael Behabtu, Dr. Jorge Mok, Dr. David Valdesueiro, and Dr. Lemuel Tong, for providing me with the opportunity to engage in a multidisciplinary and cutting-edge research project. Their collaboration and support have been instrumental in shaping my research endeavors.

I would also like to express my gratitude to my colleagues for their academic and emotional support throughout this journey. Their presence has provided a great environment for intellectual growth and inspiration. I am also immensely thankful for the support received

from all the staff at the Chemical Engineering Department, with special mention to Judy Caron. Her approachability and warm welcome have greatly contributed to my overall experience, and I am truly grateful for her support.

Finally, I would like to express my appreciation for the financial support received from the International Flavors and Fragrances Inc. (IFF) and the Natural Science and Engineering Research Council (NSERC) of Canada. Their support has significantly contributed to the successful completion of my research.

Dedication

I’d like to dedicate this work to my beloved family for their endless love and support and, to my dearest friends who were always there for me in my toughest times.

Table of Contents

List of Figures

List of Tables

List of Schematics

Nomenclature

%	Percent	**mm**	Millimetre
°C	Degree Celsius	**MCG**	Microcrystalline Glucan
3D	Three Dimensional	**MCP**	Methylcyclopropen
AFM	Atomic Force Microscopy	**MFC**	Microfibril Cellulose
AgNPs	Silver Nanoparticles	**N**	Newton
ANOVA	A One-Way Analysis of Variance	**NAL**	Nanosized Alkali Lignin
ASTM	American Society for Testing Materials	**NaOH**	Sodium Hydroxide
CaCO3	Calcium Carbonate	**NBR**	Acrylonitrile-Butadiene Rubber
CEO	Cinnamon Essential Oil	**NC**	Nanocellulose
CNC	Cellulose Nanocrystals	**NFC**	Nanofibrillated Cellulose
CNF	Cellulose Nanofibers	**NR**	Natural Rubber
cm	Centimeter	**O-H**	Hydroxyl
CMC	Carboxymethyl Cellulose	**OP**	Oxygen Permeability
CMF	Micro-Fibrillated Cellulose	**pa**	Pascal
cP	Centipoise	**PBAT**	Poly(Butylene Adipate Terephthalate)
DCP	Dicumyl Peroxide	**PBE**	Polymer Based Emulsion
DMA	Dynamic Mechanical Analysis	**PBS**	Poly(Butylene Succinate)
EDX	Energy Dispersive x-ray	**PBT**	Poly(Butylene Terephthalate)
ENR	Epoxidized Natural Rubber	**PCL**	Poly(Caprolactone)
EVA	Ethylene Vinyl Acetate	**PE**	Poly(Ethylene)
EVOH	Ethylene Vinyl Alcohol	**PEA**	Poly(Ethylene Adipate)
FTIR	Fourier Transform Infrared	**PEI**	Polyethyleneimine
g	Gram	**PET**	Poly(Ethylene Terephthalate)
GTF	Glucosyltransferases	**PGA**	Poly(Glycolic Acid)
h	Hour	**PHA**	Poly(Hydroxyalkanoates)
Hz	Hertz	**PHB**	Poly(Hydroxybutyrate)
ISO	International Organization for Standardization	**PHBV**	Poly(3-Hydroxy Valerate)
KBr	Potassium Bromide	**phr**	Parts Per Hundred Rubber
$KMnO_4$	Potassium Permanganate	**PLA**	Poly(Lactic Acid)
KOH	Potassium Hydroxide	**PP**	Poly(Propylene)
LSD	Least Significant Difference	**PPC**	Poly(Propylene Carbonate)
m	Meter	**PVA**	Poly(Vinyl Alcohol)
min	Minute	**PVC**	Poly(Vinyl Chloride)
ml	Millilitre	**PVOH**	Polyvinyl Alcohol
RH	Relative Humidity	**w/v**	Weight/Volume

rpm	Round Per Minute	**WC**	Wet cake
s	Seconds	**WCA**	Water Contact Angle
-S-S-	Sulphur-Sulphur	**Wt.%**	Weight Percentage
SEM	Scanning Electron Microscopy	**WVP**	Water Vapor Permeability
SI	Swelling Index	**WVTR**	Water Vapor Transmission Rate
TEMPO	Oxidanyl	**XPS**	X-ray Photoelectron Spectroscopy
TAAPI	Technical Association of the Pulp and Paper Industry	**XRD**	X-ray Diffraction
TBBS	N-tert-Butyl-2-Benzothiazolesulfenamide	**ZDBC**	Zinc (II) Dibutyl Dithiocarbamate
TEM	Transmission Electron Microscopy	**Zn**	Zinc
Tg	Glass Transition Temperature	**ZnO**	Zinc Oxide
TGA	Thermogravimetric Analysis	**α**	Alpha
THF	Tetrahydrofuran	**β**	Belta
Triton	Polyethylene Glycol Tert-Octylphenyl Ether	**µm**	Micrometer
W	Weight	**Δ**	Delta

List of Publications from PhD

1. **A. Adibi**, J. Kim, J. Mok, C. Lenges, L. Simon and T. H. Mekonnen. (2021) Enzymatic polymerization designed alpha-1,3 glucan particle morphology as reinforcing fillers of dipped and casted rubber films, *Carbohydrate Polymers*, **267**, 118234. https://doi.org/10.1016/j.carbpol.2021.118234.
   Impact factor- 10.723

2. **A. Adibi**, D. Valdesueiro, J. Mok, N. Behabtu, C. Lenges, L. Simon and T. H. Mekonnen. (2022) Sustainable barrier paper coating based on alpha-1,3 glucan and natural rubber latex, *Carbohydrate Polymers.*, 2022, **282**, 119121. https://doi.org/10.1016/j.carbpol.2022.119121.
   Impact factor- 10.723

3. **A. Adibi**, D. Valdesueiro, L. Simon, C. P. Lenges and T. H. Mekonnen. (2022) High Barrier Sustainable Paper Coating Based on Engineered Polysaccharides and Natural Rubber ,*ACS Sustainable Chemistry and Engineering*, **10(32)**, 10718-10732. https://doi.org/10.1021/acssuschemeng.2c03466.
   Impact factor- 9.224

4. **A. Adibi**, B. M., Trinh, and T. H. Mekonnen. (2023). Recent progress in sustainable barrier paper coating for food packaging applications. *Progress in Organic Coatings*, *181*. https://doi.org/10.1016/J.PORGCOAT.2023.107566.
   Impact factor- 6.206

5. **A. Adibi**, L. Simon, C. Lenges, and T. H. Mekonnen. (2023). Sustainable natural rubber composites: masterbatch development of epoxidized natural rubber grafted to designed enzymatic polysaccharides. *Materials Chemistry Frontiers*. https://doi.org/10.1039/d3qm00080j.
   Impact factor- 8.683

Avg Impact factor – 9.11

Chapter 1. Introduction

Rubbers, one of the most extensively employed elastomeric materials, have extensive industrial applications such as tires, pipes, sealants, and cushions [1]. The application of rubbers in their original form is very restricted due to their large free volume, inferior mechanical strength, and poor weatherability, leaving petroleum-based polymers in the lead [2]. Therefore, to enhance their physical, mechanical, and chemical resistance properties, it is essential to introduce suitable fillers and reinforcing agents and employ a crosslinking (vulcanization) process [3]. Enhancement of the physical properties can be achieved through a vulcanization process, typically carried out by using accelerators and curing agents, which lead to the formation of a three-dimensional network. Additionally, improvement in other properties, such as mechanical properties, thermal properties, electrical properties, and barrier properties, requires the incorporation of the fillers [4]. The most common reinforcing filler in the rubber industry is carbon black, known for its ability to enhance the strength of rubber, protect against UV degradation, and improve abrasion resistance [5–7].

The use of carbon black as a filler contributes to product weight increase in addition to the environmental concerns associated with the feedstock and the production process [3]. The greenhouse gas emissions linked to this specific material category are considered significant and have been classified as materials with a high energy impact, necessitating the exploration of alternative solutions[8]. Also, it was reported that inhaling carbon black causes some health issues including respiratory and cardiovascular diseases[9]. Another challenge in the preparation of the rubber composites, reinforced by rigid filler particles, is the dispersion of the filler in the matrix. Fillers, such as carbon nanotubes[10], clay[11], silica[12], and

graphene[13], promoted mechanical and barrier properties. However, poor dispersion of the fillers at higher filler loading led to deteriorating mechanical as well as barrier properties of the composites. Hence further steps, such as the modification of the fillers or employment of innovative processing techniques, in order to improve the compatibility between the rubber and the fillers need to be carried out [14].

Furthermore, mineral fillers in rubber composites require substantial energy during production and contribute to an increase in the overall weight of the composite due to their high density. The chemical modification of fillers for rubber composites, such as the silylation of silica is extensively studied and commercialized. However, in some cases, the modification process can be multi-step, complicated, and cost prohibitive. In other cases, the medication can affect the structure, morphology, and overall performance of fillers[15]. Moreover, the modification may require expensive and toxic solvents that defeat the sustainability purpose. Thus, there is a need for a simple, robust, and green process in addition to sustainable feedstock to construct sustainable rubber systems.

Typical polysaccharide derivatives utilized as fillers in polymers and rubbers are derived from biomass through various refining processes. For example, cellulose nanocrystals, microcrystalline cellulose, and cellulose powder are produced from the wood processing chain; starch is produced from agricultural crops. On the other hand, a monomer based controlled polymerization process to generate designed polysaccharide particles has not been developed for commercial and large-scale material applications until recently. In this study, alpha-1,3-

glucan polysaccharide derived from the enzymatic polymerization of sucrose is put forward as a sustainable functional filler of rubber composites.

1.1. Objectives

The goal of this research is to study the effect of highly structured polysaccharides produced via enzymatic polymerization (alpha-1,3 glucan) as a functional filler of rubber systems subsequently pursuing development of sustainable and eco-friendly rubber products. Alpha-1,3 glucan has notable properties, such as colloidal stability, high modulus, high crystallinity, high surface area, and biodegradability, which makes it a potential candidate as functional filler of rubber composites for dipped goods, paper coating, and highly cured rubber products. The mutual colloidal stability of the alpha-1,3 glucan filler and rubber latex are hypothesized to provide good dispersion of the filler in the rubber matrix despite the polarity difference between the rubber and the filler. Also, due to the various shapes and morphology of the alpha-1, 3 glucan particles, they are expected to offer unique functional attributes, such as gas and oil barrier properties to rubber composites. The overall goal of this thesis was to evaluate the functional attribute of alpha-1,3 glucan as a functional filler of rubber composites. Specific objectives include:

- To investigate the effect of alpha-1,3 glucan morphology on the physico-mechanical and barrier properties of dipped rubber goods.
- To evaluate the oil and oxygen barrier performance of rubber - alpha-1,3 glucan coating formulations for paper coating applications as well as impact of different alpha-1,3 glucan’s morphologies.

- To develop robust processing approaches for incorporating alpha-1,3 glucan in highly filled rubber vulcanizates for footwear applications. This work explores the development of epoxidized natural rubber grafted to alpha-1,3 glucan in order to promote the compatibility among the polar filler and non-polar rubber matrix.

1.2. Outline of Thesis Chapters

This PhD thesis comprises seven main chapters, each contributing to the overall objective of the project. **Chapter 1** serves as the introduction, providing the motivation behind the research and outlining the core objectives of the thesis. The remaining and subsequent chapters provide detailed literature reviewing the progress of paper coating based on biopolymers in food packaging applications and experimental research performed to achieve each objective.

→ **Chapter 2:** This chapter reviews and compiles the past and current literature and aims to provide a critical and comprehensive overview of the most impactful and important advancements in improving the barrier properties of sustainable polymer-coated paper packaging systems. Also, developing active paper packaging materials by incorporating antimicrobial agents in coatings as an attractive option for protecting food from spoilage and extending shelf-life is outlined. Biodegradability aspects, as well as future trends and opportunities of sustainable paper packaging platforms are emphasized.

→ **Chapter 3:** In this work, enzymatic polymerization derived microcrystalline glucan (MCG) polysaccharides fillers were employed as novel sustainable fillers of natural rubber (NR) films. NR films composed of 0 – 10 phr MCG were then fabricated using dipping

and casting processes. Analytical techniques, such as tensile and tear strength study, crosslink density study, and permeability testing, were utilized to determine the properties of the film composites.

→ **Chapter 4:** In this chapter, the polysaccharide alpha-1,3-glucan with spherical morphology was employed as a functional additive for natural rubber (NR) latex-based coating films. Coating formulations containing NR and 9–50 wt% alpha-1,3 glucan were prepared and then applied to paper substrates at different thicknesses. Tensile testing, water vapor permeability testing, Cobb testing, and Kit testing were utilized to evaluate the properties of the prepared paper coatings.

→ **Chapter 5:** This work employed enzymatically polymerized microcrystalline glucan (MCG) as a functional additive of natural rubber (NR)-based coating formulations. Typically, NR coating formulations containing 0–50 wt % MCG were fabricated at a constant coating thickness with a constant solid content. Also, further study on the effect of solid content and light crosslinking on the barrier properties was conducted.

→ **Chapter 6:** In this chapter, the dispersion and bonding of an inherently polar filler in a nonpolar natural rubber matrix using an *in situ* melt process grafting of epoxidized natural rubber (ENR) onto the polysaccharide, was employed to achieve enhanced material properties. The temperature and shear-mediated melt grafting in the presence of two catalysts (i.e., sodium hydroxide (NaOH) and dicumyl peroxide (DCP)) were studied. Analytical characterization techniques, such as Fourier transform infrared spectroscopy, X-ray photoelectron spectroscopy, and solvent swelling was employed to validate the formation of covalent bonds between alpha-1,3 glucan and ENR. Subsequently, ENR-

glucan masterbatch was employed as a functional masterbatch for general NR composite formulations.

→ **Chapter 7:** The final chapter of the thesis will present a comprehensive conclusion that highlights the key findings and insights derived from the preceding chapters. It will illustrate the interconnections between these findings, forming a cohesive framework for a broader understanding. Additionally, this chapter will shed light on potential future directions for further research in this field.

Chapter 2. Literature review[1]

2.1. Environmental aspect of Polymers

Developing alternatives to the petroleum economy that match or exceed performance and are inherently scalable requires us to come up with sustainable ways of producing materials from renewable resources using resource and energy-sustainable processes. Currently, uncontrolled solid-waste generation from persistent petroleum-derived polymers is correlated with increasingly widespread environmental pollution through the formation of microplastics eventually ending up in the various water bodies [16]. Traditional polymers, which have been developed over the last century are extensively used in most engineering and commodity material applications due to their excellent chemical and mechanical properties, and more importantly, based on the large-scale and low-cost manufacturing processes [17].

It was reported that over the past 70 years, there has been a substantial increase in both the quantity and variety of plastics. In 1950, only 1.5 million tonnes of plastic materials were manufactured. However, by 2017, this number had surged to 350 million tonnes, excluding popular clothing fibers like nylon and polyester[18]. The consequence of this extensive plastic production is the projected accumulation of around 1200 million metric tonnes of plastic in landfills or the environment by the year 2050[16]. With further consumption of oil-based polymers, it is inevitable to not confront problems such as a rise in the price of petroleum-

[1] A version of this chapter has been published as a review peer-reviewed journal article: A. Adibi, et al. (2023). Recent progress in sustainable barrier paper coating for food packaging applications. *Progress in Organic Coatings*, *181*. https://doi.org/10.1016/J.PORGCOAT.2023.107566.

based materials and the developing environmental crisis [19,20]. Furthermore, attempts to recycle these polymers, specifically plastics with the highest production rate, have failed as only about 5% of polymers are successfully recovered [21]. To mitigate this challenge, there is an increasing interest in finding more sustainable material options which may substitute or complement conventional polymers with renewable and/or biodegradable material alternatives [22–24].

2.2. Rubber Biocomposites

The development of sustainable bio-composite is an innovative solution to mitigate the environmental pollution induced by conventional petroleum-based polymers. Composite materials are a mixture of two or more materials that differ in physical and chemical properties the combinations lead to a material with intermediate properties of the components [25]. Biocomposites are composite materials that are comprised of at least one bio-sourced and renewable constituent [26]. The two main constituents of composites are matrix and filler. Incorporation of the filler cause enhancement of the physical and mechanical characteristics of the matrix [27]. Two key parameters that play the main role in preparing high-performance particle-filled composites are strong filler-matrix interaction along with good dispersibility of filler throughout the matrix [28]. In the process of choosing an appropriate filler for a specific polymeric matrix, it is essential to pay the utmost attention to these two parameters.

Rubber-based composites represent an essential and high functional class of performance materials required in many everyday applications. Natural rubber (NR) is a widely established biopolymer produced at a large scale with extensive industrial applications

and expanding its utility in functional materials is a promising option to mitigate the environmental impact of petrochemical-derived polymers. NR, with a chemical structure of cis-1,4-poly(isoprene), is extracted from the *Hevea brasiliensis* tree in the form of milky soap or latex [4]. Because of its appealing properties, it has widespread applications in highly crosslinked products, such as footwear, tires, gaskets, conveyor belts as well as lightly crosslinked goods, such as balloons, catheter tubes, condoms, and gloves. Natural rubber has a clear benefit over synthetic rubbers in terms of its short- to mid-term bio-degradation profile[29].

NR has an intrinsic hydrophobic structure, which makes it a valuable material in packaging applications since it provides the desired high moisture barrier [30,31]. Though pristine NR possesses excellent elasticity and reversible deformability, it has several limitations, such as low modulus, hardness, durability, tear resistance, and poor barrier performance against oil and oxygen, to effectively compete with some of the synthetic elastomer alternatives in a range of applications [2,32]. In order to potentially address flaws in the mechanical properties of NR, curing, as well as incorporating fillers, are typically employed in many if not all rubber-based applications. In the rubber industry, the two most common fillers are carbon black and silica since both present appealing reinforcing effects [3]. However, it was stated that implementing carbon black introduces major problems in terms of environmental aspects and inflicts black color [33]. Silica is used as an alternative filler due to its mineral source, but the production of silica requires substantial energy. Also, both carbon black and silica tend to create agglomerates in the rubber matrix owing to their limited

compatibility with the hydrophobic elastomers [34]. Other reinforcing filler in rubber composite systems has also been reported, such as montmorillonite clay [11], calcium carbonate [35], and carbon nanotubes [10], etc. However, several drawbacks including complicated production process as well as not being cost-effective are the main reasons, which has limited their widespread applications. It is noteworthy to mention that some biobased fillers possess unique features (e.g., low density, low abrasion impact on processing equipment, sustainability), which make them potential candidates to complement or replace the current petroleum-based or mineral-based fillers and to take further steps toward greener and more lightweight composites. For instance, the utilization of polysaccharides as fillers for polymers and rubber has received increasing attention due to their potential to provide composite reinforcement, relatively low density compared with mineral fillers, and the overall sustainability profile and extensive availability.

Polysaccharides, typically sourced from established renewable feedstock are sustainable materials composed of repeating glucose monomers linked by glycosidic bonds commonly with one primary and two secondary hydroxyl moieties[36]. Cellulose is the most abundant polysaccharide in nature that has extensive applications, such textiles, packaging and containment, construction materials, and engineered thermoplastic materials. Starch is another polysaccharide that is widely utilized in various material applications, such as paper making, component in adhesive formulations, and as a filler or functional additive in biodegradable plastics[37].

Generally, most polysaccharides are highly aggregated, hydrophilic biopolymers, and have a strong tendency to form intra and inter molecular hydrogen-bonding networks. The water solubility of polysaccharides is highly dependent on the type of glycosidic linkages (α or β), polymer chain branching, hydrogen-bonding networks, and other factors [38]. For example, cellulose (β-1,4 glucan) is highly aggregated, and water-insoluble, whereas starch is a mixture of different polysaccharide materials (α-1,4 glucans and α-1,4 / 1,6 glucans) and is typically soluble in water when heat is applied. Within the general class of polysaccharides, cellulose nanocrystals[39], chitin nano-whiskers [40], and starch nanocrystals[41] are reported in the literature as potential reinforcing fillers of natural rubber and other elastomers.

2.3. Enzymatic Polysaccharides

Most polysaccharides are derived from biomass, for instance, cellulose, starch, pectin, and carrageenan, or are derived from fermentation processes, such as xanthan, and dextran. In order to purify polysaccharides, from their origin resources considerable processing steps are employed. Enzymatic polymerization is a newer process to obtain highly pure polysaccharides with minimal processing steps [42]. Alpha-1,3 glucan is a polysaccharide that is sourced from fungal and yeast cell walls, and it was first extracted from fungal cell walls by utilizing an aqueous alkali solution [43].

Traditionally, the design of polymer structures has relied on controlling the polymer architecture during the polymerization processes, such as with polyolefins and polyacrylics, through the use of tailored polymerization catalysts and adjusting process conditions. Currently, efforts are being made to apply these concepts to the design of polysaccharide materials using enzymes. However, there is a lack of efficient and scalable methods to employ

a controlled polymerization protocol using an enzyme catalyst based on a monomer like glucose from sucrose for large-scale, commercial material applications [44]. In this thesis, a novel enzyme technology-derived polysaccharide, alpha-1,3 glucan, is utilized as a functional filler of natural rubber (NR) composites of various forms.

International Flavors and Fragrances (IFF) Inc. (Former DuPont Nutrition and Biosciences) has developed a scalable enzymatic polymerization process for the generation of engineered polysaccharides, alpha-1,3 glucan with various morphologies, from glucose derived from sucrose as demonstrated in **scheme 2.1** [45,46]. In this process, glucosyltransferases (GTFs) or commonly named glucansucrases enzymes derived from lactic acid bacteria are utilized as catalysts [47]. The alpha-1,3 glucan was produced by contacting an aqueous sucrose solution to GTF enzyme under a pH and temperature-controlled environment. Since GTFs are not thermally stable, the reaction takes place in the range of 30-50° C, and the highest activity of this type of enzyme was reported in a slightly acidic environment, pH range of 5-7 [42]. The first step of polymerization starts with splitting the α-1,2 glycosidic bond of sucrose by GTF followed by transforming the glucosyl of sucrose to enzyme and formation of a covalent enzyme-glucosyl intermediate and release of fructose as a by-product. In the next step of the process, the glycosyl group transfer from the intermediate to an acceptor molecule, water, and consequently from the hydrolysis of the intermediate, glucose is developed. However, depending on the type of acceptor molecules other reactions may happen in the process. For instance, as a result of using sucrose as an acceptor, sucrose isomers, specifically leucrose, can be generated. Developed glucose from the hydrolysis of the

intermediate, serve as the initiator of α-glucan synthesis [42,48].

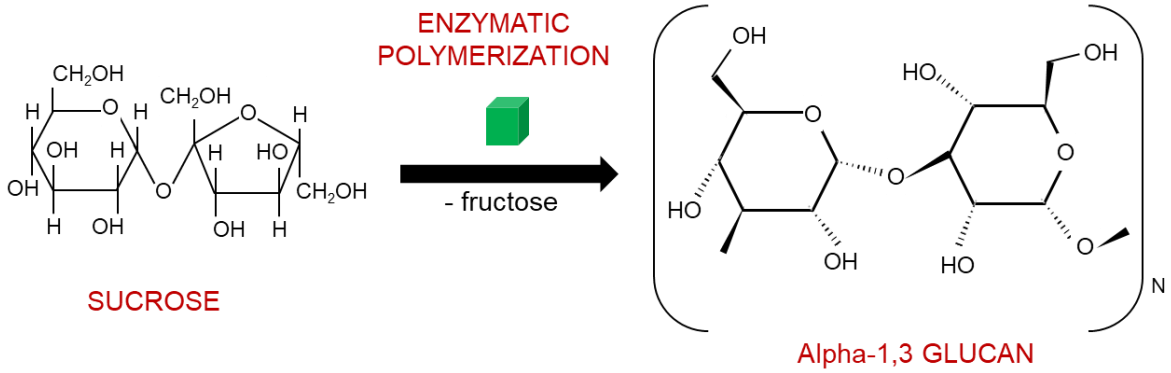

Scheme 2.1. Schematic of enzymatic reaction of alpha-1,3-glucan.

The alpha-1,3 glucan is a water-insoluble, linear, semi-crystalline polysaccharide with a typical degree of polymerization of 800 repeat units with a polydispersity in the range of 1.7-2.0 which can be controlled by the process conditions [49,50]. The isolated alpha-1,3-glucan from the process is in the form of white powder that contains 60-70% water and is highly pure (>88 wt.% purity) with a density of 1.5 g/cm^3 [44]. Thus, the lower density of these polysaccharides compared to many traditional polymer fillers, presents an opportunity to develop lightweight composites. The enzymatic polymerization to produce alpha-1,3 glucan is carried out in water and the process allows precise control of the particle morphology. Through this, various types of glucan morphologies can be accessed, including spherical aggregates (wet cake), fiber-like structures (fibrids), and plate-like systems (platelet), the microcrystalline glucan (MCG) [51].

The size of the particles varies depending on the morphology. The spherical aggregate particles have primary particle sizes between 10-30 nm which then aggregates to secondary

particles of 5-10 μm diameter. Although the aggregate particles have a high tendency to settle in water suspension, under shear they can form stable colloidal suspension [52]. In contrast, fibrid morphology of alpha-1,3 glucan provides a high aspect ratio, with 10-20 μm in width and several hundred μm in length. The last morphology of interest of alpha-1,3-glucan particles is plate-like (platelet) morphology with a diameter of 200 nm that is reported to have a high degree of crystallinity (~ 85%) [52].

The alpha-1,3 glucan polymer exhibits thermal stability up to approximately 305 °C, surpassing the melting points of various polymer systems such as polyethylene, polypropylene, poly(lactic acid), EVA, and polyhydroxyl alkanoates [44]. As a result, alpha-1,3 glucan can be effectively melt compounded with polymers as an additive, such as a nucleating agent, or as a reinforcing agent, without significant risk of process-induced thermal degradation. The combination of high crystallinity, uniformity, purity, and excellent thermal stability makes alpha-1,3 glucan a promising functional additive to polymer composite systems. In this work, the alpha-1,3 glucan with t different morphologies (spherical and platelet) has been used to explore the impact of the morphology of the reinforcing agent in the rubber composite. The availability of large-scale manufacturing of alpha-1,3-glucan provides the opportunity for a profound understanding of the characteristics of the polymer and comparing it with commercial polysaccharides like cellulose and starch.

2.4. Paper Coating

The word 'paper' originated from the plant papyrus, from which the Egyptians produced the very first crude writing material. Papers have been manufactured from bamboo, mulberry

barks, cottonseed hair, flax, sunflower stalk, and agricultural waste [53,54]. The quality of the developed paper strongly depends on its raw material due to variations in fiber length and pulp composition. Based on the smoothness and specific treatment employed to fabricate papers, the papers are often broadly divided into two categories. The first types are fine papers, which are made of bleached pulp and are typically used in printing, labelling, books, etc. and the second types are coarse papers, which are comprised of unbleached pulp and are typically used as the packaging of food and other materials [55].

The use of paper and paperboard in food packaging applications goes back to the 17th century, which gathered more popularity in the late 19th century [56]. Some characteristics of papers, such as printability, recyclability, and biodegradability, make them one of the most predominately utilized materials in the food packaging industry as primary (i.e. in direct contact with food products) and secondary (i.e. for transportation and storage of primary packages) packaging products [55]. Based on the global packaging market report in 2018, approximately 30% of materials used in the packaging industry are paper and paper boards, as presented in **Figure 2.1(a)** [57,58].

The vast majority of plastic packaging materials are considered single-use plastic packaging, making up a great percentage of the millions of tons of annual plastic debris in landfills and waterways [59,60]. According to the global primary waste generation in 2015, about 141 million tons of packaging waste was generated out of 146 million metric tons of packaging productions, which overall made up 47% of the total generated waste in 2015 (**Figure 2.1(b)**) [16]. The presence of plastic waste in the environment is threatening marine

lives, freshwater, soil environment, and the entire ecosystem [61]. Ongoing studies aim to overcome environmental concerns associated with plastic production, use and disposal. This has encouraged the transition from typically single-use, non-biodegradable, and petroleum-derived plastics into the design of sustainable packaging systems. Paper packaging design with biobased and biodegradable coating can play an important role in bringing about sustainable packaging material [62].

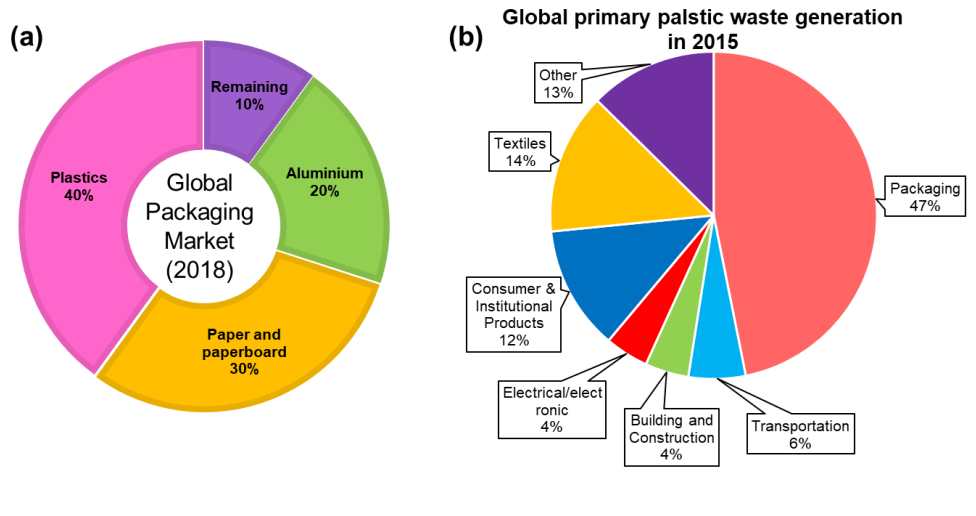

Figure 2.1. (a) materials used in the packaging market, (b) global plastic waste generation [16].

However, most papers are composed of microfibril cellulose networks, making them inherently porous and highly hydrophilic, which impose challenges in various packaging applications due to poor innate barrier performances against gases, water, and grease [63,64]. Currently, the most common approach to alleviate the inherent limitation of paper substrates is to apply surface coatings onto the paper substrates [65]. Various methods can be employed to apply either one or multiple coating layers onto the paper, including extrusion coating, curtain coating, size press coating, bar coating, and dip coating (**Figure 2.2**). Extrusion coating

is one of, if not the most, conventional processes to apply paper coating on an industrial scale. This is because it provides many benefits, such as continuous and solvent-free operations, uniform coating finishes, and effective elimination of pinholes and cracks. However, the extrusion coating process also suffers from limitations induced by other material-related factors, such as coating speed and efficiency.

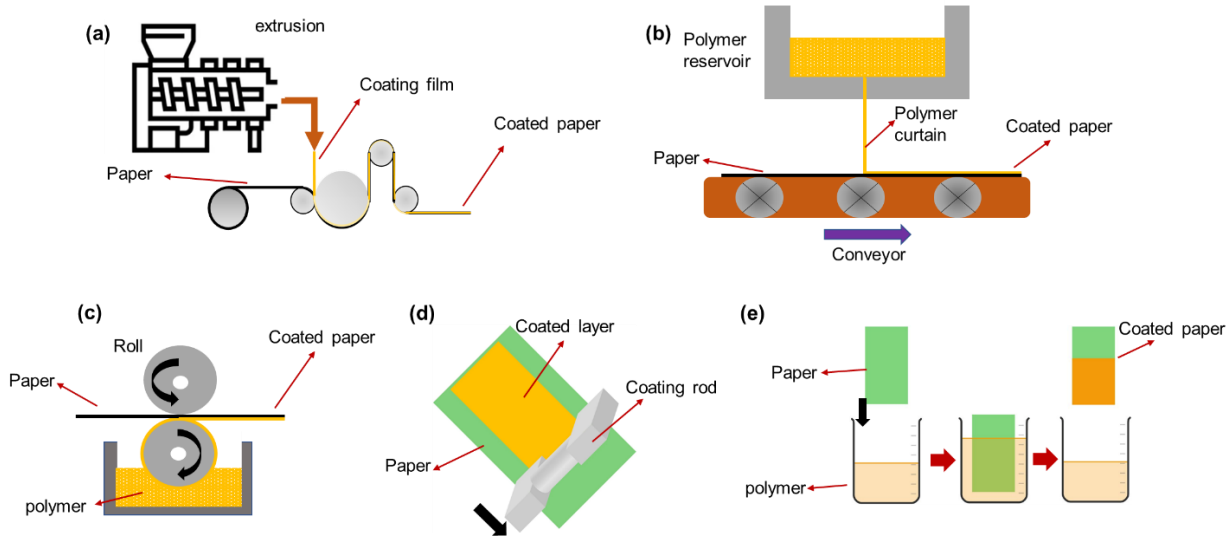

Figure 2.2. Various methods for fabricating paper coating: (a) extrusion coating, (b) curtain coating, (c) size press coating, (d) bar coating, (e) dip coating [66].

The remaining coating techniques (**Figure 2.2(b-e)**) are classified under the dispersion and solvent-based coating methods category. These methods have the advantage of requiring low coating weights to achieve desirable barrier properties, although sometimes multiple layers are required to remove the surface voids to achieve necessary properties. Similar to the extrusion coating method, in the curtain coating process, a uniform high coat weight is applied to the paper leading to complete coverage of the paper's surface [66]. In general, the size press

coating process is one of the most industrially used methods for applying aqueous coating formulation on the paper substrate where the solid content of the coating formulation is maintained at less than 10% to be able to conduct the process at allowable viscosity [67]. However, because of the low solid content, most coatings cover the base paper's surface only partially, leading to inadequate barrier properties. On the contrary, the bar coating technique provides better control over the coating thicknesses. Still, this method is only confined to laboratory or pilot scale and is not considered practical for scale-up. The dip coating process is considered a facile method for applying an aqueous coating on the paper base, but it is challenging to control the coating thickness [66].

Presently, the paper packaging industries rely primarily on utilizing synthetic petroleum-based polymers or metallization as coating layers, compromising the biodegradability attribute of papers. It will also exacerbate environmental concerns of packaging materials due to the inabilities of metalized or synthetic polymer (e.g., polyolefin) coated papers to degrade in the environment or to be reprocessed. Common synthetic non-biodegradable polymers that are frequently used as paper surface coatings include polyethylene (PE), polyethylene terephthalate (PET), polybutylene terephthalate (PBT), polyvinyl alcohol (PVOH), and paraffin wax [65,68]. A recent review by Trinh et al. provided a critical overview of the recent progress achieved in sustainable multiphase and multicomponent packaging materials.

Due to their biodegradability, abundance, and overall sustainability, there has been an increasing interest in nature-derived polymers as an alternative to petroleum-based polymers.

Examples of such nature-derived polymers or biopolymers that can be processed into coating include proteins, polysaccharides (e.g., starch, chitin, cellulose and derivatives), lignin, natural rubber etc. Aliphatic polyesters, such as poly(lactic acid) (PLA) and polyhydroxyalkanoates (PHAs) (e.g., polyhydroxybutyrate (PHB), polyhydroxybutyrate valerate (PHBV), etc.), bio-derived poly(butylene succinate)(PBS) are other biopolymers that are widely considered to be sustainable. Synthetic polymers that display a range of compostability and biodegradation attributes (e.g., polycaprolactone (PCL), polybutylene-adipate co-terephthalate (PBAT), polyglycolic acid (PGA)) are other classes of polymers that attracted substantial interest as sustainable polymer alternatives (**Figure 2.3**).

Developing packaging materials from biodegradable biopolymers has a clear upper hand regarding ecological and economic contributions since they can easily be handled in composting facilities after usage[65]. The biopolymer-based coatings can also provide favorable environmental benefits of reusability and recyclability compared to their petroleum-based synthetic polymer counterparts [65,66,69]. The proper design of sustainable polymer-based paper coating should offer essential moisture, grease, and oxygen barrier properties for packaging applications. Furthermore, sustainable polymers can serve as matrices to integrate additives, such as antimicrobials, antioxidants, coloring agents, and nutrients, to further enhance the functionalities without compromising the environmentally friendly aspect of the paper packaging material [70–72]. In addition, other application of sustainable polymer-based paper coatings can be the usage of the paper coatings in agricultural industry as stated by Bi et al. biodegradable polyester coated paper was used for controlling release of fertilizer [73]. This review paper aims to showcase the latest updates on the progress of modern paper coating

technologies that incorporate renewable and biodegradable polymeric layers. Moreover, recent progress in process and technology development for vapor, oxygen, water, and grease barrier properties of paper packaging by employing sustainable polymers is critically reviewed. Furthermore, comprehensive discussions on the biodegradability of paper packaging systems are covered in detail. Lastly, the current state of affairs and potential advancement in developing high-barrier paper coatings were also thoroughly discussed.

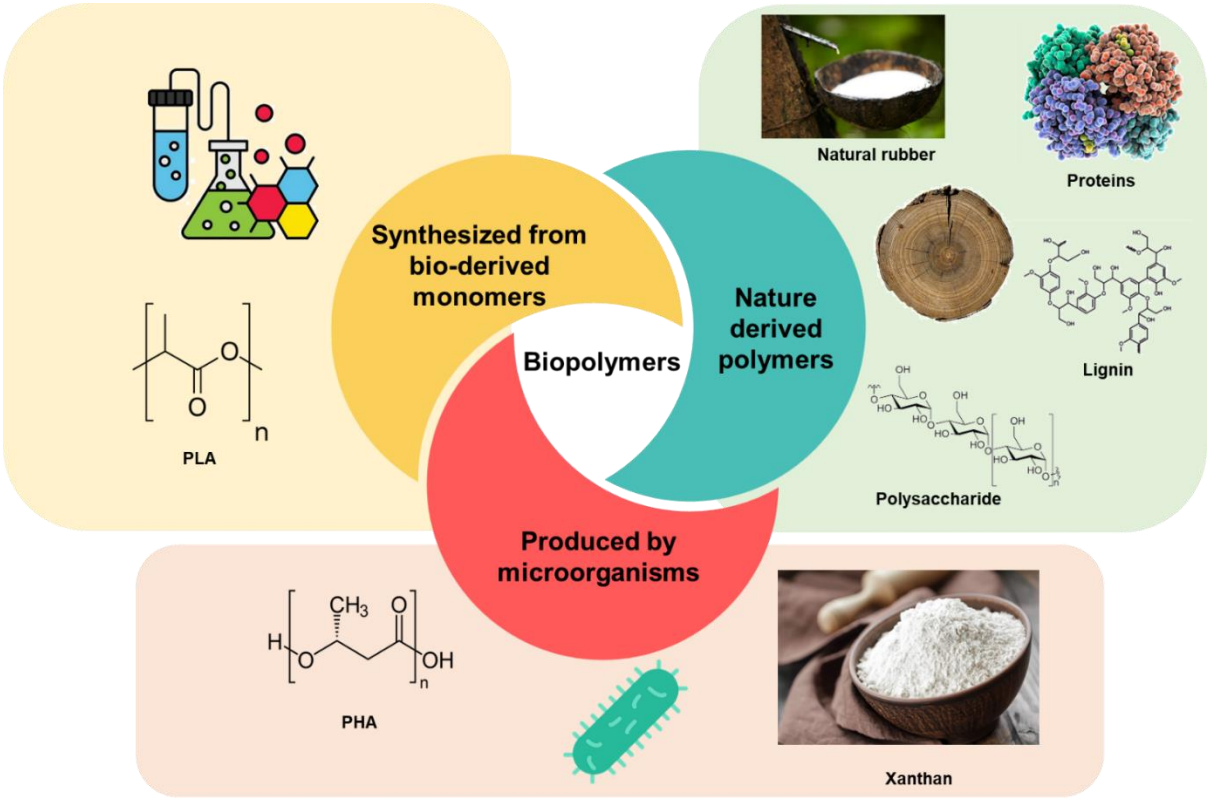

Figure 2.3. Classification of biopolymer types.

2.5. Biopolymers Used in Coatings

2.5.1. Biomass-Based Coatings

2.5.1.1. Protein-Based Coatings

Proteins are macromolecules made up of amino acids which provide structure or biological activity in plants or animals. Proteins have been successfully fabricated into films and/or coatings, which supply nutrients, and possess good mechanical, barrier, and visual properties [74]. Generally, protein-based coating films exhibit excellent oxygen barrier performance, which increases the food's shelf life and prevents food spoilage. Introducing fillers, such as nano-clay and other additives, to the protein coatings leads to greater strength, barrier enhancement, and toughness [75]. Protein-coated paper can be utilized as packaging for fruits, vegetables, meats, eggs, and dry foods [75]. Proteins that have been widely used for packaging include milk proteins (e.g., casein) [76–78], whey proteins [79,80], isolated soy protein [81,82], wheat gluten [83], and corn zein [84,85]. However, protein-based materials typically suffer from poor moisture resistance and lack of vapor barrier properties [86,87]. Thus, their use for liquid or high moisture content products is limited [88,89]. Furthermore, the application of plasticizers and some active compounds can assist the enhancement of moisture barrier performance and delay of the growth of microorganisms for protein-based food packaging applications [89]. The mechanical strength of protein-based films are usually inferior and in order to address this challenge, proteins can be modified via chemical, physical and enzymatic methods [90,91].

2.5.1.2. Polysaccharide-Based Coatings

Polysaccharides are found abundantly in nature and usually derived from renewable feedstocks, which consist of macromolecules made up of repeating monosaccharides like glucose or glucose derivative monomers linking together by glycosidic bonds, often with a primary and secondary hydroxyl group [36]. Biodegradable paper coatings, thin membranes, and standalone films are fabricated from polysaccharides for various applications, including pharmaceutical, food, medical, and industrial processes like pervaporation [92]. Most notably, these materials have been extensively used in the food packaging industry. Films developed from polysaccharides have excellent barrier performance against oil, carbon dioxide and oxygen [93]. The major drawbacks of polysaccharide films and membranes are poor water resistance, as well as low water vapor barrier properties due to their polarity and intrinsic hydrophilicity [94]. Polysaccharide materials that have been widely used as paper coatings are starch [95,96], cellulose [30,97], alginate [81], carrageenan [98], and chitosan [99–101]. Moreover, polysaccharides can be incorporated in coating layers as additives or reinforcing fillers to further enhance the barrier properties of paper coating in the form of cellulose nanocrystals (CNC) [102–104], cellulose nanofibers (CNF) [105,106], α-1,3 glucans [107,108], etc.

2.5.1.3. Lipid-Based Coatings

Lipid compounds, such as long-chain fatty acids and waxes, can be employed in developing films or coating matrices owing to their hydro-repellency. Waxes are one of the most useful natural substances to mitigate moisture permeation through packaging attributed to their hydrophobicity and low polarity [109]. Paper packaging, which is extensively utilized

in the food and drink packaging industry, is frequently wax-coated to enhance water and moisture resistance in conjunction with extending the product's shelf-life [110]. Introducing lipids in edible films and coatings not only improve barrier performance but also promote their flexibility, cohesiveness, and hydrophobicity, which consequently enhance the sensory properties, such as aroma and freshness, appearance, and tenderness [111]. Despite having excellent moisture barrier properties, lipid-based coatings have several disadvantages, such as inadequate mechanical properties, lack of homogeneity, and brittleness which can cause pinholes and cracks on the surface of the coating layers. Various attempts were made to address this challenge, including applying the coatings as emulsions or in successive multi-layers [109]. The most common lipid-based coating materials in the literature and industrial applications are beeswax [112–115], soybean oil [116–118], and paraffin wax [77,85].

2.5.1.3. Lignin-Based Coatings

Lignin is a renewable polyphenolic macromolecule that accounts for approximately 15% to 30% of the existing biomass, making it an appealing, sustainable polymer alternative [119]. In spite of the enormous amounts of lignin generated as a bioproduct of the paper and pulp industry each year, only a small fraction is used in value-added material applications, such as additives, adhesives, and dispersants, with the majority used as low-cost fuel [119]. The inherent drawbacks of lignin, such as natural complexity, incompatibility with polymer substrates, and high tendency to form agglomeration, often limit its applicability in the materials market. These weaknesses can be overcome via chemical modifications of lignin under various functionalization reactions to improve its chemical compatibility with paper substrates [120]. Other alternative approach is transforming lignin into nanoparticles using

various chemical strategies, such as antisolvent precipitation, solvent exchange, ultrasonication, interfacial cross-linking, polymerization, and biological pathways (enzymes) [121]. Lignin nanoparticles offer several advantages, such as degradability, uniform size, dispersibility, and high surface area [122]. Despite lignin's sustainability, very limited literature exists that explores lignin's potential as an additive in the paper coating formulations.

2.5.2. Aliphatic Polyesters-Based Coatings

Aliphatic polyesters are important type of biodegradable polymers. Many types of aliphatic polyesters derived from renewable resources and other polyesters have been produced that are either biodegradable or compostable. However, only a few are commercially available. Examples of such sustainable polyesters that are commercialized include PGA, PLA, PCL, PHBV, PHB, PBS, and PBAT. Among the aforementioned polymers, PLA and PHB are the most widely used materials as aliphatic bioplastics for paper coating applications. This is mainly because both polymers display high biodegradation attributes, biocompatibility, ease of solvent dissolution, and low melting temperatures (between 160 to 180 °C) for melt processing/coating technologies [123]. PHB and PHBV, derived from bacteria such as *Ralstonia eutropha*, have advantages over conventional fossil-based polymers in terms of renewability and biodegradability in various environments. As a result, it is widely considered a suitable material for food and medical packaging applications [75,123]. However, inherent brittleness and physical aging at room temperature of PHB and PHBV is limiting the usage of PHB and PHBV in food packaging applications [124]. PLA is another promising bio-polyester candidate that can act as a coating layer of paper packaging. PLA is synthesized from lactide

monomers in which these monomers are typically obtained from the fermentation of agricultural feedstocks, such as sugarcane, corn, and other sources through microbial fermentation processes [125]. Among all bio-polymers, PLA is considered to have one of the best favorable attributes toward eco-friendliness, such as low cost and abundancy of raw materials, low energy consumption during production, and biodegradability in both water and soil [124]. However, PLA suffers from low oxygen barrier properties and does not fulfill the oxygen barrier performance required in food packaging applications [126]. Moreover, PLA's relative brittleness lowers its appeal for commercial paper coating applications. Thus, blending PLA with other biodegradable polymers can be considered an efficient step toward improving its barrier properties, as well as contributing to overall cost savings [127]. Also, another approach to overcome the brittleness flaw of the prepared PLA film is solvent casting although the release of toxic and harmful organic solvents during this process gave rise to health and environmental issues specifically for food packaging applications [128]. Thus, Belletti et al. reported the preparation of aqueous emulsions of PLA for coating film formation which are non-brittle [129]. Additionally, the involvement of materials that are approved for food contact applications in the preparation of PLA dispersions in water should be considered to make it suitable material for food packaging applications.

2.6. Barrier Properties of Biopolymer Paper Coatings

2.6.1. Moisture Barrier Properties

The moisture permeation through a thin membrane such as a polymer film or a coating layer occurs in three steps: at first, the vapour molecules sorb on the surface of the membrane, followed by the diffusion of molecules through the material, and finally, the desorption of

molecules from the other surface of the membrane (**Figure 2.4**) [130–132]. The permeability coefficient, K (mol Pa^{-1} m^{-1} s^{-1}), is obtained by multiplying the diffusion coefficient, D (m^2 s^{-1}), with the sorption coefficient, S (mol m^{-3} Pa^{-1}) [131]:

$$K = D \times S \tag{2.1}$$

The permeation (P) of gaseous particles through the membrane with a specific thickness (l) is driven by the difference in the pressure gradient (ΔP), which is a steady-state property. The gas permeability can be calculated by employing Eq. (2.2) [133]:

$$P = \frac{J}{\Delta P/l} \tag{2.2}$$

J is the flux of gas diffusion (D) throughout the membrane, which is obtained by using Fick's law (Eq. (2.3)) that is based on concentration gradient (ΔC) across the membrane sides[133]:

$$J = D\frac{\Delta C}{l} \tag{2.3}$$

Which the combination of equations (2.2) & (2.3) provides a comprehensive equation for permeability:

$$P = D\frac{\Delta C}{\Delta P} = DS \tag{2.4}$$

Here S (mol.Pa^{-1}.m^{-3}) is a thermodynamic parameter inversely related to Henry's law coefficient. This equation is most recognizable as the "solution diffusion" model. Thus, permeability takes account of thermodynamic, solubility, kinetic, and diffusion contributions. Solubility is primarily dependent on the gas-membrane interactions, while the diffusivity is mainly influenced by the free volume within the polymeric membrane layer and penetrant kinetic sizes. Thus, analyzing the characterization of a membrane could lead to the evaluation

of the solubility and diffusion coefficient values and, consequently, the permeability coefficient [133,134].

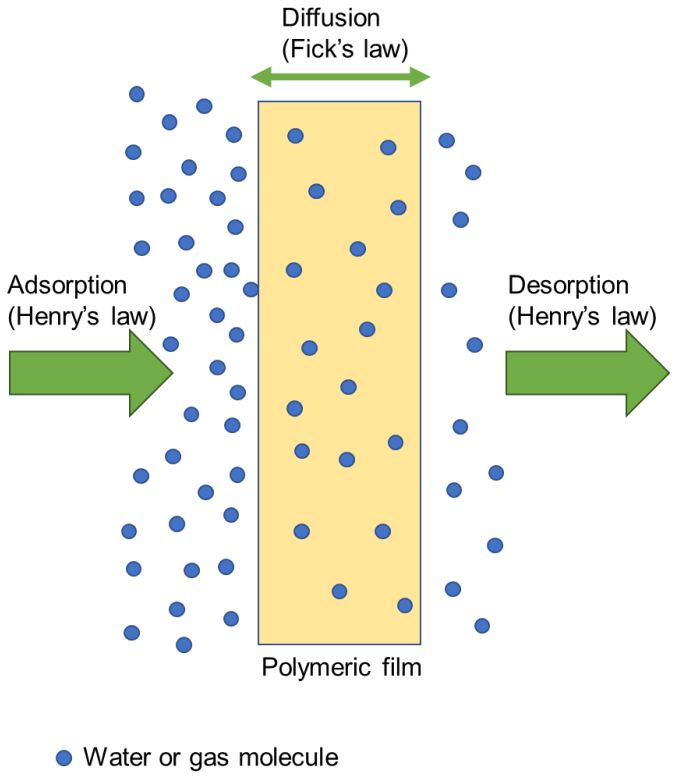

Figure 2.4. Mechanism of water vapor or gas permeation through polymeric film.

Permeation of water vapor is often evaluated with three parameters: transmission rate, permanence, and permeability. Water vapor transmission rate (WVTR) (g/m^2.day) is the volume or weight of permeant moisture conveyed through a film per cross-section area and time under equilibrium conditions (Eq. (2.5)).

$$\text{WVTR} = \frac{\text{weight passed through film}}{\text{area.time}} \tag{2.5}$$

Water vapor permeance (g/m^2.day.kPa) is defined as the transmission rate divided by the partial pressure difference across the film, and water vapor permeability (WVP) (g.μm/m^2.day.kPa) is calculated by multiplying the water vapor permeance with the thickness of the membranes, as indicated in Eq. (2.6).

$$\mathrm{WVP} = \frac{\mathrm{WVTR.thickness}}{\mathrm{partial\ pressure\ difference}} \tag{2.6}$$

As reported by Wang et al., a rough classification of moisture barriers of commonly used polymeric packaging materials can be divided into five categories, as stated in **Table 2.1** [130]. In general, barrier properties depend not only on the materials' nature but are also affected by external diffusion-controlled parameters, mainly temperature, pressure, and relative humidity (RH) [135]. Hence, barrier properties are usually investigated under equilibrium humidity and pressure conditions in a controlled environment as standards. The temperature directly impacts the diffusion and solubility coefficients, in which the permeability can get inconsistent due to the instability of temperature. Generally, an increase in temperature leads to a slight decrease in the solubility and an increase in the diffusivity of water vapor molecules through films. The increase in diffusivity results from the enhanced motion of polymer segments, as well as higher energy movements of permeant molecules [135,136]. Gas permeability also strongly depends on other parameters, such as pressure and relative humidity. Typically, an increase in gas pressure and relative humidity would negatively impact the overall barrier performance due to plasticization effects and swelling of the polymers [137,138].

Table 2.1. Moisture and oxygen barrier classifications of polymeric films [130].

Grade	Water Vapor permeability (*WVP*) (g.µm/m^2.day.kPa)	Oxygen Permeability (*OP*) (cm^3. µm /m^2.day.atm)
Poor	>3000	>40000
Low	1000-3000	4000-40000
Medium	400-1000	400-4000
High	40-400	40-400
Very high	<40	<40

Depending on the nature of the foods, food packaging materials need to fulfil essential moisture and oxygen transmission rate requirements [139]. **Figure 2.5** summarizes the moisture and oxygen barrier requirement ranges for some of the common food products. For developing food packaging, some parameters need to be considered, including material properties, thickness as well as temperature and humidity associated with its end-use to provide the required barrier performance for a given application. Generally, for a particular food packaging, either increasing the thickness or using high-barrier materials can meet the requirements of gas barrier properties. However, thicker packaging is not preferable due to increased manufacturing cost and associated weight increase that negatively affect

transportation cost and energy use. Thus, thin packaging designs with high barrier properties are preferred [130].

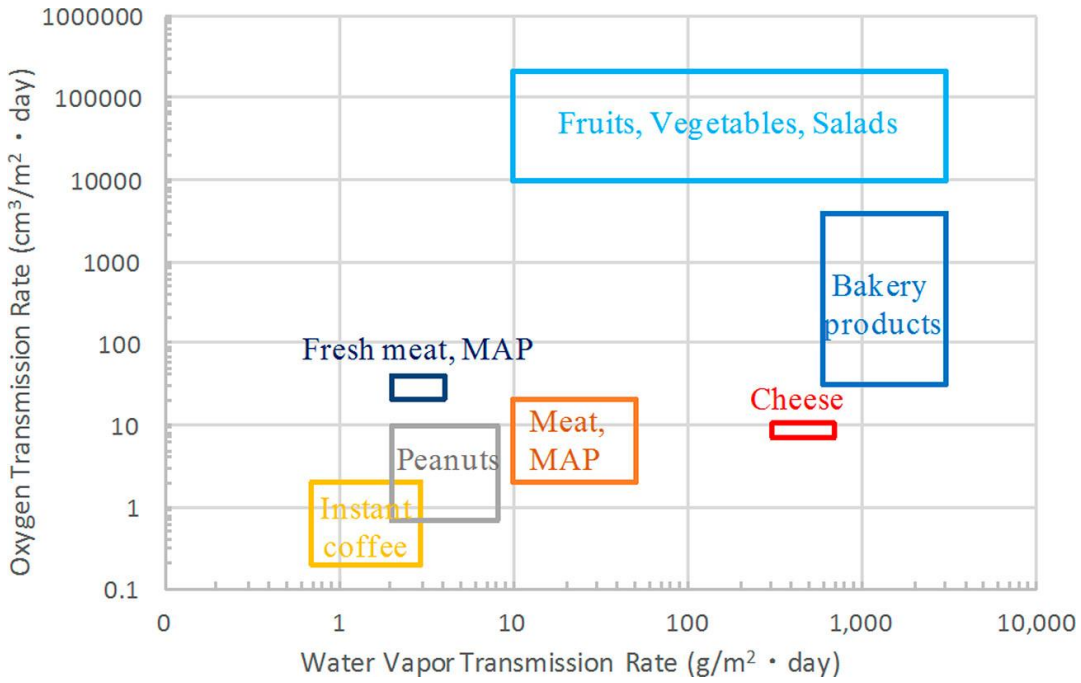

Figure 2.5. Barrier requirements of packaging material for selected food products. Adapted from [130] with permission from American Chemical Society. Copyright 2018.

Since packaged products are often exposed to moisture, the water vapor barrier properties are among the most critical attributes to consider for food packaging material design. Paper substrates, in general, have highly porous structures, which provides room for moisture penetration. Hydrophobic coatings need to be applied to reduce the susceptibility of paper substrate to moisture attack and enhance paper's resistance to the permeation of water vapor molecules. Increasing the hydrophobic properties of paper substrates and enhancing the moisture barrier performance is of great importance and recently attracted substantial research

interest, usually for developing sustainable packaging materials [140]. Traditionally, paper substrates were coated with wax. This is because the wax is relatively inexpensive, abundant, and has good moisture barrier attributes owing to its hydrophobicity. While wax coating is still practiced and available on the market, it is largely replaced by petroleum-based synthetic polymers such as polyolefins and polyvinyl alcohol due to superior barrier performance and reduced cost of these polymers [117,141].

However, innovations in wax-based coatings and modifications as moisture barrier layers are still very active simply due to their enticing attributes as biodegradable moisture-repellant materials. Zhang et al. reported that coating paper using bilayer chitosan and beeswax could promote the water vapor barrier property by up to 32 times more than the untreated paper [115]. The reduced WVTR was attributed to filling the base paper pores with beeswax during the dip coating process. The high efficiency of beeswax to enhance the WVP performance is associated with both its chemical composition and physical structure. However, it should be mentioned that since molten beeswax could easily penetrate through the base paper, the coating weight grammage can increase substantially, leading to potential failure in mechanical properties. Therefore, it was suggested to pre-coat the paper substrate with proteins or polysaccharides to make up for the smoothness deficiency of porous paper [115]. Tambe et al. utilized soybean oil as wax substitute for paper coating, and a significant decrease (53.1%) in moisture permeation through the coated paper was reported [117]. This behavior was mainly attributed to the filling up of the paper pores by the oil droplets and lodging in the paper

substrate, which consequently provided a lengthy and obstructed path for water molecules to transfer through.

On the other hand, coating with hydrophilic biopolymers such as cellulose, hemicellulose, alginate, and starch increases WVP, while enhancing other gas and substrate barrier properties [102,142,143]. Therefore, to overcome the moisture vulnerability of coated papers with these hydrophilic biopolymer layers, the addition of a hydrophobic matrix to the hydrophilic matrix need to be employed [144]. Some hydrophobic bioplastics like PLA can act as moisture resistant layers of paper substrates. Song et al. stated that nano-cellulose fiber (CNF)/polylactic acid (PLA) blend paper coating exhibits excellent moisture barrier performance due to the hydrophobic contribution from the PLA [145]. Rhim et al. investigated the effect of a single PLA coating layer on the WVP of the base paper. The PLA coating reduced the WVP by two orders of magnitude compared to the untreated paper, using only 3 w/v % PLA on the paper [146]. Parris et al. also studied the water barrier property of coating formulation composed of hydrophobic corn protein zein and paraffin wax. The WVTR of zein-wax-coated paper was considerably lower than pure zein or wax coated paper, indicating the synergetic benefits to the overall moisture resistance of the films. It is worth noting that introducing 2% zein solution in paraffin wax decreased the WVTR by approximately half the values obtained for wax-coated paper [85].Generally, base papers without coatings are highly porous materials and impose significant challenges for packaging applications as they allow penetrants to pass through the packaging coating [130]. Thus, it is crucial to control the coating weight grammage to control the WVP of coated papers [77]. This trend was observed in previous studies of cellulose-coated paper [147,148], in which increasing the coat weight of

the cellulose-based coating induced the WVP to diminish despite being hydrophilic. This trend can be ascribed to the higher coat weight caused by multiple layers bringing about effective coverage of the paper substrate pores with the coating, which results in better moisture barrier properties. Furthermore, increases in coating thickness can help extend the permeable pathways for moisture to penetrate through the coated paper [108]. Han et al. noted that WVTR of treated paper with a beeswax coating layer was remarkably reduced than untreated paperboard due to beeswax's low affinity to water vapors [112]. Moreover, the robust WVP interfacial barrier was improved by incorporating an additional adhesive layer, such as starch-based glue.

Interestingly, using a starch-based sticking agent for preparing compressed coated papers allowed the researchers to obtain a 92% decrease in WVTR (from 513 to 41 g/m^2.day). It was suggested that starch gelatinization might have taken place during the heating compression, which consequently crosslinked the polymer chains between layers and introduced additional water barrier effects. This bilayer coating system reduced the WVTR compared to single-layer beeswax-coated paper [112].

Wang et al. reported using oxalic acid-modified microfibrillated cellulose (OMFC) and nanosized alkali lignin (NAL) as multilayer coating films to a paper base, which considerably improved the moisture barrier performance. The low WVTR values can be attributed to the synergetic effects between OMFC and NAL layers owing to an increasing number of active groups formed by chemical modification and nanonization. Also, the formation of crosslinking and hydrogen bonding among cellulose and lignin networks could have resulted in extremely dense film on the paper surface, which induces as high as 93% reduction in moisture

permeation (**Figure 2.6)** [149]. This result concurs well with Adibi et al. studies that explored the influence of synergetic crosslinking of microcrystalline glucan-NR film on the barrier properties of coated papers. The crosslinked NR-based coating exhibited better moisture barrier performance than its non-crosslinked counterparts, which was attributed to the formation of -S-S- bridging bonds that further hinder moisture diffusion [107].

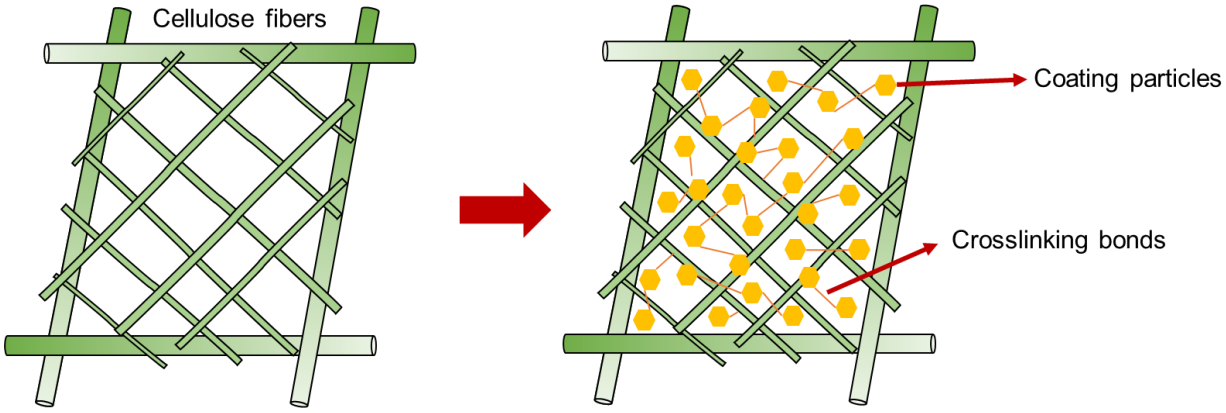

Figure 2.6. Mechanism of formation of crosslinking paper coating film on the paper base.

Table 2.2. Water vapor transmission rate (WVTR) and water vapor permeability (WVP) of biopolymer coated paper.

Coating composition	WVTR/WVP	Type of base paper	Environmental condition	Coat weight (g/m^2)	Reference
Nanofibrillated cellulose (NFC)	29.4 $g/(m^2.day)$	Unbleached kraft	23°, 50% RH	3	[140]
NFC-alkyd resin	2.4 $g/(m^2.day)$	Unbleached kraft	23°, 50% RH	20	[140]
Chitosan-zein	39 $g·\mu m/(m^2·day·Pa)$	35-liner Kraft	23°, 50% RH	23.6	[150]

Chitosan-graft-castor oil	800 g/(m^2.day)	Kraft (unbleached)	23°, 50% RH	–	[151,152]
Chitosan	658.9 g/(m^2.day)	Kraft paper	23°, 75% RH	–	[153]
Silylated soybean oil	720 g.m/m^2.day	Kraft paper	27°, 37% RH	10.45	[117]
Nanocellulose fiber-PLA	200 g/m^2.day	Paper with grammage of 150 g/m^2	23°, 50% RH	25	[145]
Sodium caseinate	0.221 mm/m^2.day.kPa	Paper packaging with grammage of 96 g/m^2	38°, 90% RH	–	[77]
Paraffin wax-Sodium caseinate	0.018 mm/m^2.day.kPa	Paper packaging with grammage of 96 g/m^2	38°, 90% RH	–	[77]
Oxalic acid modified microfibrillated cellulose	123 g/m^2.day	Filter paper with grammage of 68 g/m^2	23°, 50% RH	8	[149]
Cellulose nanofibril	300 g/m^2.day	linerboard	23°, 50% RH	10	[148]

Whey protein isolate	270 $g/m^2.day$	Paperboard from Commercial breakfast container	30°, 90% RH	–	[112]
Polycaprolactone diol	320 $g/m^2.day$	Paperboard from Commercial breakfast container	30°, 90% RH	–	[112]
Hydroxypropyl methycellulose	581 $g·\mu m/(m^2·day·kPa)$	Paper with grammage of 98 g/m^2	38°, 90% RH	3	[154]
Chitosan-beeswax	52.8 $g/m^2.day$	Paper with grammage of 76 g/m^2	38°, 90% RH	–	[115]
Zein	881 $g/m^2.day$	Kraft paper	25°, 50% RH	10	[155]
PLA	9.7 $g/m^2.day$	Paperboard with grammage of 180 g/m^2	25°, 50% RH	50	[146]
PLA	1.31×10^{-10} $g·m/(m^2·s·Pa)$	Paperboard	25°, 50% RH	89.8	[156]
PHB	1.9×10^{-10} $g·m/(m^2·s·Pa)$	Cardboard	25°, 67% RH	–	[157]
Carboxymethyl cellulose (CMC)	8.4×10^{-10} $g·m/(m^2·s·Pa)$	Filter paper	25°, 75% RH	–	[158]

2.6.2. Oxygen Barrier Properties

Oxygen permeability (OP) is another essential feature that dictates the applicability of polymeric coatings in the packaging industry. The oxygen barrier is an essential property of coating materials as it prevents detrimental contact between the product and the environment, thereby decreasing the rate of oxidation of food or pharmaceutical products, and ultimately protecting them from spoilage [114]. The oxygen barrier properties are typically evaluated by permeation testing under static state flux. A partial pressure gradient drives oxygen molecules to diffuse through materials, similar to the diffusion of water vapor molecules [97]. Polymers have an excellent oxygen barrier performance when they possess molecular structures that cause polar-polar interactions or hydrogen bonding interaction with oxygen. Thus, highly polar molecular structures tend to display high oxygen barrier properties. Thus, polymers with good oxygen barrier performance usually suffer from insufficient water vapor barrier properties [159]. Similar to the water vapor barrier property, the OP is greatly affected by the temperature and relative humidity of the surrounding environment. Generally, as the relative humidity increases, the moisture molecules plasticize the polymer used as the coating membrane, which subsequently enhances the mobility and the extensive mass transfer of oxygen molecules across the film [160]. Aulin et al. reported that at higher humidity (70% RH), there was a deleterious effect on the oxygen barrier properties of microfibril cellulose (MFC) paper coating [161]. The absorption of the water molecules into the cellulose fibrils disrupted the hydrogen bonding networks and weakened the interaction among the fibrils, which led to additional permeable routes for oxygen molecules and increased mobility of oxygen molecules [161].

Nevertheless, low OP at a high relative humidity of biobased paper coating materials was also reported in several studies [108,162,163]. The formation of the tightly packed crystallinity network within the paper fiber base can increase the tortuous diffusion paths for molecules to transfer through the coated paper, which is attributed as one of the main reasons for maintaining oxygen barrier performance at high relative humidity. Moreover, various research claimed that hydrophilic polymers have a high tendency to encapsulate the moisture around themselves, which fills up the free volumes through the paper base fibers, consequently inducing more tortuosity to the permeation paths for oxygen molecules (**Figure 2.7(a)**) [108,162]. Strong hydrogen bonding mediated interlocking among the base paper fibers and polar biobased polymers could also prevent the coated paper from swelling at high humidity.

It is noteworthy to mention that there are other factors that have significant impact on the oxygen transmission rate, such as film composition, coating film thickness, and the type of paper substrate [164]. Adibi et al. introduced microcrystalline glucan (MCG) to an NR-based paper coating to enhance the oxygen barrier performance, resulting in more than 14 times lower oxygen permeability values than pure natural rubber (NR)-coated paper. This behavior was caused by the high crystallinity of MCG particles, which induces a packed layer through the coating [107,165]. Similar results were observed for other polar additives, such as wheat gluten [166], microfibrillar cellulose and shellac [167], and regenerated cellulose [151].

Several studies demonstrate a robust relationship between crystallinity and permeability, in which a higher hierarchy of crystalline structures is associated with lower OP values [168]. Since the crystalline regions of polymer films are considered non-permeable,

employing coating material with higher crystallinity would increase the path length for the diffusion of permeant and eventually enhance the oxygen barrier properties. For example, Zhu et al. reported a substantial reduction in the OP of paper bases as they were coated with regenerated cellulose (**Figure 2.27(b)**)[151]. It was proposed that the formation of intermolecular interactions between the regenerated cellulose and the base paper fibers had led to a more compact packing and sealing of the pores of the base paper and lower the gas permeability [151]. In another work, Li et al. reported a significant reduction of OP to $0.003\ cm^3.\mu m.m^{-2}\ 24\ h^{-1}\ kPa^{-1}$ for cellulose nanocrystal coated papers, which was lower than the commercialized oxygen barrier ethylene vinyl alcohol (EVOH) under dry conditions [169]. Overall, by embedding highly crystalline and polar biopolymers in the paper coating formulations, high resistance against the permeation of oxygen molecules can be achieved.

Increasing the thickness that comes with increasing the coat weight can result in enhanced oxygen barrier properties, which are mainly associated with the increased tortuosity and closure of the pores in the paper substrates. This trend was previously observed in the work of Kjellgren et al., as shown in **Figure 2.7(c),** which stated that oxygen permeation of greaseproof paper substrate decreased significantly as the thickness of the chitosan film increased [99].

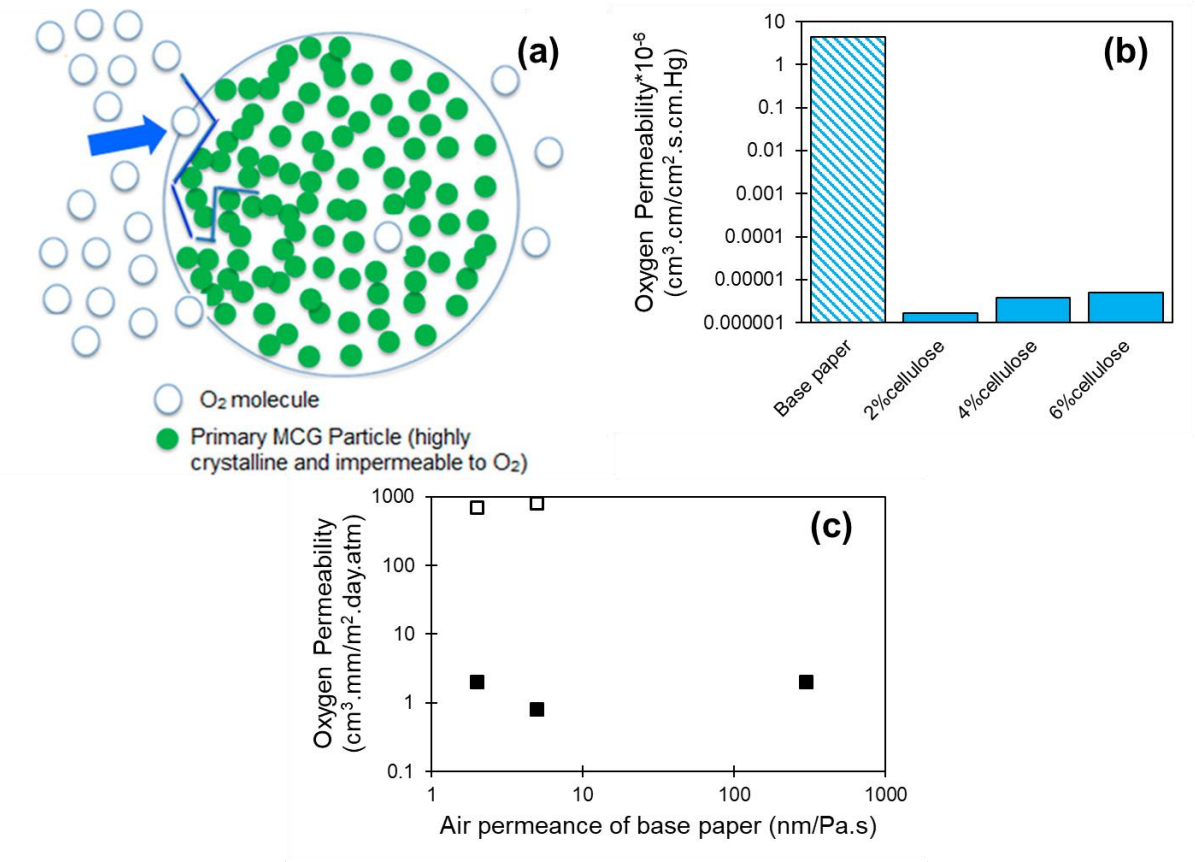

Figure 2.7. (a) Schematic of the tortuous path of oxygen permeation through the paper coated with MCG. Adapted from[107] with permission from American Chemical Society. Copyright 2022. (b) Oxygen permeability of uncoated paper and coated paper with different concentration of cellulose [151]. (c) Oxygen permeability (23 °C, 0% relative humidity) at two different coat weights, 2.4 g/m^2 (□) and 5.2 g/m^2 (■), as a function of the air permeance of the base paper [99].

The type of paper could play a vital role in determining the oxygen barrier of coated paper. Based on the different processes of paper fabrication, papers with varying porosity can be manufactured. Kjellgren et al. noted varied amounts of OP of different types of base papers

after applying coatings on them [99]. Thus, it is evident that the number of voids throughout the paper substrate can dictate the overall permeability of paper coating since highly porous papers impose major challenges to achieving good surface coverage of coatings. In the case of high porosity paper substrates, multiple and greater thicknesses of the coating film are required to fill up the pores and block oxygen molecules' path to convey through the paper coating, which could be more economically appealing.

Table 2.3. Oxygen permeability of biopolymers paper coating.

Coating composition	Oxygen Permeability (OP)	Type of base paper	Environmental condition	Coat weight (g/m^2)/thickness	Reference
Microfibril cellulose (MFC)	0.0006 cm3.μm/(m^2.day.kPa)	Kraft (wrapping), unbleached sulphate	0% RH	5 g/m^2	[161]
Chitosan	1.6 cm3.mm/(m^2.day.atm)	Greaseproof paper	37°, 0% RH	5.2 g/m^2	[99]
Regenerated cellulose	3.8125×10^{-12} cm3.cm/(cm2.s.cmHg)	Kraft (bleached)	50% RH	_	[151]
Natural rubber/Alpha-1,3 glucan	1.5×10^{-4} cm^3.m/(m2.Pa.s)	Manila paper	30% RH	20 μm	[108]
Microfibril cellulose (MFC)	482.49 cm^3.μm/(m^2.day)	Paper with grammage of 45 g/m^2	25°, 50% RH	2.62 μm	[167]

MFC and Shellac	407.53 $cm^3.\mu m/(m^2.day)$	Paper with grammage of 45 g/m^2	25°, 50% RH	12.49 μm	[167]
Wheat gluten	8328×10^{-18} mol/(m.s.Pa)	Untreated paper from bleached pulp	25°, 80% RH	57.2 g/m^2	[166]
Wheat gluten	0.75 $ml/(mm.day.m^2.atm)$	Kraft paperboard with grammage of 34.2 mg/cm^2	23°, 0% RH	_	[83]
Chitosan	0.153 $ml/(mm.day.m^2.atm)$	Kraft paperboard with grammage of 34.2 mg/cm^2	23°, 0% RH	_	[83]
PBAT-lignin (50:50)	1.13 $cm^3\cdot m/(m^2\cdot day\cdot Pa)$	Manila paper	50% RH	_	[120]
Microcrystalline glucan-NR	1.34 $cm^3\cdot m/(m^2\cdot day\cdot Pa)$	Manila paper	60%	9.6 g/m^2	[107]

2.6.3. Grease Barrier Properties

Grease resistance is another unique and critical property for paper packaging used in food protective applications, such as butter wrapping papers, baking papers, and wrapping papers for the fast-food industries (e.g., burgers and meat wraps) [103]. The grease resistance occurs as a result of the relative absence or presence of pores in the paper and it is primarily determined by the largest pore size in the paper. There is a robust correlation between the size

of the largest pore or pores, determining the grease resistance property, and the overall shape of the pore size distribution, determining the air permeation. Considering the largest pore as a simple capillary tube with length of Z (m) (thickness of the paper itself) and radius of r (m), the movement of a viscous fluid, grease, with viscosity of η (Pa.s) and under effect of an external pressure P (Pa) and a capillary pressure (Pa) 2γcos(θ)/r is evaluated by [170]:

$$dv = r^2\pi dZ = \frac{\pi r^4}{8\eta Z}\left(p + \frac{2\gamma\cos(\theta)}{r}\right)dt \tag{2.7}$$

or

$$ZdZ = \frac{r^2}{8\eta}\left(p + \frac{2\gamma\cos(\theta)}{r}\right)dt \tag{2.8}$$

Integration yields the time that it takes for the oil to convey through the paper, t (s):

$$t = \frac{4Z^2\eta}{r^2(p+2\gamma\cos(\theta)/r)} \tag{2.9}$$

The relation between the grease resistance and air permeation of coated paper was reported by Corte [171]. Kit test is one of, if not the most common tests to evaluate the grease repellency of papers or paperboards, which is specified in TAPPI Method T559. This test has been used to determine which coatings can impede the penetration of oil molecules through the paper. In this test, 12 different grease solutions containing castor oil, heptane, and toluene are dropped on the coatings, and then the coating surface is examined to observe traces of staining. The highest number of grease solutions which do not leave a dark stain on the coating film is reported as the Kit number (**Figure 2.8**). In general, a higher Kit number favors the penetration of oil solutions. This observed trend is because of the less viscosity and

comparatively more non-polar solutions, as the higher kit solutions comprised more hexane and toluene solvents and less castor oil [103,172,173]. Moreover, a material that achieves a Kit number of 8 and higher is considered grease resistance. Overall, the grease resistance of uncoated paper is inferior due to its porous structure, which offers routes for oil molecules to transfer through the paper despite inherent resistance against non-polar substances [99,174]. Hence by introducing coating layer(s) on the paper base and covering the voids on the surface of the base paper, the oil barrier-resistant properties can be alleviated [175].

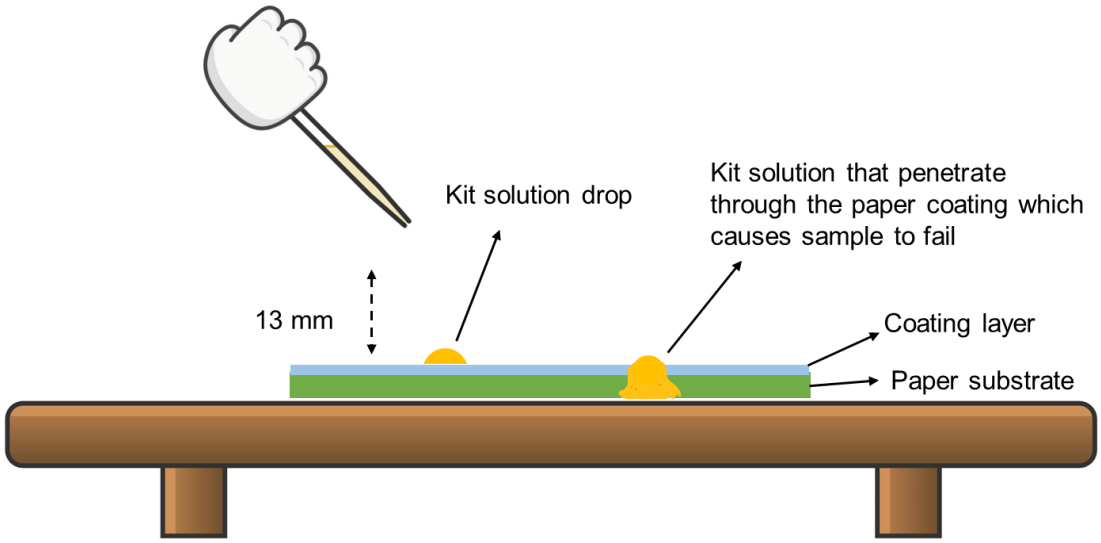

Figure 2.8. Schematic illustration of Kit test (TAAPI method T559).

Tyagi et al. reported that after the coating of the paper base with cellulose nanocrystals (CNC) films, the Kit number jumped from 0 (for the uncoated paper) to 8 and subsequently to 11 after applying multilayer coatings of CNC/cellulose nanofiber [104]. Also, Zhang et al. investigated the grease resistance of chitosan and beeswax as a paper coating [115]. The oil-stained spot was detected on the paper coated with only 1 wt.% chitosan; on the other hand, no

trace of oil-stained was spotted for 1 wt.% chitosan-beeswax paper coating, indicating that beeswax was the main contributing factors in improving the grease resistance in their paper coating systems. Enhancement in the mechanical properties of the coated paper was noted, which was mainly ascribed as improving surface deficiency by applying chitosan and beeswax [115]. Additionally, the effects of the coating thickness on the grease resistance were examined in other studies. In a recent investigation on a paper coating composed of alpha-1,3 glucan-Natural rubber (NR), when the thickness of the coating layer increased from 20 to 100 μm, the highest Kit number (Kit value 12) was achieved. Hence alpha-1,3 glucan-NR paper coating is comparable to commercial paper packaging or containment materials, for instance, polyethylene (PE) coated paper [108]. Effective sealing of the voids, in addition to the introduction of the tortuous path via alpha-1,3 glucan particles for oil molecules to convey through the paper substrate pores, brought about appealing grease resistance performances for the coated paper (**Figure 2.10**). Wang et al. reported the same trend for cellulose paper coating, demonstrating that the grease barrier properties incrementally improved as the cellulose deposit weight gradually increased [149]. Remarkably, Park et al. and Trezza et al. noted higher grease barrier properties of soy protein and corn zein compared with commercially used polyethylene-laminated paper [82,84]. Also, Wang et al. reported that using carboxymethyl chitosan and sodium alginate as paper coating exhibited good oil barrier performance with a Kit number of 8 [176]. Also, Fein et al. reported that NR-CNF paper coatings passed a 12 Kit number; however, some defects were introduced after folding, which enabled grease penetration into the coated paper [177]. NR, unlike CNF, is oleophilic and does not provide

enough grease resistance. As shown in **Figure 2.9,** the introduction of NR to the coating formulations could have disrupted the protective CNF layer against grease.

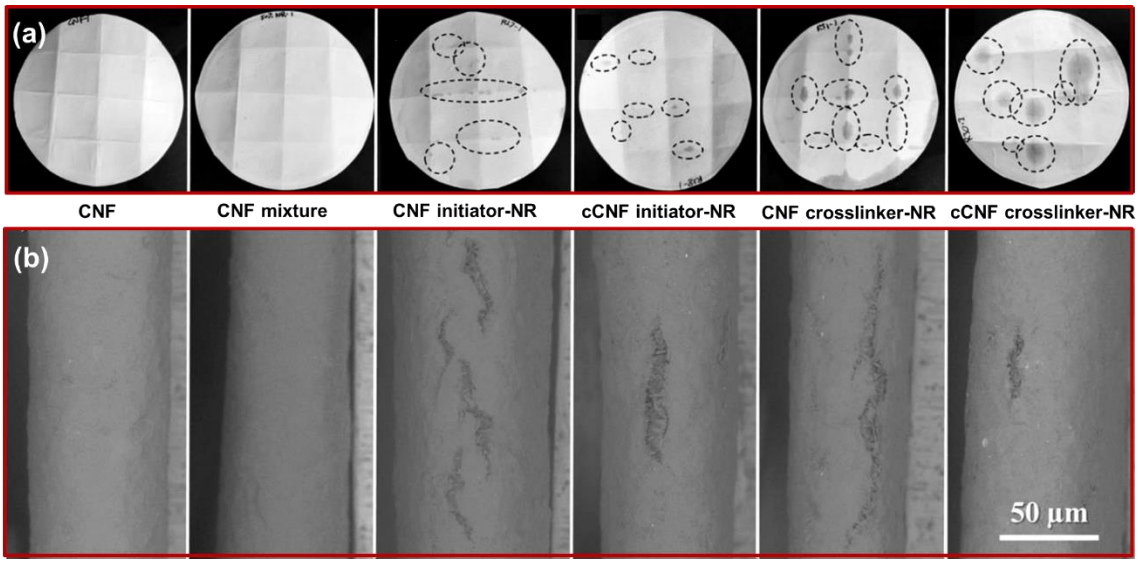

Figure 2.9. (a) Images of coating surfaces after 12 kit-test were dropped on folds encompassing the four center squares on each sample. Ellipses indicate regions of grease penetration. (b) SEM Images of fold edges at 100X magnification. Adapted from [177] with permission from Elsevier. Copyright 2020.

Waxes are widely used in food packaging and fruit preservation. Additionally, waxes can be combined with other ingredients to generate emulsions that can be used for paper coating applications. The employment of such wax emulsion has gained commercial interest due to the ease of separating the cellulose fiber from the wax during the paper repulping process thus allowing paper recycling [116,178]. Additionally, emulsions are easier to apply on the paper base and more ecofriendly compared to conventional extruded coatings [118]. Liu et al. investigated utilizing microcrystalline wax emulsion as paper coating material, and as the

emulsifier dosage increased, the kit number first increased and then slightly decreased [179]. This trend highlighted the excessive addition of the oleophilic and hydrophilic emulsifiers that could weaken the oil-resistance performance of the coated paper. Also, the effect of the microcrystalline wax emulsion loading coat was explored in the work, in which increasing coating weight results in the enhancement of the grease resistance from 0 (for uncoated paper) to 8 (with a coating load of 10 g/m^2). The employment of microcrystalline wax emulsion as coating effectively fills the pores, which prevents oil molecules from permeating through it and hence, protects the papers from oil penetration. In a different work, Li et al. developed paper coatings with chitosan-graft-caster oil copolymer, which further supported the higher oil resistance of coated paper [152]. Furthermore, utilizing a dual-layer of chitosan-zein as coating layers was investigated by Kansal et al., and the hydrophilicity of the chitosan provided the paper with high grease barrier properties (with a Kit value of 12), while zein had poor oil resistance and was mainly introduced to the coating for water repellency [150].

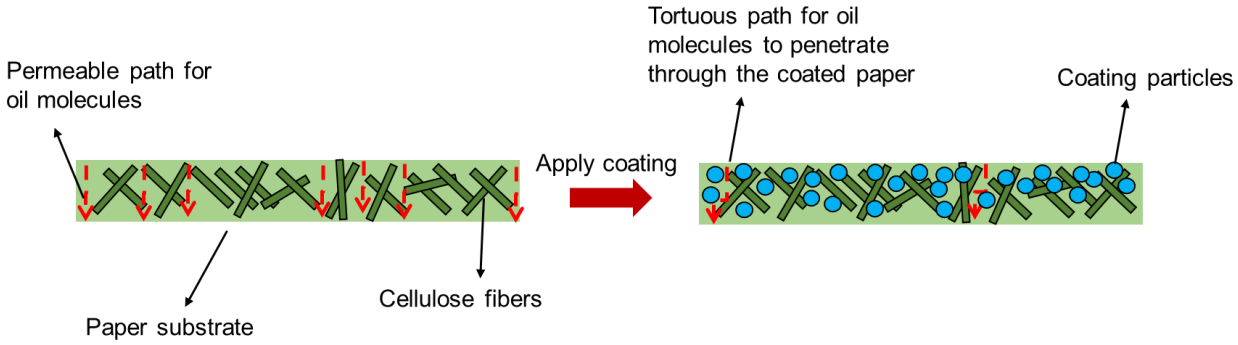

Figure 2.10. Schematic illustration of the mechanism of improvement of grease barrier performance by applying coating on the paper.

2.6.4. Water Resistance Properties

For packaging applications, meeting the required water resistance properties is essential for coated papers to direct contact with wet products is common. Since paper packaging substrate is highly hygroscopic and hydrophilic as they are made from cellulose containing a high degree of polar functional moieties, hydrophobic and/or superhydrophobic surface coatings are often implemented to help reduce the wetting behaviors and to improve the water-repellent traits to enhance the wettability performances of paper packaging layers. The water-repellent attributes are usually measured by the water contact angle (WCA) between the liquid droplets and the contact surface of coatings. For standard flat paper surfaces, the WCA typically ranges from 0-90°, indicating inherent hydrophilic behaviours. The WCA for hydrophobic coating surface must fall in the range of 90-150°, while the superhydrophobic coating surface must show an almost perfect sphere with WCA greater than 150° [180]. Additionally, the coating of papers is considered hydrophobic only when they have a sliding angle, in which the water droplets can roll off the surface when tilted at an angle. Therefore, coated paper's wet strength is a better way to evaluate its strength when it comes in contact with water, and this is an occasion that frequently occurs with food packaging.

An untreated paper easily loses its physical integrity when exposed to water as the water wet the cellulose fibers and causes swelling, resulting in a disruption in the fibers network and leaving somewhere between 3% to 10% of the original dry strength (at 50% relative humidity) [181]. Thus, it is vital to employ coatings capable of impeding the deterioration influence of water on the base paper. Adibi et al. examined the effect of the NR-alpha-1,3 glucan coating film on the wet strength of the paper. The researchers submerged the

paper coating samples in water for a specific time and immediately conducted tensile strength testing. It was observed that the uncoated paper experienced catastrophic mechanical strength deterioration. On the contrary, the coated samples showed substantial tensile property retention. Also, a progressive improvement in the paper's wet strength was reported with increasing the loading content of the alpha-1,3 glucan, which was owing to two main reasons; first, occupying the fiber pores and leaving no free space for water molecules to get collected and secondly, the high affinity of alpha-1,3 glucan to the cellulose fibers which induced strong mechanical interlocking and hydrogen bonding that effectively hinder water molecules penetration [108].

Enhancement in the tensile strength of coated paper was stated by Sun et al. in chitosan-guanidine coated paper. The wet strength of treated paper was weakened as the concentration of the chitosan decreased, which implied that chitosan introduced extra hydrogen bonding among the fiber networks, hence better wet strength with the coated paper [182]. These results correlate well with Rohan et al. that also demonstrated wet strength retention with the employment of PBAT-lignin coating. Applying a layer of a relatively non-polar modified lignin assisted the samples with extra water repellence, which led to a retention of the wet strength of the coated samples. The filling of the micro-voids between the cellulose fibers in the paper by the dispersed lignin particles that consequently prevent water seepage through the pores was suggested [120].

Superhydrophobic coating is a relatively novel and advanced class of materials that can be very useful for packaging applications owing to their self-cleaning, anti-liquid, anti-dirt, and anti-corrosion properties. Vigorous chemical modification or surface treatments on coating

materials are required to reduce the surface tension energy and, thus, achieve a superhydrophobic surface for paper packaging. Zhang et al. fabricated superhydrophobic paper with a mixture of beeswax and carnauba wax as coating, followed by annealing [113]. The contact angle was ~160°, and water droplets rolled off easily from the paper coating surface. In another study, Arbatan et al. reported the preparation of superhydrophobic paper in two steps [183]. At first, the paper was dipped into aqueous suspensions of precipitated calcium carbonate pigments and cellulose nanofibers. In the second step, the coated papers were treated with a solution of alkyl ketene dimer in n-heptane. Contact angle measurements displayed contact angles above 150° and rolling angles of less than 5°, as presented in **Figure 2.11**, which confirmed the superhydrophobicity of the coated paper [183]. Khanjani et al. also produced superhydrophobic paper by spin-coating a dispersion of nanostructured fluorinated cellulose esters [184]. The contact angles post-coating was higher than 150° while the untreated paper was super hydrophilic as the water droplets quickly penetrated through it.

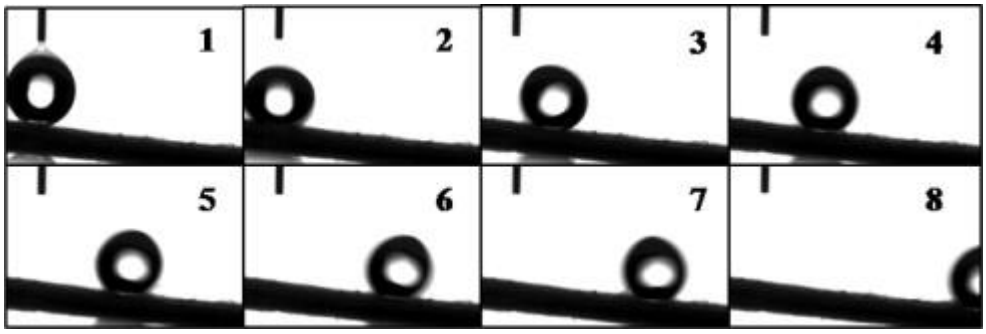

Figure 2.11. The water rolling-off angle: figures (1–8) are images of a 5 μl water droplet being placed on the tilted (5°) surface of superhydrophobic paper. The water droplet began to roll off

the superhydrophobic paper surface as the tilting angle of the surface increased to 5°. Adapted from [183] with permission from Elsevier. Copyright 2012.

2.6.5. Rheology of Coatings

Rheology of paper coating formulations is among the critical attributes that dictates the quality of the coating applications, such as blade and extrusion coating. This is because the rheology of the coatings could influence the flow patterns, flow rate, momentum transfer, and subsequently influence the coating weight. In extrusion coating, the melt rheology of a polymer has a great impact on coating speed while adhesion and melt strength dictate coating efficiency. Cheng et al. demonstrated that due to the relatively low melting index and poor adhesion of the pristine PLA, high-power extrusion equipment is needed for shaping PLA products [185]. Therefore, modification of PLA is required in order to address its poor melt flow rheology. PLA modified with animal gelatin resulted in enhancement of its adhesion strength along with facilitating thin film and lamination fabrication process. Usually, the concentration of the gelatin-based plasticizer for extrusion coating is in the range of 0.5-2.5 wt% depending on the extrusion equipment, type of paper base, and specific laminate requirements **Figure 2.12**.

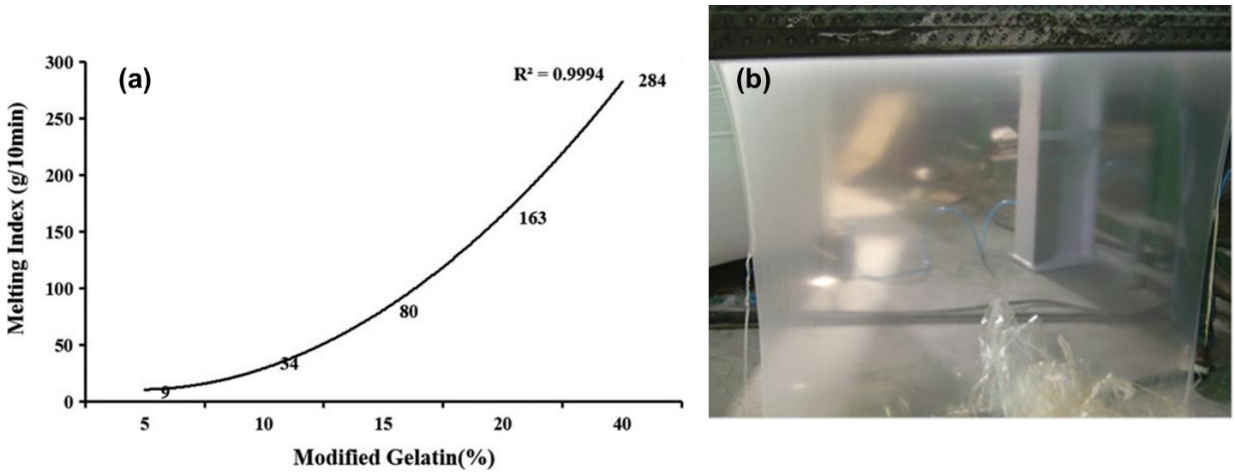

Figure 2.12. (a) Melting Index of modified PLAs obtained at 190°, (b) modified PLA melt curtain. Adapted from [185] with permission from Wiley. Copyright 2015.

The rheological properties of paper coating greatly affect the quality of the coated paper too [186]. Moreover, the dynamic viscosity of the coating formulations governs the surface uniformity and flow behavior of the coating formulations. Usually, for liquid coating systems, the addition of a thickener or rheology modifier is vital to obtain suitable rheology [187]. For instance, a common thickener and co-binder is carboxymethylcellulose (CMC), which alters the rheological properties of the coating film, thereby affecting its quality [188]. Liu et al. stated that nanocellulose (NC) can be utilized as a rheology modifier in paper coating [189]. It was mentioned that the rheological behaviors of NC suspensions are greatly dependent on their features, like dimensional size, particle size, surface charge, and dispersion microstructure. The NC suspensions exhibited shear-thinning behavior due to the breaking down of the network constructed by strong hydrogen or ionic bonds among NCs at elevated shear strength. With the addition of NC to the coating, the viscosity considerably increased at low shear rates resulting in more shear-thinning behavior. Therefore, when the coating containing NC is applied on the

paper and after the shear force is applied, a highly viscous layer could be formed on the paper base [189]. Shorey et al. studied the rheological properties of esterified lignin and PBAT blend as a paper coating [120]. It was mentioned that with increasing the lignin content in the formulation, the overall viscosity of the coating formulations increased, which was mainly due to the effect of lignin on the flow characteristics by restricting the mobility of polymer chains. Also, the presence of lignin in the coating formulation led to a shear-thinning behavior, which is favorable in wet coating fabrications [120].

2.6.6. Other Prospective Properties

Paper packaging has also recently found applications in active packaging, one of the most appealing sectors in the food packaging industry. Modern paper-based food packaging is designed to be able to provide excellent barrier properties for food protection, as well as to contain active ingredients to maintain the freshness of enclosed food products [62]. These active packaging systems employ various technologies that can further reduce spoilage rates and extend food products' shelf-life. These approaches include employing oxygen and ethylene scavengers, moisture absorbents, and antimicrobial and antioxidant agents [190,191]. While the direct addition of active compounds in food formulations is a common practice to preserve food, it poses some significant drawbacks. Firstly the potential inactivation of active substances and secondly having limited options as the substance must be safe enough for consumption. On the contrary, other types of active compound incorporation, such as embedding in the coating polymer substrates, on the surface as coatings, or in the headspace sachets/bags can have enhanced potency and effectiveness in terms of preservation and mitigate some of the challenges posed by direct addition [192,193]. For instance, polymer

coating systems may serve as potential inclusion units for these active volatile and non-volatile compounds, which promote both the barrier effect and preservation potentials of these paper-based packaging materials [109]. Ethylene, oxygen, and moisture scavenger/inhibitor compounds are incorporated as composite additives in coating layers to complement the protection and safeguard properties of paper and paperboard packaging materials [62,194,195]. For instance, ethylene scavengers, such as potassium permanganate, silica, and clay mineral, have been previously investigated as techniques to inhibit the releases of ethylene gases, which are responsible for the ripening processes (browning, softening, weight loss) of vegetables and fruits. Rodriguéz employed PLA-based hydrophobic coating with various clay-based ethylene gas absorbents such as clinoptilolite, sepiolite, and sepiolite permanganate [196]. However, the hydrophilic nature of these clay-based additives slightly reduced the water barrier improvement provided by hydrophobic PLA coating, though the reduction was not substantial and the sufficient water permeability level was satisfied. In another study, Ni et al. utilized a combination of ethylene inhibitors (1-methylcyclopropen (1-MCP), ethylene captivator potassium permanganate ($KMnO_4$), and antimicrobial cinnamon essential oil (CEO) microcapsule) in ethyl cellulose-based paper coating to extend the shelf life of climatic mushroom Agaricus bisporus (**Figure 2.13**) [197]. The combination of these different active compounds successfully inhibited the mushrooms' enzyme activities and continuously absorbed and removed ethylene production through the packaging atmospheres, thus providing sufficient shelf-life extension for storage and transportation periods. Since different ethylene scavengers and inhibitors control the influence of ethylene production by different

mechanisms, combinations of these compounds could have a more potent impact on the preservation effects of paper packaging products.

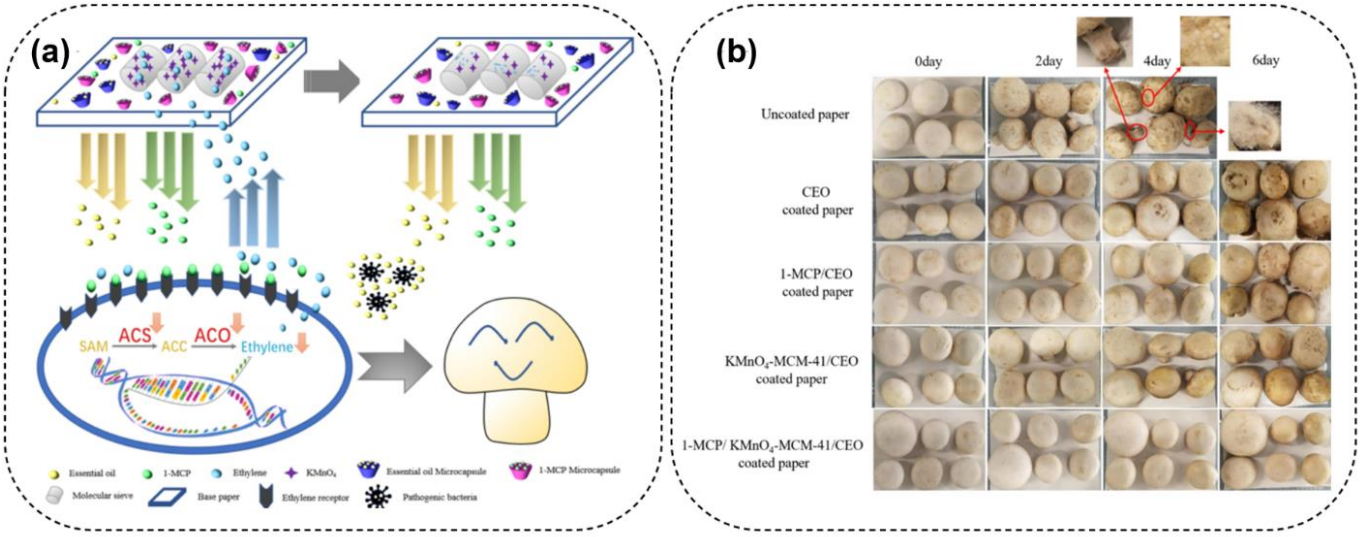

Figure 2.13. (a) Mechanism of scavenger, antioxidant, and antimicrobial agents to extend the shelf-life of mushroom. (b) Preservation of mushroom with coated paper over the course of 6 days. Adapted from [197] with permission from Elsevier. Copyright 2021.

In addition to scavengers, antimicrobial and antioxidant active agents are frequently integrated into paper-based packaging materials as they provide extra merits for preserving fresh foods, particularly stopping microbial growth and oxidative attacks, in addition to barrier properties. Compounds with antimicrobial and antioxidant activities can be derived from inorganic substances (metal and metal oxide micro/nanoparticles), organic (plants, essential oils, chitosan/chitin), or other sources (enzymes, bacteriocins) [198,199]. However, inorganic compounds seem more dominant in paper packaging as antimicrobial and antioxidant agents due to their effective potency. Ni et al. investigated the antimicrobial activities of incorporating

ZnO nanoparticles in the starch-based film with carboxymethyl cellulose (CMC) used as a bridging agent to homogeneously disperse the ZnO nanoparticles in the starch matrix to achieve the maximum antimicrobial activity. [200] However, the use of inorganic materials raises concerns about the biodegradability and recyclability of paper coating products. Thus, there is upsurging research on developing organic and safe functional additives that provide biodegradability or recyclability.

Recently, studies have shown that chitosan/chitin has been utilized in active packaging as an "all-in-one" material due to its coating-forming capabilities, and antimicrobial, antioxidant, and barrier properties [201–204]. Moreover, chitosan/chitin are biodegradable and compatible with paper substrates, promoting renewability functions that are quintessential for these biodegradable packaging materials [205]. Bordenave et al. employed chitosan-based coatings that were modified with palmitoyl chloride and stearic fatty acid by grafting onto the OH^- moieties of chitosan, which promote excellent grease-barrier and antimicrobial properties of the film [201]. Additionally, the WVP values of modified chitosan did not drop though the coating became more hydrophobic, which was attributed to the porous microstructure after the modifications. However, the antimicrobial properties of chitosan/chitin have been reported to become less potent with time. Thus, adding other active compounds to retain the required antimicrobial and antioxidant properties of packaging materials is required [206]. For instance, Jung et al. developed a paper coating composite from starch-chitosan blends embedded with silver nanoparticles (AgNPs) [206]. The additional AgNPs not only helped reduce the antimicrobial activities in the chitosan-starch coating, but also inhibited the fungal activities

on the paper substrates, making the bio-based coatings more appealing as active packaging materials. Additionally, other natural active compounds such as plant extracts [207,208], citric acid [209], and essential oil [210,211] are frequently utilized as antimicrobial and antioxidant packaging. The use of these bio-based and biodegradable materials should be further developed over inorganic additives to produce complete biodegradable paper packaging products for product shelf-life extension.

2.7. Biodegradability Aspect of Bio-based Packaging

Biodegradable food packaging is becoming one of the most popular demands in the market and an area of researchers' interest because of environmental pollution concerns (**Figure 2.3**). Paper packaging made up of synthetic petroleum-based plastics, such as PP, PE, and ethylene vinyl acetate (EVA) coating, have clear disadvantages over the new class of biodegradable polymers owing to their non-biodegradability despite their excellent barrier and mechanical properties as barrier layers of paper packaging. Moreover, some synthetic and non-biodegradable plastics can pose safety concerns in addition to their substantial contribution to the accumulating pollution problems caused by microplastic fragments and toxic additives leaking into the food chain. It is reported that 64.3% of microplastic debris from packaging materials has polluted the marine environment and severely affected marine ecology [212]. Other studies show that some synthetic plastics commonly used in food packaging (e.g., polystyrene and polyamides) can lead to severe health hazards such as cancer, allergies, and system dysfunction [213]. Thus, the use of bio-based and biodegradable polymer options for food packaging material design is essential.

The term "biodegradable," according to ASTM standard D-5488-94d definitions, means "capable of undergoing decomposition into carbon dioxide, methane, inorganic compounds, and biomass.". Biodegradation occurs mainly due to microorganisms' enzymatic actions, which can be evaluated using standard tests over a specific period, typically within 6 months in composting conditions [214]. The biodegradation process starts with the secretion of enzymes from microorganisms that hydrolyze the corresponding polymer chain structures, resulting in the depolymerization of macromolecules into monomers and oligomers. And then oligomers and monomers are uptaken as biomass which induces the production of CO_2 and H_2O. The reactions that take place during the degradation of bio- and fossil-based polymers are shown through **Figure 2.14**[215]**.**

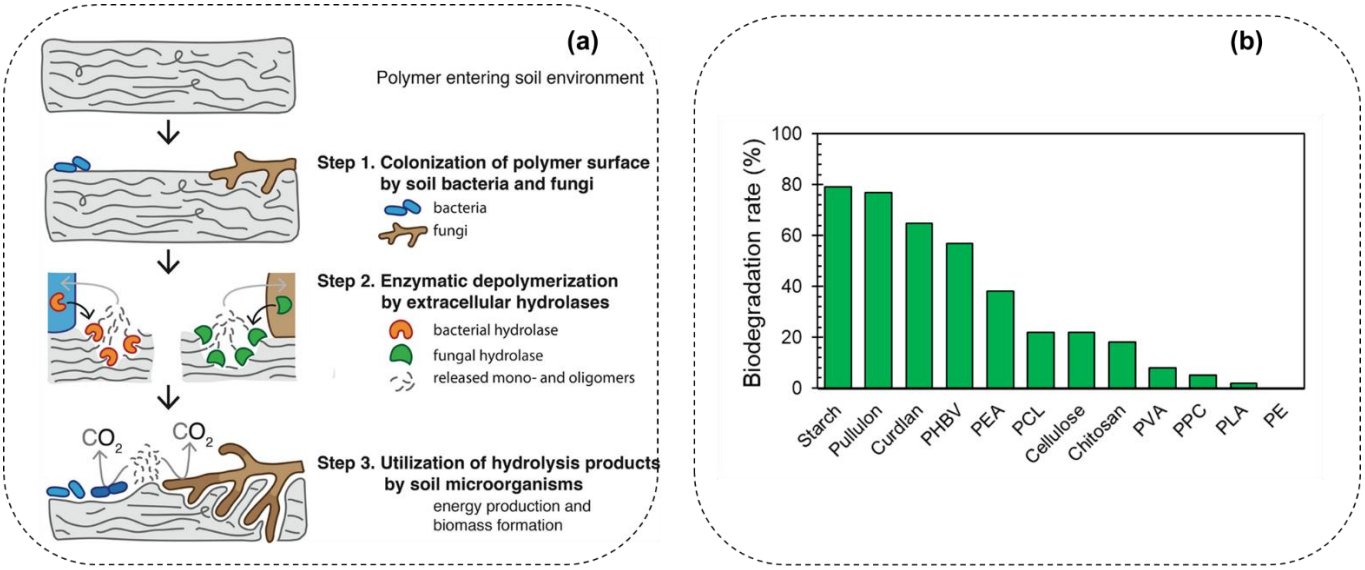

Figure 2.14. (a)Three fundamental steps involved in polymer biodegradation in soils. Adapted from [215] with permission from American Chemical Society. Copyright 2019. (b) Biodegradation rate of different polymers [216,217].

Cardboard paper has been used for packaging and wrapping applications, but its biodegradability is limited due to the fibers network density and the inclusion of chemical additives that obstruct the biodegradation processes [218]. Kraft paper, on the other hand, is comprised of a high-density and content of lignin, and in most cases, is produced in semi-bleached or untreated conditions. As a result, the theoretical biodegradable fraction of kraft paper is 36%, and currently most composting facilities do not accept kraft papers [218].

Eco-friendly food packaging, also known as green packaging, is made up of renewable materials which are biodegradable and/or can be recycled or reused. Studies have shown that cellulose-based packaging films exhibit low toxicity along with low environmental risks associated with them [219]. Utilizing bio-based polymers in packaging accelerates the rate of biodegradation, which can be counted as a step forward toward alleviating the environmental pollution crisis (**Figure 2.15**). One study showed a high biodegradability rate of PBE/PBAT bio-nanocomposite within 20 days of testing in the marine environment [220]. This behavior can be due to the attacks on the polymeric chains by microorganisms and algae leading to polymer chain cleavage. For instance, a review by Siracusa et al. stated that blending PET with aliphatic polyesters results in forming weak spots that favor the degradation through hydrolysis [221]. Also, the addition of starch into other polymeric materials has shown to increase the disintegration percentage up to 60% [213]. Therefore, introducing bio-based polymers as a coating to the paper packaging system could favor coated paper's bio-disintegration rate.

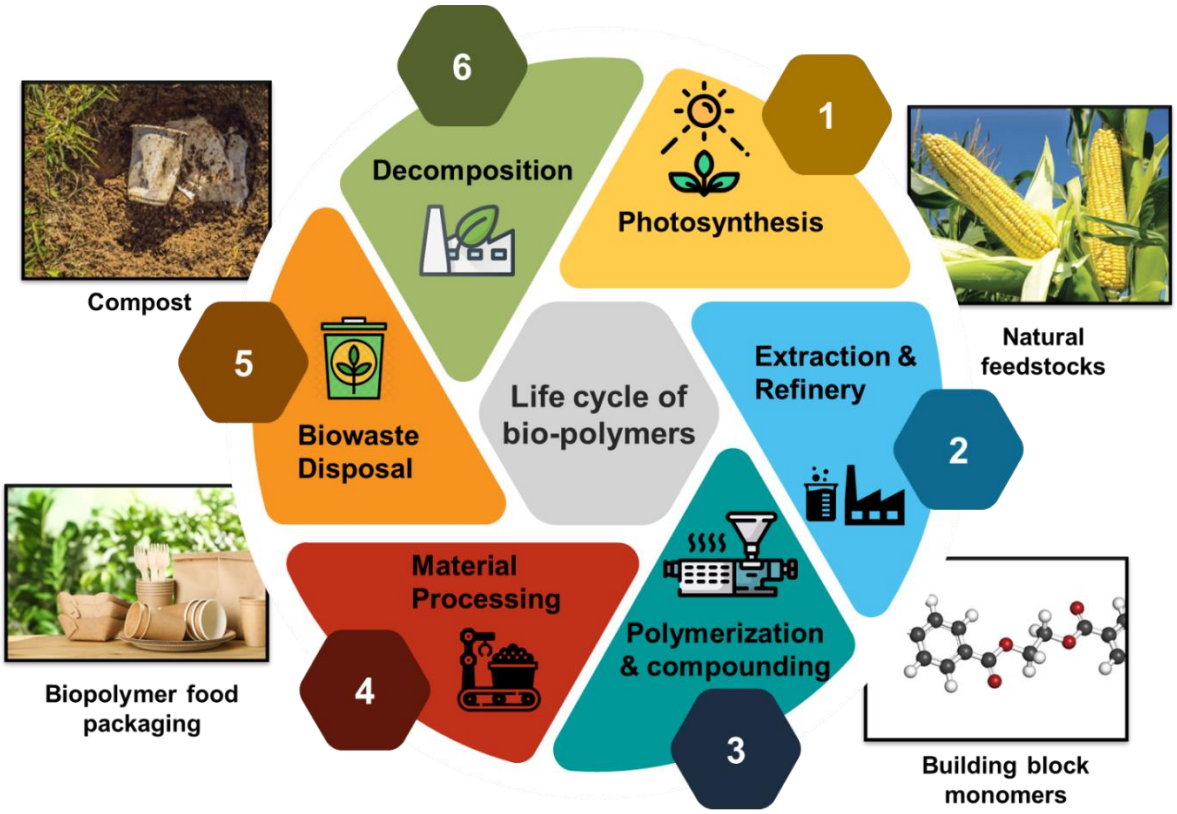

Figure 2.15. Life cycle of biopolymers [222].

2.8. Summary and Future Trends of Green Packaging Materials

The deployment of eco-friendly polymer composites for paper coating applications offers exciting opportunities for the safety and quality of food and the sustainability of packaging materials. Moreover, the multifunctional properties of paper packaging accrued by sustainable coating materials in conjunction with functional additives have great merit for society. Important considerations that need to be accounted for the development of successful packaging materials include i) cost-effectiveness of food packaging material manufacturing, since expensive equipment is mostly involved in the process, ii) eco-friendly additives and agents for green packaging material, iii) regulations and legislation for packaging must be

applied to achieve a high level of food safety and transparency for consumers [220]. Packaging applications often require low WVP and OP, as well as being mechanically sturdy and resistant enough against water and oil to protect the packed food for an extended time.

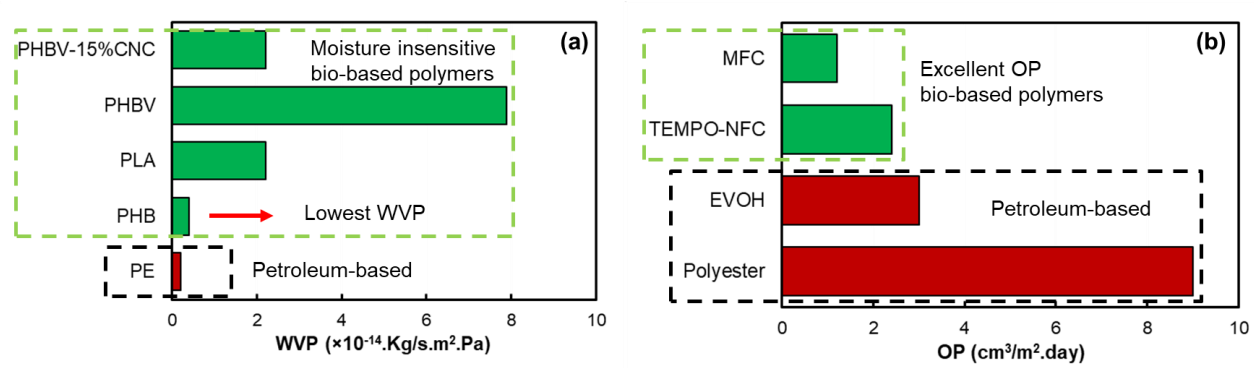

Figure 2.16. (a) Comparison of WVP among bio-based and petroleum-based polymers as paper coatings, (b) comparison of OP among bio-based and petroleum-based polymers as paper coatings [66].

After analyzing available literature on the barrier properties of bio-based polymers and their potential for use as paper coatings, several biopolymers were found to compete with existing petroleum-based commercialized packaging materials (**Figure2.16**). Petroleum-based materials such as PE are known to show outstanding barrier performance and can withstand high humidity conditions without compromising mechanical and barrier properties. Thus, it is often used as standard material for packaging applications [223]. Non-polar biopolymers such as PLA, PHB and PHBV usually show good water barrier properties; specifically, PHB is so far known as a biopolymer with the most comparable WVP to that of petroleum-based polymers such as PE [66]. Nature-derived biopolymers, such as starch, protein, and cellulose,

are inherently polar and allow water vapor permeation easily, especially at higher relative humidity conditions where they are more susceptible to moisture attacks [224,225]. Therefore, it is essential to improve their water-resistance performance through hydrophobic treatments for their effective utilization in paper coating applications. Also, in order to further enhance the barrier properties of hydrophilic biopolymers, incorporating other hydrophobically modified biopolymers or lipid-based biopolymers as blend or filler can be conducted. For instance, the addition of modified CNC to PHBV matrix promotes the WVP [226]. Notably, biopolymers with high crystallinity, such as MFC and NFC, have excellent barrier properties and perform better than conventional polymers (**Figure 2.16(b)**). In addition, most hydrophilic biopolymers exhibit excellent grease resistance when covering the paper base surface effectively. Currently, credible information on the cost of sustainable paper coating material is not easily available partly because most sustainable polymer systems are still under intense research and development. Nevertheless, for sustainable paper coating to succeed in the market, their cost has to be comparable to the incumbent materials besides their performance. Also, complete life cycle assessment needs to be established to appreciate their sustainability.

Chapter 3. Enzymatic polymerization designed polysaccharide particle morphology as a reinforcing filler of dipped and casted rubber films[2]

3.1. Introduction

Developing alternatives to the petroleum economy which match or exceed performance and are inherently scalable requires us to come up with sustainable ways of producing materials from renewable resources using resource and energy sustainable processes. Currently, uncontrolled solid-waste generation from persistent petroleum-derived polymers is correlated with increasing widespread environmental pollution through formation of microplastics eventually ending up in the various water bodies [16]. Traditional polymer materials which have been developed over the last century are extensively used in most engineering and commodity material applications due to their excellent chemical and mechanical properties, and more importantly, based on the large scale and low-cost manufacturing processes [17]. Attempts to recycle these polymers, specifically plastics with the highest production rate, have failed as only about 5% of polymers are successfully recovered [21]. To mitigate this challenge, there is an increasing interest in finding more sustainable material options which may substitute or complement conventional polymers with renewable and /or biodegradable material alternatives [22,23].

Rubber products represent an essential and high functional class of performance materials required in many everyday applications. Natural rubber (NR) is a widely established

[2] A version of this chapter has been published on peer-reviewed journal as a review article: A. Adibi, et al. (2021). Enzymatic polymerization designed alpha-1,3 glucan particle morphology as reinforcing fillers of dipped and casted rubber films. *Carbohydrate Polymers*, **267**, 118234. https://doi.org/10.1016/j.carbpol.2021.118234.

biopolymer manufactured at large scale with extensive industrial applications and expanding its utility may be a promising option to enable the expanded use of this sustainable, and high-performance biopolymer. NR, with the chemical structure of cis-1,4-poly(isoprene), is extracted from the *Hevea brasiliensis* tree in the form of milky soap or latex [4]. Because of the appealing properties, it has widespread applications in highly crosslinked products such as footwear, tires, gaskets, conveyor belts as well as lightly crosslinked goods, such as balloons, catheter tubes, condoms, and gloves. While there is a well-established market for the use of NR in glove applications [227], it still lags behind nitrile rubber due to allergic sensitivity concerns from the protein residues that are inherently in natural rubber. The current COVID pandemic is already pushing the limits of PPE use, including nitrile-based gloves which is leading to the generation of large quantities of non-biodegradable solid waste, often littered under uncontrolled disposal conditions. Natural rubber has a clear benefit over synthetic rubbers in terms of its short- to mid-term bio-degradation profile. The use of functional fillers can certainly enhance its functional performance, which may justify the added cost for removing protein impurities. Though pristine NR possesses excellent elasticity and reversible deformability, it has several limitations, such as low modulus, hardness, durability, and tear resistance, to effectively compete with some of the synthetic elastomers alternatives in a range of applications [2]. In order to potentially address this market opportunity and to improve the mechanical properties of NR, curing, as well as incorporating fillers, are typically employed in many if not all rubber-based applications. Filler systems which can be processed into the composite at the nano-scale such as montmorillonite clay [11], silica [228], calcium carbonate [35], and carbon nanotubes [10] have been used to enhance the mechanical properties of NR.

The use of such filler systems in rubber is especially appealing over micron-scale fillers as the significantly higher surface area at lower scale enables effective interaction with the rubber polymer at the molecular level and as a result property enhancements can be achieved at low filler loading levels. However, at increasing filler content, the NR matrix becomes susceptible to poor filler dispersion, which may lead to the deterioration of the mechanical properties. Therefore, optimizing the filler concentration to maximize performance is a key design consideration.

Polysaccharides, typically sourced from established renewable feedstock (e.g. cellulose or starch), are sustainable materials composed of repeating glucose monomers linked by glycosidic bonds commonly with one primary and two secondary hydroxyl moieties[36]. Generally, polysaccharides are highly aggregated, hydrophilic biopolymers, and have a strong tendency to form intra and inter molecular hydrogen-bonding networks. The water solubility of polysaccharides is highly dependent on the type of glycosidic linkages (α or β), polymer chain branching, and hydrogen-bonding networks and other factors [38]. For example, cellulose (β-1,4 glucan) is highly aggregated, and water-insoluble, whereas starch is a mixture of different polysaccharide materials (α-1,4 glucans and α-1,4 / 1,6 glucans) and is typically soluble in water when heat is applied. The utilization of polysaccharides as fillers for polymers is receiving increasing attention due to the potential to provide composite reinforcement, relative low density compared with mineral fillers, and the overall sustainability profile of a readily renewably sourced material. Within the general class of polysaccharides, cellulose nanocrystals[39], chitin nanowhiskers [40], and starch nanocrystals[41] are reported in the literature as potential reinforcing fillers of natural rubber and other elastomers.

Recently, IFF (Former DuPont Nutrition and Biosciences) has described the engineered polysaccharide, α-1,3 glucan, from the enzymatic polymerization of glucose derived from sucrose [45,46]. The α-1,3 glucan is a water-insoluble, linear, semi-crystalline polysaccharide [49]. The enzymatic polymerization is carried out in water and this process allows for the control of the particle morphology. Through this, various types of glucan morphologies can be accessed, including spherical aggregates (wet cake), fiber-like structures (fibrids), and a plate-like systems (platelet), the microcrystalline glucan material used in this work (MCG) [51]. The isolated polysaccharide has a highly agglomerated structure with a higher surface area, typically in the 2-10 micron range; however, further analysis indicates that under shear various aggregated structures become accessible. The primary particle size range is within the 10 to 30 nm range (by AFM), but the accessible particle size range accessed in formulations representing the MCG system are in the 0.2-1 micron range, and can also further aggregate and form various morphologies in the microscale [229].

This study seeks to elucidate the influence of these novel engineered polysaccharides with specific morphology on the mechanical properties, barrier properties, as well as crosslink density of natural rubber-based composites. In this study, two different methods, casting and dipping, were employed to produce thin films. Analytical techniques, such as tensile and tear strength, crosslink density, and permeability analyses, were utilized to determine the properties of the film composites.

3.2. Materials and Methods

3.2.1. Materials

Microcrystalline glucan (MCG) derived from enzymatic polymerization is provided as stable colloidal dispersion in water (6-10 wt.%), obtained from IFF (DuPont Nutrition and Biosciences). Cellulose nanocrystals (CNCs) were obtained from CelluForce Inc (Montreal, QC, Canada). Stabilized natural rubber (NR) latex (60 wt.% solid content) was supplied by Chemionics Corporation, OH, USA. Zinc oxide powder (ZnO), potassium hydroxide pellets (KOH), tetrahydrofuran (THF), and polyethylene glycol tert-octylphenyl ether (Triton) were purchased from Sigma Aldrich, USA. Zinc (II) dibutyl dithiocarbamate (ZDBC) (98 wt.%), Calcium Carbonate, and Calcium Nitrate were obtained from Fisher Scientific Inc., Canada. Sulfur with 99.5% purity was obtained from Acros Organics.

3.2.2. Methods

3.2.2.1. Particle Characterization

The zeta potential of the MCG was analyzed using a Malvern Zetasizer (Westborough, MA) in an aqueous dispersion of MCG (0.1 wt. %) dispersed in deionized water. Three measurements were conducted for each test, and a folded capillary cell (Zetasizer nanoseries, DTS 1061) was utilized for the zeta potential test. The surface morphology of the MCG particles was imaged using the FE SEM. The thermal stability of MCG was evaluated using Thermogravimetric analysis (TGA) (METTLER TOLEDO TGA 2) in the dynamic mode under nitrogen flow. Prior to the test, the MCG was dried in a convectional oven (105 °C overnight), and heated at a rate of 5 °C/min from room temperature to 500°C. The MCG was

also characterized by Fourier Transform Infrared Spectroscopy (FTIR, Bruker Tensor 27) and compared with cellulose nanocrystals (CNCs). For this, 10 mg of dried MCG and 200 mg of dried KBr were pressed together into pellets and scanned from 4000 to 400 cm^{-1} wavenumber.

3.2.2.2. Formulation and Film Fabrication

Rubber latex formulation for preparing rubber films consisted of sulfur curing agent, activating agent, and MCG is shown in **Table 3.1**. The preparation procedure was initiated by pre-dispersing the curing agent, activating agent, and filler in water via homogenization (5 min shear mixing at 25,000 rpm) using a PowerGen 700 homogenizer, followed by sonication. The concentrations of MCG as fillers in the composite film formulation were varied in parts per hundred (phr) with respect to the natural rubber with the following experimental design; 0 (control), 1 phr (0.94 wt.%), 3 phr (2.8 wt.%), 5 (4.54 wt.%), 7.25 (6.46 wt.%), and 10 phr (8.7 wt.%). After adding the pre-dispersed mixture to NR, dipping and casting methods were employed to produce prototype film specimens. For the dipping process, constant viscosity formulations were employed to develop consistent and stable films on the film former (Scheme 1). Hence, the formulations were diluted with water to achieve the reference viscosity of 37.2 cP, which was the NR latex's viscosity. Brookfield digital viscometer was used to monitor the viscosity of the formulations. For the casting method, a total solids content of 40 wt.% was maintained to obtain films with uniform thickness.

Table 3.1. Formulation compositions for rubber latex.

COMPONENTS	PARTS PER HUNDRED (PHR)
NR latex	100
MCG	0, 1, 3, 5, 7.25 , 10
3% KOH Solution	1.5
Sulphur	1.5
ZDBC	0.7
ZnO	1.3

Dipped Film Fabrication

The pre-dispersed latex formulation was mixed at 400 rpm for 2 h at 40 °C using a hot plate with a magnetic stir bar as a maturation process. Fabrication of the rubber latex film was initiated by dipping a rectangular glass in a coagulant solution (**Table 3.2**) for 10 seconds, drying at 80 °C for 15 min, then cooling at room temperature for 1 minute. The glass coated with the coagulant solution, as shown in Table 2, was then gently dipped in the matured latex formulation for 40 seconds prior to curing at 100°C for 2 h, as displayed in **Scheme 3.1**. This method is typically used in the industry for dipped goods production [230].

Table 3.2. Formulation compositions for coagulant solution.

Components	Parts Per Hundred Rubber (phr)
Deionized water	100
Calcium nitrate	50
Calcium carbonate	0.8
Triton	0.06

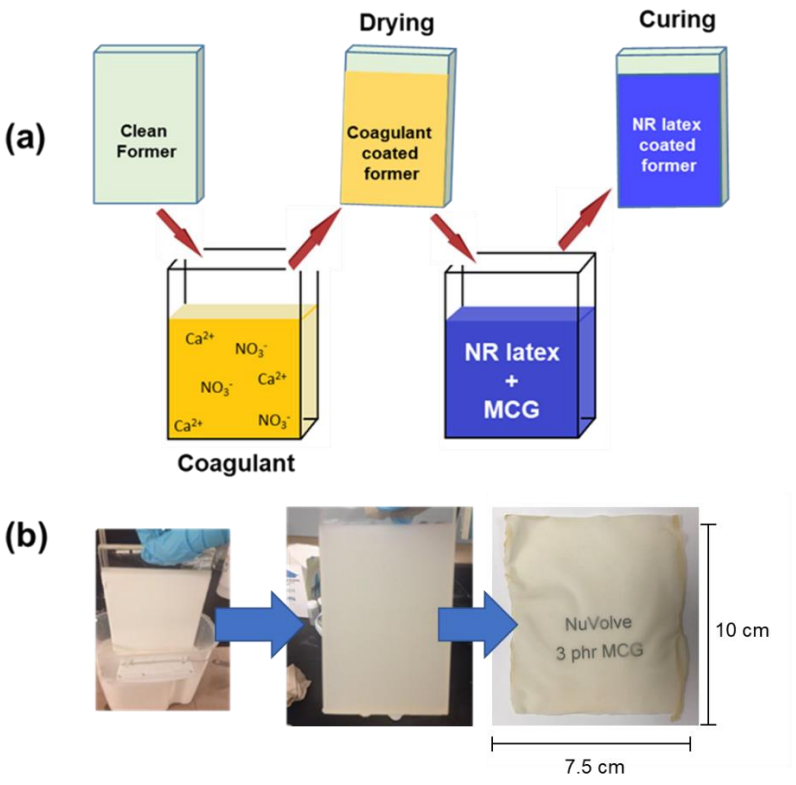

Scheme 3.1. Schematic demonstration of the dipping process (a) Cartoon describing the dipping process; (b) image displaying manual dipping and the generated film.

Cast Film Preparation

The latex formulation comprised of 40 wt.% solids was casted on glass molds to produce films with uniform thickness. After drying at room temperature, the films were cured at 100°C for 2 h, as illustrated in **Scheme 3.2**.

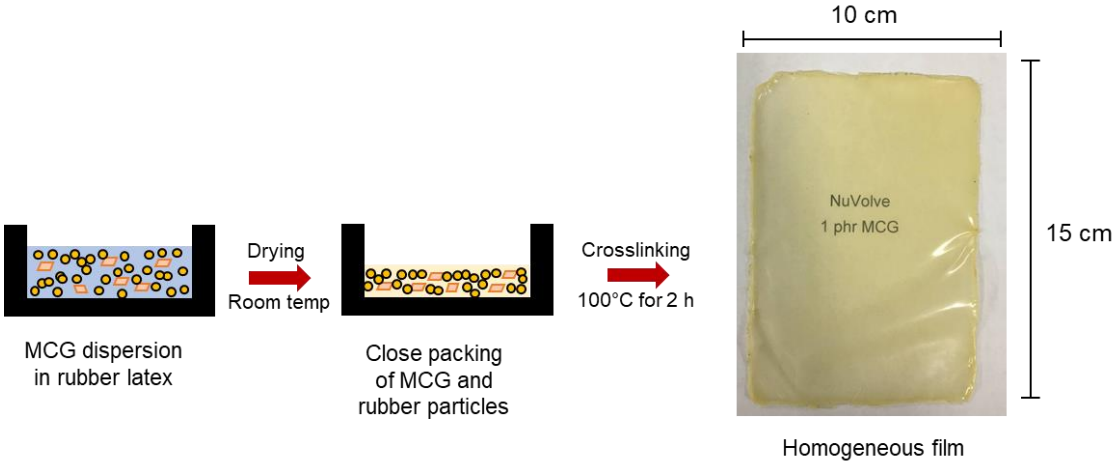

Scheme 3.2. Schematic demonstration of the casting process.

3.2.3. Film Characterization

3.2.3.1. THF Swelling and Crosslink Density Study

The evaluation of the crosslink density of the composite films was accomplished via the THF swelling method. Rubber films were cut into 25 mm × 15 mm pieces, which were then immersed in THF until reaching equilibrium swelling, which was found to be 72 h. Each sample's weight was tracked at various time intervals by wiping the excess THF off the surface of the films and immediately weighing. The swelling index (*SI*) was calculated to investigate

the degree of swelling as described in Equation (3.1), where W_1 (g) and W_2 (g) are the weight of the samples before and after submerging in THF for a specific amount of time, respectively. This test was conducted in triplicates for each sample, and the average swelling index was reported.

$$SI = \frac{W_2 - W_1}{W_1} \tag{3.1}$$

The crosslink density (ν_{cross}) was calculated using the Flory-Rehner equation[231,232]:

$$\nu_{cross}\left(\frac{mol}{g}\right) = -\frac{ln(1-\nu_r) + \nu_r + \chi\nu_r^2}{2\rho_r V_s\left(\sqrt[3]{\nu_r} - \frac{\nu_r}{2}\right)} \tag{3.2}$$

where ν_r is the volume fraction of the equilibrium swollen rubber, χ is the Flory-Huggins polymer-solvent interaction parameter (0.393), V_s is the molar volume of the solvent (81.08 m^3/mol), and ρ_r (0.908 g/cm^3) is the density of rubber. To calculate ν_r, Equation (3.3) was utilized:

$$\nu_r = \frac{\frac{W_{before} - W_{filler}}{\rho_r}}{\frac{W_{before} - W_{filler}}{\rho_r} + \frac{W_{after} - W_{filler}}{\rho_s}} \tag{3.3}$$

where W_{before} (g) is the weight of the rubber films before swelling, W_{after} (g) is the weight of the rubber films after swelling, W_{filler} (g) is the weight of the filler, and ρ_s (0.89 g/cm^3) is the density of the solvent.

3.2.3.2. Morphology Analysis

The degree of dispersion of the MCG in the NR latex films was evaluated by using a scanning electron microscope (FEI Quanta FEG 250 SEM). In this test, specimens were cut immediately after immersing in liquid nitrogen and then coated with gold.

3.2.3.3. Tensile Testing

The rubber films were cut into strips with specific dimensions (70 mm×10 mm) in accordance with ASTM D882-18. The tensile test was conducted on five specimens with a 500 mm/min strain rate using a Tensile Testing Equipment (AGS-X Shimadzu, Japan) using 0.5 kN load cell.

3.2.3.4. Tear Strength Testing

The tear test was conducted in accordance with ASTM D624-12 using a tensile testing unit (AGS-X, Shimadzu, Japan). A type T trouser specimen with dimensions of 50 mm × 20 mm and an initial cut length of 10 mm were tested with a crosshead speed of 50 mm/min.

3.2.3.5. Dynamic Mechanical Analysis (DMA)

For dynamic mechanical analysis (DMA) testing, rectangular strip specimens with a width of 6.5 mm were cut from rubber films prepared by the dipping method. The test was conducted with an initial grip separation of 12 mm using a 50 μm amplitude, frequency of 1 Hz, and applied force of 0.01 N on TA Instruments, DMA Q800. The samples were equilibrated at -90°C for 1 minute then heated at a rate of 3 °C/min to 20°C.

3.2.3.6. Thermogravimetric Analysis (TGA)

TGA analysis was carried out under nitrogen flow with the rate of 30 mL/min initially in isothermal and then in dynamic mode by using a TGA instrument (METTLER TOLEDO TGA 2). The samples were first heated to 100 °C for 5 min to remove water, then the temperature was ramped up to 500°C at a heating rate of 5 °C/min.

3.2.3.7. Water Absorption Testing

A water absorption test was conducted in triplicates to study the effect MCG's on the

response of the composite films to moisture. Specimens with 25 mm × 15 mm dimensions were dried overnight in a convection oven at 80°C prior to the test. After weighing the dry samples, they were submerged in glass cups filled with 200 mL of water, and the weight change was monitored at various time intervals over 7 days.

3.2.3.8. Permeability Testing

The impact of MCG on the barrier properties of the rubber composite films was analyzed against water and ethanol as a volatile solvent, as stated by ASTM E96. Cups containing water and ethanol were tightly sealed with the rubber composite films, and throughout the 7 days, the weight change was tracked. This experiment was performed under constant relative humidity in a desiccator. The water vapor transmission rate (*WVTR*) and solvent transmission rate were then calculated using the following equation ASTM E96/E96M-16:

$$WVTR = \frac{G}{t \cdot A} \tag{3.4}$$

where *G* is the weight change (g), *t* is time (hr), and *A* is the cross-sectional area of the cup mouth (m^2). Additionally, the water vapor permeability was calculated using the following equation [233]:

$$WVP = \frac{(WVTR) \times l}{\Delta p} \tag{3.5}$$

where l is the thickness of the films (m), and Δp is the partial water vapor pressure difference (Pa) between the two sides of the film.

3.3. Results and Discussion

3.3.1. Engineered Polysaccharide Characterization

The engineered polysaccharide, α-1,3-glucan, was provided by IFF. The polysaccharide is formed in an enzymatic polymerization process starting from sucrose. as described in the literature[44,51,234]. This polysaccharide is water insoluble and is isolated from the polymerization process as aggregated, highly associated structure. Through enzyme catalyst and process control the formation of various particle morphologies and the degrees of crystallinity can be adjusted [44,51,229]. Even though this semi-crystalline polysaccharide is hydrophilic, it is not soluble in water and can form a stable colloidal dispersion in water under shear that displays a shear-thinning behavior [235].

The α-1,3 glucan, utilized in this work is isolated with a specific microcrystalline structure (MCG), a feature enabled directly by the enzymatic polymerization or within the overall polymerization process. The morphology of the MCG was studied using various imaging techniques (**Figure 3.1(a-c)**). The SEM images (**Figure 3.1(c)**) indicated the platelet morphology of the MCG, which was rather unique for this material as compared to other polysaccharides such as cellulose nanocrystals (CNCs), starch nanocrystals, or chitin, which typically have either rod or spherical shape. The optical micrograph images (**Figure 3.1(c)**) exhibited that the MCG particles consisted of aggregated, fractal-like particles with a high surface area. This specific particle system in addition to colloidal stability also demonstrates consistent stability across a wide pH range, the colloidal stability and the viscosity response are only marginally impacted. Even at a pH of 2, the MCG dispersion remains controlled and no decomposition or hydrolysis is observed. The zeta potential of the MCG was measured, and it has a neutral surface charge over the investigated pH range (2 to 10). This value is in

complete agreement with the surface charge that has been previously reported by Kedzior et al. [52]. Kedzior et al.[52] reported that MCG dispersed under the described conditions has 200 × 200 nm length by width, and 10 nm in thickness.

The variation in the primary structure, morphology, and surface area are plausible reasons for the observed variations. The crystallinity index of the MCG calculated from X-ray diffraction (XRD) was 85% (**Figure 3.1(d)**), which makes it comparable with CNCs [236] and highly structured cellulose found in bacterial cellulose [44].The thermal stability of fillers is an important factor that needs to be studied, as the majority of the polymer processing operations are performed at elevated temperatures. The thermal stability/degradation of dried MCG powder was evaluated using TGA. The onset thermal degradation temperature of the MCG was 270°C, which was close to cellulose nanocrystals (CNCs), as shown in **Figure 3.1(e)**. The TGA results indicated that the MCG has a slightly better thermal stability as compared to the CNC, since the peak thermal degradation of the MCG was between 270°C to 340°C, while the CNC degraded before reaching 300°C. FTIR results presented in **Figure 3.1(f)** displayed that MCG and CNCs have similar spectra. It was noted that the MCG and CNCs have similar characteristic peaks. The most prominent peaks were at 3380 cm^{-1} (O-H stretching), in the range of 2800-2900 cm^{-1} (C-H stretching)[237,238], at 1360 cm^{-1} (C-H and C-O bending vibrations of the polysaccharides) [239], at 1430 cm^{-1} (CH_2 bending mode) [240], at 1160 cm^{-1} (coupling modes of C-O and C-C stretching) [241], and at 1090 cm^{-1} (C-O-H bending modes) [241].

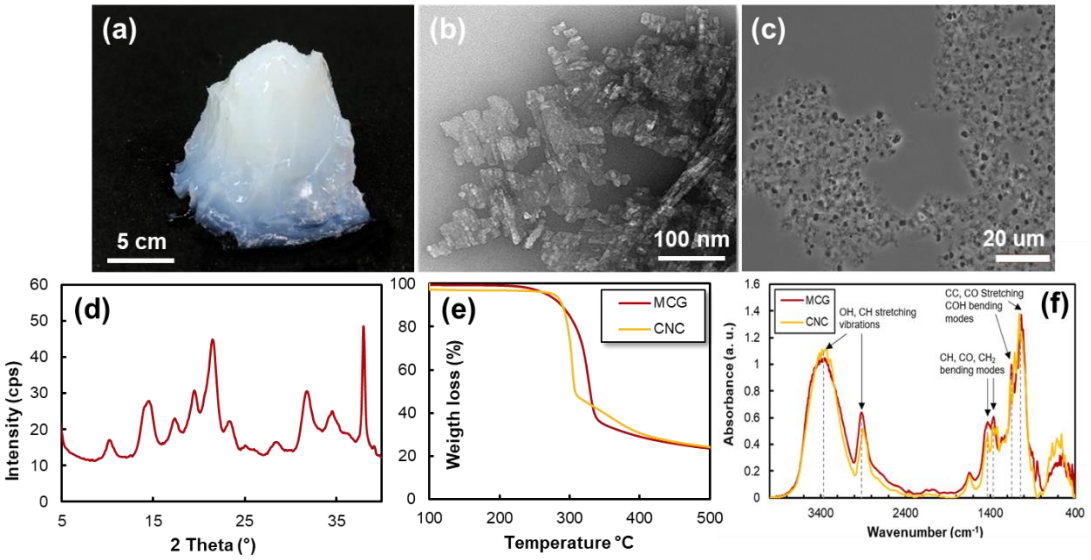

Figure 3.1. (a) Image of MCG colloid (7% solid content); (b) SEM images of MCG particles, (c) optical micrograph images of MCG, (d) XRD patterns of the MCG, (e) TGA comparison of MCG and CNCs: (f) FTIR spectra of the MCG and CNC.

3.3.2. THF Swelling and Crosslink Density

The crosslink density plays a major role in the mechanical properties of rubber-based composites and is typically determined by monitoring the swelling of the rubber in suitable solvents, such as toluene and tetrahydrofuran. In the swelling method, solvent molecules penetrate through the polymer chains, causing changes in the dimension and weight of the rubber composite. Higher crosslinking levels in the films prevent solvent molecules from diffusing through the material, resulting in a lower swelling ratio as opposed to lower crosslinking levels. In this work, the swelling ratio of dipped and casted composite films were evaluated, and the degree of crosslinking was calculated using the Flory-Rehner equation (Equations 1-3), and results are presented in **Figure 3.2(a-b)**.

The majority of the THF uptake occurred during the first 2 h of the test, followed by a reduction in the sorption rate until reaching the swelling equilibrium. In general, composite films containing fillers have a lower degree of swelling compared to the unfilled NR films in both the casting and dipping methods. The crosslinking bonds, along with nanofiller network, obstruct the diffusion of solvent molecules, resulting in a substantial decrease in solvent absorption. Sinclair et al. 2019 have reported the same trend in solvent uptake by adding cellulose nanofibers (CNF) in styrene-butadiene rubber nanocomposite, which aligns with the MCG rubber composite film results. The incorporation of CNFs reduces the absorbency, as well as the rate of absorption since the nanofiller particles act as a barrier against the solvent molecules and hinder solvent penetration through the nanocomposite while also restricting the rubber chain movement. A notable reduction in solvent uptake occurred at a higher degree of CNFs, associated with the formation of filler-filler networks [242].

Similar enhancement in MCG-NR composite films' crosslinking density that increases with increasing MCG levels was noted in this study as shown in **Figures 3.2(c-d)**. As expected, the filler in the composite led to a higher crosslink density in the composite. However, at 10 phr MCG content, a reduction was observed, which can be attributed to the beginning of agglomerated filler network formations. The observed results are in line with previous findings, where the NR latex films filled with carrageenan exhibited higher crosslink density measurement compared to the unfilled NR latex films [243]. The high tendency of carrageenan for having physical entanglement with NR latex could hinder the chain mobility, which led to a decrease in solvent diffusion and an apparent increase in the crosslinking density.

Additionally, Maslowski et al. 2019 suggested that strong filler-polymer interactions in natural rubber composites filled with crop residues could be reasons for an increase in the crosslink density of rubber.

Comparing the dipping and casting film fabrication processes, the resulting casted films exhibit an overall lower solvent swelling index and consequently higher crosslinking density. This was likely attributed to the time variation during the NR curing process in the film fabrication step. In the case of the casting process, the NR and NR-MCG films were first dried at ambient temperature for up to 48 h prior to the high-temperature curing as opposed to the dipped films, which were cured right after the dipping process without the need for the drying process step. As such, the casted film formulations spent a longer time with the activators and the curing agent sulfur to generate a comparatively higher degree of crosslinking.

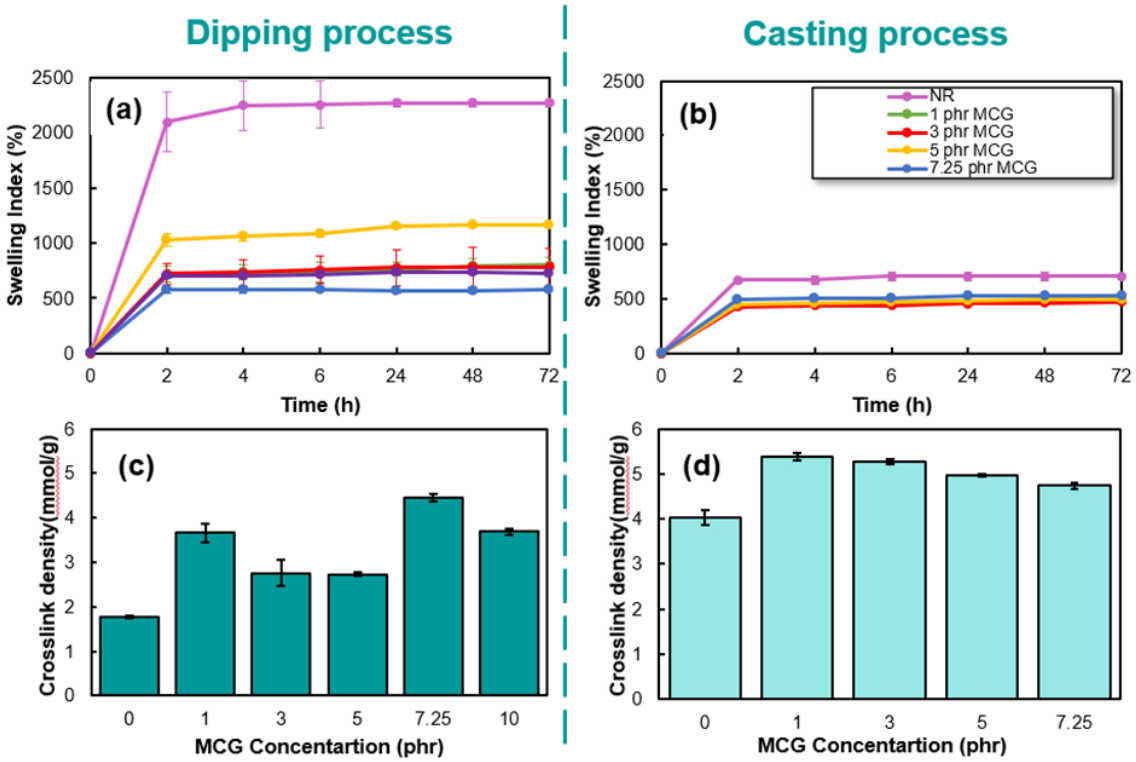

Figure 3.2. Equilibrium swelling in THF of NR and NR-MCG composites for: (a) films prepared by dipping method, (b) films prepared by casting method. Crosslink density of NR and NR-MCG camposites for: (c) films prepared by dipping method, (d) films prepared by casting method.

3.3.3. Morphology Analysis

SEM was used to evaluate the degree of dispersion of MCG in the NR latex composite as shown in **Figure 3.3**. The images were generated from the cross-section of the films where a cryogenic fracture was applied for preparing the specimens. The bright white particles, pointed by the arrows in the pure NR films, are identified as ZnO (emitting high energy electrons, as confirmed by energy-dispersive x-ray spectroscopy (EDX) analysis, **Figure 3.4**

and **Figure 3.5**. It was apparent that the incorporation of the MCG as a filler aided in dispersing the ZnO particles homogeneously, which may contribute to the higher crosslink density of the rubber composite films as opposed to the unfilled NR films.

These results agree with the findings from the CNC-NR nanocomposite study, which were reported in other studies [14,244]. By mapping the Zn particles, Blanchard et al. found that adding CNC, the amount of ZnO agglomerates decreased and eventually disappeared at a higher loading of the CNC. Also, the potential Zn-cellulose network formation may improve the dispersion of Zn throughout the films [14]. Since the MCG particles were not distinguishable under the SEM analysis, EDX was employed to analyze the dispersion of oxygen associated with MCG by capitalizing on the high oxygen content of MCG. It is important to highlight here that the observed oxygen can be associated with the ZnO as well. Since Zn mapping was also employed, the location of ZnO was already known; thus, it was possible to stipulate the distribution of the MCG based on the EDX – oxygen mapping. As illustrated in **Figure 3.4** and **Figure 3.5**, the EDX analysis revealed that the MCG and sulfur have uniform dispersion throughout the composite films in both the dipping and casting methods indicating the good dispersion of the colloidal MCG in the rubber latex as well as in the subsequent films. However, no distinction between the dipping and casting processes on the dispersion of MCGs in the composite films were made based on the SEM and EDX studies.

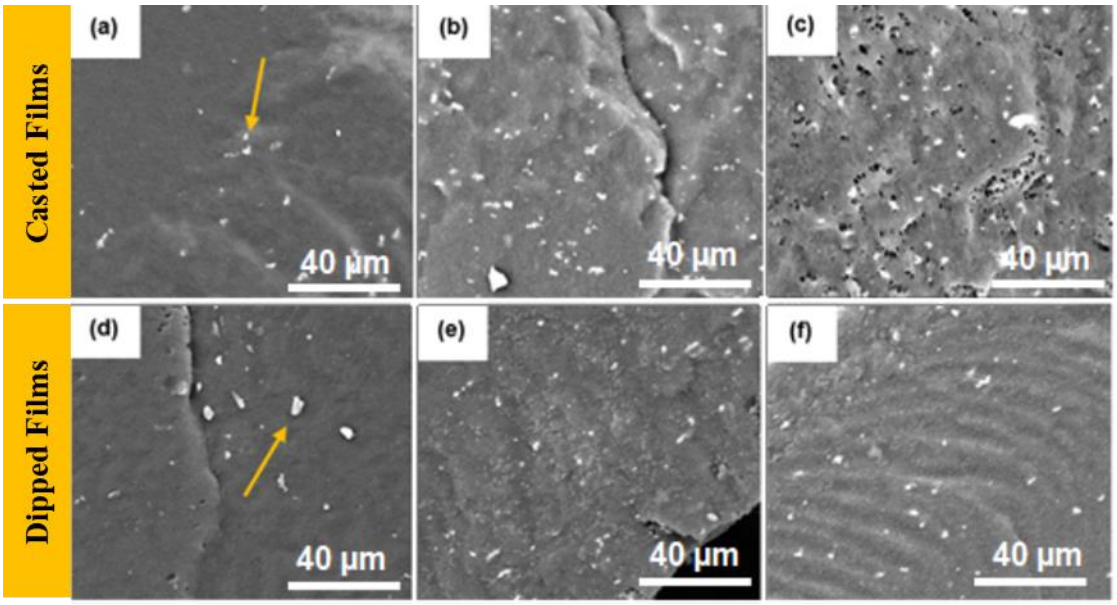

Figure 3.3. SEM images for films prepared by casting method containing: (a) 0 phr MCG, (b) 5 phr MCG (c) 7.25 phr MCG, films prepared by dipping method containing: (d) 0 phr MCG, (e) 5 phr MCG, (f) 7.25 phr MCG.

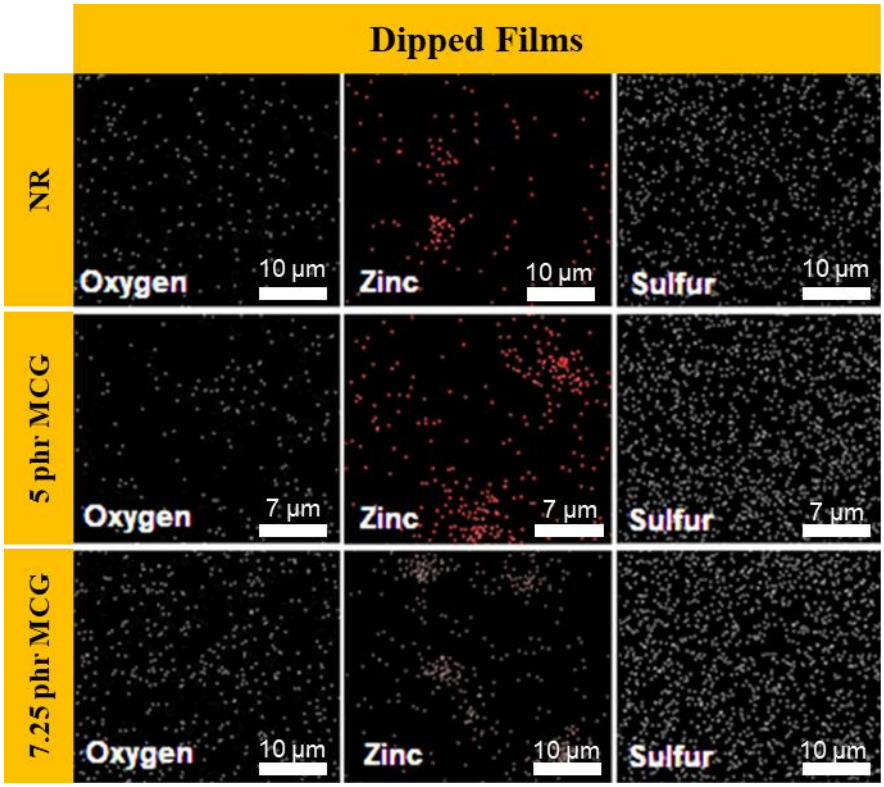

Figure 3.4. Dipped films EDX mapping of cured NR and NR-MCG composites for oxygen, zinc, and sulfur.

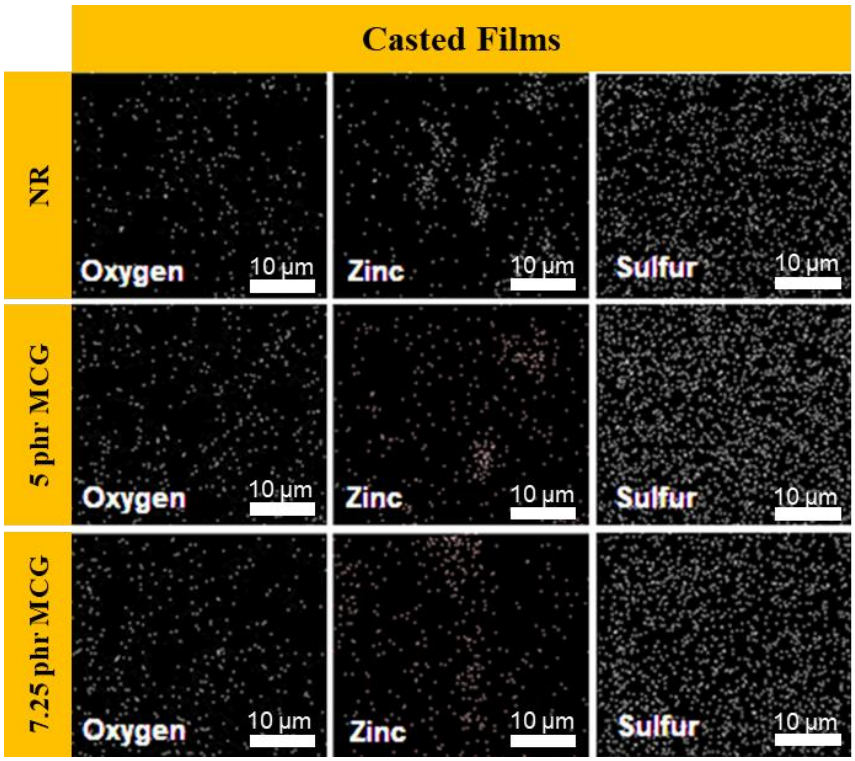

Figure 3.5. Casted films EDX mapping of cured NR and NR-MCG composites for oxygen, zinc, and sulfur.

3.3.4. Tensile Testing

The mechanical properties of the films were evaluated to study the effect of the MCG as a reinforcing filler of rubber films. Typical stress-strain curves, tensile strength, elongation at break, modulus of elasticity, toughness calculated from the area of the stress-strain curves for the dipped and casted films are presented in **Figure 3.6** and **Figure 3.7**, respectively. A notable reinforcing effect of the MCG on the rubber films was noted from the substantial improvement in the tensile strength of both the dipped and casted film formulations, as noted from **Figure 3.6(a-b)** and **Figure 3.7(a-b)**. The maximum improvement was noted at 7.25 phr

and 5 phr MCG loadings in the dipped and casted films, respectively. It was evident that there was a maximum tensile strength of the films, as the strength decreases beyond a certain MCG concentration. This reduction in the tensile strength occurred at 7.25 and 10 phr MCG for the casting and dipping processes, respectively, which was in line with the general colloidal behavior of particles at a higher loading agglomeration emerges that results in poor polymer – filler interaction and thus a decrease in tensile strength.

The concentration of MCG at which the tensile strength started to decrease was higher for the dipping method because the dipping method does not require a drying method as in the casting method. The long drying employed in the casted films provides the particles ample time to interact with each other and form aggregated and agglomerated structures, which led to the observed tensile strength reduction at a relatively lower MCG loading as compared to the dipping method. The excellent colloidal dispersion of MCG that allowed efficient stress transfer from the elastomer to the filler in conjuncture with the high crystallinity mediated stiffness of MCG led to the observed enhancement in the tensile strength and modulus of the composite films [245]. Furthermore, the higher crosslinking of the MCG-filled NR films compared to the unfilled NR could also have contributed to the higher resistance vs rupture. The most significant improvement in tensile strength was observed with the addition of 1 phr MCG, where the strength was improved by 178% and 145% for dipping and casting methods, respectively. A similar improvement in tensile strength of NR was obtained after increasing the concentration of CNCs up to 5 phr (Blanchard et al., 2020).

As expected, the elongation at break gradually reduced with the addition of MCG, which was due to the incorporation of the rigid filler in the matrix that reduce the mobility of

the rubber chains. Additionally, crosslinking bonds between the chain segments prevent untangling of some chains, consequently decreasing the elongation at break. The same results were shown by incorporating sago starch in the natural rubber matrix, where the introduction of a more crystalline region from the sago starch made the films more vulnerable under applied force and thereby failed at a lower elongation percentage [246]. CNCs also caused a similar reduction in the elasticity of a range of elastomers, such as styrene-butadiene rubber [247], polychloroprene [248,249], nitrile rubber [244], and natural rubber [250].

A progressive enhancement of elastic modulus at 50% and 100% elongation can be observed with increasing MCG concentration in both dipped and casted films (**Figure 3.6(c)** and **Figure 3.7(c)**). The addition of the rigid filler, as well as the enhancement in the crosslinking density, are the two main factors that promoted the increase in the elastic modulus of the composite films. This is because incorporating a rigid filler within the NR matrix may hinder the chain mobility, which leads to the observed higher resistance against deformation when an external force is applied on the films, as also noted from the increasing slope of the stress-strain curves (**Figure 3.6(a)** and **Figure 3.7(a)**).

The toughness of the films, which represents the films' absorbed energy up to the point of rupture, increased until a certain point with the addition of the MCG additive. It is noteworthy to mention that a dramatic increase in toughness was observed in both the casting and dipping methods. This is attributed to the high tensile strength and modulus with a slight loss in elongation at break. The toughness was evaluated by integrating the stress-strain curve (**Figure 3.6(e)** and **Figure 3.7(e)**). The higher energy required to rupture the films is attributed

to the presence of the MCG making an effective network and crosslinking bonds with the rubber matrix. At a higher loading of the MCG, the tensile strength increased while elongation reduced, which leads to a drop in toughness. The higher crosslinking obtained with MCG fillers could also play an important role in the observed increase in toughness. These results align well with results by Khalid et al. for the radiated natural rubber/carbon nanotubes composite [251]. The authors found that radiation aided in promoting the degree of crosslinking, which provides an improvement in toughness, and with further radiation applied, a remarkable decline was reported for toughness.

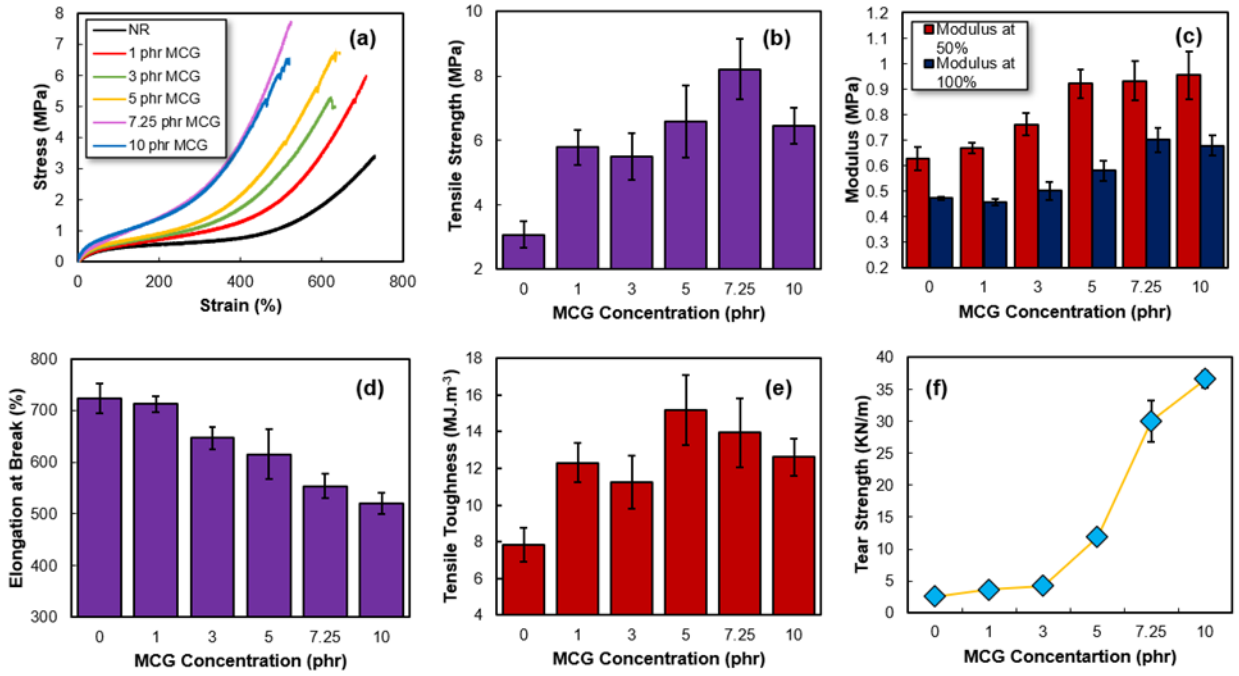

Figure 3.6. Tensile and tear properties of dipped films (a) typical stress-strain curve; (b) tensile strength; (c) modulus at 50% and 100 % elongation; (d) Elongation at break; (e) Tensile toughness; (f) Die T tear strength.

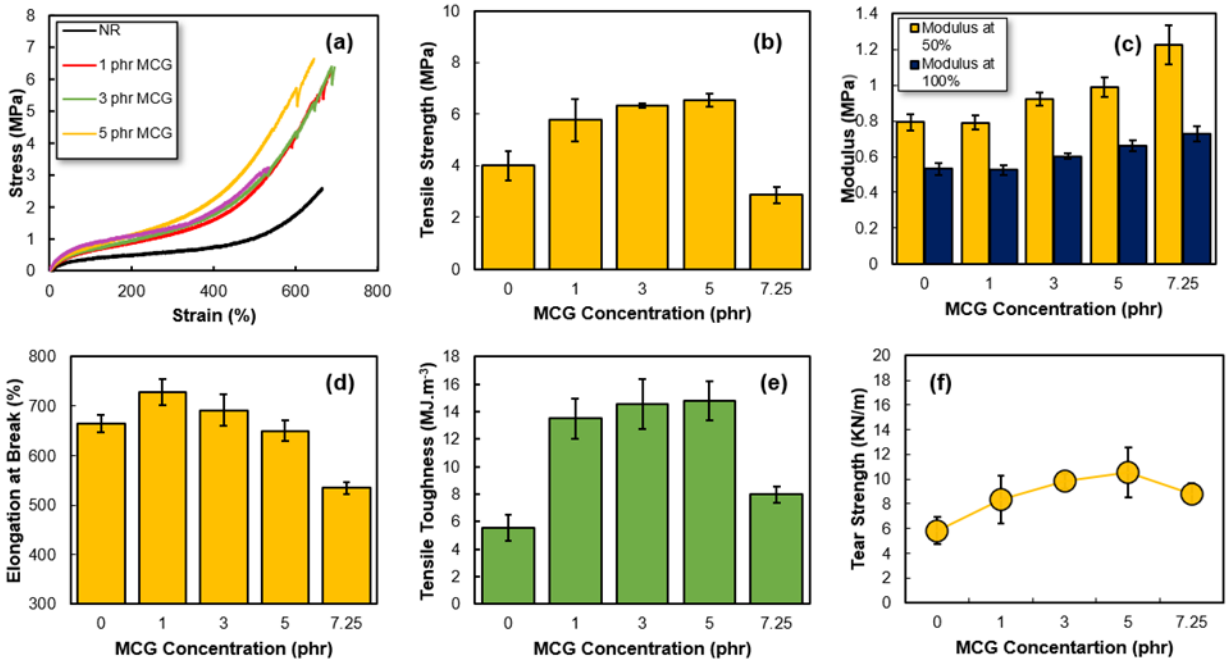

Figure 3.7. Tensile and tear properties of casted films (a) typical stress-strain curve; (b) tensile strength; (c) modulus at 50% and 100 % elongation; (d) Elongation at break; (e) Tensile toughness; (f) Die T tear strength.

3.3.5. Tear Propagation

For commercial applications of NR latex composite systems tear resistance is a critical performance dimension and significant quality control requirements are typically in place to ensure product performance in this area to ensure reliable performance the derived safety and performance of the products. High tear resistance is needed in dipped goods materials, including gloves, condoms, and balloons. The effect of the MCG on the propagation of cracks through the length of the composite films was investigated using trouser cut specimens, commonly called Die T test. The MCG particles provided a direct improvement in preventing tear propagation, as depicted in **Figure 3.6(f)** and **Figure**

3.7(f) for both the dipping and casting process generated films. A noticeable 10-fold improvement at 10 phr MCG concentration was observed for the dipped films. This attractive performance improvement was likely due to the excellent dispersion of the MCG within the NR matrix and the underlying stiffness of the highly crystalline MCG with the unique platelet-type particle morphology. At a lower concentration of the MCG (e.g. 1 phr MCG loading), minimal improvement in tear resistance was observed as the films were easily torn in the areas where there was not sufficient MCG incorporation. Moreover, a jump in the tear strength as MCG additive levels increase from 3 to 5, and continuously to 7.25 phr, confirm the possibility of filler percolation network formation in the films that can lead to a tortuous path for the tear to propagate. The same trend was displayed in other rubber films [14,247,249]. These tear results indicate the promising attribute of using MCG in the NR films.

For example, the tear resistance for commercially available nitrile gloves is typically 14.9 kN/m [252]. In contrast, the dipped rubber films in this research shows a tear strength of 2.5 kN/m for the baseline, unfilled NR system, while the NR-film composite containing the MCG filler shows 36 kN/m, respectively indicating that the MCG has remarkably elevated the tear resistance of the model film system.

3.3.6. Thermo-Mechanical and Thermal Properties of the Films

Tan delta (tan δ), damping factor curves, presented in **Figure 3.8(a)**, were obtained from dynamic mechanical analysis (DMA) on the pure NR and NR/MCG reinforced films, which were prepared by the dipping method. The temperature point where tan δ peaks are observed

represents the glass transition temperature (Tg) associated with the onset of long-range segmental mobility. Factors that affect the segmental mobility, such as chain stiffness and available free volume for segmental motion, directly impact the Tg. It is obvious from the graph that there was a reverse relationship between the MCG loading levels and the height of the tan delta peak. An increase in the MCG loading led to a decrease in tan δ intensities which is mainly attributed to restricting the segmental mobility of NR polymer chains around the incorporated fillers caused by strong rubber-filler interfacial interaction[253,254]. Additionally, decreasing the concentration of matrix, which is capable of relaxation, with the addition of the filler can be count as another plausible evidence for a reduction in the intensity of tan delta[255,256]. Furthermore, the lower quantity of tan delta intensities in the NR/MCG films indicating a reduction in the elasticity of the films as a result of the generation of less deformable films from the greater crosslinking density and reinforcement by the MCG in agreement with Das et al. [257]. However, the Tg remained unchanged at approximately -58°C, despite the change in the MCG loading. Similar results of unchanged Tg in nanocomposites were reported for the NR containing nano-calcium carbonate ($CaCO_3$) [258]. The NR and MCG systems do not have any specific interactions, such as polar-polar or ionic, along the NR chains and MCG. Therefore, the Tg of the composite remained unchanged.

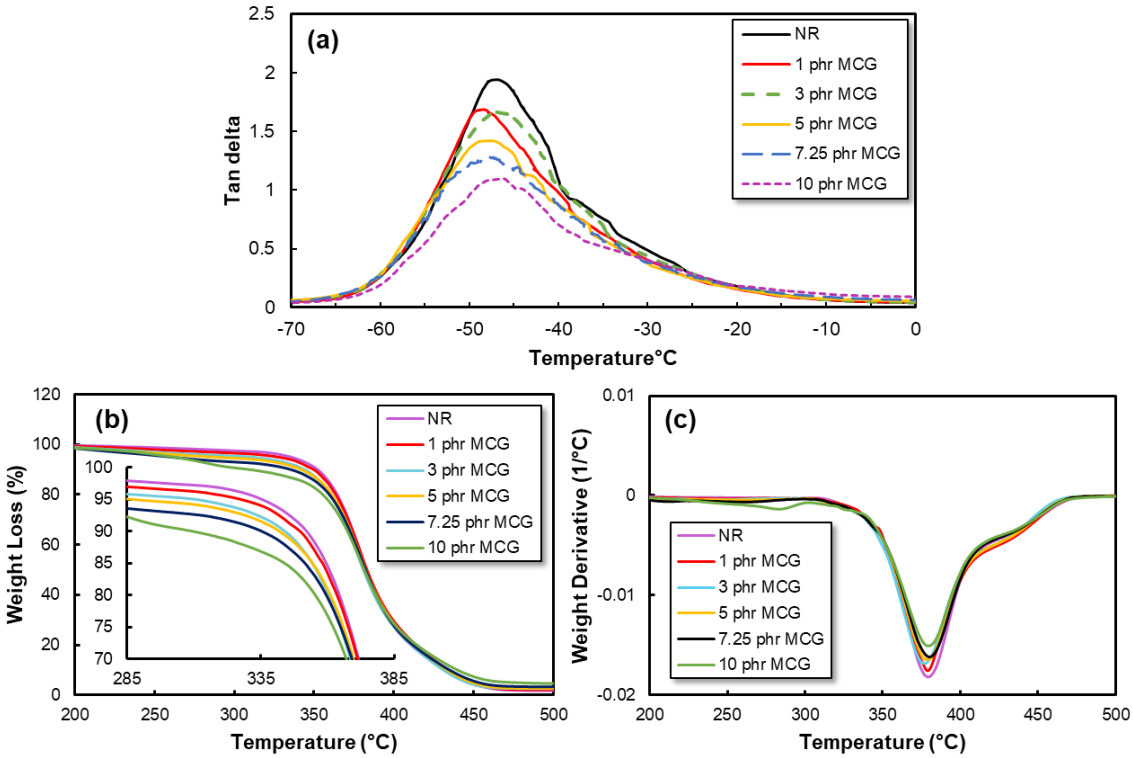

Figure 3.8. Dynamic mechanical analysis: (a) tan delta, Thermogravimetric analysis: (b) Weight loss and (c) derivative weight loss curves of NR and NR-MCG composites.

The thermal degradation behavior of the films was investigated using TGA and the progress of degradation is illustrated in **Figure 3.8(b-c)**. As a result of chain cleavage, as well as scission of the crosslinking bonds, the degradation of the rubber polymers occurred, and the main decomposition happened in the range of 280°C to 450°C. The onset temperature of the degradation process of the films containing MCG gradually decreased as the MCG loading increased. Also, other peaks around 280°C were observed from the derivative curve likely attributed to the thermal degradation of the MCG. Blanchard et al. reported a similar trend for natural rubber composite reinforced by cellulose nanocrystals [14]. The lower thermal stability in the presence of MCG has been observed due to the effect of early degradation of MCG. The

same outcomes by incorporating nanocellulose were shown by Abraham et al., as maintaining the same thermal stability as natural rubber was only possible at the lowest percentage of nanocellulose. Also, with the further addition of cellulose, a similar thermal stability decrease was noted [259].

3.3.7. Water Absorption

The water uptake of composite films after immersing in distilled water was investigated, as depicted in **Figure 3.9(c)**. Over the first 8 h, the composites with 5 and 7.25 phr MCG, along with NR had the highest water uptake values. In contrast, during the long-term testing period, an increase of the MCG content in the NR composite displayed an opposite trend by declining the water uptake rate. The higher water absorption of the MCG-filled films may be due to the general hydrophilic nature of a polysaccharide based filler system such as the MCG, which may inherently associate with moisture via hydrogen bonding [260]. The decrease in the rate of water absorption with the increase in the MCG additive content was noted in the longer-term (seven days) studies. This observation may be rationalized by MCG embedded in the NR matrix reducing the effective extend of free volume in the NR matrix, especially at these higher concentrations, which may lead to less free volume available for the retention of water molecules, which in turn reduces the overall water uptake. These results are consistent with the previous study of acrylonitrile-butadiene rubber (NBR) films using a nanocellulose filler by Ogunsona et al. [244]. This study reported that changes in the micro-voids and the increase in the crosslinking density of the rubber chains was responsible for reducing water uptake. Upon the addition of nanocellulose, the available micro-voids for water molecules diminished,

which induced a denser material and made it difficult for water to diffuse. Moreover, the crosslinking network restricted the swelling degree of the rubber films[244].

3.3.8. Permeability Testing

3.3.8.1. Water Vapor Permeability (WVP)

The water barrier performance of the prepared composite films was investigated under a constant relative humidity environment, and results are presented in **Figure 3.9(a-b)**. The water vapor transmission rate values are directly proportional to the difference in relative humidity, and the behavior can be explained with Fick's law[261,262]. As seen from the weight difference graphs at different time intervals (**Figure 3.9(a)**), the water permeation increased with the MCG loading up to 7.25 phr, followed by a decline at 10 phr MCG. Since higher MCG loading creates a tortuous path for penetration, the continuous permeation route formed by the percolated MCG network is the proposed mechanism for increasing the WVP that was observed in **Figure 3.9(b)**. At high MCG loading levels (10 phr and above), the platelet MCG morphology fills free volume along with a higher degree of crosslinking, creating a more complex route for diffusion, leading to the observed drop in the WVP at 10 phr MCG. Bras et al. reported a similar trend upon the addition of cellulose whiskers in natural rubber [263]. In this study, a greater WVP was noted because of the cellulose whiskers' high hydrophilic nature. However, the formation of the cellulose network via hydrogen bonding led to a decrease in WVP. The relatively high-water permeation of the NR-MCG composites as opposed to the unfilled NR is appealing for glove applications, as it can prevent the buildup of sweat inside the gloves by allowing the moisture to diffuse out.

3.3.8.2. Solvent Vapor Permeability (SVP)

Barrier performance against solvent is of a high priority for glove applications since the gloves should be able to protect hands from solvents. To test the barrier behavior of NR-MCG composite films, ethanol was selected as the solvent material. Although ethanol is a volatile solvent and travels much faster through the films than water, the results showed that the solvent permeability decreased when the MCG content increased, as highlighted in **Figure 3.9(d)**.This finding is well supported by the fact that the MCG forms a network of hydrophilic fillers in conjuncture with the increase in the crosslinking density that caused the observed difficulties for solvent molecules to diffuse through the films [14]. The ethanol barrier property was enhanced with the increase in the MCG loading and consequently, the crosslink density. Likewise, the incorporation of silicate nanomaterials in NBR resulted in an improved solvent barrier when a good filler-rubber interaction is achieved [12]. Generally, obtaining an enhancement in the barrier properties against ethanol indicates that the MCG reinforced NR films can be of great importance in practical applications, such as gloves.

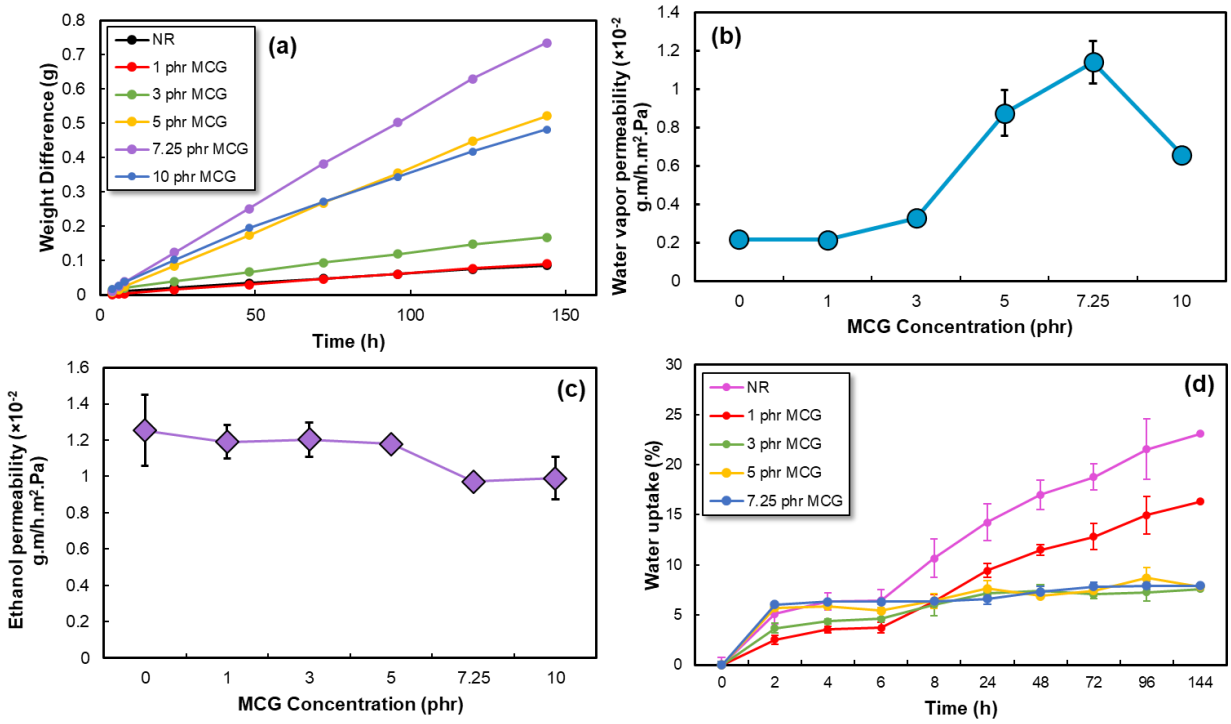

Figure 3.9. (a) Vapor permeation loss of water through NR and NR-MCG nanocomposites, (b) water vapor permeability and (c) ethanol permeability, (d) water absorption of NR and NR-MCG nanocomposites.

3.4. Concluding Remarks

The colloidal microcrystalline glucan (MCG) obtained from enzymatic polymerization has a controlled, and specific plate-like morphology, with high surface area, high crystallinity, low density compared with mineral fillers, and good thermal stability. This colloidal MCG system displayed good dispersibility in rubber latex composite films prepared by both dipping and casting processes. The physico-mechanical characterization indicates a noteworthy enhancement in mechanical properties, such as tensile strength, modulus of elasticity, and tear strength. The improvement in mechanical properties was achieved due to the good dispersion

of the MCGs in the rubber latex and eventually in the cured matrices. Also, the formation of the tortuous path by percolated MCG promoted the barrier properties, as well as tear strength of the composite films. Overall, the incorporation of MCGs brought about appealing rubber film properties that are desired for a range of lightly-crosslinked dipped goods, including gloves and condoms. The rubber composite films produced using the MCG filler system emerges as a promising candidate to provide performance enhancements for a NR-based composite as required for typical commercial applications. At the same time, the increasing interest in an overall more sustainable material solution that reduces the overall green house gas impact by using composites with overall renewable content. In addition, pending the extent of crosslinking, the overall composite will likely also show biodegradability performance to avoid the formation of persistent micro-plastic entering the environment through uncontrolled disposal.

Chapter 4. Sustainable barrier paper coating based on alpha-1,3 glucan and natural rubber latex[3]

4.1. Introduction

Many traditional polymers originating from fossil resources are in discussion regarding their potential for severe environmental pollution concerns associated with the production and disposal, especially as regulations are driving towards greenhouse gas avoidance metrics. Nearly all plastic packaging that has been produced is sourced from petroleum feedstock and disposed of after a short period of use which about five million tonnes of plastic waste per year accumulating in oceans and landfills [264,265]. Furthermore, the natural limitation of petroleum resources in some geographies and depletion concerns in others, and the implications of some polymers, especially in packaging, coating, and biomedical uses [266], constitute additional concerns. To mitigate these challenges, efforts are directed towards shifting the production of polymers from petrochemical feedstock to renewable resources (e.g., making plastics from plants), as well as the development of biodegradable polymers [267]. Therefore, developing sustainable, ideally also biodegradable, and safe material alternatives as new packaging materials provoked widespread attention to mitigate the outlined challenges of conventional packaging materials [268].

Paper is extensively used in the food packaging industry in various forms [269]. However, the direct use of paper for food packaging applications is limited due to the inferior

[3] A version of this chapter has been published on peer-reviewed journal as a review article: **A. Adibi**, D. Valdesueiro, J. Mok, N. Behabtu, C. Lenges, L. Simon and T. H. Mekonnen. (2022) Sustainable barrier paper coating based on alpha-1,3 glucan and natural rubber latex, *Carbohydrate Polymers.*, 2022, **282**, 119121. https://doi.org/10.1016/j.carbpol.2022.119121.

mechanical properties (e.g., wet tensile strength and tear strength) and insufficient barrier properties against water, oil, and oxygen. A promising technique to alleviate the inherent limitation of paper substrates and enhance critical properties of this packing alternative is the application of surface coatings, for example, water-based coatings which can be applied at high speed and can be led to the use of biopolymers [270].

Fillers are used in water borne barrier coatings, are inexpensive inorganic materials, such as kaolin, calcium carbonate [271]. Moreover, due to the morphology and high aspect ratio of inorganic fillers, they can provide great barrier properties by introducing further tortuosity [272,273]. Inorganic fillers can also be incorporated in the paper substrate during the fabrication process to fill voids with a net effect of smooth surface and enhanced barrier properties [274]. The drawbacks associated with incorporating inorganic fillers in paper coating includes inferior compatibility and adhesion, making the use of adhesive and compatibilizer essential [275,276]. Mineral fillers also causes embrittlement, potential for pinholes, and generation of defects-[277]. With regard to the biodegradability of coatings, the use of bio-based organic fillers, such as polysaccharides instead of inorganic fillers is considered more advantageous [271].

Natural rubber (NR) is a natural biopolymer harvested from *Hevea brasiliensis* plant as a milky colloidal suspension and typically provided as a water-based latex [263]. With the typical cis-1,4-polyisoprene chemical structure of the polymer (**Scheme 4.1**), NR is reactive and a natural-sourced hydrocarbon polymer which has found a wide range of industrial applications, usually through extensive formulation and processing with typical applications

in floor mats, hoses, belts, gloves, ropes, and most widely in vehicle tires, etc. [278]. Since NR latex displays biological mineralization, it can be regarded as renewable, sustainable, and inherently biodegradable polymer if further crosslinking and formulation is avoided or significantly limited. Products made from uncured NR exhibit good biodegradation in several environments [279]. The environmental benefits, its stable aqueous latex form, and its hydrophobicity that may provide good moisture barrier properties may enable NR-based formulations to provide appealing properties for paper coating applications [30,31]. Despite its moisture barrier properties, utilizing NR as a paper coating is not common due to its low tensile strength and typically insufficient barrier performance vs. for example, oxygen and grease/oil.

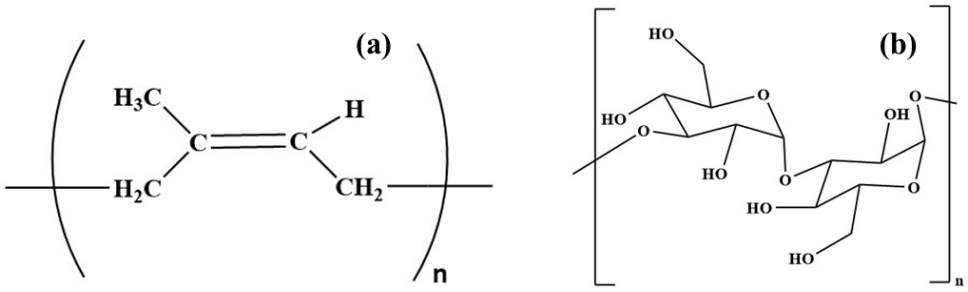

Scheme 4.1. Structure of a) natural rubber, b) alpha-1,3-glucan.

Polysaccharides are renewably sourced materials (e.g., cellulose or starch) comprised of monosaccharides linked by glycosidic bonds with three hydroxyl moieties on each repeating anhydroglucose unit. Due to their hydroxyl groups, polysaccharides can form strong hydrogen bond networks for example, within the cellulose in paper when used in paper coating formulations[275]. Additionally, polysaccharides are generally biocompatible, biodegradable, and non-toxic, making them appealing materials for food contact applications, such as paper coating. However, polysaccharides are also hydrophilic and display a high water absorption rate and poor moisture barrier properties [177,280]. Thus, it is not feasible to use widely

commercially available polysaccharides (e.g., starch) as a sole component for high-performance paper coating formulations

In recent years, IFF (formerly DuPont Nutrition and Biosciences) has developed a biocatalysis process to enable access to tailored polysaccharides, for example, alpha-1,3-glucan (Scheme 1), from enzymatic polymerization of glucose from sucrose with controlled morphology and structure [38,49]. The alpha-1,3-glucan has high purity, is a water-insoluble, linear, high-Tg polymer with high crystallinity (crystallinity index up to 0.70), and exhibits stable colloidal stability in its never-dried form [44,281]. Through the engineered polymerization processes, tailored morphologies are accessible, including spherical aggregates (wet cake), fibrids, and platelet-type particle structures (microcrystalline glucan, MCG) (Kedzior et al., 2021). The alpha-1,3 glucan in wet-cake form shows spherical particle morphology and a particle size between 5-10 μm in its aggregated form and is utilized as a functional filler within an NR-latex system in this work.

This study aims to investigate the barrier performance of the combination of alpha-1,3 glucan and NR latex in paper coating applications. It is hypothesized that the mutual aqueous colloidal dispersion of alpha-1,3 glucan and NR latex forms a stable latex system that can be applied to provide a consistent and functional barrier coating on cellulosic paper substrates. The effect of various composition ranges on the film-forming properties and barrier performance versus water vapor, oil, and oxygen are studied. Analytical techniques such as tensile testing, water vapor permeability testing, Cobb testing, and Kit testing were utilized to determine the properties of the prepared paper coatings.

4.2. Materials and Methods

4.2.1. Materials

The alpha-1,3 glucan colloid (40 wt.% solids, 60 wt.% water) of alpha-1,3 glucan, made from enzymatic polymerization of glucose from sucrose, with surface area of 9.7 m^2/g was provided by International Flavors & Fragrances Inc.(IFF). Stabilized natural rubber (NR) latex (60 wt.%. solids, 40 wt.% water) was purchased from Chemionics Corporation, OH, USA. Toluene, n-heptane, and castor oil were purchased from Sigma Aldrich. Polyvinyl alcohol (PVOH) with a molecular weight of 72,000 g/mol was obtained from MP biomedicals and heptane was supplied by OmniSolv. Manila papers, which are made from semi-bleached wood fibers with a thickness and grammage of 0.24 mm and 204 g/m^2, respectively is sourced from a local stationery store (Waterloo, ON, Canada) were used as the paper substrate.

4.2.2. Characterization of alpha-1,3 glucan

To observe the morphology of alpha-1,3 glucan particles, 10 μL of dispersed polysaccharides (10 wt.%) were spun at 6,000 rpm at room temperature. A Dimension Icon® scanning probe Atomic Force Microscopy (AFM) (Bruker, Santa Barbara, USA) was then employed to collect images. Alpha-1,3 glucan dispersions (5 wt.%, 7.5 wt.% and 10 wt.%) were prepared by dispersing the wet cake in deionized water using a kitchen blender for 10 min. A Brookfield digital viscometer was then used to measure the viscosity. The particle size of dispersed alpha-1,3 glucan particles in water was also measured using Malvern Zetasizer (Westborough, MA). For this, the dispersion was diluted to a concentration of 0.1 wt.% in deionized water and three measurements were conducted.

4.2.3. Coating Fabrication

The coating formulations consist of NR, wet cake of alpha-1,3 glucan, and water while maintaining a constant total solids content of 10 wt.% for all formulations. The fabrication procedure was initiated by pre-dispersing the alpha-1,3 glucan wet cake in water with a kitchen-type blender at high speed (10x) until achieving a viscous dispersion (~ 2,600 mPa.s, 15 wt.%). The alpha-1,3 glucan dispersion prepared as such was then mixed with a calculated quantity of NR latex and distilled water to obtain the required formulations. In the formulations, the concentration of alpha-1,3 glucan in the coating film formulations was varied between 0 (control) and 100 parts per hundred rubber (phr) alpha-1,3 glucan (wet cake) as shown in **Table 4.1** while maintaining the total solid at 10 wt.% by adding water. The formulations were then mixed on a stir plate at 500 rpm for 10 min followed by homogenization (25,000 rpm x 3 min) to obtain a uniform dispersion. Finally, the coatings were applied on Manila paper substrates utilizing a Doctor blade with a gap of 200 μm (wet thickness) to obtain 20 μm dry thickness. It is important to highlight that the 20 μm coating thickness is a calculated value and a slight variation from 20 μm is expected to due to the penetration of the wet coating into the paper structure. The coated papers were then allowed to dry at room temperature for 24 h prior to testing. For 100 μm thickness coating, five coating layers, each with 20 μm dry thickness. Each layer was allowed to dry for 24 h before the next layer was applied.

Table 4.1. Composition and nomenclature of coating film formulation.

Sample labels	Parts per hundred (phr) of NR, dry basis	Parts per hundred (phr) of wet cake (wc), alpha-1,3 glucan dry basis	Wt.% of alpha-1,3 glucan	Sample designations

NR	100	0	0	NR Control
NR-10wc	100	10	9.09	NR+ 10 phr wc
NR-30wc	100	30	23.08	NR + 30 phr wc
NR-50wc	100	50	33.33	NR + 50 phr wc
NR-70wc	100	70	41.18	NR + 70 phr wc
NR-100wc	100	100	50.00	NR + 100 phr wc

4.2.4. Characterization of the Coatings

4.2.4.1. Dynamic Viscosity Measurement

The dynamic viscosity of the coating formulations was investigated by a rheometer (HAAKE MARS, Thermo scientific). The steady-state viscosity of the NR/alpha-1,3 glucan formulations was reported at shear rates ranging from 0.03-100 s^{-1}. A 35 mm stainless steel parallel plate with a plate gap of 1 mm was utilized for the tests. The test was conducted at 27 °C.

2.2.4.2. Morphology Analysis

The uniformity of the films that were applied on the paper along with the existing voids on the surface of the paper coatings were evaluated by using a scanning electron microscope (FEI Quanta FEG 250 SEM). In this test, the coated papers were cryofractured and gold coated to assess the surface and cross-sectional morphology of the specimens.

4.2.4.3. Contact Angle Measurement

Contact angle measurements of the control and coated papers surface were conducted using a custom-built system equipped with a programmable syringe pump (New Era Pump Systems Inc.) and a video camera to study the interaction of water with the formulated coatings. About 3 μL of deionized water was dropped on the surface of the coated paper and images were captured at 0, 30, and 60 s. The contact angle was then calculated using ImageJ software.

4.2.4.4. Mechanical Properties

Dry Tensile Strength: Seven specimens were cut from the coated paper samples into 70 mm x 20 mm strips. The tensile test was conducted according to ISO 1924-2/3 with a 100 mm/min strain rate, using tensile testing equipment (AGS-X, Shimadzu, Japan).

Wet Tensile Strength: To determine wet strength, seven specimens were dipped in distilled water for 30 s and 1 min in accordance with ASTM D829-97. After that, the excess amount of water on the surface of the paper coating was blotted with a paper towel, and tensile testing was carried out immediately using the same tensile testing procedure as above.

4.2.4.5. Cobb Test

Water Cobb Test: The water Cobb test was run for 2 min as stated by TAPPI T441 using five replicate specimens. About 10 cm^2 of circular samples were cut, placed on the Cobb cylinder that contained a measured quantity of water, and tightly clamped by exposing the paper coating side towards the water. The Cobb cylinder was then reversed, and the paper coating was allowed to contact the water for 2 min. Subsequently, the coated paper was

weighed after removing the excess water via gentle blotting. The weight difference before and after the test defines Cobb's value as described by equation (4.1):

$$Cobb\ value({}^{g}/_{m^2}) = (m_2 - m_1) \times {}^{10000}/_{Area(\ cm^2)} \quad (4.1)$$

where m_2 and m_1 are the weight of the sample after and before the test, respectively.

Oil Cobb Test: The oil Cobb test was employed in a manner similar to the water test to evaluate the amount of oil absorbed by the sample in 1 min. In this test, canola oil was utilized, and five measurements were carried out for each formulation in the Cobb test and the average was reported.

4.2.4.6. Water Vapor Barrier

The effect of the coating on the barrier performance of the coated paper against water vapor was evaluated according to ASTM E96. For this method, cups were partially filled with water and then sealed tightly with coated paper so that the coating was exposed to the water vapor. The change of weight of the cups was tracked for seven days. This test was carried out in triplicates for each coating formulation. The water vapor permeability (*WVP*) was then calculated by obtaining the water vapor transmission rate (*WVTR*) and utilizing the following equations:

$$WVTR = \frac{\Delta G}{t\ .\ A} \quad (4.2)$$

$$WVP = \frac{(WVTR) \times l}{\Delta p} \quad (4.3)$$

where ΔG is the weight change (g), t is time (hr), A is the cross-sectional area of the cup mouth (m^2), l is the thickness of the paper coatings, and Δp is the partial water vapor pressure difference between the two sides of the film (1 Pa).

4.2.4.7. Oxygen Barrier

Oxygen permeability (*OP*) was investigated using a custom-made bubble flowmeter. The specimens were cut in the shape of circles with a certain dimension (4.8 cm in diameter), placed in the chamber with the coating exposed to pure oxygen and the other side of the paper coating was attached to the bubble flow meter system as shown in Scheme S1. By recording the required time for the bubble to travel 20 mL through a burette, the flow rate was calculated. This test was conducted at a fixed pressure of 13.8 kPa and at different initial moisture contents of the coated paper, i.e., 30%, 60%, and 99%. In order to adjust the moisture content of the coated papers, the specimens were kept in a desiccator where the relative humidity was tracked with a digital hygrometer immediately before the *OP* test. The *OP* was measured as using Eq. (4.4):

$$OP = \left(\frac{V}{t.A}\right) \times \frac{l}{\Delta P} \tag{4.4}$$

where $V/(t.A)$ is the flux of the oxygen flow rate ($cm^3/m^2.s$), l is the thickness of the paper coatings (m), and ΔP is the oxygen gas pressure difference between the two sides of the coated paper.

4.2.4.8. Kit Test

The grease resistance of the paper coatings was analyzed by the Kit test in accordance with T559. In this test, 12 different grease solutions (**Table A1**) containing varying amounts

of castor oil, n-heptane, and toluene were prepared and applied on the coating surface. Each grease solution was then applied on at least five replicate samples where new samples were used as repeats, and the surface of the coating was examined to observe any trace of staining. The highest number of grease solutions which did not leave any dark spot on the paper coatings was reported as the Kit number. A higher Kit number presents better grease resistance of the sample. A sample that attained a Kit number of 8 was reported as grease resistant.

4.2.5. Effect of Coating Thickness on the Barrier Properties

Since paper is a porous substrate containing interconnected voids, which forms a permeable porous network, the coating thickness plays an important role in blocking the voids and bringing about barrier properties. In this study, selected paper coating formulations with three different thicknesses (5, 20, and 100 μm) were fabricated in order to study the effect of the thickness on the barrier properties of the paper coatings, using *WVP*, *OP*, the oil Cobb test, and the Kit test.

4.2.6. Comparison of Coating with Commercial Material

To obtain a better perspective of the effectiveness of the NR/alpha-1,3 glucan formulation as a viable coating, the selected formulations were compared with commercial coatings that are widely utilized in the food-packaging industry. For this, two different commercial polymer coatings, polyvinyl alcohol (PVOH) and polyethylene (PE) were selected due to the great moisture and oil barrier capability of PE, and the outstanding oxygen barrier performance of PVOH. To prepare the PVOH coating, PVOH was dissolved in distilled water (10 wt.%) at 90 °C under stirring (600 rpm), cooled, and applied on the paper substrate using

a doctor blade to obtain 20 ± 3 μm thickness. For a PE coating example, a commercial food container coated with PE (100 μm) was sourced from a restaurant chain and used for the study. The *WVP*, *OP*, oil Cobb test, and Kit test were performed on these two paper coatings for comparison with the formulated coating. The calculations were adjusted wherever required to account for the thickness variation of the PE coating with the other formulations.

4.2.7. Statistical Analysis

All tests were replicated at least three times and results were presented as mean ± standard deviation. Statistical evaluation of the data were conducted using Minitab version 19. To identify significant differences among means, single factor analysis of variance (ANOVA) was employed to the data with an LSD criteria of 95% confidence level ($P < 0.05$).

4.3. Results and Discussions

4.3.1. Alpha-1,3 Glucan Characterization

The engineered polysaccharide, alpha-1,3 glucan, can be obtained in a biocatalysis process from sucrose using a glucosyltransferase (GTF) enzyme. The enzymatic process can provide the ability to control the morphology as well as the degree of crystallinity [44]. The resultant polysaccharide is water-insoluble and has an aggregated structure. Even though this semi-crystalline polysaccharide is water-insoluble, and it has a tendency of settling due to its neutral surface charge, it can form stable colloidal dispersions in water under shear [165]. In this work, the spherical morphology of the alpha-1,3 glucan wet cake systems have been utilized for this assessment. In order to obtain a better perspective of the morphology of alpha-1,3 glucan, an AFM and SEM imaging were employed, as shown in **Figure 4.1(b - d)**. It was

observed that the primary particles may be in the range of 25-35 nm within the highly aggregated structure which are providing micrometer type systems within the dispersed water system.

By applying high shear, the aggregated structure of the alpha-1,3 glucan forms a stable colloidal dispersion in water with a typical particle a size of 0.2-1 μm, as shown in **Figure 4.1(a)**. Dispersions prepared as such were combined with NR latex to prepare the coating formulations. The increase in the concentration of the rigid alpha-1,3 glucan particles in water resulted in a higher viscosity of the suspension. At 10 wt.% concentration, a viscous colloidal dispersion (~ 2,600 mPa.s) in a similar range as that of honey or corn syrup was noted (**Figure 4.1(f)**). This indicated that the application of high shear could break the aggregated structures of the wet cake polysaccharides.

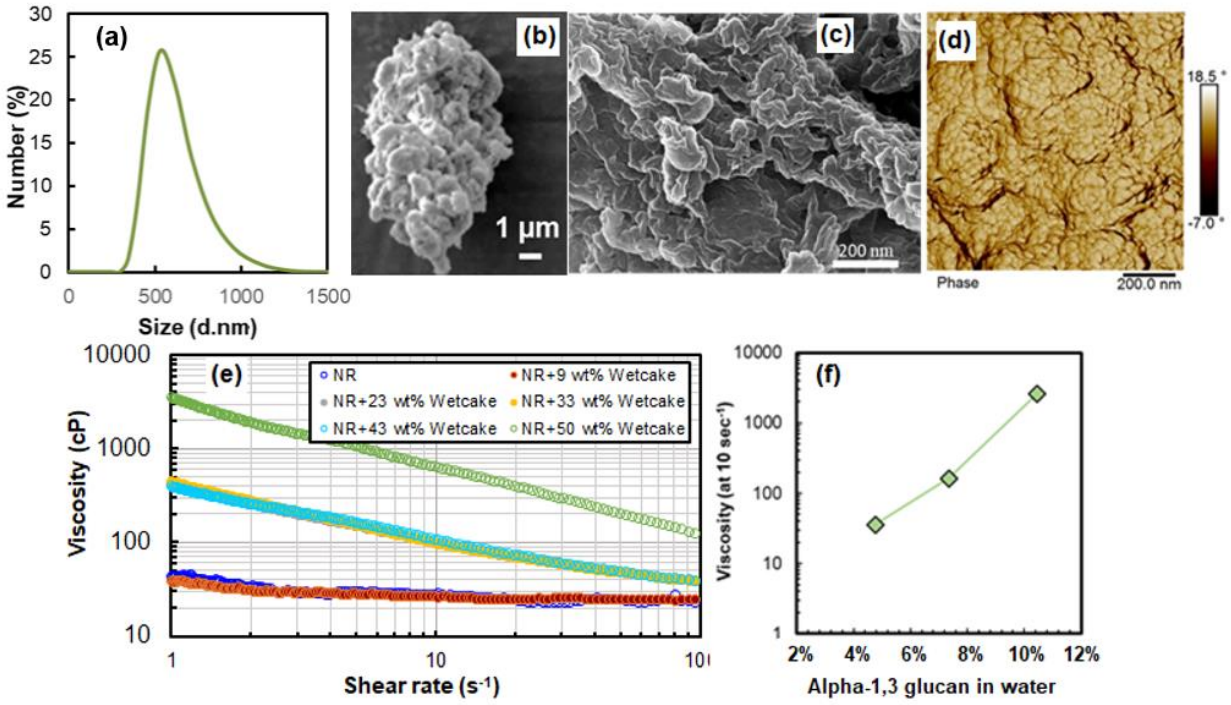

Figure 4.1. a) Particle size of dispersed alpha-1,3 glucan in water, b) SEM image of dried alpha-1,3 glucan aggregate, c) SEM image of dispersed alpha-1,3 glucan in water, d) AFM phase images of alpha-1,3 glucan particles, e) Dynamic viscosity of NR/alpha-1,3 glucan wet cake (wc) suspensions: viscosity against shear rate, f) viscosity of alpha-1,3 glucan dispersions in water at various concentrations.

4.3.2. Dynamic Viscosity

The dynamic viscosity of the coating formulation was investigated to understand the flow behavior of the coating formulations and the resulting uniformity. Moreover, the effect of alpha-1,3 glucan on the dynamic viscosity of the formulation was evaluated. In general, the rheology of suspensions, can be dependent on particle characteristics such as particle shape and size, surface charge, and dispersion microstructure (for example Liu et al., 2017). In the paper formulations prepared in this study using the NR/ alpha-1,3 glucan formulation systems unique differences are observed, the solid content of these formulations was typically 10 wt.% in this study. The changes in the dynamic viscosity with increasing shear rate are presented in **Figure 4.1(e)**. The alpha-1,3 glucan loading concentration has a positive correlation with the suspension viscosity increase due to the latex colloids mobility restrictions by the stiffer alpha-1,3 glucan particles.

It is noted that lower levels of alpha-1,3 glucan loading (up to 30 phr) did not visibly change the dynamic viscosity. Further increase of the alpha-1,3 glucan concentrations to 50 and 70 phr substantially increased the viscosity. While all coating formulations displayed shear thinning behavior, higher alpha-1,3 glucan loading formulations showed severe cases. This is

attributed to the alpha-1,3 glucan aggregate breakdown as a result of the increase in shear, which could be favorable in the process of coating fabrication [39,282]. It is likely that this behavior can also be affected by shear rate (Deborah number) and the particles can behave viscoelastic (Lapasin & Pricl, 1995).

4.3.3. Morphology of Coatings

To study the change in the morphology of the paper as a result of the employed NR/ alpha-1,3 glucan coatings, scanning electron microscope (SEM) images were collected as shown in **Figure 4.2**. The uncoated paper surface displayed voids and pores indicated with red arrows (**Figure 4.2(a)**), and uneven surface with recognizable individual fibers intertwined with each other. However, after applying the coating, the cellulose fibers of the paper can hardly be distinguished and most of the voids were covered, leading to a relatively smooth surface which is in complete agreement with previous findings [106,283]. Additionally, the SEM images of the cross-section of the uncoated paper exhibited the physical interlocking of the cellulose fibers, which results in the formation of pores throughout the paper. In **Figure 4.2(e)**, which represents the cross-section of coated paper with NR, a distinguishable interface between the paper and NR was visible. The substantial variation in the polarity of the cellulose in the paper substrate will not typically allow an intimate interaction. On the other hand, with the addition of the alpha-1,3 glucan, hardly any interface can be detected due to the great compatibility between the alpha-1,3 glucan and the fibers of the paper; this result is consistent with results obtained with other types of coatings such as better filling of pores and creating a more uniform surface of the paper coating, as reported by previous studies. Also, in **Figure**

4.2, the degree of dispersion of alpha-1,3 glucan in the NR films was evaluated. As highlighted in **Figure 4.2(j)**, it was observed that at lower concentration of alpha-1,3 glucan(10 phr), and uniform dispersion of the filler particles was obtained.

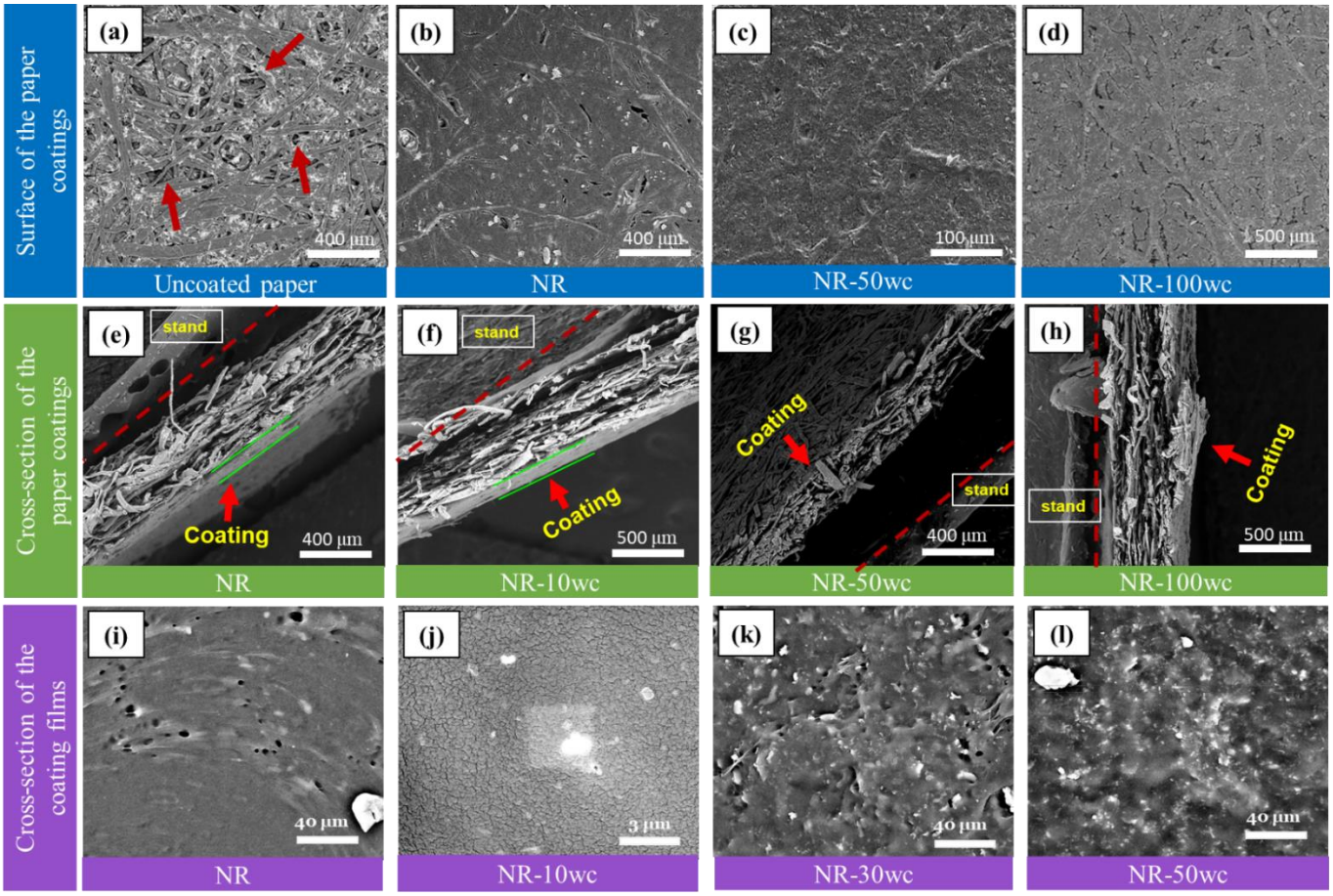

Figure 4.2. SEM images of the surface of: a) uncoated paper, b) NR coating film on the paper, c) NR+ 50 phr alpha-1,3 glucan wet cake (wc) coating film on the paper, d) NR+ 100 phr wc coating film on the paper, SEM images of cross-section of: e) NR coating film on the paper, f) NR+ 10 phr wc coating film on the paper, g) NR+ 50 phr wc coating film on the paper, h) NR+

100 phr wc coating film on the paper, i) NR film, j) NR+ 10 phr alpha-1,3 glucan film, k) NR+ 30 phr wc film, l) NR+ 50 phr wc film.

4.3.4. Contact Angle

The wettability of the surface of the coatings was assessed by measuring the contact angle with water. The variation of contact angle during a certain amount of time is shown in **Figure 4.3**. The small contact angle of the paper base can be due to the hydrophilic nature of paper and its porous structure. It was expected that, with the introduction of the alpha-1,3 glucan in the coating, the degree of hydrophilicity of the coating will increase, causing the contact angle to drop below 90° which matches well with previous findings [148,283]. It is noteworthy to mention that after 1 min of contact between the water droplet and the surface, the contact angle did not change significantly (**Figure 4.3**), which exhibits the stability of the coatings. On the other hand, the water droplets completely penetrate through the base paper after 30 s.

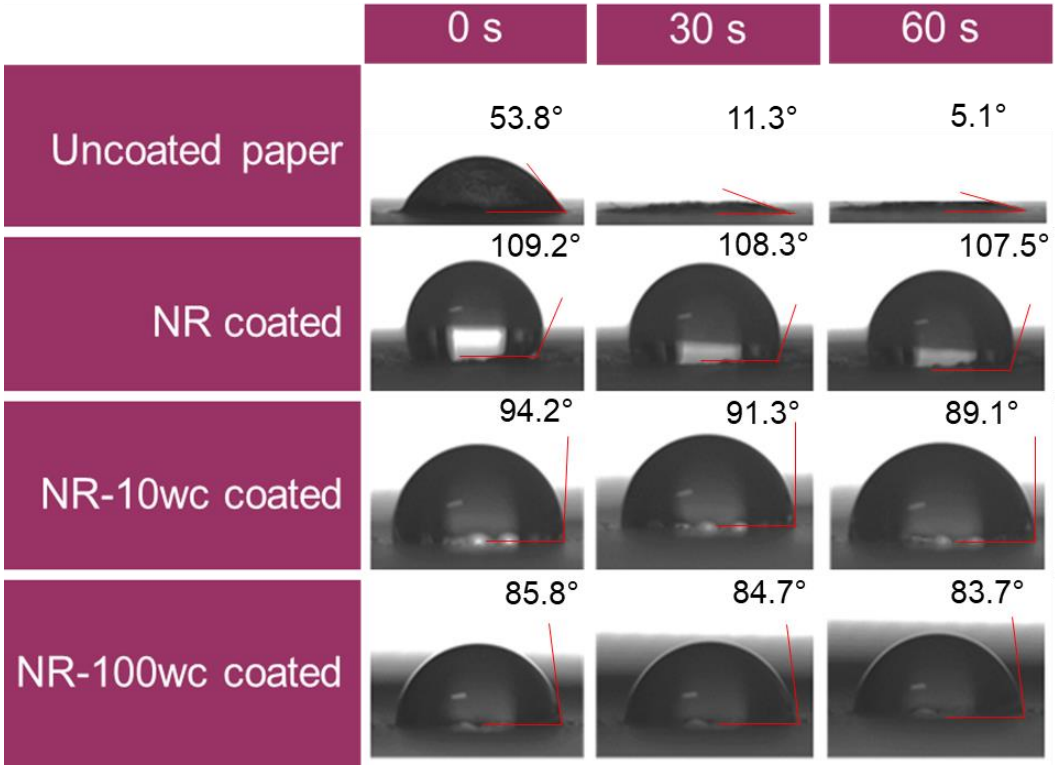

Figure 4.3. Contact angle of uncoated paper and coated papers.

4.3.5. Dry and Wet Tensile Properties

Tensile strength is a parameter representing the resistance against failure of the material under tension. In general, the major determining factor of tensile strength of coated paper is the base paper substrate [284]. While polymer coatings are typically less stiff than paper, they can act as adhesives of the paper fibers and enhance the strength. It is evident from **Figure 4.4 (a)** that applying coating film on the base paper has resulted in slightly higher tensile strength than the uncoated paper. Also, the incorporation of the alpha-1,3 glucan in the coating formulation had a positive influence at increasing the tensile strength of the coated paper in comparison to pure NR. This was attributed to the structural similarity of the alpha-1,3 glucan

with the cellulose fibers constituting the paper substrate leading to an intimate physical interlocking and hydrogen bonding. Moreover, the alpha-1,3 glucan particles are small enough to travel through the pores and voids in the paper substrate cellulose fibers and block pores while forming strong interactions as shown in **Scheme 4.2**. Afra et al. [285] reported a similar outcome of higher tensile strength by utilizing cellulose nanofibrils (CNF) as a coating constituent. On the contrary, the elongation at break of paper, remained almost unchanged (below 3%) from the baseline irrespective of the coating formulation variation indicating that the applied coating (20 μm) did not noticeably affect the paper substrate's flexibility. The influence of formulated coatings on the foldability and flexibility of the paper was evaluated by comparing the water Cobb of unfolded coated paper specimen and folded specimens (folded vertically and horizontally). As shown in **Figure A1**, the water Cobb values of the folded samples were not statistically significant ($p > 0.05$) from the unfolded samples. This indicates that the employed coating retained the water barrier properties despite the folding and as such the paper coatings lend their flexibility to the paper substrate.

Enhancement in the elastic modulus was observed by employing the coating layers on the paper substrate as shown in **Figure 4.4(b)**. This was ascribed to the adhesion and filling of pores by the NR latex in conjuncture with the migration of the alpha-1,3 glucan particles between the pores of cellulose fibers which lock the movement of the fibers, presenting higher resistance against deformation under tension. Similar modulus increase of paper substrate was reported using micro-fibrillated cellulose as a coating [286]. Furthermore, Hashemi Najafi et al. stated that with increasing starch content in the latex-starch films, the tensile modulus improved [287].

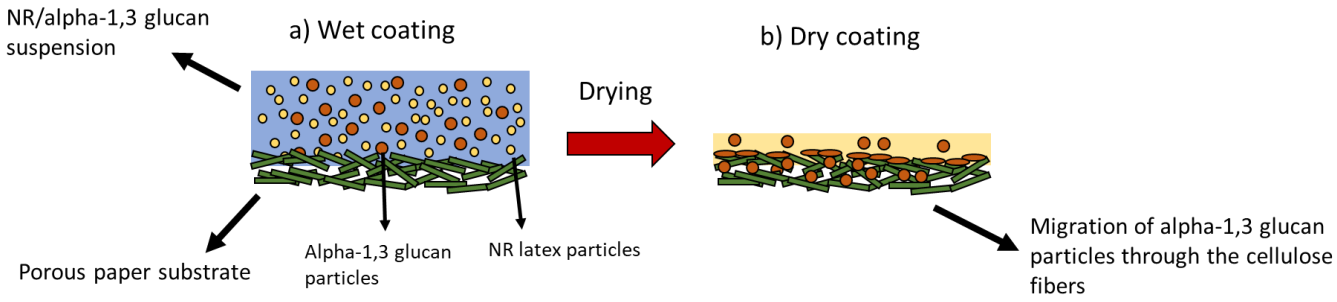

Scheme 4.2. The mechanism of formation of coating film on the paper substrate.

The wet tensile test was conducted to explore the effect of the coating on the wetted tensile properties of the coated paper, as wet contact is relevant in food packaging. While the mechanical strength deterioration was catastrophic for the uncoated paper, it is visibly better for the coated samples. It is known that the submersion of paper in water weakens and losses its integrity quickly as the water disrupts the non-bonded and hydrophilic cellulose fibers apart easily. Interestingly, a progressive improvement in the wet strength and modulus of the coated specimens was noted with increasing concentrations of alpha-1,3 glucan for both 30 s and 1 min submersion (**Figure 4.4(c)** and **Figure 4.4(d)**). This trend was likely caused by (i) the hydrophobic NR coating layer constituent that partially prevents water penetration; (ii) the blocking of the paper substrate cellulose fibers pores with the micron-sized alpha-1,3 glucan particles; (iii) the strong interactions between the alpha-1,3 glucan particles and the cellulose fibers resulting in mechanical interlocking and hydrogen bonding during the coating process that effectively blocks the penetration of moisture. The improvement in the tensile properties of the coated specimens' trend is in line with the corresponding dry strength. Also, as noted from the SEM analysis of the cross-sectional area of paper coatings made with alpha-1,3 glucan, the interface of coating film and the paper base was undistinguishable, confirming the

strong bonding among the coating particles and cellulose fibers. It is important to mention that this method has limitations in that the water could penetrate through the edge as well as on the non-coated side of the paper, which could result in debonding of the cellulose fibers in the paper substrate and subsequently degradation of tensile properties up on wetting.

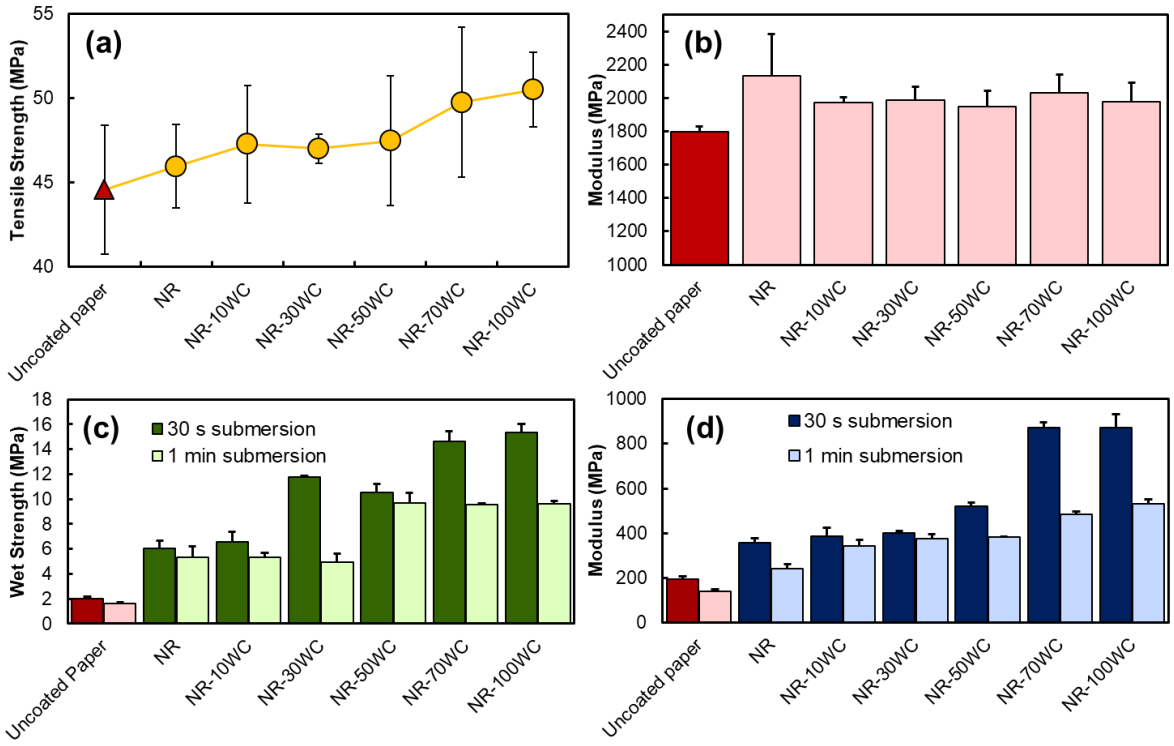

Figure 4.4. Tensile and modulus properties of paper coatings: a) dry tensile strength, b) dry elastic modulus, c) wet strength, d) wet modulus.

4.3.6. Barrier Properties

4.3.6.1. Water Cobb Test

The water Cobb test was employed to investigate the extent of water penetration prevention the formulated coating could provide to the paper substrate. In this method, the

coating was allowed to come in direct contact with the water for 60 and 120 s and the Cobb value is calculated (Eq. 1) based on the absorbed water. As illustrated in **Figure 4.5(a)**, the lowest Cobb value belonged to the NR coating as a result of its hydrophobicity. By introducing the alpha-1,3 glucan in the coating formulation, the Cobb value increased. However, the water absorption of the NR/alpha-1,3 glucan coating has tremendously decreased, in the range of 6-18 times, compared to the uncoated paper, which can be considered as an appealing result for food packaging applications. These values are in agreement with a previous study on chitosan paper coating [99].

4.3.6.2. Oil Cobb Test

The oil Cobb test was utilized to observe the oil absorption capability of paper coatings. The oil Cobb values have a reverse relation to the water barrier performance of the coatings, as indicated in **Figure 4.5(b)**. The results indicated that applying any of the coatings enhanced the oil barrier property of the substrate. Even though the coatings promoted the oil barrier performance in general, the reduction was not remarkable as attributed to some voids remaining after the application of the thin layer coating (20 μm), which were observed on the SEM images. It was noteworthy that the lowest oil Cobb value was recorded with 10 phr (9.09 wt.%) alpha-1,3 glucan loading. This behaviour can be associated with the well dispersed state of the alpha-1,3 glucan in the NR as proved by the SEM images as well as possible formation of a percolated network of alpha-1,3 glucan particles, which effectively hinders the penetration of oil through the paper substrate.

4.3.6.3. Water Vapor Barrier Property

The effect of the coating formulations on the water vapor permeability of coated papers was studied and results are highlighted in **Figure 4.5(c)**. This test was conducted at room temperature and constant relative humidity since *WVP* is sensitive to environmental conditions [135]. As noted from *WVP* results, applying NR on the paper led to a drop in *WVP* values, which is attributed to the hydrophobicity of NR. A remarkably reduction in the *WVP* was recorded by using the NR-10wc (9.09 wt.% alpha-1,3 glucan) formulation. This value is attribute to the uniform dispersion of alpha-1,3 glucan through the coating film which led to the formation of a more tortuous path for water molecules to penetrate through the paper. This result strengthens the possibility of a formation of percolated network at 9.09 wt.% loading. The same trend was observed in a study of a modified nanocellulose/polylactic acid (PLA) coating in which better water vapor barrier properties were obtained when the content of nanocellulose fibers (NFC) was close to the percolation threshold (5 wt.%) [145]. The decrease in the transmission of water vapor can be associated with the homogenous and compact coating layer, which retards the transporting of water molecules through the paper. Further increase of the alpha-1,3 glucan in the formulation likely creates aggregates leaving a permeable route for moisture transport. Since alpha-1,3 glucan particles are hydrophilic, they further exacerbate moisture absorption followed by desorption, which was observed as an increase in the *WVP*. This trend is consistent with a study of nano-fibrillated cellulose (NFC)/chitosan nanoparticles for paper coating [19]. It was reported that the increase in *WVP* values with the incorporation of NFC is associated with the high hydrophilicity of NFC.

4.3.6.4. Oxygen Permeability

In food packaging, the oxygen barrier has high importance in prolonging the shell-life of food [151]. Hence, the oxygen permeability of prepared paper coatings was investigated to evaluate the ability of alpha-1,3 glucan and NR to act as oxygen barriers. As can be observed from **Figure 4.5(d)**, the pure NR coating slightly improved the oxygen barrier capabilities of the substrate. However, introducing the alpha-1,3 glucan in the coating led to a noticeable enhancement in the oxygen barrier by up to about 55%. The alpha-1,3 glucan particles, with a crystallinity of up to 65% [44] accrued from intra- and intermolecular hydrogen bonding provided high oxygen barrier. These results are consistent with previous findings for coatings with cellulose nanocrystals [169] and regenerated cellulose as a coating [151]. Researchers have found that hydrogen bonding among the nanocellulose, which formed a strong nanocellulose network, induced a more packed layer of coating and resulted in lower oxygen permeability. The high polarity of the alpha-1,3 glucan associated with the –OH functional groups, would prevent an easy diffusion and passage of oxygen through the coating as opposed to the NR only based coating.

While there is a good improvement in the oxygen barrier with the coating, it requires further enhancement to achieve the superior barrier properties desired in food packaging. It is important to mention that, based on SEM images, a coating thickness of 20 μm did not seem sufficient to cover all of the pores present in the paper substrate. Thus, increasing the coating thickness could be a good strategy to ensure that the pores are covered (as presented in section 3.2). Similar challenges with the use of micro-fibrillated cellulose (CMF) for cardboard coating were noted in other studies [102,130].

The effect of humidity on the *OP* of the coated paper was also investigated. Results shown in **Figure 4.5(e)** indicated that higher relative humidity of the surrounding environment reduced the *OP* of the coating. This is rather counterintuitive, and it can be attributed to the hydrogen bond mediated association and encapsulation of water vapor around the alpha-1,3 glucan particles and the paper substrate. Such bonded water is expected to impede the passage of non-polar oxygen through it. Likewise, a similar trend was previously reported by Song et al. in both polyethyleneimine (PEI)/poly(acrylic acid) and PEI/clay films [163]. Researchers believed that hydrophilic polymers are capable of improving the barrier properties as the water molecules fill the free volumes within the multilayer films which induce greater tortuosity to the permeation path for oxygen molecules. Also, another plausible reason for greater oxygen barrier property at high relative humidity, was the swelling of glucan in the film which further blocks free volume in the rubber film to block the permeation of oxygen across.

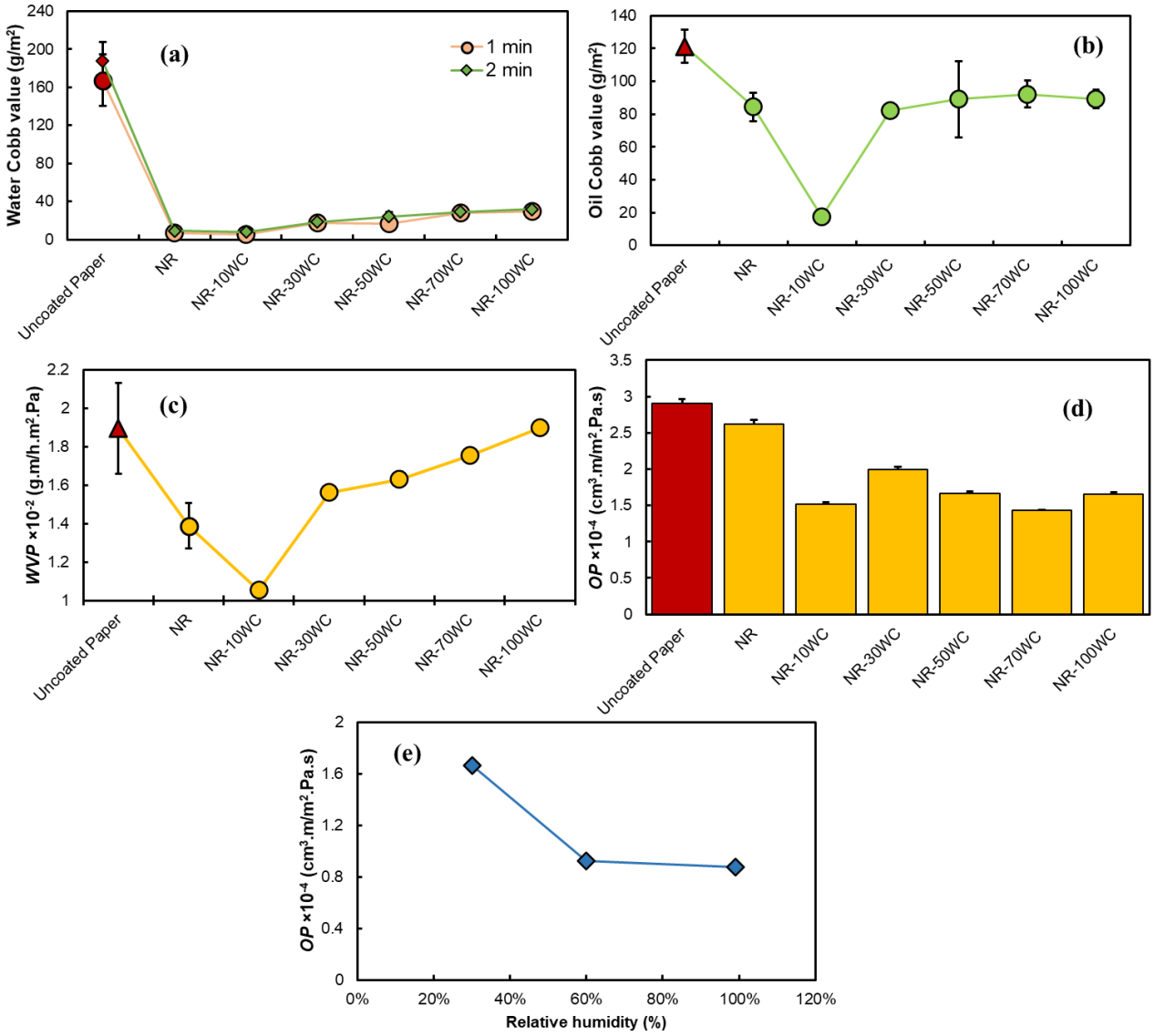

Figure 4.5. (a) Cobb test, (b) oil Cobb test, (c) water vapor permeability, (d) oxygen permeability of NR/alpha-1,3 glucan coated paper, (e) oxygen permeability at different initial moisture content at 22 ° for the NR-33 wt.% alpha-1,3 glucan coated paper.

4.2.5. Kit Test

In order to examine the grease resistance of the coated papers, a Kit test was employed. As can be observed from **Table 4.2**, the lowest Kit number was correlated with uncoated paper, which confirmed its high porosity. By employing coating, the Kit number started to increase as the coating films covered the pores throughout the paper and induced a tortuous path for the oil molecules. It is noteworthy to mention that, at 9 wt.% concentration of the alpha-1,3 glucan (NR-10wc), the highest Kit number was achieved. Further increase in the alpha-1,3 glucan loading content reduced the Kit number to four and eventually dropped to one for NR-100wc (50 wt.% alpha-1,3 glucan). This trend highlighted that as the concentration of the alpha-1,3 glucan increased, the performance of the coating resembled the paper substrate. Overall, the combination of the alpha-1,3 glucan with the NR at optimal concentration provides good grease resistance. While the NR is an important component to improve the grease resistance, without the alpha-1,3 glucan, the resistance it offers is not sufficient. Levoine et al [102] reported a Kit number of 2.5 for a micro fibrillated cellulose (MFC) coated paper, which is comparatively lower than the Kit number achieved for NR/alpha-1,3 glucan coating.

Table 4.2. Kit number of NR/alpha-1,3 glucan coated papers.

Coating composition	Uncoated paper	NR	NR-10WC	NR-30WC	NR-50WC	NR-70WC	NR-100WC
Kit number	0	3	10	4	4	4	1

4.3.7. Effect of Thickness on the Barrier Properties

Coating thickness is one of the dominant parameters in determining barrier performance, thus in this work, the effect of thickness on barrier properties was probed. Three different thicknesses, 5, 20, and 100 μm coating films, were prepared and their barrier performance against water, oil, and oxygen was explored. The water vapor barrier property results (**Figure 4.6(a)**) displayed that as thickness increased, water vapor permeability diminished. This trend suggested that larger thicknesses, produced from multiple layers of applied coating films on the paper, assisted in providing a better moisture barrier due to effective coverage of the paper substrate pores with the coating. Moreover, the thickness increase results in an extension of the migration path length for moisture to penetrate through and desorb from the coated paper. Similar observations were reported for chitosan-coated paper. When the coating weight and consequently the thickness were increased, the coating films provided lower *WVP* values and they were able to hinder the transmission of water vapor molecules through the paper [288].

Furthermore, the influence of thickness on the oil barrier performance was inspected by the oil Cobb and Kit tests. As highlighted in **Figure 4.6(b)**, a significant reduction in oil Cobb values was obtained by increasing the thickness of coating films on the paper. It is noteworthy to mention that the Cobb value was reduced by more than 99% compared to the untreated paper as coating thickness reached 100 μm. Successful sealing of the pores, in addition to the formation of a tortuous path via alpha-1,3 glucan particles for oil molecules to penetrate through the paper voids, resulted in the appealing oil barrier performance of the

coated paper. On the contrary, in terms of coatings with 5 μm, poor barrier ability against oil was demonstrated which was owing to the existence of voids on the surface of the coated paper. Aulin et al. reported a similar trend upon increasing the thickness of micro-fibrillated cellulose coating films [161]. It is important to highlight that the highest Kit number (12) was recorded for PE coated paper with a thickness of 100 μm thickness due to the excellent grease barrier properties of PE [286] and the sufficient thickness. The Kit test result obtained for the NR/alpha-1,3 glucan coating (**Table A2**) in this study is aligned with the result reported by Wang et al. for a multilayer cellulose coating [149].

The prevention of oxygen molecule permeation in coating films is one of the important challenges for food packaging applications. The thickness increase aided the paper coating to effectively impede the transportation of oxygen molecules through the material, as shown in **Figure 4.6(c)**. The increase in tortuosity and oxygen diffusion path length increase are the suspected reason for the enhancement of oxygen barrier with increasing coating thickness. Park et al. noted the opposite correlation of the thickness of the protein films, corn-zein, and wheat gluten with oxygen permeability [289].

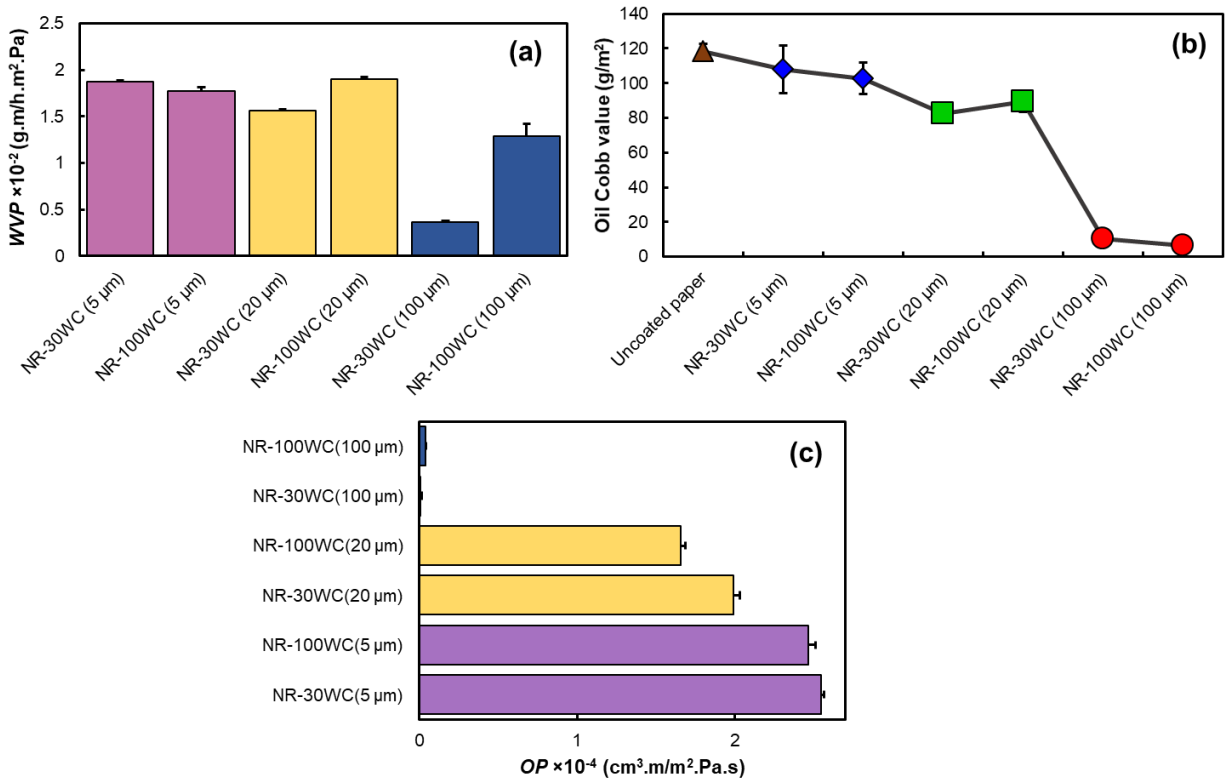

Figure 4.6. a) Water vapor permeability, b) oil Cobb test, and c) oxygen permeability of paper coatings with varying the thickness of the coating films.

4.3.8. Comparison of Formulated Coating with Commercial Coatings

In order to ensure that the formulated paper coating in this study is viable in the food packaging industry, the barrier properties of the manufactured NR/alpha-1,3 glucan coating films were compared with commercialized PE and PVOH paper coating films. As illustrated in **Figure 4.7**, the NR-wc coating with 20 µm thickness provided better oxygen barrier than PE, but less barrier than PVOH. On the other hand, the water barrier was less than PE, but better than PVOH. Overall, the combined oxygen and moisture barrier properties of the NR/alpha-1,3 glucan coating was in between the PVOH and PE, adjusted for thickness. Despite

the fact that the formulated coating contained hydrophilic alpha-1,3 glucan particles, the *WVP* of the NR/alpha-1,3 glucan with 100 μm thickness was just slightly higher than the *WVP* of PE, which is remarkable considering that it provides much better oxygen barrier than PE.

To compare the oil barrier properties of the PE and NR-wc coating films, an oil Cobb test was conducted. The oil Cobb results demonstrated that by increasing the thickness of the NR/alpha-1,3 glucan coating, and similar Cobb values as PE coating films can be achieved (**Figure 4.7(d)**). Furthermore, the effect of humidity on the *OP* of PVOH and NR-wc coating films was studied and was compared with the formulated coating, as shown in **Figure 4.7**. It is obvious that moisture has a deteriorating effect on the oxygen performance of the PVOH due to the plasticizing effect of moisture on PVOH that subsequently led to the swelling relaxation of polymer chains [262,290]. On the contrary, the increase in humidity has a positive effect on the *OP* of the NR-wc coating. These results indicate that the formulated paper coating can compete with the existing commercial paper coatings in the market.

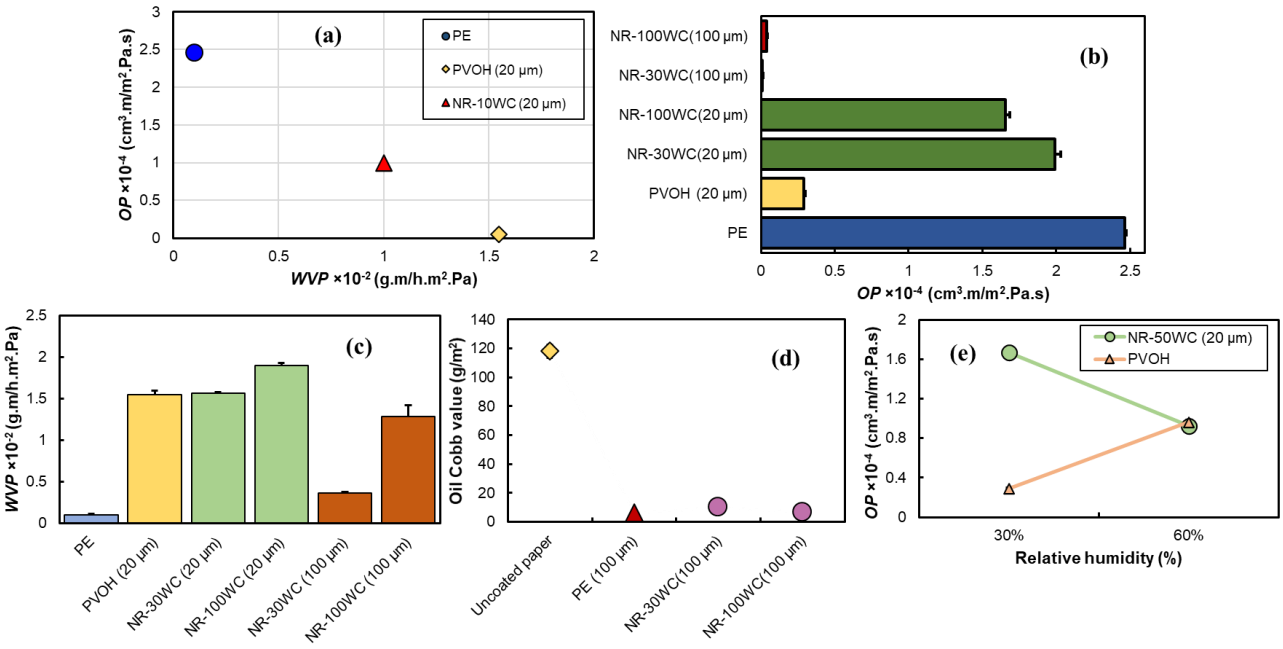

Figure 4.7. a) Oxygen and water vapor permeability comparison of NR/alpha-1,3 glucan coating with PVOH and PE, b) oxygen permeability comparison of NR/alpha-1,3 glucan coating at different thicknesses with PVOH and PE, c) water vapor permeability comparison of NR/alpha-1,3 glucan coating at different thicknesses with PVOH and PE, d) oil Cobb value comparison of NR/alpha-1,3 glucan with PE, e) effect of initial moisture content on the NR/alpha-1,3 glucan and PE as paper coating.

4.4. Concluding Remarks

The engineered polysaccharide, alpha-1,3 glucan, is derived from enzymatic polymerization of sucrose and provides a new sustainable and biodegradable material option providing unique and differentiated properties. The ability to directly convert sucrose allows for a highly feedstock efficient process that has the potential to emerge with a probable life cycle profile. The enzymatic polymerization process has inherently enabled to provide

materials for food contact applications in packaging. These alpha-1,3 glucan particles were incorporated as a functional additive in natural rubber (NR) latex systems to formulate a sustainable paper coating material. The coating performance evaluation results indicated that these formulated coatings improved the mechanical properties of the paper substrate, including the dry and wet strength, and modulus, without changing the flexibility and fold resistance, attributed to the good interactions between the coating films and cellulose fibers of the base paper substrate. At sufficient thickness, this coating system allows for successfully sealing of the paper substrate pores. As a result, notable barrier property improvements versus oil, oxygen, and water vapor were achieved. The NR coating formulation with 10 phr alpha-1,3 glucan (9.09 wt.%) provided an improved moisture, oxygen and grease barrier. Higher loading levels can be detrimental to the moisture barrier properties of the coating. Overall, the NR/alpha-1,3 glucan coating films produced in this study demonstrated high mechanical strength and barrier properties, both of which are essential properties in the food packaging industry. This demonstrates that the studied NR-alpha-1,3 glucan coating system may be an appealing option for sustainable paper-based flexible packaging alternatives advancing to commercial deployment.

Chapter 5. High Barrier Sustainable Paper Coating Based on Engineered Polysaccharides and Natural Rubber [4]

5.1. Introduction

Paper is a versatile material widely used in the food packaging industry due to its good mechanical properties and general affordability but also more recently based on increased interest in aspects of sustainability such as biodegradability and general recyclability.[109,153,285] Paper is typically comprised of a physical network of cellulose fibers in combination with other additives resulting in a composite with high porosity and hydrophilicity. While the porosity and hydrophilicity can be beneficial in certain applications, these properties impose challenges in packaging applications which require barrier performance. For example, food packaging applications require viable barriers to water, oil, and oxygen [99,161]. Therefore, special treatments are needed to improve the barrier property of paper substrates to meet the necessary criteria for packaging applications [148]. Surface coatings are one of the most common approaches to overcoming the lack of sufficient barrier properties and achieving specific functionalities [291,292]. Currently, the paper packaging industry mainly utilizes fossil-derived synthetic polymers as coating layers, and their lack of environmental degradability, along with poor recyclability, aggravate environmental concerns [144]. Common synthetic polymers that have been utilized as surface coatings are polyethylene

[4] A version of this chapter has been published on peer-reviewed journal as a review article: **A. Adibi**, et al. (2022). High Barrier Sustainable Paper Coating Based on Engineered Polysaccharides and Natural Rubber ,*ACS Sustainable Chemistry and Engineering*, **10(32)**, 10718-10732. https://doi.org/10.1021/acssuschemeng.2c03466.

(PE), wax, polyethylene terephthalate (PET), and polybutylene terephthalate (PBT) [68]. It is worthwhile to mention that the majority of the aforementioned synthetic polymers are not recovered in these applications and usually pollutes land sites and water bodies [16]. In 2015, approximately five million tons of plastic waste was generated that ended up in landfills, incinerators, and as litter leaking into the environment [61,98]. This alarming environmental concern has accelerated the interest in using sustainable polymer alternatives for packaging design to replace current petroleum-based substrates and coating materials [89].

Natural rubber (NR) is an abundant renewable biopolymer extracted from the rubber tree (*Hevea brasiliensis*) in the form of a milky colloidal suspension [263]. With the typical cis-1,4-polyisoprene chemical structure of the polymer (Scheme 1), NR is considered one of the most utilized elastomers and has extensive applications, particularly in coatings, adhesives, condoms, tires, gloves, and power transmission belts [14]. Properties such as excellent film-forming ability, high moisture barrier, recyclability, and flexibility could make NR a superb alternative as a coating for application in the packaging market. While uncured NR is capable of slowly biodegrading in the soil [29,293,294], the incorporation of bio-fillers (i.e. starch, cellulose, chitosan) can accelerate the disintegration to further accelerate biodegradation [295–297]. Nevertheless, at this point the utilization of NR in paper coatings is still limited [31,32]. This is because NR has certain limitations, such as poor mechanical, oil, and weather resistance, that need to be addressed in order to achieve the essential requirements to fulfil the paper coating market needs. Additionally, NR latex can cause allergic reactions induced by enzymes. Hence in order to eliminate the restriction of being directly used in the food application, deprotonation is highly needed. Employing polysaccharides as functional

additives can compensate for the drawbacks of NR to make it an appealing and environmental-friendly material alternative to replace conventional polymers [15].

Polysaccharides are also among the most abundant natural polymers, originating from plants, marine biomass, fungi, and bacteria. They are comprised of repeating monosaccharides units connected by glycosidic bonds [298] and are typically biocompatible, biodegradable, and non-toxic [299] and hence can be appealing components in paper coating fabrication. The most common polysaccharides, starch, chitosan, alginate, etc., have hydroxyl moieties, which can interact with the hydroxyl groups of cellulose fibers in paper via hydrogen bonding resulting in strong adhesion [275]. One of the feasible approaches to making polysaccharides applicable in food packaging is combining them with other film-forming materials [280]. However, the principal drawbacks of polysaccharides are poor water and moisture barrier and mechanical properties, which restrict their extensive applications [300]. Furthermore, most nature-derived polysaccharides are not pure and display extensive variation in their molecular structure and morphology depending on their source (geography, season, cultivar, etc.).

More recently, a novel approach was employed to produce engineered polysaccharide, alpha-1,3 glucan, by IFF Inc. The alpha-1,3 glucan was obtained by enzymatic polymerization of glucose derived from sucrose. This reaction is conducted with the use of an enzyme catalyst selected from the general class of glucosyltransferase (GTF) enzymes [49,281,301]. The alpha-1,3 glucan generated as such is a water-insoluble, linear, highly crystalline, with a high surface area [50]. Despite their high tendency to form agglomeration, alpha-1,3 glucan can be dispersed in water under shear to form a stable colloidal suspension. Furthermore, the enzymatic polymerization process allows control of morphologies, including spherical

aggregates, fibrids, and platelet particles referred to as microcrystalline glucan (MCG) [52]. In this work, platelet morphology MCG particles were used to promote oxygen and oil barrier properties owing to their morphology, high crystallinity, and high surface area. Therefore, formulating MCG into NR may be able to efficiently address the flaws of NR in terms of barrier properties and be able to generate desirable sustainable paper coating formulations.

The main objective of this work was to investigate the fabrication of a paper coating that provides good mechanical and barrier properties while maintaining environmental attributes. Also, it assesses the contribution of alpha-1,3 glucan in NR formulation in terms of barrier properties. In addition, the effect of light-crosslinking on the mechanical as well as barrier performance of formulated NR/MCG paper coatings is investigated. Analytical techniques, such as tensile strength studies, rheology studies, permeability testing such as water vapor and oxygen, Cobb test, and Kit test, were employed to evaluate the characteristics of the formulated paper coatings.

5.2. Experimental

5.2.1. Materials

Enzymatically polymerized polysaccharide, microcrystalline glucan (MCG), with surface area of 9.7 m^2/g was provided by IFF Inc (Wilmington, DE, USA). The utilized MCG was a colloidal dispersion in water (6.6 wt.%) [44]. Stabilized natural rubber (NR) latex (60 wt.% solid content) was supplied by Chemionics Corporation, OH, USA. Toluene, n-heptane, zinc oxide powder (ZnO), potassium hydroxide pellets (KOH), and sodium hydroxide (NaOH) pellets were purchased from Sigma Aldrich, USA. Zinc (II) dibutyl dithiocarbamate (ZDBC) (98 wt.%) was obtained from Fisher Scientific Inc., Canada. Sulfur with 99.5% purity was

obtained from Acros Organics. Semi-bleached Manila paper, with a thickness and grammage of 0.26 mm and 204 g/m^2, respectively was sourced from a local stationery store (Waterloo, ON, Canada) and used as the substrate.

5.2.2. Characteristics of Microcrystalline Alpha-1,3 Glucan (MCG) Platelets

5.2.2.1. Rheology of Alpha-1,3 Glucan

To explore the rheology of the MCG dispersed in water, an amplitude sweep method was employed using a rheometer (HAAKE MARS, Thermo scientific). The dynamic viscosity of the MCG dispersion at multiple concentrations (2 wt.%, 5 wt.%, 7.5 wt. %, 10 wt. %, 15 wt.%, and 20 wt.%), were evaluated at shear strains ranging from 0.1-100 %. Prior to dispersing MCG in water, the water content of the MCG was reduced using a rotavapor (BUCHI R-124) and then it was subsequently dispersed in water at the desired concentration on a stir plate (500 rpm for 2 h). Tests were conducted using a parallel plate rheometer (35 mm diameter, 1 mm plate gap) at room temperature.

5.2.2.2. Stability of MCG in Rubber Latex

Stability test was conducted in order to study the compatibility of NR and MCG as well as the influence of varying concentrations of the MCG on the stability of NR/MCG formulation. In this method, the NR/MCG formulations were diluted to 20 wt.% and were monitored for 4 days. Also, the change in the particle size of the coating formulations was evaluated for four days using a Zetasizer (Malvern, Westborough, MA).

5.2.3. Coating fabrication

The coating formulations comprised NR, MCG, and water. The water content of the MCG was reduced from 93.4 wt.% (received sample) to 80 wt.% by using a rotary evaporator (rotavapor, BUCHI R-124) at 85 °C and used as a masterbatch for all the coating formulations. The fabrication procedure of the coating formulation was initiated by pre-dispersing the MCG in water on a stir plate (500 rpm for 2 h). The pre-dispersed MCG was then mixed with calculated amounts of NR latex and distilled water to achieve the required solid content. The concentration of MCG in the coating film formulations was 0, 2, 5, 10, 25, 50 wt.% (dry weight basis) with respect to the concentration of natural rubber in the formulation, as shown in **Table 5.1**. The formulation compositions were further mixed on a stir plate (500 rpm x 10 min) followed by homogenization (20,000 rpm x 4 min) to obtain a uniform dispersion. At 50 wt.% concentration of the MCG, the coating formulation resulted in high viscosity that prevented a uniform dispersion of the MCG in the rubber latex. To overcome the mixing issue, 0.5 wt.% NaOH pellets relative to the MCG was incorporated in the formulations. The coating formulations were subsequently applied on the paper substrate using a doctor blade to get 20 μm dry thickness. Afterwards, the coated paper was left to dry at room temperature for 24 h prior to testing (**Scheme 5.1**). Also, the grammage of the paper coating was calculated in five replicate samples, and the average is reported in **Table 5.1**.

Table 5.1. Composition and grammage of paper coating samples.

Sample label	**Wt.% of NR, dry basis**	**Wt.% of MCG, dry basis**	**Grammage (g/m^2)***
NR	100	0	8.4 ± 0.8^a
NR-2%MCG	98	2	8.4 ± 1.1^a

NR-5%MCG	95	5	8.6 ± 0.5^{a}
NR-10%MCG	90	10	9.6 ± 0.1^{b}
NR-25%MCG	75	25	12.2 ± 0.9^{c}
NR-50%MCG	50	50	16.9 ± 4.1^{c}

*Grammage (g/m^2) = mean (n = 5) ± standard deviation, varying superscript letters within a column indicate statistically different ($P < 0.05$)

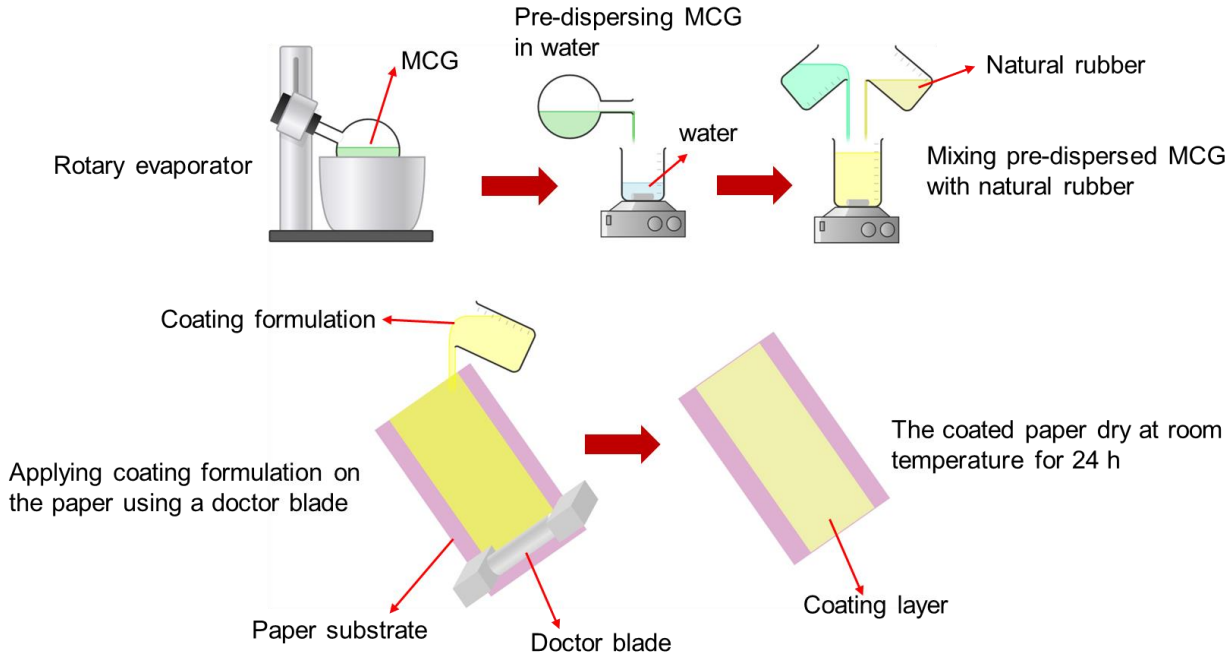

Scheme 5.1. Schematic illustration of coating fabrication procedure.

5.2.4. Characterization of the coatings

5.2.4.1. Rheology Analysis

An amplitude sweep method, using a rheometer, was used to evaluate the rheology of the NR/MCG coating formulations. The viscosity, loss modulus, and storage modulus of the NR/MCG formulations were evaluated (0.1-10 % shear strain) at room temperature.

5.2.4.2. Morphology Analysis

A scanning electron microscope (FEI Quanta FEG 250 SEM) was used to examine the homogeneity of the coatings as well as the voids present on the paper coatings surface. Prior to the test, the specimens were cryofractured and coated with gold to evaluate their surface and cross-sectional morphology.

5.2.4.3. Contact Angle Measurement

The contact angle of the control and coated paper surfaces were performed using a custom-made optical sessile drop system. Deionized water (3 μL) was allowed to drop on the coated paper surface and images were taken with a video camera after 0, 30, and 60 s to assess how the water interacted with the formulated coatings. Measurements of the contact angles of water droplets were carried out using ImageJ software.

5.2.4.4. Mechanical Properties

Dry Tensile Strength: Tensile tests were conducted using a Universal tensile testing equipment (AGS-X series, Shimadzu, Japan) with a 100 mm/min strain rate and a 500 N load cell according to ISO 1924-2/3. Specimens were cut into strips (70 × 10 mm), with a gauge length of 50 mm. For each coating formulation, seven specimens were tested, and the average ± standard deviation was reported.

Wet Tensile Strength: Wet tensile tests were performed according to ASTM D829-97. In this test, at least eight test specimens were immersed in distilled water (30 s and 1 min), followed by the removal of the excess water on the coated paper's surface, and then tensile testing was conducted like the dry testing method.

Adhesion Strength Analysis: A shear test was employed to study the adhesion strength between the coating film and the paper substrate using the tensile testing equipment (AGS-X series, Shimadzu, Japan). The specimens were cut into strips of 10 mm in width and 40 mm in length. Afterward, 20 mm of the length of the coated part was peeled off from the paper and was taped to be inserted into the grips. The shear rate was tested at a crosshead speed of 20 mm/min according to ASTM F2824. For each sample, seven specimens were tested, and the average was reported.

5.2.4.5. Cobb Test

The water Cobb test was carried out on five replicate test specimens by using custom-built Cobb equipment in accordance with TAPPI T441. First, about 30 cm^2 of circular samples were prepared, fixed underneath the Cobb cylinder so the coated surface faced upward, and then a specific amount of water was then poured into the Cobb cylinder. After 2 min of water exposure, the water was poured out completely, and the sample was blotted dry to remove any excess water. Subsequently, the coated paper was weighed in order to determine the Cobb value, which is based on weight difference (Eq. 5.1):

$$Cobb\ value\left({}^{g}/_{m^2}\right) = (m_2 - m_1) \times 10000/Area(\ cm^2) \qquad (5.1)$$

where m_1 and m_2 are sample weights before and after the test, respectively.

Similarly, the oil Cobb test was implemented to measure the quantity of oil penetrated through the coated paper in 1 min. Canola oil at room temperature was used in the test, in which five measurements were taken for each sample to calculate the average value.

5.2.4.6. Kit Test

The Kit test was conducted to evaluate the grease resistance of the paper coatings according to T559. For this test, 12 different standard grease formulations shown in **Table A1** composed of varying quantities of toluene, castor oil, and n-heptane were applied on the coating surface. After 15 s of contacting the grease solutions with the coated samples, the grease drop was wiped, and the coating surface was examined for traces of staining. The strongest grease solution, represented by the highest number, that did not leave dark spot trace on the coated paper surface is reported as the Kit value. Samples with higher Kit number are considered grease resistant. The test was run on at least five replicate samples.

5.2.4.7. Water Vapor Barrier

The influence of the coating in enhancing the water vapor barrier performance of the coated paper was studied as per ASTM E96. For this method, Teflon cups containing distilled water were tightly sealed with the coated paper samples, in such a way that the coating surface faces the water vapor. Over seven days of testing, the weight change of the samples was tracked. This test was carried out in a constant relative humidity environment, and three measurements was conducted for each coating formulation. Consequently, the water vapor transmission rate (*WVTR*) and subsequently the water vapor permeability (*WVP*) was calculated by employing Eq. (2) and Eq. (3):

$$WVTR = \frac{\Delta G}{t \,.\, A} \tag{5.2}$$

$$WVP = \frac{(WVTR) \times l}{\Delta p} \tag{5.3}$$

where t is time (hr), A is the cup's mouth cross-sectional area (m^2), l is the coated paper's thickness (m), ΔG is the weight change (g), and Δp is the partial water vapor pressure difference (1 Pa) between the film's two sides.

5.2.4.8. Oxygen Barrier

The oxygen permeability (*OP*) tests were carried out using a bubble flowmeter system (**Scheme B1**). For the test, circular coated paper samples (4.8 cm in diameter) were sealed in a two-chamber cartridge attached to an oxygen source from the bottom chamber and a bubble flow meter from the top end of the chamber. The flow rate was determined by recording the time a soap bubble took to travel 20 mL through a burette. The pressure difference between the two chambers was fixed at 13.8 kPa, which allowed the oxygen to permeate through the samples. The *OP* test was carried out at various humidity exposure levels of the coated paper, i.e., 15%, 30%, 60%, and 100%, to explore the effect of the humidity on the barrier performance of the formulated coatings. To expose the samples to the specified humidity, they were placed in a humidity adjusted desiccator equipped with a digital hygrometer and allowed to equilibrate for 2h. The test was then immediately performed, and the OP value was calculated using Eq. (5.4):

$$OP = \left(\frac{V}{t.A}\right) \times \frac{l}{\Delta P} \tag{5.4}$$

where l is coated paper's thickness (m), $V / (t. A)$ is the oxygen flow rate ($cm^3/m^2.s$), and ΔP is the oxygen gas pressure difference.

5.2.4.9. Effect of Solid Content on the Barrier Properties

To investigate the impact of the solid content of the formulations on the barrier properties of the paper coatings, selected coating formulations with a higher solid content of 40 wt.% were prepared. Since increasing the solid content in the formulation led to higher viscosity, NaOH (0.5 wt.% of the solid weight of alpha-1,3 glucan) was utilized to enhance the mixing process. The barrier property tests were carried out on these coatings and compared with 20 wt.% solid content-based formulations.

5.2.4.10. Effect of Rubber Crosslinking on the Barrier Properties

Since crosslinking introduce a covalent bond to the network, it is expected that it will generate additional complex diffusion path for fluids and facilitates greater barrier properties. Therefore, lightly crosslinked paper coatings were fabricated for a fundamental investigation of the influence of light crosslinking on the barrier properties of the coating. Formulations for crosslinked paper coating consisted of sulfur curing agent (1.5 phr), KOH (3 wt.%), activating agent (ZDBC, 0.5 phr), ZnO (1.3 phr), and MCG (**Table 5.1**). The preparation procedure was initiated with the pre-dispersion of the MCG in water and then adding the curing agent, activating agent, and filler to the MCG dispersion and mixing via homogenization (4 min shear mixing at 20,000 rpm) and sonication. After adding NR to the pre-dispersed mixture, the formulation was mixed on a hot plate (400 rpm at 40 °C for 2 h) as part of the maturation process [165]. Then the coating formulation was applied on a paper substrate, dried at 23 °C, and crosslinked (100°C for 2 h).

5.2.4.11. Statistical Analysis

All experiments, unless otherwise stated, were replicated at least three times and data were presented as mean ± standard deviation. A one-way analysis of variance (ANOVA) was carried out to identify significant changes in data followed by Tukey' HSD multiple comparisons for mean comparison (0.05 significance level) using Minitab statistical software.

5.3. Results and Discussions

The microcrystalline glucan (MCG) additive used in the study forms a stable dispersion in water over a wide pH range (0-10) [165]. It has a platelet morphology with dimensions of about 200 nm x 200 nm and 5 nm thickness based on TEM imaging estimation (**Figure 5.1(a)**). Moreover, it has high crystallinity (~85%) with an average particle size in the range of 0.4 – 0.6 µm [165].

5.3.1. Rheology of the MCG

To investigate the effect of varying concentrations of the MCG on the viscoelastic properties of MCG suspensions, an amplitude sweep test was carried out over a shear strain of 0.1-100 %. As depicted in **Figure 5.1(b-c)**, the overall moduli increased with the MCG concentration. Also, at all the studied concentrations, the storage modulus (G′) exceeded the loss modulus (G″), which exhibited the dominancy of the elastic behavior [302,303]. Li et al. reported the same behavior for the cellulose nanofiber (CNF) suspensions due to the formation of the 3D network among CNFs, which led to a solid-like structure of the CNF suspensions [304]. Additionally, the linear moduli behavior at low shear strain corresponds to the linear viscoelastic properties [305].

Dynamic viscosity of the varying concentration of MCG suspensions was collected as illustrated in **Figure 5.1(d)**. It was observed that dynamic viscosity progressively increased as

the MCG content increased. The strong physical interlocking among the MCG particles significantly contributed to promoting the viscosity of the suspensions [120]. At low shear strain, a plateau was noted that indicated the independency of the viscosity against shear strain representing Newtonian behavior [306]. Further increase in shear strain results in shear-thinning behavior, which can be mainly associated with the disruption and break up of the MCG networks under shear [39].

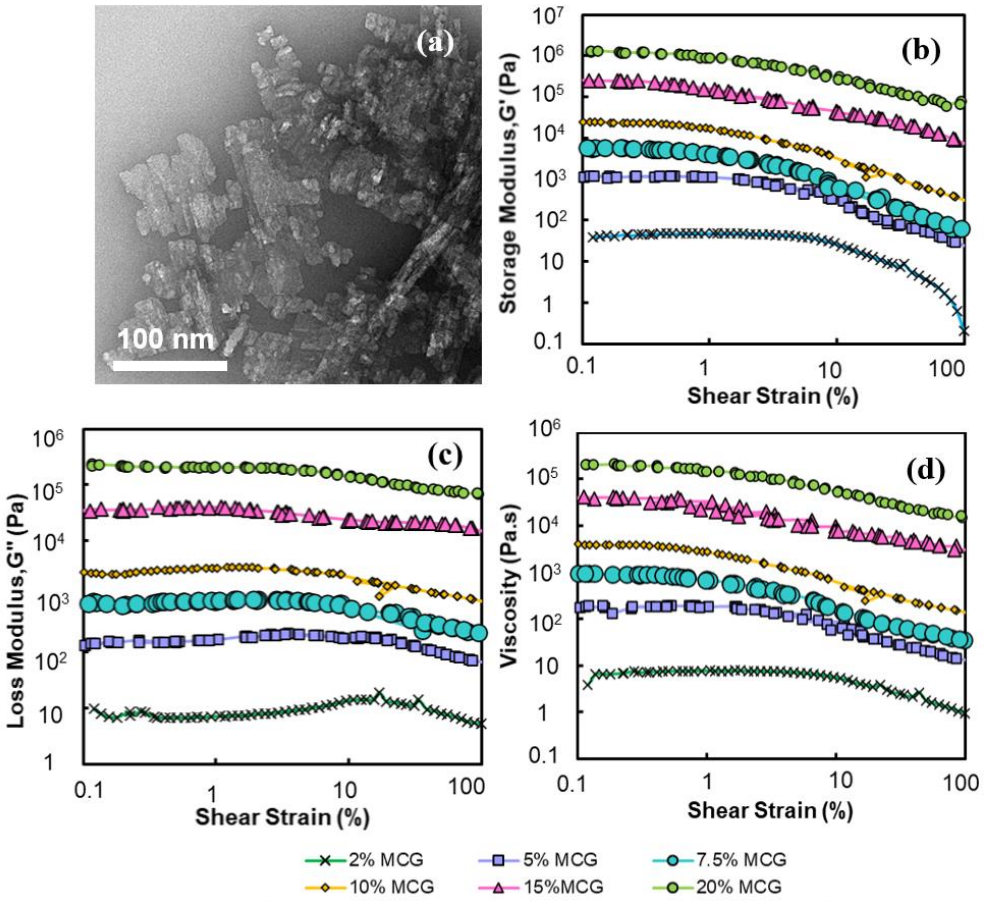

Figure 5.1. a) TEM image of MCG, b) storage modulus of MCG dispersion in water, c) loss modulus of MCG dispersion in water, d) viscosity of MCG dispersion in water.

5.3.2. Stability of MCG in Rubber Latex

The stability of the MCG in the NR latex formulation was evaluated by assessing the sedimentation behaviour of the mixtures. Images of a diluted NR/MCG formulation that shows a change in stability over 4 days were collected and are shown in **Figure 5.2(b-d)**. It was evident that even after 4 days, the MCG particles were stable in the NR latex. At high loadings, the stability of the 50% MCG formulation started to be impacted. Furthermore, a particle distribution evaluation, as shown in **Figure 5.2(a-c)**, did not display major changes, which supports the visual observation that indicated the high stability of the MCG in NR formulation. This can mainly be due to the mutual colloidal stability of the MCG and NR latex. Nevertheless, when the concentration of the MCG is high (50 wt.%), sedimentation was observed in these particular samples after Day 3 (**Figure 5.2(c-d)**). This is likely associated with the tendency of the MCG particles, which have high surface area, to form agglomerations, resulting in the generation of MCG clusters that may form sediments under gravity. Prior to 3 days, no aggregation was observed. The two differentiated peaks observed in **Figure 5.2(c)** were attributed to separating the agglomerated and suspended particles. Similar observations were reported when hydroxyethyl cellulose was dispersed in NR latex [307].

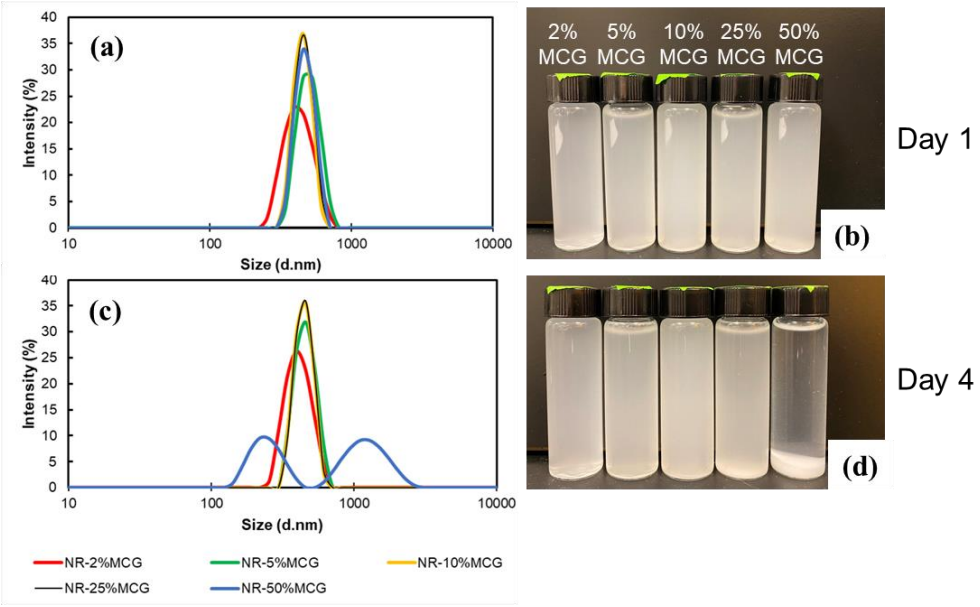

Figure 5.2. a) Particle size of diluted NR/MCG coating formulations at day 1, b) image of diluted NR/MCG coating formulations at day 1, c) particle size of diluted NR/MCG coating formulations at day 4, d) image of diluted NR/MCG coating formulations at day 4.

5.3.3. Rheology of Coatings

To study the effect of the MCG on the rheological properties of NR latex along with the processability of the formulated coatings, rheology as a function of strain rate (%) was collected. The storage modulus (G′) and loss modulus (G″) versus the shear rate at a constant frequency of 1 Hz were generated to assess the viscoelastic behavior of the NR/MCG formulation, as indicated in **Figure 5.3(a-b)**. The increment in concentration of MCG resulted in higher storage and loss modulus representing a more robust gel network caused by the MCGs [308,309]. The modulus of the suspensions mostly depended on the concentration and the interactions between the particles, and hence as the disperse phase increases, the modulus

became larger [310]. Also, another observation worth noting was a higher G′ than G″ throughout the strain rate range due to the gel-like behavior of NR latex with contained the MCG additive [114,311].

Furthermore, the dynamic viscosity of the coating formulations was evaluated to shed light on their flow behavior. As shown in **Figure 5.3(c)**, increasing the concentration of the MCG induced higher viscosity, which can be associated with the restriction of latex colloids' mobility by rigid MCG particles. A steep decrease in the viscosity caused by increasing shear strain for all formulations represented shear-thinning behavior. The formulations displayed such behaviour due to the disruption in the MCG network resulting in a viscosity decrease [282,312].

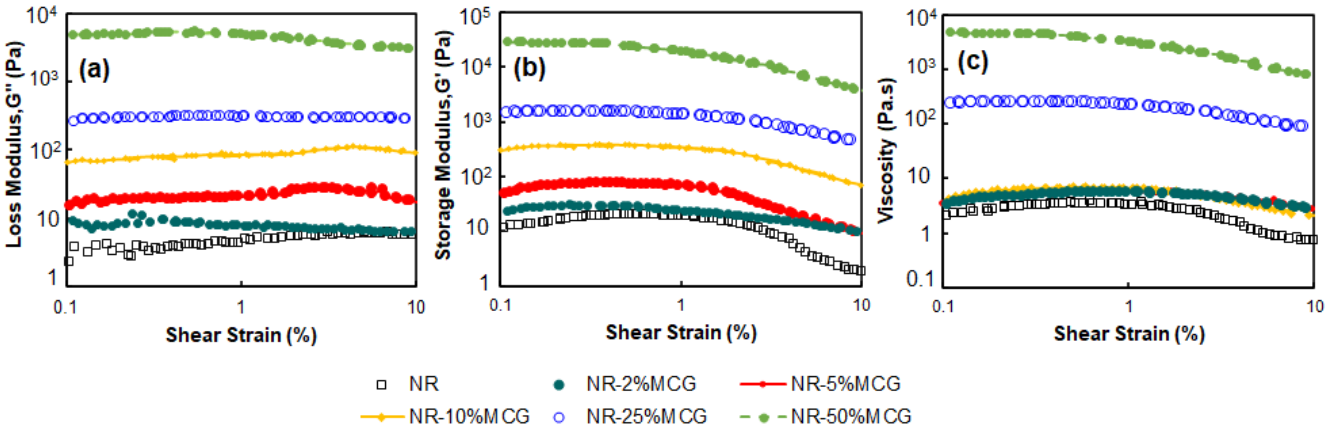

Figure 5.3. a) Storage modulus of NR/MCG coating formulations, b) loss modulus of NR/MCG coating formulations, c) viscostity of NR/MCG coating formulations.

5.3.4. Morphology of Formulated Coatings

In order to evaluate the uniformity of the coating film on the paper's surface, the morphology of the formulations and their ability to fully block voids on the paper was studied.

For this, scanning electron microscope (SEM) imaging was employed, and the results are displayed in Figure **5.4(a - f)**. Uncoated paper has an uneven surface, and the cellulose fibers can be easily recognized in **Figure 5.4(a)**. Also, the presence of the voids on the paper's surface was evident in the cross-sectional images of the base paper (**Figure 5.4(g-j)**). However, after coating this base paper with the NR/MCG formulations, the surface becomes relatively smooth and individual fibers are mostly covered and indistinguishable on the surface. Also, in general, the NR/MCG formulated coatings are homogeneously distributed on the base paper, while noticeably, the pure NR coating does cover the pores only partially, as shown in **Figure 5.4(b)**, which was suspected to be due to the difference in the polarity of the NR and the cellulose fiber substrate that prevents intimate interaction.

In contrast, full coverage of the pores on the paper's surface was accomplished by incorporating the MCG in the NR formulations. This was due to the structural similarity of MCG with cellulose and hence high compatibility resulting in better filling of the pores. Overall, the MCG-based formulations enhanced the uniformity and improved the overall coating quality, similar to other studies[30,145,151,286]. However, at the highest concentration of the MCG (50 wt.%), the paper fibers were visible again together with the deposited MCG particles, ascribed to the lack of sufficient NR to cover the paper fibers. The cross-section of the coating film is indicated by a red arrow and exhibits good interaction of the coating film and the paper, which can be attributed to the high affinity of the MCGs to the cellulose fibers as shown in **Figure 5.4(g – j)**.

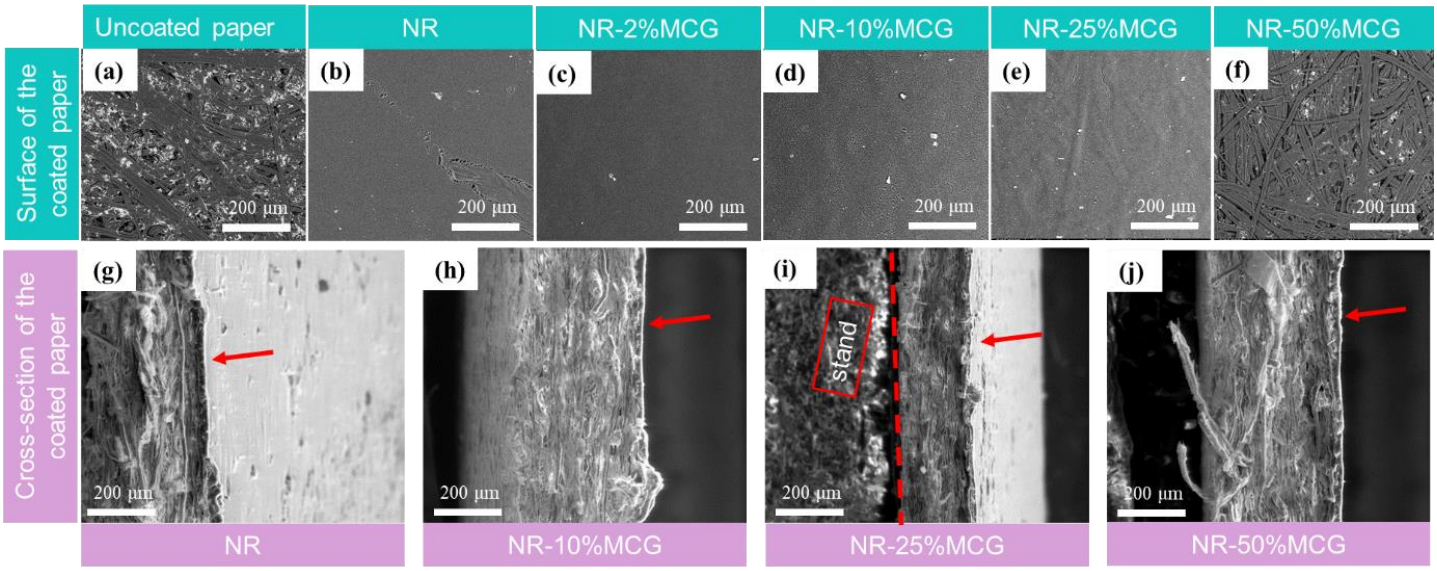

Figure 5.4. SEM images of the surface of: a) uncoated paper, b) NR coating film on the paper, c) NR-2%MCG coating film on the paper, d) NR-10%MCG coating film on the paper, e) NR-25%MCG coating film on the paper, f) NR-50%MCG coating film on the paper , SEM images of cross-section of: g) NR coating film on the paper, h) NR-10%MCG coating film on the paper, i) NR-25%MCG coating film on the paper, j) NR-50%MCG coating film on the paper.

5.3.5. Wettability

The wettability of the coating was characterized by measuring the water contact angle with the coated paper's surface. Contact angle variation at 0, 30 s, and 60 s of contacting the coating side of the coated paper with a water droplet is presented in **Figure 5.5**. The baseline uncoated paper exhibited the smallest contact angle reflecting its hydrophilicity. As expected, after 30 s, the water droplet penetrated through the baseline paper due to the paper's porosity. However, all the NR-MCG formulation-based coatings displayed contact angles above 90°.

Moreover, these coated paper samples maintained their hydrophobicity over the 1 min duration. It was noted that with the increasing addition of MCG into the coating formulation, the hydrophilicity also slightly increased, as observed from the reduction in contact angle. Nevertheless, the contact angle change was rather minimal indicating that the NR phase dominates the surface-water phase interaction. This may likely be attributed to the platelet morphology of the MCG that efficiently hinders the diffusion of water molecules. Additionally, after 1 min of exposing the coated paper to a water droplet, the water contact angle remained almost unchanged, indicating the coatings' stability.

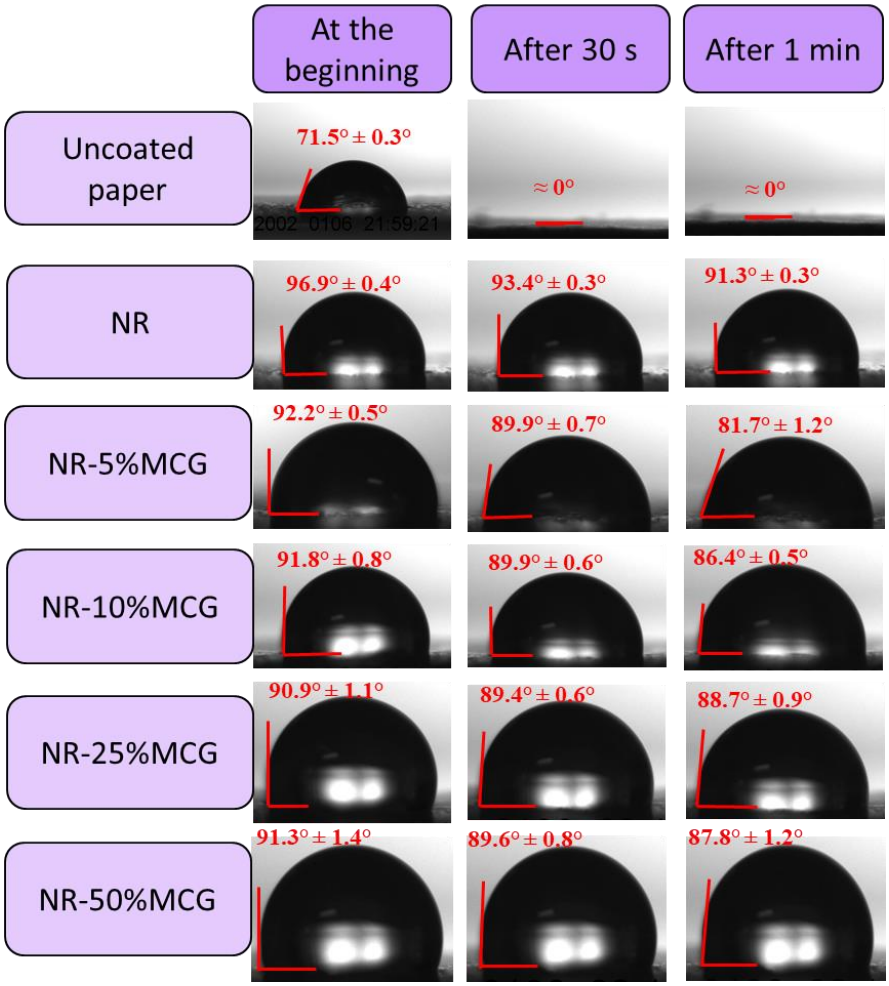

Figure 5.5. Contact angle of NR-MCG coating formulations.

5.3.6. Mechanical Properties

5.3.6.1. Dry and Wet Strength

Tensile testing was employed to evaluate potential changes in the physical integrity of the paper as a result of the coating. In general, the base paper has the most important contribution in determining the mechanical properties, such as tensile strength. Applying the series of NR-formulated coatings positively influences the tensile properties and results in a slight improvement in tensile strength. Additionally, the incorporation of MCG in the coating further enhanced the tensile strength, as evidenced by **Figure 5.6(a)**. Improvement in the tensile strength was mainly attributed to the high affinity of the MCG to the paper fibers besides filling the paper pores, which ultimately may induce efficient stress transfer. These results are in line with results reported by Zakaria et al. as using chitosan in paper coating examples enhanced the paper strength and ductility [313]. On the other side, the elongation at break remained unchanged (below 3%) for the base paper and all the coating formulations (**Figure B1**). This indicates that the coating film did not have a major impact on the flexibility of the paper substrate (**Figure B2**). Türe et al. also reported that wheat gluten/montmorillonite clay as coating did not affect the elongation at break compared to the paper substrate [314]. In the case of elastic modulus, the NR coating alone slightly reduced the modulus noted for the base paper (**Figure 5.6(b)**). This is not surprising as NR has high elasticity and inferior modulus. With the incorporation of the MCG in the formulation, improvement in modulus was noted. This was because the MCG can interact with the cellulose paper fibers and potentially form a

strong interlock along with covering the paper voids, consequently promoting the resistance against deformation. Likewise, Tanpichai et al. noted an increase in the modulus after applying chitosan to the paper substrate [315].

Wet strength provides better insight for assessing the coated paper's strength when in contact with water, and this is a condition that food packaging undergoes frequently. Overall substantial reduction in the wet tensile strength was noted compared to the dry tensile strength. This can be explained by the fact that this method was carried out by submerging one side of coated specimens in water, which allows water to penetrate, soak, and weaken the paper fiber's physical interlocks, disrupting the structural integrity of the paper. It was noted that both the wet modulus and wet strength of the paper are enhanced by applying the coating, as highlighted in **Figure 5.6(c-d)**, respectively. This can be ascribed to the shielding of the paper fibers from penetration via the water of the NR latex in conjuncture with strong interlocking between the MCG and paper fibers and hydrogen bonding which preserve the paper from water damage.

Furthermore, occupying the pores via the MCG particles reduces the water diffusion space. This is in agreement with previous results with the use of chitosan as a coating that led to enhancement in wet strength of paper [182]. Nevertheless, a reduction in the wet strength and modulus was observed at higher MCG loading, attributed to the hydrophilicity of MCGs. Moreover, the agglomeration of MCGs at higher loading can leave behind unfilled spots for water diffusion. Additionally, higher MCG loading means less NR in the formulation that provided much of the moisture attack.

5.3.6.2. Adhesion Strength

The adhesion strength of the NR/MCG formulated coating to the base paper was probed by measuring the required force to peel off the coating from the paper, as shown in **Figure 5.6(e)**. Incorporating the MCG into the coating formulation brought about greater adhesion between the coating film and the paper, as displayed in **Figure 5.6(f)**. Also, increasing the concentration of the MCG positively correlated with the adhesion strength. At 25 wt.% loading content of the MCG, the adhesion strength almost doubled compared to the pure NR coating. These results were attributed to the great compatibility between the MCG and the cellulose fibers and the formation of strong bonds among the -OH functional groups. This trend is in complete agreement with previous observations [316–318].

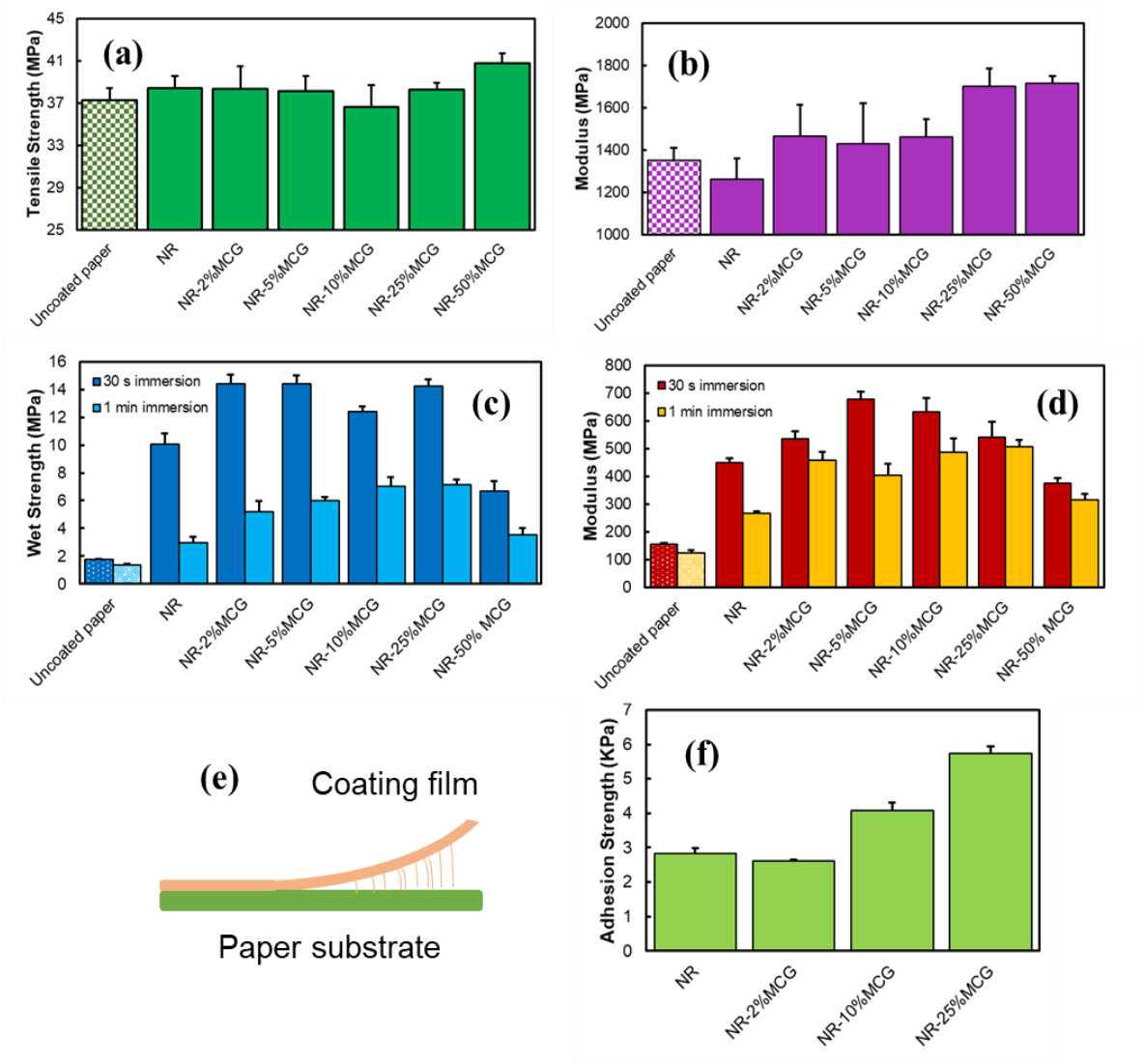

Figure 5.6. Tensile and modulus properties of paper coatings: a) dry tensile strength, b) dry elastic modulus, c) wet strength, d) wet modulus, e) schematic of adhesion strength analysis, f) adhesion strength of paper coatings.

Barrier Properties

5.3.7. Cobb test

5.3.7.1. Water Cobb Test

The water Cobb value has a reverse correlation with water barrier performance, and it was used here to assess the effect of the various coating formulations on the water absorption of the paper after 120 seconds of exposure. As depicted in **Figure 5.8(a)**, the uncoated paper substrate has high water Cobb value due to the paper's hydrophilicity. Applying the NR coating has considerably reduced the water Cobb value. Despite the hydrophilicity of MCG and its tendency to absorb water, a reduction in the water absorption was noted with the use of the NR/MCG coatings. This can be attributed to the high affinity of the rigid filler particles to the cellulose fibers filling the pores that subsequently impede water diffusion. The incorporation of 2 – 10 wt.% MCG in the formulation dramatically reduced the water absorption by roughly 99.5% compared to the untreated paper. This trend is consistent with a study of chitosan as a paper coating; however, the water absorption has dropped only by 12% compared to the paper base, which is far lower than the NR/MCG formulated coating [319]. However, with further addition of the MCG, the water absorption has increased, which can be associated with the agglomeration of the fillers within the NR coating, leaving some areas susceptible to the passage of water molecules. Moreover, beyond a certain critical limit of the MCG concentration, the hydrophilicity associated with its –OH moiety will be significant and expected to contribute to the overall water absorption of the coated paper.

5.3.7.2. Oil Cobb Test

The oil Cobb test was performed on the coated papers to determine absorption resistance to canola oil. The coatings, which effectively blocked the paper's pores as noted

from the SEM images, resulted in reduced oil absorption, as shown in **Figure 5.8(b)**. Additionally, as the concentration of the MCG increased, a progressive enhancement in the oil barrier property has transpired. This observation can be attributed to the high polarity of MCG as well as the filling of the pores between the cellulose fibers, which induced a tortuous path for oil molecules to diffuse through the paper coating. To emulate the real-life applications of the coated papers, food boxes were made of uncoated, NR-coated, and NR-10% MCG-coated paper samples. Then oily rice obtained from a local grocery store was placed in the boxes, and the oil leaching towards the backside of the paper was monitored for 24h. As exhibited in **Figure 5.7**, the best oil barrier performance was achieved using NR-MCG paper coating, in which almost no stain appeared after 24h.

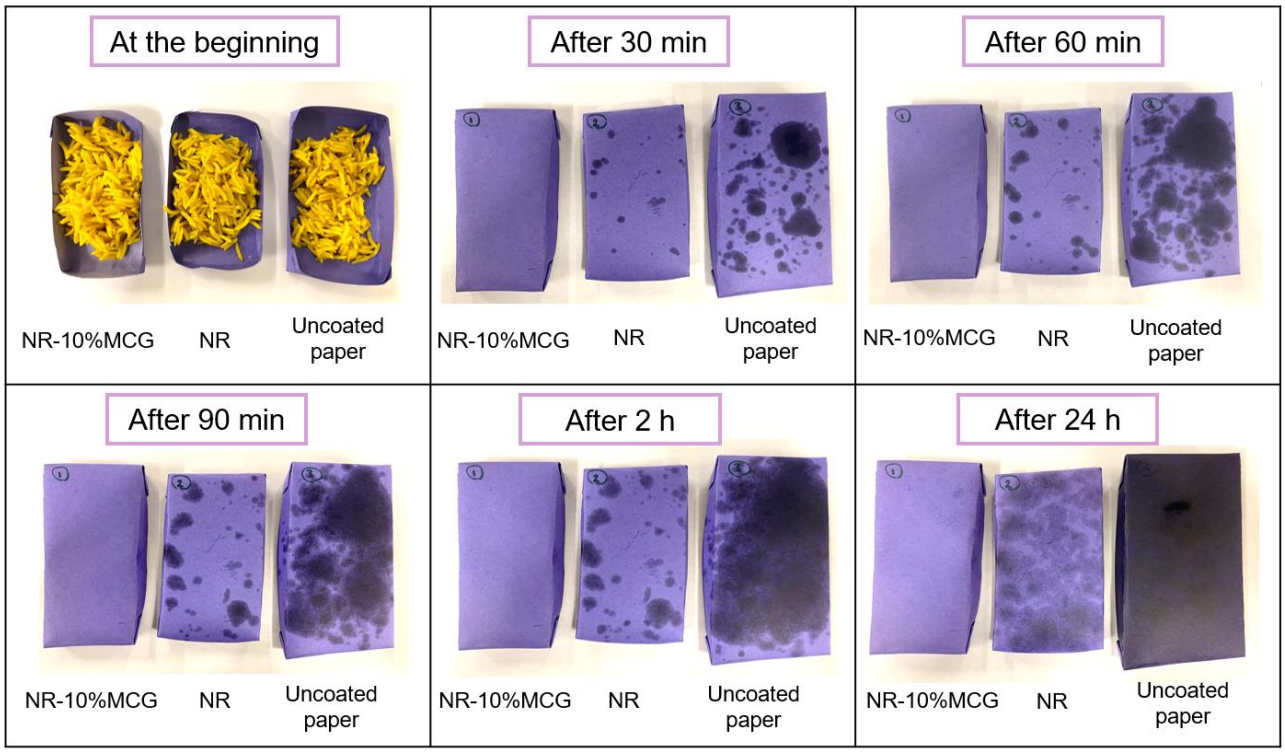

Figure 5.7. Oil barrier performance of paper coating samples.

5.3.8. Kit Test

The kit test is one of the most common methods to examine the grease resistance of coated papers. As shown in **Table 5.2**, the lowest kit value belongs to the paper substrate, which strengthens the fact that the paper base contains many voids. Also, applying NR coating on the paper improves its grease barrier but not sufficiently since NR is an oleophobic material. However, the introduction of MCG in the coating formulation has increased the Kit value dramatically, and it is noteworthy to mention that it achieved the highest Kit number possible (Kit value 12) at 5 wt.% of MCG (**Figure B3**). The MCG presents hydrophilic characteristics along with great affinity towards the base paper's cellulose fibers resulting in the effective closure of the pores, and hence meeting the criteria for being a great grease resistance material.

Moreover, the platelet morphology of the MCG particles is the other important factor that plays a vital role in oil barrier properties as the rigid platelet filler formed a complex route for grease molecules to penetrate the coated paper. The trend indicated that NR alone is not adequate to provide the required grease resistance, and its combination with the MCG has successfully brought superior grease resistance for the coated paper. This trend agrees with the results reported by S. M. Mazhari Mousavi et al. [283] and Fein et al. [177] where cellulose nanofibril (CNF) enhanced the grease resistance of paper coating materials.

Table 5.2. Kit number of NR/MCG coated papers.

Coating composition	Uncoated paper	NR	NR-2%MCG	NR-5%MCG	NR-10%MCG	NR-25%MCG	NR-50%MCG
Kit number	0	4	6	12	12	12	12

5.3.9. Moisture Barrier Property

The moisture barrier is one of the most crucial features of food packaging since the products are exposed to moisture frequently. The degree of resistance opposing the water vapor transmission through the coated paper was investigated using the water vapor permeability test (*WVP*). The temperature and relative humidity were maintained constant throughout the experiment as these two factors dramatically affect the *WVP* [145]. As displayed in **Figure 5.8(c)**, the inherently hydrophobic NR as a coating layer assisted in mitigating the moisture adsorption and significantly reduced the *WVP* across the coated paper. However, as anticipated, as the concentration of the MCG increased, the moisture diffusivity gradually increased as well. This phenomenon is attributed to the hydrophilic nature of the MCG, which creates permeable routes for transmission of moisture and makes the paper coating susceptible to water vapor attack. The increment in *WVP* by the addition of the MCG is in line with the previous results [320], in which utilizing thermoplastic starch as a component of a barrier film led to significant moisture transmission, resulting in the generation of sensitive films to water vapor attack.

5.3.10. Oxygen Permeability

The oxygen barrier is also among the most vital properties that dictate the applicability of the coatings for food application. This is because oxygen has a deteriorating impact on the oxidative stability and rancidity of food products. Thus, there is a great desire to prevent oxygen permeation through packaging films and coatings to ultimately prolong the shell life of food. Therefore, the oxygen barrier performance of the formulated NR/MCG coating was

evaluated. As shown in **Figure 5.8(d)**, utilizing NR as coating exhibited a minimal improvement in the oxygen permeability (OP) of the paper substrate.

On the other hand, introducing the MCG into the coating formulation enhanced oxygen barrier performance. It appears that 5 wt.% MCG loading is the optimal concentration, and it has reduced the oxygen permeation more than 14 times compared to the pure NR coated paper. This behaviour is because of the high crystallinity of MCG, with about 85% [44,165] accrued from inter-and intramolecular hydrogen bonding, which comes with a more packed layer within a coating (**Figure 5.8(f)**). These values corroborate well with previous results by using polar additives, such as wheat gluten [166], microfibrillar cellulose and shellac [167], and regenerated cellulose [151]. Overall, embedding the highly crystalline and polar MCG particles in the NR formulation provided an improved oxygen barrier.

Relative humidity is one of the dominant elements in determining the OP of packaging materials. Hence, in this approach, the OP test was carried out at varying relative humidity levels, i.e., 15%, 30%, 60%, and 100%, to have a better perspective of its influence on the oxygen permeation of the coated paper. As shown in **Figure 5.8(e)**, surprisingly, increasing relative humidity led to a statistically significant enhancement in the oxygen barrier property (**Table B1**). This unexpected behavior might be attributed to the adsorption of water to the MCG as well as cellulose fibres, resulting in the filling of the remaining voids and creating a more complex path for oxygen molecules to diffuse through (**Scheme 5.2**). Also, the strong interlock between the MCG and the cellulose fibers likely causes the reluctance of the coated paper to swell. The unexpected behavior noted in this study is consistent with previous results

[108], in which a higher humidity had a positive effect on the barrier performance of the NR/alpha-1,3 glucan paper coating. It is anticipated that hydrogen bonding, as well as the encapsulation of the water vapor around alpha-1,3 glucan particles and paper substrate, can be the major reasons for lower OP at higher humidity. While the result is reproducible and the observed enhancement in oxygen barrier at higher moisture is statistically significant ($p < 0.05$), it requires further detailed and focused investigation to confirm the suspected mechanism.

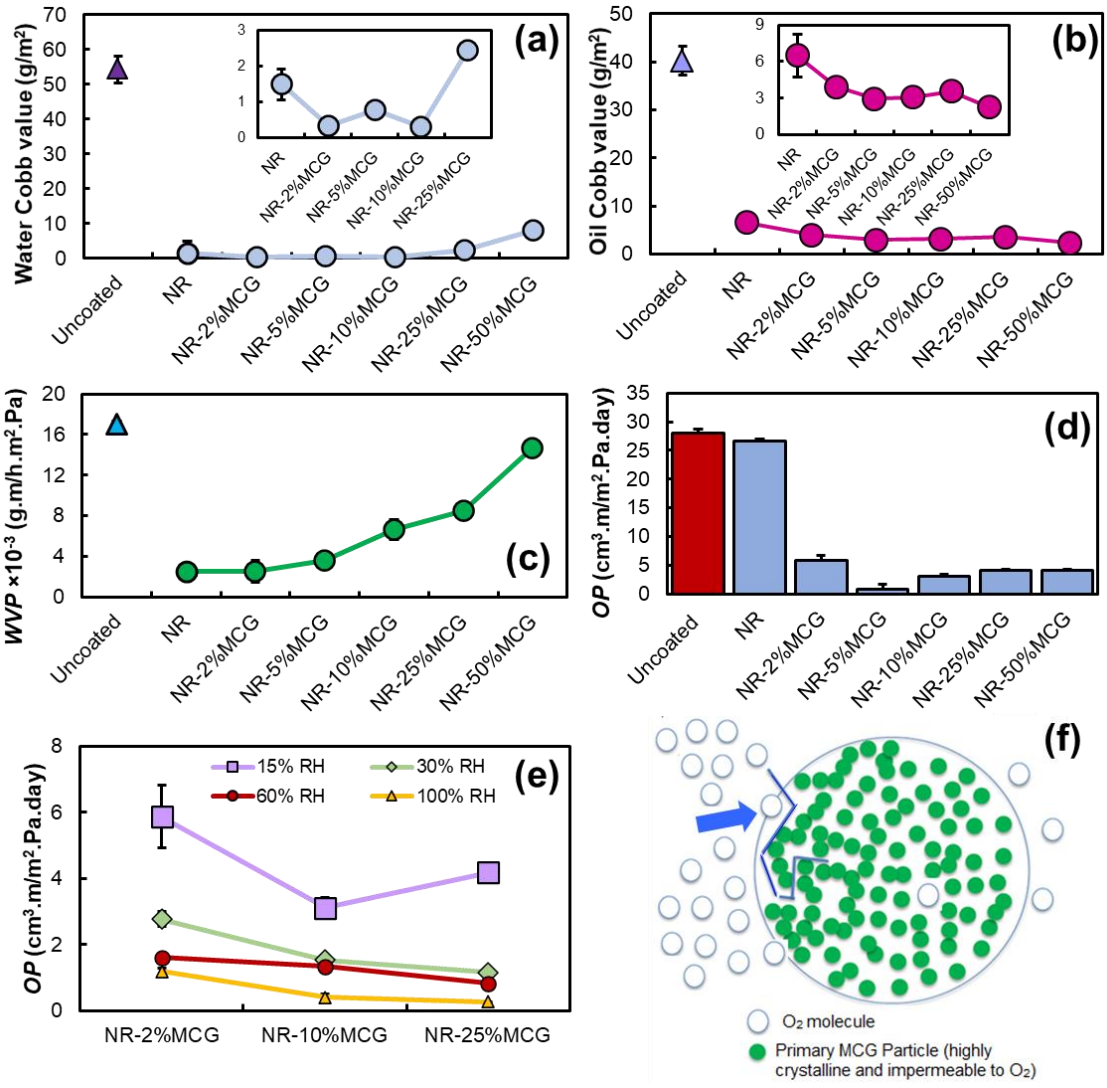

Figure 5.8. (a) water Cobb test, (b) oil Cobb test, (c) water vapor permeability, (d) oxygen permeability of NR/MCG coated paper, (e) oxygen permeability at different initial moisture content at 22 °C of NR/MCG coated paper, (f) schematic of the tortuous path of oxygen permeation through the MCG filled coating formulation.

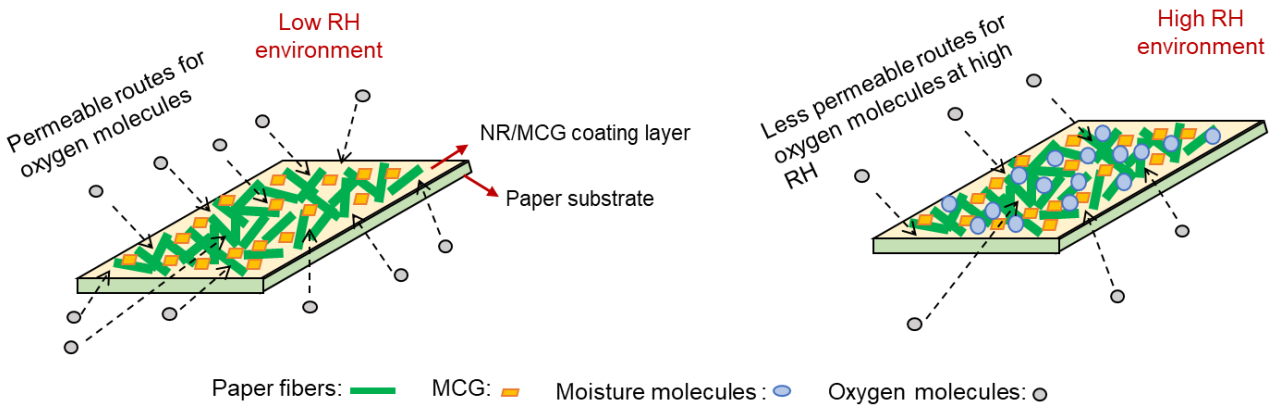

Scheme 5.2. The mechanism of penetration of oxygen molecules at low and high RH environment.

5.3.11. Effect of Solid Content on the Barrier Properties

To examine the effect of solid content, NR/MCG coating with 40 wt.% solid content was prepared in selected formulation ratios. For the fabrication of the coating, one layer of coating was applied on the paper to obtain 20 μm thickness, while for 20 wt.% solid content, two layers were applied on the paper. Also, the grammage of the high solid content formulation was calculated and considering the standard deviation, the grammage did not change compared to the 20 wt.% solid content samples. In spite of the application of a single coating layer of high solid content coating samples, the samples indicated relatively similar oil Cobb and WVP values to the lower solid content counterparts with two layers, as displayed in **Figure 5.9(a-b)**. However, a slight reduction in the OP results with the high solid content paper coating was noted in comparison to the lower solid content specimens. This trend agrees well with OP results of cellulose nanofiber/carboxymethyl cellulose blend as a paper coating[106].

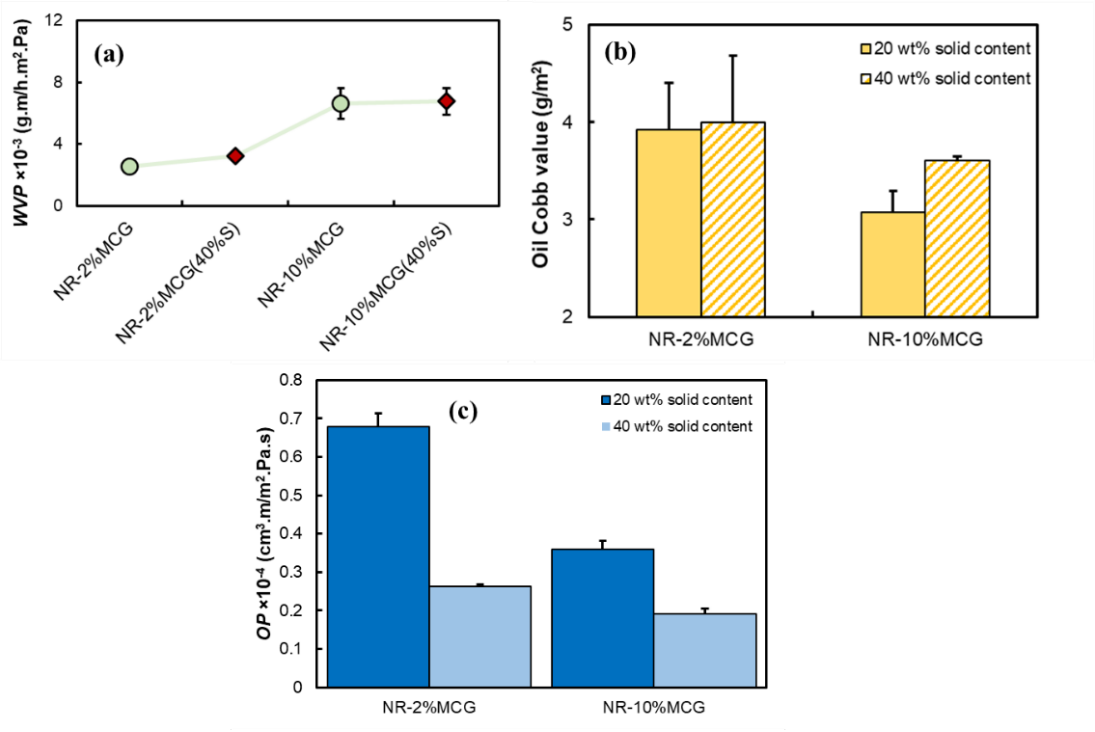

Figure 5.9. a) Water vapor permeability, b) oil Cobb test, and c) oxygen permeability of paper coatings with varying the solid content of coating formulations.

5.3.12. Effect of Crosslinking on the Paper Coating Properties

The effect of NR crosslinking was explored on the mechanical and barrier properties of NR/MCG formulated coatings. The crosslinking density was kept low (~ 4 mmol/g) by controlling the concentration of the crosslinking agent and catalysts to ensure the coating films are only lightly crosslinked by following previously published work [165]. As expected, the dry tensile strength of the crosslinked samples improved in comparison to the uncrosslinked counterpart (**Figure 5.10(a)**). However, the crosslinking reduced the wet strength, making the observation more noticeable at 30 s immersion (**Figure 5.10(b)**). This could be attributed to the crosslinking process that involved exposing the coated paper to a reasonably high

temperature (100 °C for 2 h) with a risk of deteriorating the integrity of the cellulose fibers and other additives (e.g., starch additives) in the paper resulting in the observed reduction in the tensile properties. The WVP results are displayed in **Figure 5.9(c)**, showing that the crosslinked coated paper enhanced the moisture barrier property compared to the uncrosslinked sample. This is suspected to be due to the formation of -S-S- bridging bond that further hinders moisture diffusion. It is noteworthy to mention that the degree of enhancement rises as the concentration of the MCG increases indicating the complementary benefits of the platelet MCG and the -S-S- bridging bonds. These results are in good agreement with previous works of crosslinked soy, and whey-protein coated paper [80] as well as a crosslinked starch paper coating [321].

Furthermore, both the water Cobb value and oxygen permeation dropped significantly as crosslinking bonds were introduced in the coating films, as shown in **Figure 5.10(d)** and **5.10(e)**, respectively. Outstanding oxygen barrier performance with a permeation of only 0.16 $cm^3.m/m^2.Pa.day$ was achieved in the 25 wt.% MCG formulation. This was a 99.4% decrease from the samples coated with only NR. Herrera et al. reported the positive influence of crosslinking of nanocellulose on the barrier properties of the paper coating [162]. Other researches have also shown improvement in the oxygen barrier and reduction in the water absorption of crosslinked rubbers [12,249,322,323]. Also, the Kit values of the crosslinked coating systems exhibited excellent grease barrier properties using as low as 2 wt.% MCG concentration, as shown in **Table 5.3**. These observations are suspected to be mainly due to the reduction of the rubber free volume and lack of diffusion route due to the crosslinking bridges. Overall, the crosslinked paper coatings revealed remarkable barrier properties, which

makes the formulated NR/MCG a viable candidate for food packaging applications. While the crosslinking could impact the rate of disintegration and biodegradability of a NR based formulation, it may enhance re-pulping steps and the overall recycling of the paper-based packaging product potentially allowing for recovery of the rubber phase. This is because the lightly crosslinked rubber is less sticky than the green rubber making it easily separable.

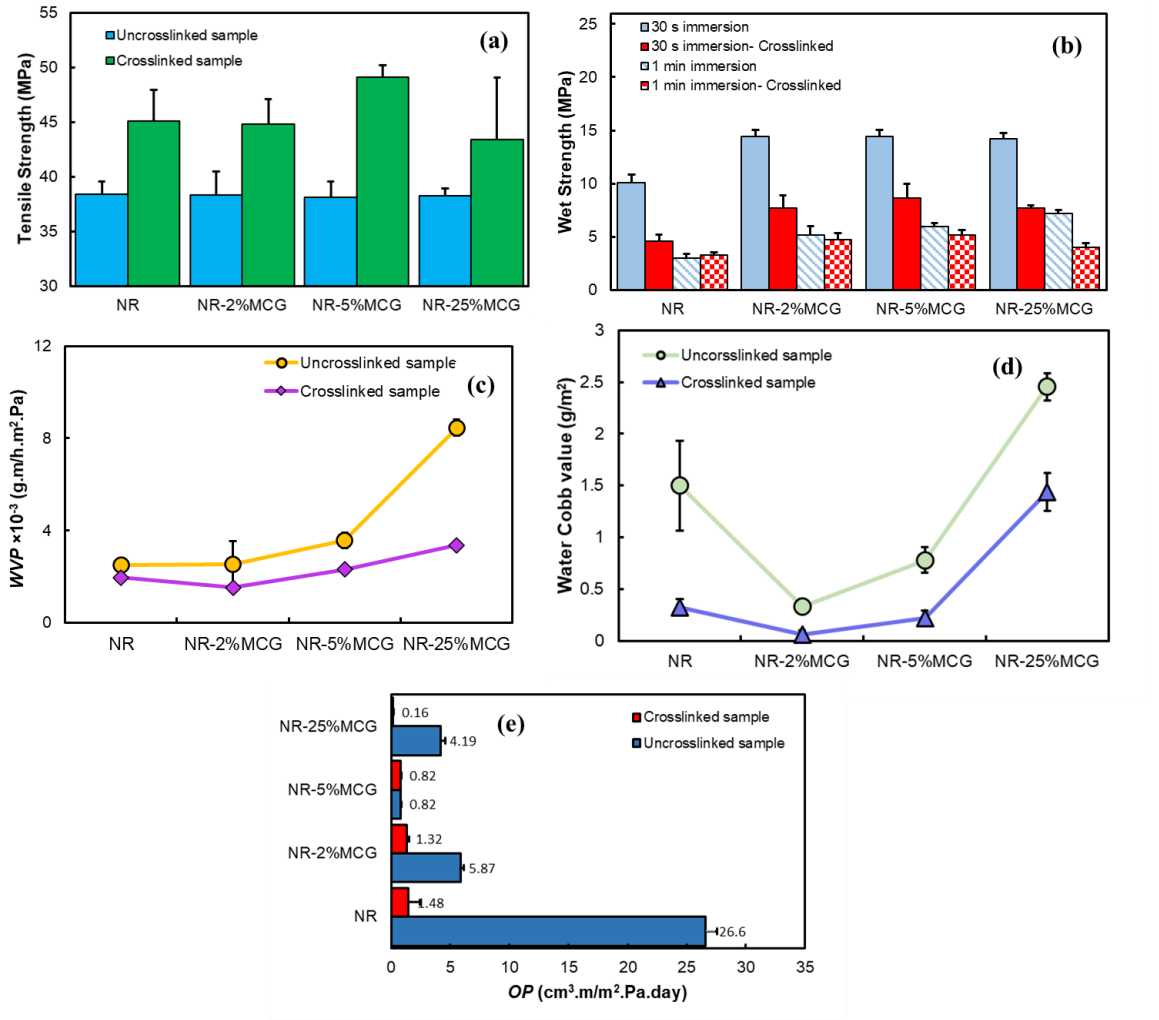

Figure 5.10. a) Dry tensile strength comparison of crosslinked NR/MCG and uncrosslinked NR/MCG coating, b) wet strength of comparison of crosslinked NR/MCG and uncrosslinked

NR/MCG coating, c) water vapor permeability comparison of crosslinked NR/MCG and uncrosslinked NR/MCG coating, d) water cobb test comparison of crosslinked NR/MCG and uncrosslinked NR/MCG coating, e) oxygen permeability comparison of crosslinked NR/MCG and uncrosslinked NR/MCG coating.

Table 5.3. Kit values of crosslinked NR/MCG coating.

Paper coating composition	Kit number
Crosslinked NR	8
Crosslinked NR-2%MCG	12
Crosslinked NR-5%MCG	12
Crosslinked NR-25%MCG	12

5.4. Concluding Remarks

The MCG derived from enzymatic polymerization of glucose from sucrose have a high surface area, low density, and high crystallinity with a typical platelet morphology. This additive was utilized in natural rubber (NR) based coatings with the goal of assessing potential applications as food packaging materials. The mutual colloidal stability of the MCG in the NR phase assisted in the excellent dispersion stability and compatibility of the MCG in the NR coating formulation. Formulated NR/MCG coatings improved both the dry and wet strength as well as modulus compared to the uncoated paper substrate without compromising the flexibility of the coated paper. Also, the incorporation of MCGs in the NR formulations led to strong adhesion strength of coating films to the paper substrate due to the high affinity of the

MCGs to the paper fibers – this suggests that only one coating will be required in this process and avoids the need for additional adhesive layers. The series of coatings investigated in this study indicated outstanding oil, grease, and oxygen barrier properties with a good compromise regarding water vapor and water barrier performance. By introducing a light crosslinking in the paper coating formulations, further enhancements in barrier properties were achieved. Overall, the developed NR/MCG paper coating systems provide good mechanical and barrier properties, which should meet the requirements for many product categories in the food packaging market. This may enable the utilization of paper-based packaging formats to replace traditional thermoplastic resin-based solutions. The approach described here may also offer a multitude of crucial barrier performance characteristics required for the viable shelf-life performance of packaged goods from one single coating step on the base paper substrate compared with incumbent, multilayer complex flexible packaging solutions. This alone provides an exciting opportunity to enable a sustainable paper-based packaging material alternative that is inherently based on renewable feedstocks, recycle-enabled, and biodegradable within various food-contact environments.

Chapter 6. Sustainable natural rubber composites: masterbatch development of epoxidized natural rubber grafted to designed enzymatic polysaccharides [5]

6.1. Introduction

Rubber products are essential and high-performance materials that have extensive industrial applications. Natural rubber (NR) is a biopolymer that occupies a substantial portion of the high-value rubber market and continues to be essential for key industrial applications. Tuning NR's properties and utility in composites continue to drive innovation for more widespread utilization of this high-performance biopolymer. At the same time, sustainable sourcing of natural rubber receives increasing attention within a bio-circular economy. The utilization of NR, in its original, not-reinforced form, is rare and limited due to its large free volume and inferior performance as material. Therefore, introducing appropriate reinforcements and a crosslinking (vulcanization) process is crucial to obtain optimal physico-mechanical properties and chemical resistance [3]. Carbon black remains dominant and has been the pioneer of reinforcing fillers in the rubber industry [9]. However, carbon black is typically manufactured using a high energy-consuming production process, and typically using petroleum tar as a feedstock. The overall greenhouse gas footprint for this material category is considered significant and has been classified as a material of high energy impact in need of

[5] A version of this chapter has been published on peer-reviewed journal as a review article: A. Adibi, et al. (2023). Sustainable natural rubber composites: masterbatch development of epoxidized natural rubber grafted to designed enzymatic polysaccharides. *Materials Chemistry Frontiers*. https://doi.org/10.1039/d3qm00080j.

alternative material solutions[8]. Other filler systems such as silicas, calcium carbonate, clay, talcum, or titanium dioxide are also used as alternative or partial substitutes for carbon black in rubber composites with varying success[12]. However, typically these fillers are considered non-reinforcing, while the true performance of a reinforcing filler is achieved through direct interaction between filler and elastomer matrix.

The rubber industry is increasingly assessing the development of rubber composites that incorporate various sustainable fillers as alternatives without compromising reinforcement performance, in addition providing energy savings during processing and overall composite weight reduction. In parallel, the interest for replacing or complementing carbon black with sustainable fillers is to improve or reduce the overall environmental footprint of the composite. Sustainable filler systems derived from biomass or through the conversion of biomass in biological processes are appealing alternatives to replace or complement carbon black, silicas, or higher-density mineral-based fillers.

Polysaccharides are receiving increasing attention as sustainable filler of rubber goods due to their potential to provide reinforcing properties, relatively low density compared with mineral fillers, and ease of chemical modifications to create a link between the filler system and the elastomer matrix. Several polysaccharides have been reported as reinforcing fillers of natural rubber and other elastomers in the literature, including cellulose nanocrystals [39,324,325], chitin nanowhiskers [40], starch nanocrystals [41], cellulose fiber [326–328], microcellulose [329].

IFF has developed a biocatalysis process to enable access to designed enzymatic biomaterials such as the polysaccharide alpha-1,3 glucan (glucan). The glucan material isolated from the enzymatic polymerization process provides access to particles with controlled morphology. The polymerization of glucose from sucrose in the presence of an enzyme catalyst selected from the general class of glucosyltransferase (GTF) enzymes has been developed to industrial scale [38,49,108]. The glucan generated as such is a water-insoluble, linear, semi-crystalline polysaccharide (50-70% crystallinity) with a typical degree of polymerization of 800 repeat units with a polydispersity in the range of 1.7-2.0 [44,281]. Also, through the engineered polymerization processes, different morphologies are accessible, including spherical aggregates, fibrids, and platelet particles referred to as microcrystalline glucan (MCG) (**Scheme 6.1**)[52].

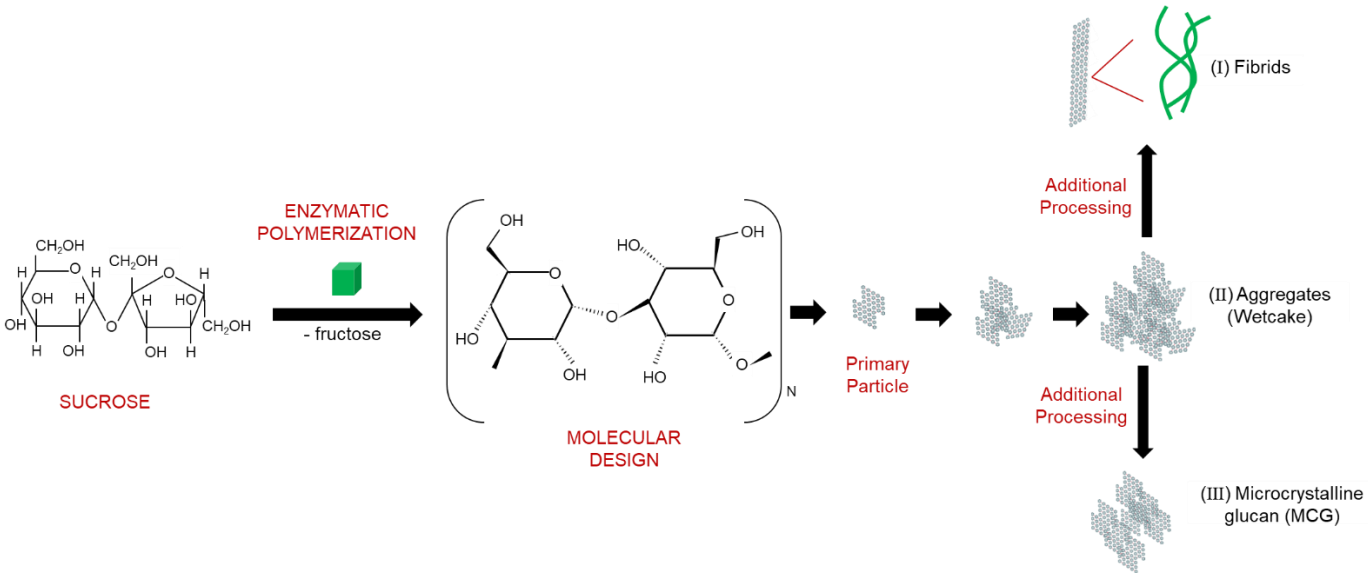

Scheme 6.1. Schematic of enzymatic polymerization of glucan and its various morphologies.

In order for fillers in rubber to fully demonstrate their reinforcement potential, both strong interfacial interactions and effective dispersion of the fillers in the matrix are essential [330]. The hydrophobic NR matrix is typically incompatible with hydrophilic fillers including polysaccharides and as a result, the weak interfacial interactions between the rubber matrix and the fillers provide an inferior reinforcing effect [331]. Thus, in order to address the compatibility limitation of a polysaccharide such as glucan with NR, modifying the glucan with macromolecules that are compatible with rubber is proposed in this study. For this, epoxidized natural rubber (ENR), obtained by epoxidizing natural rubber (NR) under acidic conditions was selected as the modifier of glucan [331]. This is because ENR is compatible with NR and the epoxide functional group of ENR can react with the -OH moieties of glucan through ring-opening etherification to generate ENR – grafted glucan [332–334].

Additionally, the oxygenous groups of ENR make it more polar than NR, allowing it to be more compatible with polar fillers, such as glucan. For instance, the improved compatibility of ENR with polar fillers including cellulose nanocrystals [335–338], lignin [339], silica[331,340], clay [341], starch [342], and chitosan [343] to fabricate ENR composites is reported. In this study, a high temperature and shear-mediated reaction of the oxirane group of ENR with the electronegative hydroxyl groups of glucans via a ring-opening reaction to form covalent grafts is investigated.

A solvent free, batch mixer-based reactive process was employed to carry out the reaction of ENR with glucan. The effect of the use of additives such as peroxide and alkaline environment on the reaction efficiency was evaluated. By using the optimized processing parameters identified in this first part of the study (temperature, shear rate, reaction time,

catalyst level), next an ENR – glucan masterbatch was produced. Notably the temperature was selected based on preliminary optimization work. Temperatures ranging from 115 °C to 200 °C were investigated. The higher ranges caused degradation of the material whereas the lower temperatures were not even sufficient to cause any reaction. And since there is no solvent in the system, high temperature in conjuncture with shear are needed to achieve the desired grafting. Spectroscopy, rheology, mechanical properties, and solvent swelling studies were employed to evaluate the properties of the generated masterbatch. Subsequently, the masterbatch prepared this way (one-to-one ratio of glucan to ENR, by weight) was employed as a modified filler for cured natural rubber formulations. The properties of such a cured and reinforced rubber system with and without the masterbatch filler was then evaluated to elucidate the performance of the generated masterbatch. Remarkably, an important insight of this work is that the batch mixer-based reactive process is a solvent-free, scalable, and mature technology broadly deployed in the rubber industry. In addition, the generated ENR – glucan masterbatch provided excellent property enhancement in the cured NR formulation. Thus, it can be anticipated that the masterbatch production approach to enhance the dispersion of glucan in rubber formulations can be appealing for commercial deployment in a range of highly cured rubber products, including conveyor belts, footwear, automotive parts, seals, and gaskets, etc.

6.2. Materials and Methods

The alpha-1,3 glucan referred to here as glucan, that is produced via enzymatic polymerization of sucrose was obtained from International Flavors & Fragrances Inc. (IFF, Wilmington, DE, USA). Bale ENR, 50% epoxide content, was obtained from Muang Mai

Company Ltd (Muang, Thailand). Sodium hydroxide (NaOH), dicumyl peroxide (DCP), zinc oxide powder (ZnO), and stearic acid were purchased from Sigma -Aldrich (Oakville, ON, Canada). Stabilized natural rubber (NR) latex with 60 wt.% solid content, was provided by Chemionics Corporation (OH, USA). N-tert-Butyl-2-benzothiazolesulfenamide 97% (TBBS), calcium carbonate ($CaCO_3$), and Sulphur were purchased from Fisher Scientific (ON, Canada). Silica was purchased from GELEST. INC. (Morrisville, PA).

6.2.1. Preparation of ENR-glucan Master-Batch

The ENR-glucan masterbatch was prepared in a HAAKE Rheomix 3000 batch mixer/extruder (Thermo-Fisher Scientific Inc., Waltham, MA, USA) at a mixing temperature and screw speed of 160 °C (across three heating zones) and 80 rpm, respectively. The batch-mixing process was carried out using two catalysts, NaOH (7 % (w/v) solution) and DCP. The procedure was initiated by adding 100 g of ENR into the batch mixer. Glucan powder (100g) was then gradually added, and the blend was mixed until constant torque was developed as depicted in **Figure 6.1.** Then, a specified amount of catalysts (NaOH or DCP), as shown in **Table 6.1**, was incorporated into the composition, and the reaction was conducted for 5 mins (**Figure C1**). After the mixing was completed, the samples were quickly removed from the batch melt compounder and cooled with forced air to terminate the reaction. The control formulations (neat ENR, ENR-glucan blend) were also prepared without the use of any catalyst by utilizing the aforementioned procedure. Also, the ENR master batch was prepared with silica and $CaCO_3$ for comparison (**Table 6.1**).

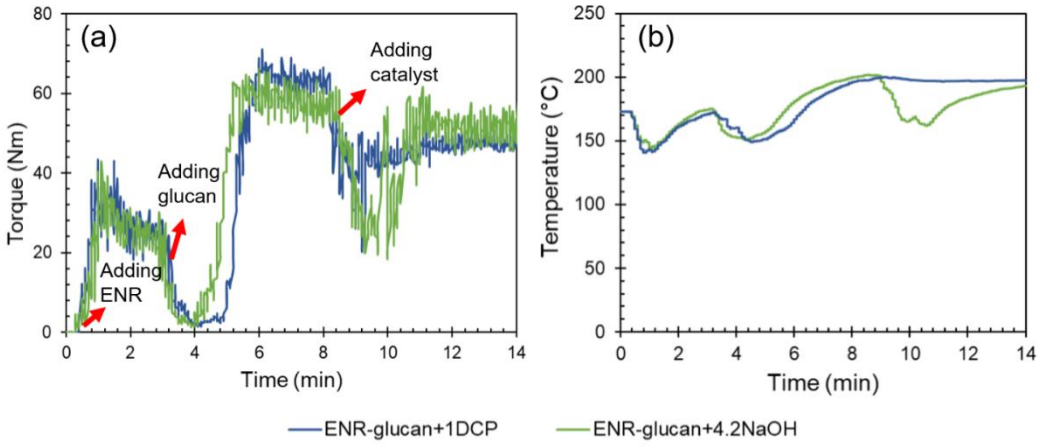

Figure 6.1. (a) Torque and (b) temperature progress with the batch mixing process time for ENR-glucan+1DCP and ENR-glucan+4.2 NaOH.

Table 6.1. Formulation of ENR-glucan masterbatch blend.

Components	**Glucan formulations (parts per hundred (phr))**	**Silica formulations (parts per hundred (phr))**	**$CaCO_3$ formulations (parts per hundred (phr))**
ENR	100	100	100
Glucan	100	0	0
DCP	0, 0.1, 0.5, 1	0	0
NaOH	0, 1.4, 2.8, 4.2	0	0
Silica	0	100	0
$CaCO_3$	0	0	100

6.2.2. Characterization of ENR-glucan Masterbatch

6.2.2.1. Fourier Transform Infrared Spectroscopy (FTIR)

FTIR (Thermo Nicolet Nexus 670 FTIR-ATR) spectra were obtained by placing the samples on the ATR and collecting an average of 32 scans.

6.2.2.2. X-ray Photoelectron Spectroscopy (XPS)

The surface chemistry of the blends, along with the influence of glucan and catalysts on the functional groups of the blends, was investigated using a ThermoScientific ESCALab 250 X-ray Photoelectron Spectrometer (XPS). Samples prepared as small cubes (5 mm x 5 mm x 4 mm) were used for the XPS analysis. CasaXPS software was employed to extract and analyze the collected spectra.

6.2.2.3. Toluene Swelling

The swelling index of the masterbatch blends was evaluated by the toluene swelling method. About 0.5 g samples were taken from each formulation and were accurately weighed and submerged in toluene for 72 h. The final weight of each sample was recorded by wiping the excess toluene off the surface, and the level of swelling was investigated by computing the swelling index (SI) in accordance with Equation (6.1). Where W_1 (g) and W_2 (g) are the weight of the samples before and after submerging in toluene, each specimen was tested in triplicates, and the average SI is calculated.

$$SI = \frac{W_2 - W_1}{W_1} \tag{6.1}$$

6.2.2.4. Injection Molding of ENR-glucan Samples

To prepare tensile and rheology (disc) test specimens, the various formulations were injection molded using a Haake Mini-jet Pro (Thermo-Fisher Scientific inc., Waltham, MA,

USA). Prior to the test, the samples were dried at 80 ^{o}C overnight to remove any residual moisture. For all the formulations, the molding was carried out with a cylinder temperature, mold temperature, injection pressure, injection back pressure, and injection time, 150 ^{o}C, 30 ^{o}C, 850 bar, 500 bar, and 10 s, respectively, except for ENR and ENR-glucan in which the mold temperature was reduced to 50 ^{o}C.

6.2.2.5. Tensile Property Testing

The tensile properties of the ENR-glucan masterbatch blends were evaluated using a tensile testing unit (Shimadzu-AGS X) equipped with 10 kN load cell. For this, the injection molded ENR-glucan masterbatch samples were tested at room temperature and 50% relative humidity at a crosshead speed of 500 mm/min according to the ASTM D638. At least seven replicates were tested for each formulation, and the average was reported. Furthermore, in order to investigate the degree of interaction and mechanical reinforcement of glucan with the ENR system, silica, and calcium carbonate were utilized as two common reinforcing agents for comparison.

6.2.2.5. Hardness Analysis

The hardness of the masterbatch formulations was tested using a digital durometer (Shore D) in accordance with ASTM D2240. Stacks of specimens with a thickness of about 6 mm were placed on a flat surface and indented with the durometer. As soon as the indentor firmly contacted the specimen, the data was collected from the digital reading. The test was contacted at three points along the stacked samples, and the average was computed and reported.

6.2.2.6. Rheology Evaluation

The rheology of the ENR-glucan masterbatch blends was explored using a parallel plate rheometer (Haake Mars III) under a frequency sweep. Disc-shaped specimens with a diameter and thickness of 25 mm and 2.5 mm, respectively were used for the rheology test. The masterbatches' viscosity, loss modulus, and storage modulus were reported over a frequency range of 0.01 to 100 rad/s.

6.2.3. Fabrication of NR Composites

An ENR-glucan masterbatch blend formulation that displayed high tensile strength and modulus was selected and employed as a filler in a typical NR composite formulation. For comparison, glucan and ENR were also introduced to the NR composite system separately. The NR composites were processed via batch mixing (HAAKE Rheomix 3000) with a rotor speed and temperature of 80 rpm and 50 °C, respectively. The procedure began with adding a specified amount of NR into the batch mixer and masticated until constant torque was achieved which occurred within roughly 3 mins (**Scheme 6.2**). Then calculated amount of glucan or glucan and ENR, or ENR-glucan masterbatch as fillers were gradually added to the NR and mixed for another 4 mins as shown in **Table 6.2**. Finally, the curing agents were added into the batch mixer and processed for 3 mins, and quenched with forced air. The total mixing time of the procedure was 10 mins.

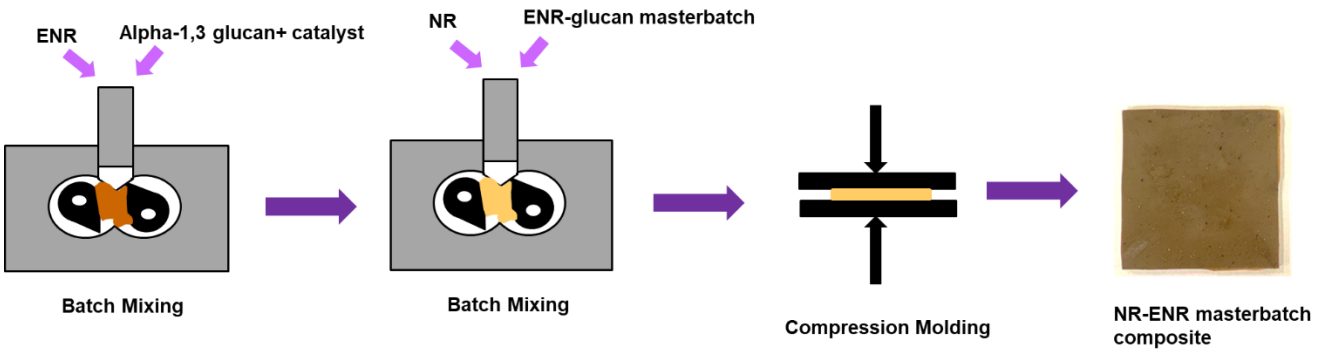

Scheme 6.2. Schematic of fabrication of NR composites.

Table 6.2. Formulation composition for NR composites.

	Sample label			
Composition (phr)	NR (control)	NR-glucan-ENR	NR-glucan	NR-ENR masterbatch
NR	100	80	100	80
Glucan	0	20	20	0
ENR	0	20	0	0
ENR masterbatch	0	0	0	40
Sulphur	1.5	1.5	1.5	1.5
Stearic acid	1	1	1	1
TBBS	1.5	1.5	1.5	1.5
Zinc oxide	3	3	3	3

6.2.4. Vulcanization Process

The vulcanization of all premixed samples was performed in an electrically heated hydraulic press (Carver press, IN, USA) that has a 20 cm × 20 cm platen at 165 ◦C and 14 t

using approximately 22 g of samples. The optimum cure time (T_{c90}) of the NR composites, was determined using a rubber process analyzer (Pioneer MDR 2000) as per ASTM D 2084 as per a previous study [8]. Accordingly, the vulcanization of all samples was carried out on the hot press (T_{c90} = 3.9 min), and the cured sheets were removed from the hot press and dipped into DI water to quench.

6.2.5. Characterization of the NR Composites

6.2.5.1. Crosslink Density

The crosslink density (ν_{cross}) was calculated using toluene swelling data by employing the Flory-Rehner Equation [165,231,232]:

$$\nu_{cross}\left(\frac{mol}{g}\right) = -\frac{ln(1-\nu_r)+\nu_r+\chi\nu_r^2}{2\rho_r V_s\left(\sqrt[3]{\nu_r}-\frac{\nu_r}{2}\right)} \tag{6.2}$$

where ν_r is the volume fraction of the equilibrium swollen rubber, χ is the Flory-Huggins polymer-solvent interaction parameter (0.393), V_s is the molar volume of the solvent (108.56 m^3/mol), and ρ_r (0.97 g/cm^3) is the density of rubber. To calculate ν_r, Equation (6.3) was utilized:

$$\nu_r = \frac{\frac{W_{before}-W_{filler}}{\rho_r}}{\frac{W_{before}-W_{filler}}{\rho_r}+\frac{W_{after}-W_{filler}}{\rho_s}} \tag{6.3}$$

where W_{before} (g) is the weight of the rubber sheet samples before swelling, W_{after} (g) is the weight of the rubber samples after swelling, W_{filler} (g) is the weight of the filler, and ρ_s (0.87 g/cm^3) is the density of the solvent.

6.2.5.2. Scanning Electron Microscopy (SEM)

The morphology of ENR-glucan blends was explored using an Oxford Instruments Quanta FEG 250 Environmental SEM coupled with an energy-dispersive X-ray system (EDX) (Abingdon, Oxon, UK) without any sputter coating. And prior to the test, samples were cryofractured, and the SEM images were taken from the cross-section.

6.2.5.3. Atomic Force Microscopy (AFM)

The surface morphology of NR composites was examined using AFM (ASYLUM Cypher, Pacific Nanotechnology, inc.). Images of samples ($10 \times 10\ \mu m^2$) were taken at a scan rate of 0.5 Hz. The tapping phase mode was used to detect the degree of glucan particle dispersion within the NR matrix.

6.2.5.4. Tensile Testing Analysis

The tensile strength, modulus, and elongation at the break of the NR composites were evaluated via a Shimadzu-AGS X tensile testing unit equipped with a load cell of 0.5 kN and a crosshead speed of 500 mm/min as per ASTM 412. Seven replicates were tested, and the average was reported.

6.2.6. Statistical Analysis

All tests reported in this work are carried out in triplicate and results are reported as mean ± standard deviation. To differentiate significant differences among means, single factor analysis of variance (ANOVA) was employed to the data with a least significant difference (LSD) criteria of 95% ($P < 0.05$) confidence level.

6.3. Results and Discussions

6.3.1. Characterization of ENR-glucan Masterbatch Blends

6.3.1.1. Fourier Transform Infrared Spectroscopy (FTIR)

FTIR was used as a screening tool to investigate the chemical reaction between ENR and glucan, as presented in **Figure 6.2**. Glucan exhibited some common characteristic peaks at 3600-3000 cm^{-1} (O-H stretching), 2900-2800 cm^{-1} (C-H stretching), and 1140 cm^{-1} (C-O stretching) [114,165,241,344]. The control ENR showed peaks at 3000-2800 cm^{-1} (C-H stretching), 1650 cm^{-1} (C=C stretching), and 1452 and 1378 cm^{-1} (C-H deformation) [337,345,346]. The peaks at 872 and 1250 cm^{-1} are attributed to the asymmetrical and symmetrical stretching vibration of the C-O-C of the epoxidized groups in ENR chains [336,338]. For ENR-grafted glucan, an increase in the intensity of the broad peak in the range of 3000-3600 cm^{-1} associated with the OH peaks of glucan is observed. In addition, a new peak at 1140 cm^{-1} depicted an ether group that confirms the formation of chemical bonding between ENR and glucan, which was absent in the neat ENR (**Figure C2**). Also, there is a successive reduction in the intensity of the peaks associated with the epoxy groups in the ENR-glucan blends. Compared to the neat ENR, the adsorption around 872 cm^{-1} of the ENR-glucan samples slightly shifted to a lower wavenumber, which corroborates the formation of intermolecular hydrogen bonds between the hydroxyl groups of glucan and oxygenous group of ENR as illustrated in **scheme 6.3** [332,336]. Similar IR intensities were observed in the study of ENR-regenerated cellulose that indicated the chemical bonds created between ENR and regenerated cellulose [332].

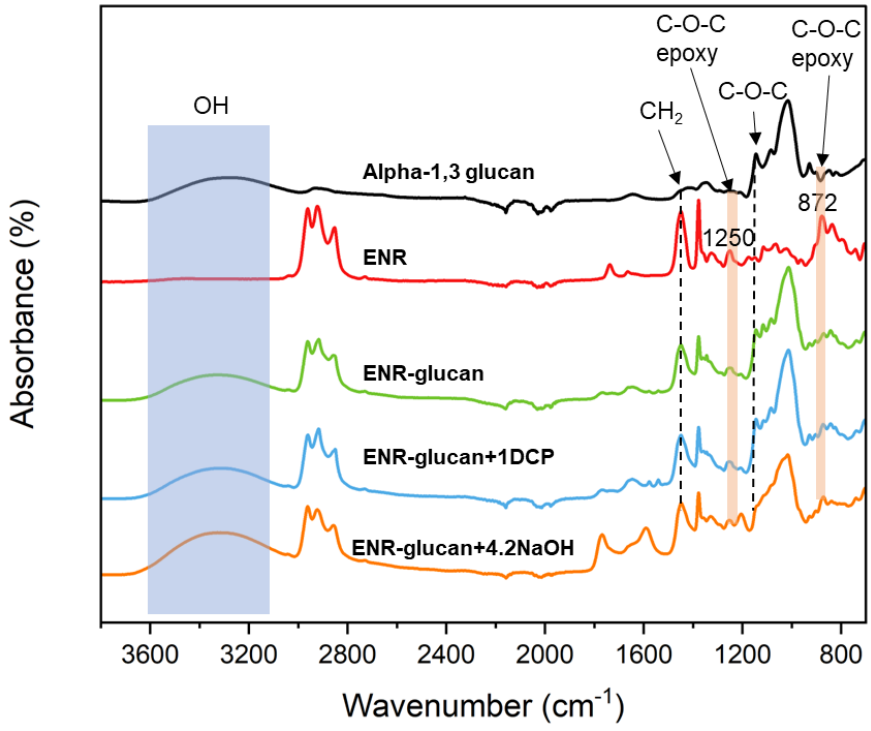

Figure 6.2. FTIR spectra of neat ENR and ENR-glucan composites.

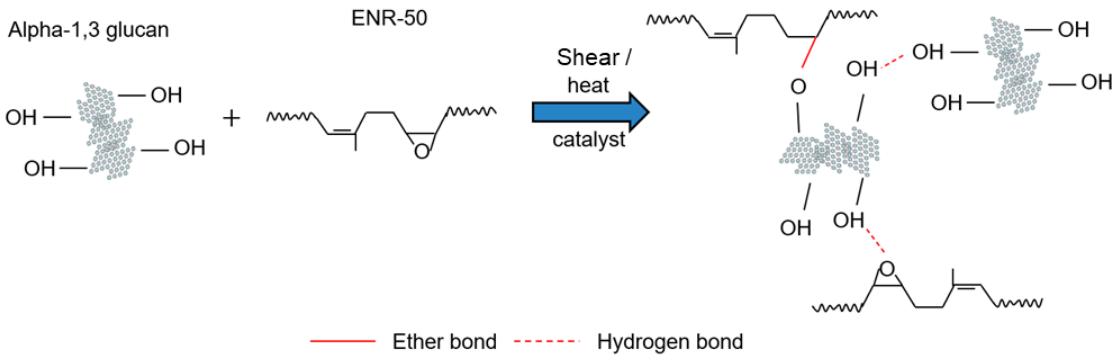

Scheme 6.3. The plausible reaction between ENR and glucan.

6.3.1.2. X-ray Photoelectron Spectroscopy (XPS)

XPS is a powerful technique to investigate the constitution, chemical structure, and the physical and chemical interactions that occur on materials' surfaces or interfaces. The investigation of the C 1s and O 1s spectra of ENR and its masterbatch with glucan was conducted in this study to investigate the interactions between ENR and glucan. **Figure 6.3(a)** and **Table 6.3** show the low-resolution XPS spectra and the atomic contents of different elements in the ENR and ENR-glucan masterbatch, respectively. According to the low-resolution XPS spectra of all samples, peaks at binding energies 103, 281, and 528 eV correspond to Si 2p, C 1s, and O 1s, respectively. Based on the atomic composition in the individual samples in **Table 6.3**, an increase in the O/C ratios for all masterbatch samples indicates the presence of more oxygen-containing groups associated with glucan in the ENR-glucan composites compared to the neat ENR [340,347]. For instance, in the case of ENR-glucan masterbatch without a catalyst, an O/C ratio of 20% was noted due to the high oxygen content of glucan and feasible hydrogen bonds which is in complete agreement with the FTIR results.

Moreover, **Figure 6.3(b-e)** shows high-resolution C1s spectra of neat ENR and ENR-glucan masterbatch, which exhibit four groups: C-C, C-H, C-O-C, C=C, and C=O. Neat ENR showed a broad C-O-C peak, which became narrower for ENR-glucan without using a catalyst, which could be a result of the participation of C-O-C in hydrogen bond formation. It was noted that the C-O-C peak for the ENR-glucan using DCP and NaOH as catalysts remained broad and convoluted. This indicated that although these groups took part in hydrogen bond formation, more C-O-C bonds were generated from the epoxy ring opening and subsequent

ether bond formation [337]. Therefore, these results provide further evidence that grafting has occurred between the ENR and glucan, which was previously observed by FTIR measurements.

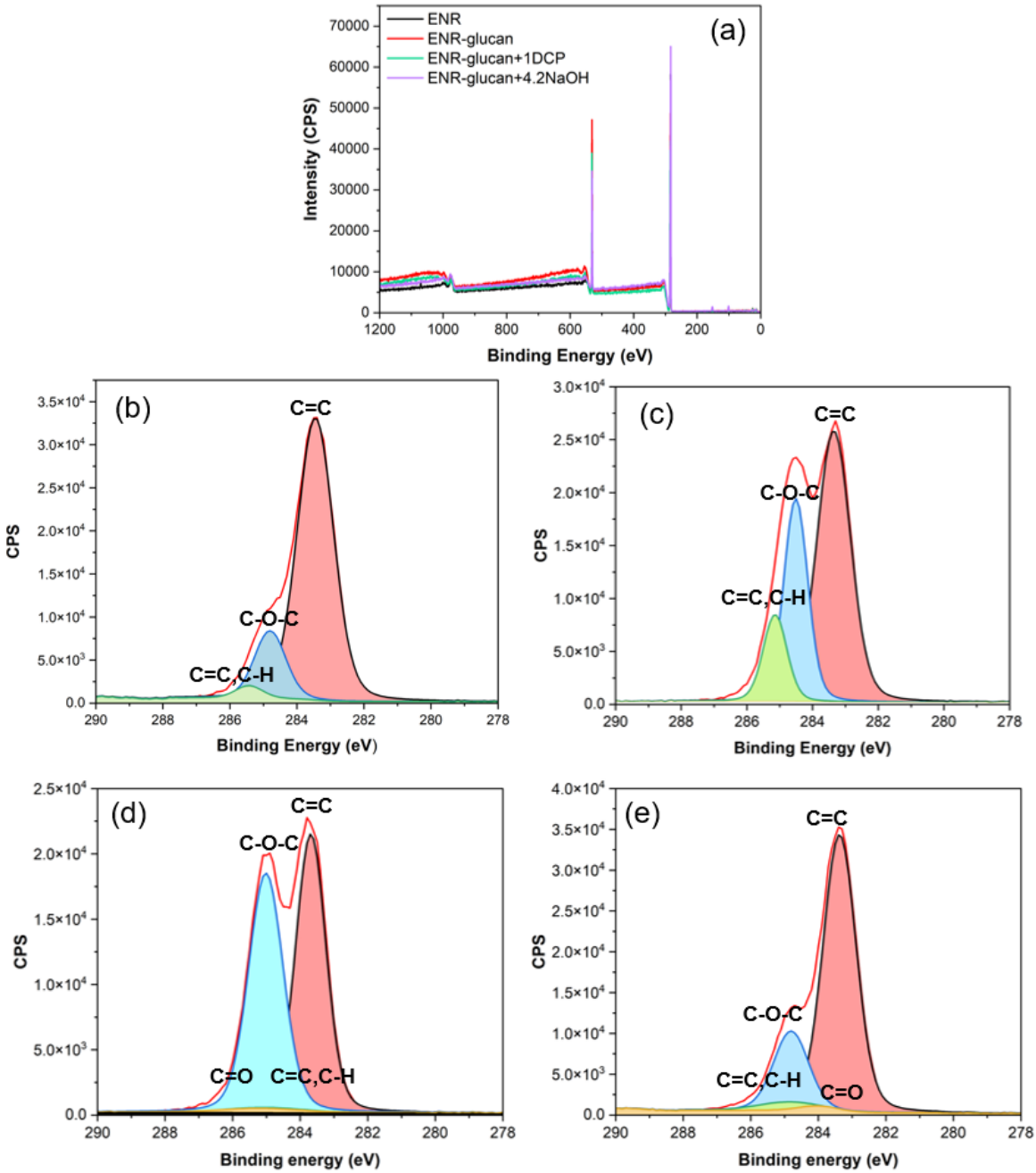

Figure 6.3. (a) Low-resolution XPS spectra of ENR and all ENR-glucan composites and high-resolution deconvoluted spectra of C 1s for (b) ENR, (c) ENR-glucan, (d) ENR-glucan with using 1 phr DCP, and (e) ENR-glucan with using 4.2 phr NaOH.

Table 6.3. Atomic compositions and O/C ratios for ENR and ENR-glucan composites.

Sample	Element Constitution (%)			
	C 1s (%)	O 1s (%)	Si 2p (%)	O/C ratio
ENR	88.31	10.79	0.9	0.12
ENR-glucan	82.95	17.05	0	0.20
ENR-glucan+1DCP	82.93	17	0.07	0.20
ENR-glucan+4.2NaOH	84.6	13.48	1.92	0.16

6.3.1.3. Toluene Swelling

In order to explore the creation of insoluble gel induced by the network between the ENR and glucan, masterbatch samples were subjected to toluene swelling analysis. **Figure 6.4** indicated that the baseline ENR was fully dissolved in toluene within the first day of the swelling test due to the absence of any network between the ENR chains to hinder the penetration of the solvent molecules through the rubber. On the contrary, the ENR-glucan masterbatch blends were only swollen and remained intact, revealing the grafting of ENR onto glucan and network formation, which substantiates previous FTIR and XPS findings. The formed networks as a result of the covalent bond grafts reduced the ENR-solvent interaction

and hence avoided the dissolution of ENR. The ENR-glucan masterbatch (**Figure 6.4(b)**), without any catalyst, was also not soluble in toluene, indicating the high-temperature and high-shear mediated epoxy ring opening of the ENR and grafting onto the glucan structure as noted from the FTIR spectra as well as XPS analysis.

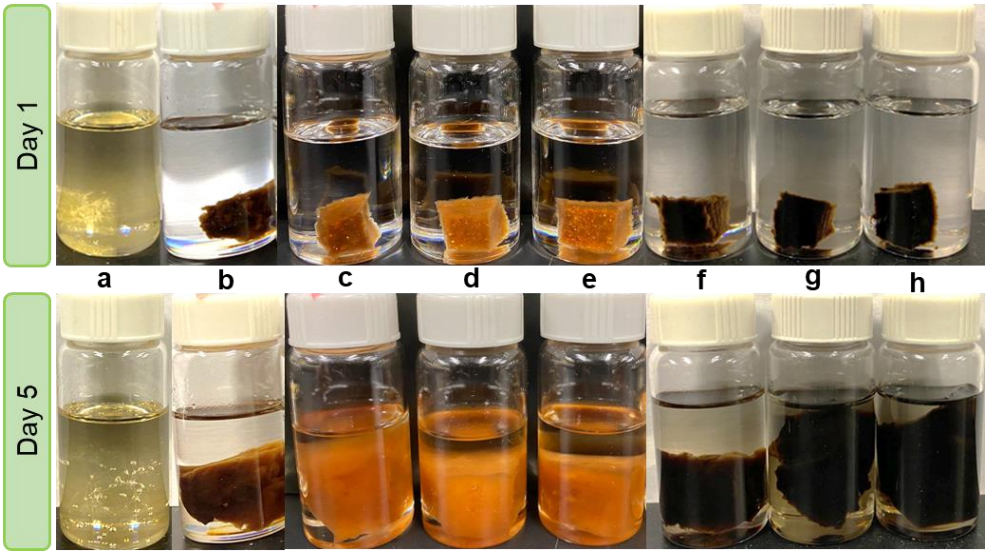

Figure 6.4. Toluene swelling analysis of (a)ENR, (b)ENR-glucan, (c)ENR-glucan+0.1DCP, (d)ENR-glucan+0.5DCP, (e)ENR-glucan+1DCP, (f)ENR-glucan+1.4 NaOH, (g)ENR-glucan+2.8 NaOH, (h)ENR-glucan+4.2 NaOH.

Based on the swelling experiment data, the swelling index of the ENR-glucan masterbatch was calculated and presented in **Figure 6.5**. It is noteworthy to mention that the lowest swelling index belonged to the masterbatch produced with DCP catalyst indicating the effectiveness of DCP as a catalyst for the opening of the epoxy ring, which consequently induced more grafting of ENR on the glucan. Overall, the swelling experiments' results agree

with the FTIR study's result (**Figure 6.1**) which exhibited the formation of the grafted network between ENR and glucan owing to the creation of the ether bond.

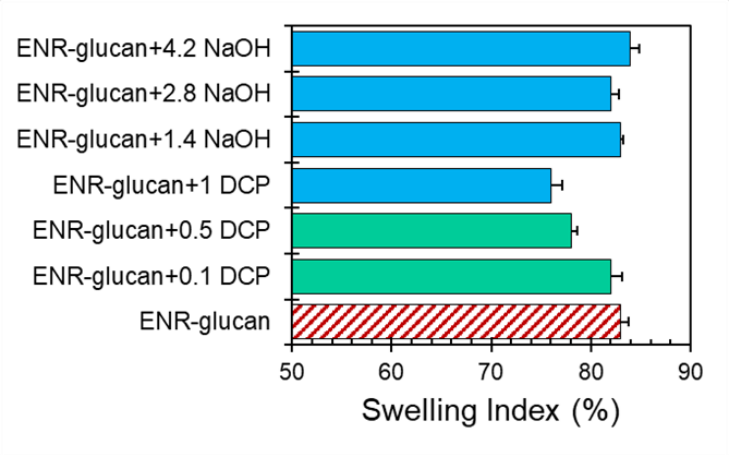

Figure 6.5. Swelling index of ENR-glucan composites.

6.3.1.4. Tensile Properties

Predominant parameters which dictate the reinforcing capability of the fillers in filled composites are the concentration and dispersion of fillers besides the interaction between the fillers and the matrix. The tensile strength, stress-strain curve, elongation at break, and elastic modulus of the baseline ENR and ENR-glucan masterbatch samples are displayed in **Figure 6.6**. The incorporation of the glucan substantially improved the tensile strength results (**Figure 6.6(d)**) for all the ENR-glucan composites compared to the neat ENR. The enhancement in the tensile strength could be attributed to the robust interactions through the covalent grafting and hydrogen bond interaction between the ENR and glucan. Considerable enhancement in the tensile strength of ENR-glucan blend without catalyst strengthens the hypothesized grafting between the ENR and glucan due to elevated batch mixing temperature as well as high shear

stress. Strikingly, ENR-glucan using 0.1 phr DCP achieved the utmost tensile strength amongst all samples of 5.5 MPa, which is 550% higher than the neat ENR. These superior reinforcement results are induced by the grafting of ENR onto the polysaccharide backbone coupled with hydrogen bonds, which can endure the load stresses and effectively transfer the load from the rubber matrix to the rigid fillers. These findings are aligned with the previous study of ENR-oxidized starch by Tong et al., in which the incorporation of the oxidized starch as filler improves the tensile strength [342].

As expected, the elongation at break decreased by introducing high fillers loading fillers in the rubber matrix as the rigid fillers restricted the chain mobility and suppressed strain crystallization in the matrix. Moreover, covalent bonds among the chain segments impede the untangling of some chains, resulting in reduced elongation at break [3]. Varghese et al. reported the same trend as the incorporation of silicates in the ENR matrix led to a decrease in the elongation at break [348]. Also, Nie et al. showed that as the loading of cellulose nanocrystals as fillers in the ENR matrix increased, the elongation at break dropped because of the continuous development of the hydrogen bonding network, which limits the movement of the ENR chains [349].

Important factors that play an essential role in determining the modulus of filled composites are the extent of dispersion of fillers in the matrix as well as the nature of chemical interactions within the composite. As depicted in **Figure 6.6(e)**, the incorporation of glucan led to considerable improvement of elastic modulus, which can be ascribed to the formation of filler-polymer networks in the composite. Additionally, introducing rigid filler to the rubbery

matrix obstructs chain movement, which brings about higher resistance against deformation under applied force, as also noted from the increasing slope of the stress-strain curve. This result is in excellent agreement with Bhakri et al., which reported a remarkable modulus increase of ENR by incorporating microfibrillated cellulose as fillers [350].

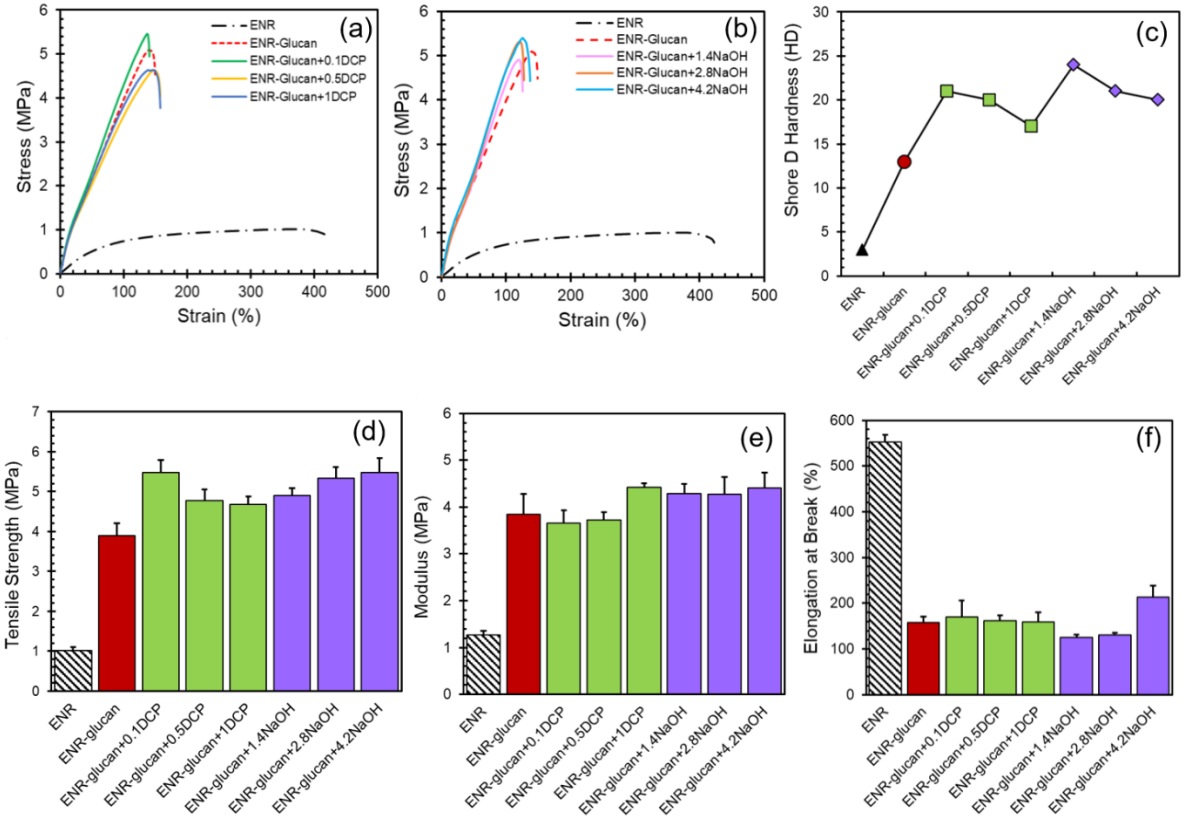

Figure 6.6. (a) stress-strain curve of ENR-glucan composites using DCP, (b) stress-strain curve of ENR-glucan composites using DCP, (c) shore D hardness of neat ENR and ENR-glucan composites (d) tensile strength, (e)elastic modulus, and (f) elongation at break of neat ENR and ENR-glucan composites.

The results of the hardness tests illustrate the effects of filler concentration and chemical interactions within the composite as shown in **Figure 6.6(c)**. The hardness significantly increased with the introduction of a higher concentration of glucan filler into the ENR matrix. Notably, the hardness of glucan particles was compared with cellulose nanocrystals (CNC) using nanoindentation analysis, and the results indicated a higher modulus, consequently, greater hardness of glucan than CNCs (**Figure C3**). As the filler concentration and grafts within the composites strongly influence the hardness, the increase in hardness can be attributed to network formation within the composite since the same level of filler was incorporated in all nanocomposites. Additionally, elastic modulus values corroborate the trend in hardness as the hardness tends to increase with an increase in the elastic modulus [351,352]. This trend concurs well with the previous finding of ENR-lignin composite which hardness was substantially increased as lignin content increased for heat-treated rubber composites [339]. The higher hardness of the ENR-lignin composite was attributed to the stronger lignin-rubber interactions at higher lignin content [339]. A comparison of silica and calcium carbonate with glucan was also carried out in order to examine the prospects of glucan compared with other reinforcing materials, and the results are shown in **Figure 6.7**. In terms of tensile strength, modulus, and hardness, considerably enhanced results were achieved with glucan compared to silica and calcium carbonate. Despite silica (average particle size 780 nm) and calcium carbonate (average particle size 1.6 μm) had substantially smaller particle sizes compared to the glucan (average particle size 15 μm) used in this study (**Figure C4**), which could lead to finer dispersion, the glucan displayed improved mechanical properties. This was attributed to the temperature and shear-mediated etherification between the -OH moieties of glucan with

the epoxy groups of ENR that led to covalent grafting. Such bonding is unlikely to happen with clay and calcium carbonate. Furthermore, hydrogen bond interaction is expected in glucan – ENR masterbatch (**Scheme 6.3**). Additionally, the density of the ENR masterbatch composites with glucan, silica, and calcium carbonate was evaluated and presented in **Figure 6.7(e)**. These results indicate a higher density of composites with silica and calcium carbonate compared to the glucan thus the volume fraction of glucan is higher, which corroborates the assumption of finer dispersion of silica and calcium carbonate than glucan.

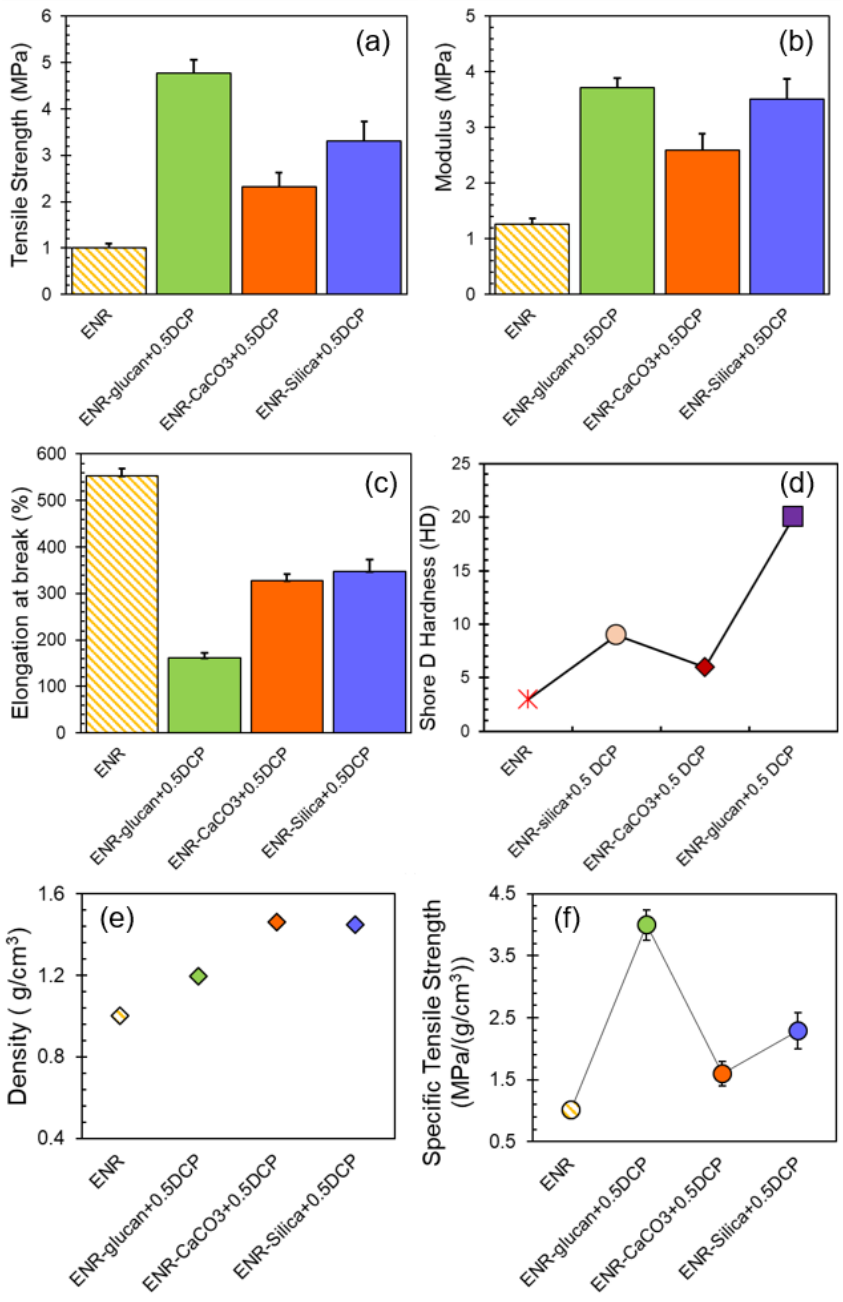

Figure 6.7. Comparison of mechanical properties between glucan, silica, and calcium carbonate; (a)tensile strength, (b)modulus, (c) elongation at break, (d) hardness, (e) density, and (f) specific tensile strength.

6.3.1.5. Rheology

The rheology properties of the ENR-glucan composites were evaluated to investigate the microstructure and viscoelastic properties of the composites. The storage modulus (G'), loss modulus (G''), and complex viscosity as a function of frequency are presented in **Figure 6.8**. As expected, a steep decrease in the complex viscosity caused by increasing frequency for all formulations was noted that representing shear-thinning behavior. This behavior was initiated by changes in the microstructure of the masterbatch composites, followed by the untangling of the ENR chains, which consequently resulted in more free volume within the ENR composite and, thus, a reduction in the viscosity[107]. Overall, the incorporation of the glucan in the ENR system led to a higher viscosity of the composite, which can be associated with the occupation of the free volume of the ENR matrix succeeded by restriction of the ENR chains movement [337,353]. It was evident that using a catalyst for producing the masterbatch composite positively correlates with the viscosity increase as composites with a catalyst displayed greater viscosity than the samples without a catalyst. This could be attributed to the formation of more irreversible ether bond grafting of the ENR onto the glucan with the assistance of the catalyst. The covalent bonds in the composites led to the prevention of the rubber chains' disentanglement.

The inclusion of glucan led to significantly higher storage and loss modulus compared to pure ENR, representing the creation of the robust network caused by glucan within the composites. Also, it is worth mentioning that using a catalyst in the formulation increased the storage modulus, which validates the efficiency of the catalyst for the grafting between ENR

and glucan. This behavior reveals that the rigidity of the composites relies not only on the concentration of the glucan but the presence of the network within the composites. Also, another observation worth noting was a higher G′ than G″ throughout the frequency range due to the elastic solid-like behavior of ENR-glucan composites, implying the promoted interactions through the composites [311,354]. Furthermore, the same trend was observed in pure ENR, as G′ was greater than G″, indicating the prominently elastic nature of the ENR [333].

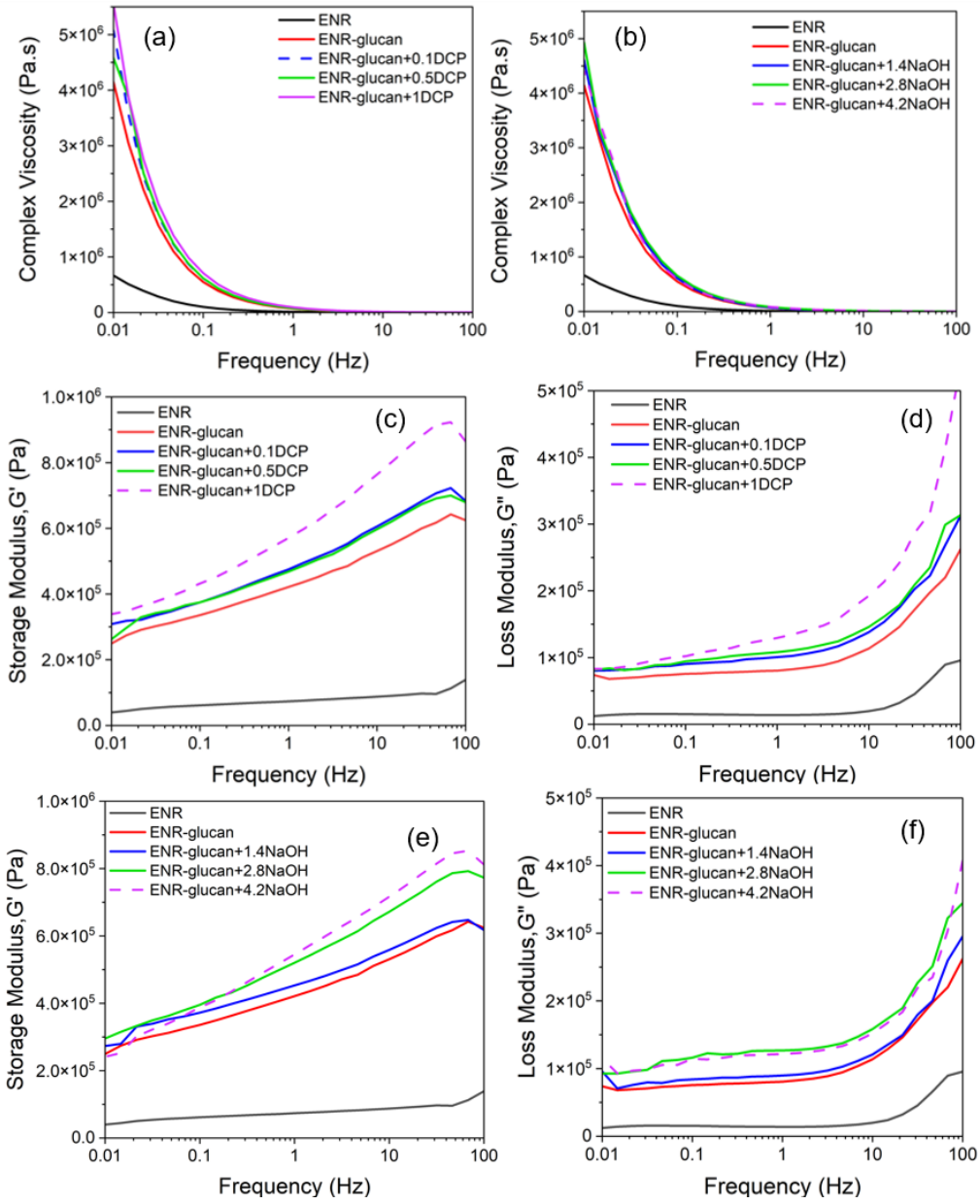

Figure 6.8. (a)Complex viscosity of ENR-glucan composites using DCP, (b)complex viscosity of ENR-glucan composites using NaOH, (c)storage modulus, (d)loss modulus of ENR-glucan composites using DCP, (e) storage modulus and, (f) loss modulus of ENR-glucan composites with using NaOH.

6.3.2. Characterization of NR Composites

Based on the obtained results from the ENR-glucan masterbatch blends, ENR-glucan masterbatch generated using 0.1 phr of DCP displayed appealing properties. It was thus utilized as a carrier of glucan in cured rubber formulations. Comparison of the direct blending of glucan versus the masterbatch was compared to elucidate the benefits of utilizing the masterbatch formulation.

6.3.2.1. Crosslink Density

Crosslink density is a critical determinant of the mechanical properties of rubber composites, and it is typically measured by monitoring their swelling in an appropriate solvent. Solvent molecules penetrate the rubber chains in the swelling method, causing changes in the rubber composite's dimensions that vary on the level of crosslinking. As a general rule, the solvent absorbency of rubbers is inversely proportional to the crosslink density for good solvents. Rubber crosslink densities can then be calculated by using the Flory-Rehner Equation, which relates swelling to crosslink density [355]. Rubber composite samples containing fillers have a lower tendency to swell than those without fillers since fillers slow down solvent diffusion into the rubber and restrain chain mobility. As noted in **Figure 6.9**, the crosslink density of NR rubber increased as glucan was introduced into the NR matrix compared to pure NR, which could be attributed to the strong filler-polymer interactions, which led to a decrease in solvent penetration through rubber composites and an apparent increase in the crosslink density. Increasing crosslink density by the addition of the filler was also previously stated in NR-cellulose nanofiber and NR-crop residues [242,356].

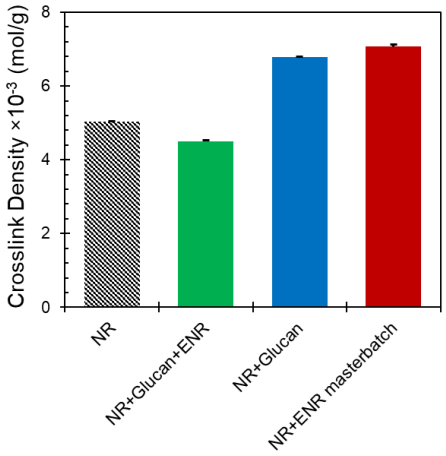

Figure 6.9. The crosslink density of pure NR and NR composites.

6.3.2.2. Scanning Electron Microscopy

SEM was employed to examine the morphology and degree of dispersion of glucan in the NR matrix, as depicted in **Figure 6.10**. Images were generated from the cross-sections of sheets after specimens were prepared via a cryogenic fracture. According to the energy-dispersive x-ray spectroscopy (EDX) analysis, the bright white particles, highlighted by red circles in the SEM images, are ZnO particles that emit high-energy electrons. It appears that the incorporation of glucan filler helped to disperse the ZnO particles homogeneously, thereby contributing to a higher crosslink density of the rubber composites compared with the unfilled NR samples. Additionally, the crosslinking density results suggest that the presence of glucan could enhance the ZnO dispersion in the rubber matrix. Similar observations were reported for NR-cellulose nanocrystals (CNC) [14] and nitrile butadiene rubber (NBR) – CNC composites [244]. Furthermore, by EDX mapping, Blanchard et al. found out that the amount of ZnO agglomerates decreases as potential Zn-polysaccharide network formation and increase torque as a result of the viscosity increase may have promoted the dispersion of Zn in the

rubber matrix [14]. As noted in **Figure 6.8(d)**, the formulation that contained the NR-ENR masterbatch displayed no visible accumulation of bright particles indicating the high dispersion of ZnO. Although **Figure 6.8(b-d)** exhibited good overall dispersion of glucan, the NR-ENR masterbatch showed a more homogenous distribution and dispersion of the glucan particles.

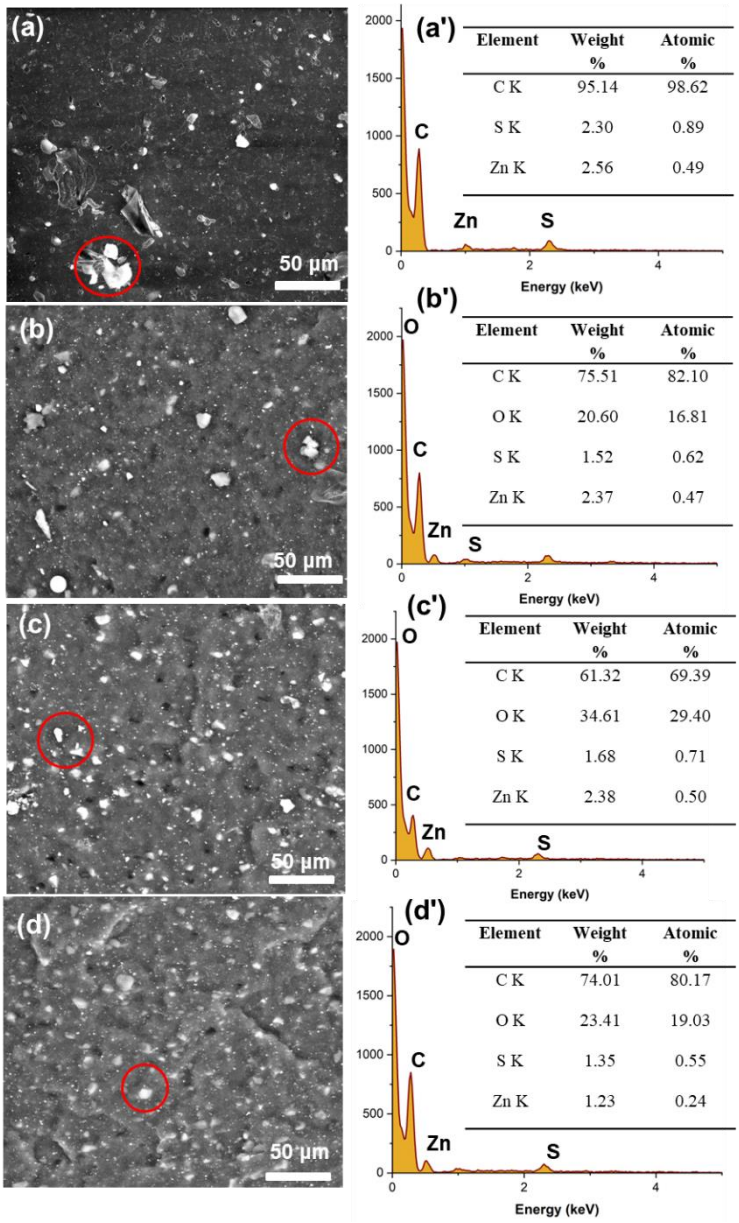

Figure 6.10. SEM images of (a)pure NR, (b)NR-glucan-ENR, (c)NR-glucan, (d)NR-ENR masterbatch and EDS images of (a')-(d').

6.3.2.3. Atomic Force Microscopy

In polymer composites, phase images obtained from the tapping mode of atomic force microscopy (AFM) imaging provide a useful way to study filler dispersion and distribution as varying stiffness can be detected [353]. The morphology of NR composites obtained from the tapping mode of AFM imaging is shown in **Figure 6.11**. It was demonstrated that stiffer materials, in this case, ZnO and glucan particles, have a more positive phase shift and appear as brighter regions [357]. The AFM image of pure NR composite film exhibited an accumulation of brighter regions in a small spot, revealing poor ZnO dispersion. Additionally, by incorporating glucan, a more uniform distribution of ZnO and glucan was accomplished, which strengthens the possibility of the contribution of glucan in dispersing the ZnO particles through the rubber composites, which was previously observed by SEM analysis.

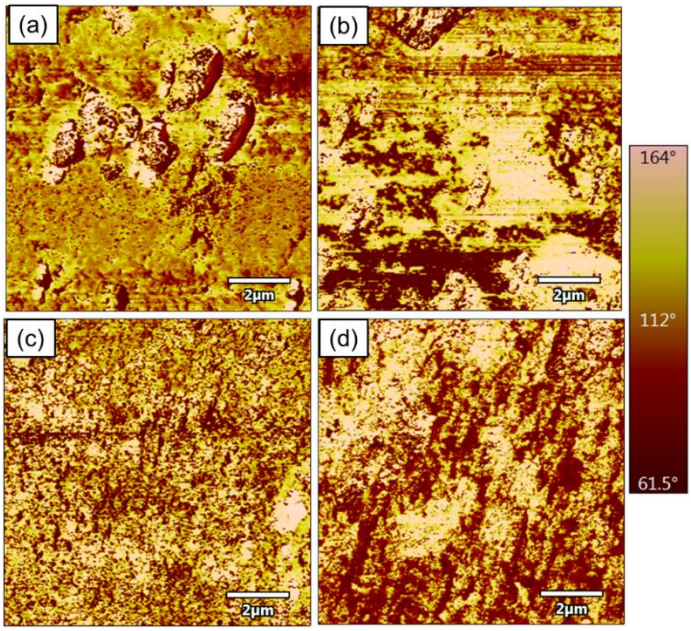

Figure 6.11. AFM phase image of (a)NR, (b)NR-glucan-ENR, (c)NR-glucan, and (d)NR-ENR masterbatch.

6.3.2.4. Tensile Testing

The employment of ENR-glucan masterbatch in the NR composite and its impact on the fundamental material properties was evaluated using tensile testing. The tensile strength, elongation at break, elastic modulus, modulus at 50%, 100%, and 300% elongation, and typical stress-strain curves are presented in **Figure 6.12**. There was a significant increase in the tensile strength with the addition of glucan into the NR matrix. Notably, the NR-ENR masterbatch provided the highest tensile strength (27 MPa) of the NR composite, which was comparable to the tensile strength performance of commercialized nanosized carbon black-filled NR for the same loading levels [358]. The superior tensile strength property of NR-ENR masterbatch could be ascribed to the excellent dispersion of filler in the ENR and hence NR in conjuncture

with the higher crosslink density, which led to higher resistance to stress. This is because the ENR worked as an interfacial modifier which assisted in the better dispersion of glucan [331]. As expected, the strain at break decreased with the inclusion of rigid glucan particles in the NR rubber films. Rigid filler particles as well as the crosslinking network between the chain segments, inhibit untangling of some chains, thereby decreasing elongation at break [359]. Despite the reduction in comparison to the unfilled NR, the ENR-glucan based NR composite formulation provided high elasticity (~840%), indicating the high toughness of such formulations.

Moreover, the incorporation of the glucan led to the enhancement of modulus due to the increasing stiffness of the composite induced by adding rigid fillers. Notably, the elastic modulus of the ENR - glucan masterbatch based NR composite increased by a whopping 270% compared to the unfilled NR samples. This result substantiates the effectiveness of utilizing ENR-grafted glucan as a masterbatch to enhance the tensile properties of NR composites, attributed to the compatibility of the ENR with the NR matrix.

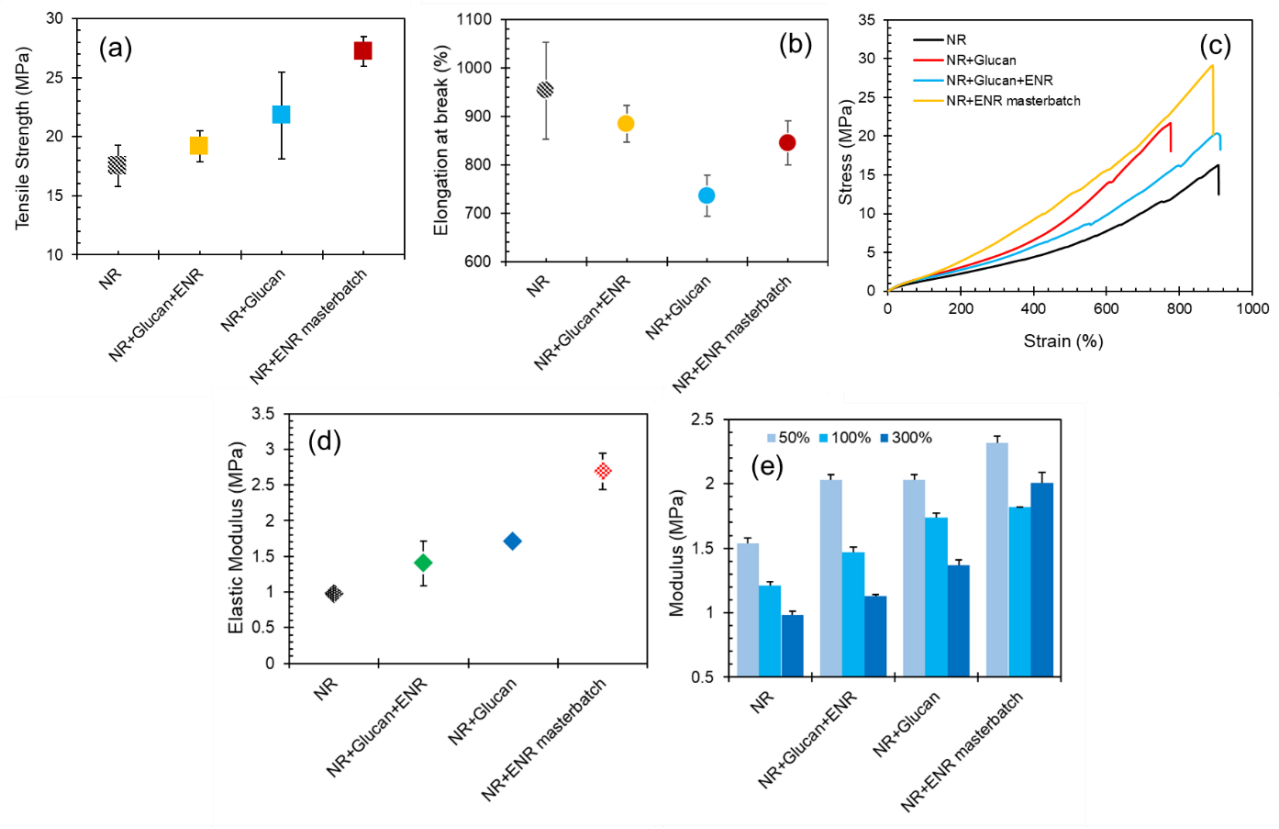

Figure 6.12. (a)Tensile strength, (b)elongation at break, (c)typical stress-strain curve, (d)elastic modulus, and (e)modulus at 50,100, and 300% of pure NR and NR composites.

6.4. Concluding Remarks

The designed enzymatic polysaccharide, glucan, was processed with ENR to obtain a chemically grafted ENR-glucan masterbatch using a one-step, scalable *in situ* batch melt compounding process. As a result of this work, a significant insight was gained that batch mixers-based reactive processes are solvent-free, scalable, and mature technologies widely used in rubber manufacturing. The ENR-glucan masterbatch exhibited robust interactions between the matrix and filler owing to the formation of covalent ether bonds and hydrogen

bonds between the ENR matrix and glucan, which was validated with FTIR, XPS, and toluene swelling. Selected ENR-glucan masterbatch samples were subsequently melt-mixed with NR formulations to generate NR composites. The mechanical properties of the resulting composite displayed that the employment of the ENR masterbatch leads to superior mechanical properties equivalent to common commercial fillers, such as carbon black. This indicates that the designed enzymatic polysaccharide, glucan, has outstanding potential for applications as a sustainable filler in rubber and elastomer systems.

Chapter 7. Conclusions and Future Work

7.1. Conclusions

In this research, the employment of enzymatic polymerized polysaccharide, alpha-1,3 glucan, as a functional additive and filler of rubber was studied. The impact of various morphology of alpha-1,3 glucan on the physico-mechanical properties of rubber composites and dipped rubber goods, as well as on the barrier properties of paper coating was studied. A robust procedure was developed for the incorporation of incorporating alpha-1,3 glucan (wet cake and MCG)ain hydrophobic NR matrix to generated various levels of filled rubber composites.

In the first study, the incorporation of a platelet morphology alpha-1,3 glucan (MCG) in the NR led to a remarkable enhancement in the tear strength, tensile properties, toughness, and an increase in water vapor permeability but a decrease in alcohol permeation. This behavior is appealing in gloves, where high sweat permeation from hands to the environment and limited to no solvent penetration from the environment to the skin is desired. The study indicated that the enzymatically polymerized MCG are effective reinforcing fillers for NR latex and potentially other elastomers offering the potential for appealing physical property improvements. The second and third experimental research studies investigated the development of NR-alpha-1,3 glucan based paper coating for food packaging applications. It was noted that paper coating based on NR and spherical particle alpha-1,3 glucan exhibited outstanding tensile properties and balanced oxygen and oil barrier performance. Also, it was revealed that at sufficient thickness, this coating system successfully seals paper substrate's

pores. As a result, notable barrier property improvements versus oil, oxygen, and water vapor were achieved. However, higher loading levels can be detrimental to the moisture barrier properties of the coating.

In a follow up study, platelet alpha-1,3 glucan, MCG, was employed in NR coating systems. The formulated NR/MCG coatings demonstrated notable improvements in mechanical strength without compromising the flexibility of the coated paper. Furthermore, the incorporation of MCGs in the NR formulations resulted in strong adhesion strength between the coating films and the paper substrate resulting in eliminating the need for additional adhesive layers. Also, it was unveiled that NR/MCG formulated paper coatings provided outstanding barrier properties against oil, grease, and oxygen, which was further improved by introducing a light crosslinking in the paper coating. Overall, the developed NR/MCG paper coating systems demonstrated favorable mechanical and barrier properties, making them suitable for various food packaging applications.

Finally, the last study showed that by employing one-step, solvent free, mature technology and scalable in situ batch melt compounding, chemical grafted ENR-glucan masterbatch was successfully developed. Then formation of covalent bonds among ENR and glucan was validated with FTIR, XPS, and toluene swelling analysis. Subsequently, the selected ENR-glucan was utilized as reinforcing filler of NR composites, which led to superior mechanical properties equivalent to commercial fillers, such as carbon black. These findings suggest that the enzymatically designed polysaccharide, glucan, possesses exceptional potential for use as a sustainable filler in rubber and elastomer systems.

Biomass derived polysaccharides, such as cellulose, chitin, and starch, has been used in material applications (e.g., paper) for centuries. More recently, there is a renewed interest in utilizing them as sustainable alternative or complement to the mature petrochemical derived polymers. However, these polysaccharides lack purity and the molecular design precision round in designed polymers as they are mostly extracted from diverse agri-forestry feedstock. Enzymatic polymerization of simple sugars into polysaccharides allows to develop high purity, precise structure, desired morphology, and colloidal features. The unique characteristics of alpha-1,3 glucan provide it with a distinct advantage in improving the mechanical and barrier properties of rubber composites in comparison to other polysaccharides such as cellulose and starch. It is worth mentioning that alpha-1,3 glucan demonstrates properties that are on par with commercially available fillers. Alpha-1,3 glucan is an example of such enzymatically polymerized polysaccharide that demonstrated appealing functional filler attribute as well as sustainability requirements in rubber composites for a range of applications.

7.2. Future Works

A potential avenue for future research would be to evaluate the impact of alpha-1,3 glucan on the biodegradation of NR composites and the effect of crosslinking density on the biodegradation of NR-alpha-1,3 glucan composites. Although the NR has long-term biodegradability profile, the kinetics of NR biodegradation is a slow process attributed to the limited progress of bacterial growth on rubber substrates [29]. It is expected that incorporating biopolymers in rubber composites could enhance biodegradation. Additionally, investigating the recyclability of NR-alpha-1,3 glucan composites could be proposed as another area of future work.

Another future research direction could involve building upon the findings of Chapter 6 by incorporating the platelet morphology microcrystalline glucan (MCG) in the preparation of epoxidized natural rubber (ENR) masterbatch. The platelet morphology of MCG suggests the potential for achieving outstanding mechanical properties. Since alpha -1, 3 glucan is a relatively new polysaccharide (that is not yet commercially available), its potential for other polymer or composite material applications is largely untapped. Thus, future research can investigate chemical modification chemistries, structure and morphology fine-tuning during the polymerization, and composite processing platforms to broaden the application of alpha -1, 3 glucan in various polymer and material systems.

References

[1] Fukui S, Ito T, Saito T, Noguchi T, Isogai A. Surface-hydrophobized TEMPO-nanocellulose/rubber composite films prepared in heterogeneous and homogeneous systems. Cellulose 2019;26:463–73. https://doi.org/10.1007/s10570-018-2107-6.

[2] Danafar F, Kalantari M. A Review of Natural Rubber Nanocomposites Based on Carbon Nanotubes. J Rubber Res 2018;21:293–310. https://doi.org/10.1007/bf03449176.

[3] Chang BP, Gupta A, Muthuraj R, Mekonnen TH. Bioresourced fillers for rubber composite sustainability: current development and future opportunities. Green Chem 2021. https://doi.org/10.1039/D1GC01115D.

[4] Bokobza L. Natural rubber nanocomposites: A review. Nanomaterials 2019;9:12. https://doi.org/10.3390/nano9010012.

[5] Low DYS, Supramaniam J, Soottitantawat A, Charinpanitkul T, Tanthapanichakoon W, Tan KW, et al. Recent Developments in Nanocellulose-Reinforced Rubber Matrix Composites: A Review. Polym 2021, Vol 13, Page 550 2021;13:550. https://doi.org/10.3390/POLYM13040550.

[6] Noguchi T, Endo M, Niihara K, Jinnai H, Isogai A. Cellulose nanofiber/elastomer composites with high tensile strength, modulus, toughness, and thermal stability prepared by high-shear kneading. Compos Sci Technol 2020;188:108005. https://doi.org/10.1016/j.compscitech.2020.108005.

[7] Parambath Kanoth B, Claudino M, Johansson M, Berglund LA, Zhou Q. Biocomposites from Natural Rubber: Synergistic Effects of Functionalized Cellulose Nanocrystals as Both Reinforcing and Cross-Linking Agents via Free-Radical Thiol-ene Chemistry. ACS Appl Mater Interfaces 2015;7:16303–10. https://doi.org/10.1021/acsami.5b03115.

[8] Ojogbo E, Tzoganakis C, Mekonnen TH. Effect of extrusion, batch-mixing, and co-coagulation on the dispersion of CNCs in natural rubber - CNC nanocomposites. Compos Part A Appl Sci Manuf 2021;149:106580. https://doi.org/10.1016/j.compositesa.2021.106580.

[9] Lynge E. Identification of Research Needs to Resolve the Carcinogenicity of High-Priority IARC Carcinogens. Lyon, France: World Health Organization,; 2009.

[10] Krainoi A, Kummerlöwe C, Nakaramontri Y, Vennemann N, Pichaiyut S, Wisunthorn S, et al. Influence of critical carbon nanotube loading on mechanical and electrical properties of epoxidized natural rubber nanocomposites. Polym Test 2018;66:122–36. https://doi.org/10.1016/j.polymertesting.2018.01.003.

[11] Arroyo M, López-Manchado MA, Herrero B. Organo-montmorillonite as substitute of carbon black in natural rubber compounds. Polymer (Guildf) 2003;44:2447–53. https://doi.org/10.1016/S0032-3861(03)00090-9.

[12] Hwang WG, Wei KH, Wu CM. Mechanical, thermal, and barrier properties of NBR/organosilicate nanocomposites. Polym Eng Sci 2004;44:2117–24. https://doi.org/10.1002/pen.20217.

[13] Hernández M, Bernal M del M, Verdejo R, Ezquerra TA, López-Manchado MA. Overall performance of natural rubber/graphene nanocomposites. Compos Sci Technol 2012;73:40–6. https://doi.org/10.1016/J.COMPSCITECH.2012.08.012.

[14] Blanchard R, Ogunsona EO, Hojabr S, Berry R, Mekonnen TH. Synergistic Cross-linking and Reinforcing Enhancement of Rubber Latex with Cellulose Nanocrystals for Glove Applications. ACS Appl Polym Mater 2020;2:887–98. https://doi.org/10.1021/acsapm.9b01117.

[15] Thakore S. Nanosized cellulose derivatives as green reinforcing agents at higher loadings in

natural rubber. J Appl Polym Sci 2014;131:40632. https://doi.org/10.1002/APP.40632.
[16] Geyer R, Jambeck JR, Law KL. Production, use, and fate of all plastics ever made. Sci Adv 2017;3:e1700782. https://doi.org/10.1126/SCIADV.1700782/SUPPL_FILE/1700782_SM.PDF.
[17] Ojeda T. Polymers and the Environment. Polym. Sci., InTech; 2013. https://doi.org/10.5772/51057.
[18] Welden NA. The environmental impacts of plastic pollution. Plast Waste Recycl Environ Impact, Soc Issues, Prev Solut 2020:195–222. https://doi.org/10.1016/B978-0-12-817880-5.00008-6.
[19] Hassan EA, Hassan ML, Abou-zeid RE, El-Wakil NA. Novel nanofibrillated cellulose/chitosan nanoparticles nanocomposites films and their use for paper coating. Ind Crops Prod 2016;93:219–26. https://doi.org/10.1016/j.indcrop.2015.12.006.
[20] Zhang W, Yang X, Li C, Liang M, Lu C, Deng Y. Mechanochemical activation of cellulose and its thermoplastic polyvinyl alcohol ecocomposites with enhanced physicochemical properties. Carbohydr Polym 2011;83:257–63. https://doi.org/10.1016/j.carbpol.2010.07.062.
[21] Hong M, Chen EYX. Future Directions for Sustainable Polymers. Trends Chem 2019;1:148–51. https://doi.org/10.1016/j.trechm.2019.03.004.
[22] Faruk O, Bledzki AK, Fink HP, Sain M. Progress report on natural fiber reinforced composites. Macromol Mater Eng 2014;299:9–26. https://doi.org/10.1002/mame.201300008.
[23] Li S, Wang Y, Xu W, Shi B. Natural Rubber-Based Elastomer Reinforced by Chemically Modified Multiscale Leather Collagen Fibers with Excellent Toughness. Cite This ACS Sustain Chem Eng 2020;8:5091–9. https://doi.org/10.1021/acssuschemeng.9b07078.
[24] Zhu Y, Romain C, Williams CK. Sustainable polymers from renewable resources. Nat 2016 5407633 2016;540:354–62. https://doi.org/10.1038/nature21001.
[25] Mente P, Motaung TE, Hlangothi SP. Natural Rubber and Reclaimed Rubber Composites – A Systematic Review. Polym Sci 2016;2:1. https://doi.org/10.4172/2471-9935.100015.
[26] Shchipunov Y. Bionanocomposites: Green sustainable materials for the near future. Pure Appl Chem 2012;84:2579–607. https://doi.org/10.1351/PAC-CON-12-05-04.
[27] Zafar R, Zia KM, Tabasum S, Jabeen F, Noreen A, Zuber M. Polysaccharide based bionanocomposites, properties and applications: A review. Int J Biol Macromol 2016;92:1012–24. https://doi.org/10.1016/J.IJBIOMAC.2016.07.102.
[28] Egwaikhide AP, Okieimen FE, U. L. Rheological and Mechanical Properties of Natural Rubber Compounds Filled with Carbonized Palm Kernel Husk and Carbon Black (N330). Http://WwwSciencepublishinggroupCom 2014;1:50. https://doi.org/10.11648/J.SJC.20130105.11.
[29] Rose K, Steinbüchel A. Biodegradation of Natural Rubber and Related Compounds: Recent Insights into a Hardly Understood Catabolic Capability of Microorganisms. Appl Environ Microbiol 2005;71:2803. https://doi.org/10.1128/AEM.71.6.2803-2812.2005.
[30] Jin K, Tang Y, Liu J, Wang J, Ye C. Nanofibrillated cellulose as coating agent for food packaging paper. Int J Biol Macromol 2021;168:331–8.
[31] Wang H, Easteal A, Edmonds N. Prevulcanized natural rubber latex/modified lignin dispersion for Water Vapour Barrier Coatings on Paperboard Packaging. Adv. Mater. Res., vol. 47- 50 PART 1, Trans Tech Publications; 2008, p. 93–6. https://doi.org/10.4028/www.scientific.net/amr.47-50.93.
[32] Samyn P, Driessen F, Stanssens D. Natural Rubber Composites for Paper Coating Applications. Mater. Proc. 2020, Vol. 2, Page 29, vol. 2, MDPI AG; 2020, p. 6832. https://doi.org/10.3390/ciwc2020-06832.

[33] Roy K, Pongwisuthiruchte A, Chandra Debnath S, Potiyaraj P. Application of cellulose as green filler for the development of sustainable rubber technology. Curr Res Green Sustain Chem 2021;4:100140. https://doi.org/10.1016/J.CRGSC.2021.100140.
[34] Sui G, Zhong WH, Yang XP, Yu YH, Zhao SH. Preparation and properties of natural rubber composites reinforced with pretreated carbon nanotubes. Polym Adv Technol 2008;19:1543–9. https://doi.org/10.1002/PAT.1163.
[35] Cai HH, Li SD, Tian GR, Wang HB, Wang JH. Reinforcement of natural rubber latex film by ultrafine calcium carbonate. J Appl Polym Sci 2002;87:982–5. https://doi.org/10.1002/app.11410.
[36] Ojogbo E, Ogunsona EO, Mekonnen TH. Chemical and physical modifications of starch for renewable polymeric materials. Mater Today Sustain 2020;7–8:100028. https://doi.org/10.1016/j.mtsust.2019.100028.
[37] Lörcks J. Properties and applications of compostable starch-based plastic material. Polym Degrad Stab 1998;59:245–9. https://doi.org/10.1016/S0141-3910(97)00168-7.
[38] Marcinko JJ, Lenges C, Kim K, Harvey M. Nuvolve engineered polysaccharides as performance-enhancing additives for latex wood adhesives. For Prod J 2020;70:293–301. https://doi.org/10.13073/FPJ-D-19-00058.
[39] Mariano M, El Kissi N, Dufresne A. Cellulose nanocrystal reinforced oxidized natural rubber nanocomposites. Carbohydr Polym 2016;137:174–83. https://doi.org/10.1016/j.carbpol.2015.10.027.
[40] Dominic C.D. M, Joseph R, Sabura Begum PM, Raghunandanan A, Vackkachan NT, Padmanabhan D, et al. Chitin nanowhiskers from shrimp shell waste as green filler in acrylonitrile-butadiene rubber: Processing and performance properties. Carbohydr Polym 2020. https://doi.org/10.1016/j.carbpol.2020.116505.
[41] Angellier H, Molina-Boisseau S, Dufresne A. Mechanical properties of waxy maize starch nanocrystal reinforced natural rubber. Macromolecules 2005;38:9161–70. https://doi.org/10.1021/ma0512399.
[42] Kralj S, Khandige S, Guan R, Boetkjaer K, Behabtu N, Lenges C, et al. Microbial and Enzymatic Polysaccharides. Kirk-Othmer Encycl Chem Technol 2020:1–55. https://doi.org/10.1002/0471238961.1309031803152005.A01.PUB2.
[43] Bacon JSD, Jones D, Farmer VC, Webley DM. The occurrence of α(1–3)glucan in Cryptococcus, schizosaccharomyces and Polyporus species, and its hydrolysis by a Streptomyces culture filtrate lysing cell walls of Cryptococcus. Biochim Biophys Acta - Gen Subj 1968;158:313–5. https://doi.org/10.1016/0304-4165(68)90153-0.
[44] Mekonnen TH, Behabtu N, Lenges C. Enzymatic polymerization derived engineered polysaccharides as reinforcing fillers of ethylene vinyl acetate composites. Carbohydr Polym 2020;241:116252. https://doi.org/10.1016/j.carbpol.2020.116252.
[45] Corr SA. Metal oxide nanoparticles. In: O'brien P, editor., The Royal Society of Chemistry; 2013.
[46] O'brien J, Opper K. Novel Composition for Preparing Polysaccharide Fibers. US Pat App 13/645,570 2012.
[47] Behabtu N, Kralj S. Enzymatic Polymerization Routes to Synthetic–Natural Materials: A Review. ACS Sustain Chem Eng 2020;8:9947–54. https://doi.org/10.1021/ACSSUSCHEMENG.0C01664.
[48] Puanglek S, Kimura S, Enomoto-Rogers Y, Kabe T, Yoshida M, Wada M, et al. In vitro synthesis of linear α-1,3-glucan and chemical modification to ester derivatives exhibiting outstanding thermal properties. Sci Reports 2016 61 2016;6:1–8.

https://doi.org/10.1038/srep30479.
[49] Heinze T, Pfeifer A, Koschella A, Adelman D, Howe L, Behabtu N, et al. Engineered Polysaccharides: α-1,3-Glucan Acetates Showing Upper Critical Solution Temperature in Organic Solvents. Macromol Chem Phys 2019;220:1–8. https://doi.org/10.1002/macp.201900112.
[50] Lenges C, Behabtu N, Mok J, Sendijarevic I, Sendijarevic A. Engineered polysaccharide alpha-1,3 glucan as isocyanate-reactive component in viscoelastic polyurethane foams. J Appl Polym Sci 2021;138:49979. https://doi.org/10.1002/app.49979.
[51] Behabtu N, Kralj S. Enzymatic Polymerization Routes to Synthetic-Natural Materials: A Review. ACS Sustain Chem Eng 2020. https://doi.org/10.1021/acssuschemeng.0c01664.
[52] Kedzior SA, Cranmer-Smith S, Behabtu N, Kim K, Lenges C, Bryant SL, et al. Elucidating the effect of enzymatic polymerized polysaccharide particle morphology on emulsion properties. Carbohydr Polym 2021;251:117112. https://doi.org/10.1016/j.carbpol.2020.117112.
[53] Rudi H, Resalati H, Eshkiki RB, Kermanian H. Sunflower stalk neutral sulfite semi-chemical pulp: an alternative fiber source for production of fluting paper. J Clean Prod 2016;127:562–6. https://doi.org/10.1016/J.JCLEPRO.2016.04.049.
[54] Smook GA (Gary A. Handbook for pulp & paper technologists 1992:419.
[55] Deshwal GK, Panjagari NR, Alam T. An overview of paper and paper based food packaging materials: health safety and environmental concerns. J Food Sci Technol 2019;56.
[56] Marsh K, Bugusu B. Food Packaging—Roles, Materials, and Environmental Issues. J Food Sci 2007;72:R39–55. https://doi.org/10.1111/J.1750-3841.2007.00301.X.
[57] Semple KE, Zhou C, Rojas OJ, Nkeuwa WN, Dai C. Moulded pulp fibers for disposable food packaging: A state-of-the-art review. Food Packag Shelf Life 2022;33:100908. https://doi.org/10.1016/J.FPSL.2022.100908.
[58] Tonjes DJ, Greene KL. A review of national municipal solid waste generation assessments in the USA. Waste Manag Res 2012;30:758–71. https://doi.org/10.1177/0734242X12451305.
[59] Qasim U, Osman AI, Al-Muhtaseb AH, Farrell C, Al-Abri M, Ali M, et al. Renewable cellulosic nanocomposites for food packaging to avoid fossil fuel plastic pollution: a review. Environ Chem Lett 2020 191 2020;19:613–41. https://doi.org/10.1007/S10311-020-01090-X.
[60] Phelan A (Anya), Meissner K, Humphrey J, Ross H. Plastic pollution and packaging: Corporate commitments and actions from the food and beverage sector. J Clean Prod 2022;331:129827. https://doi.org/10.1016/J.JCLEPRO.2021.129827.
[61] Jia L, Evans S, Linden S van der. Motivating actions to mitigate plastic pollution. Nat Commun 2019 101 2019;10:1–3. https://doi.org/10.1038/s41467-019-12666-9.
[62] Gaikwad KK, Singh S, Negi YS. Ethylene scavengers for active packaging of fresh food produce. Environ Chem Lett 2020;18:269–84. https://doi.org/10.1007/S10311-019-00938-1/FIGURES/5.
[63] Bhardwaj S, Bhardwaj NK, Negi YS. Effect of degree of deacetylation of chitosan on its performance as surface application chemical for paper-based packaging. Cellulose 2020;27:5337–52. https://doi.org/10.1007/S10570-020-03134-5/TABLES/5.
[64] Han JH, Krochta JM. Physical Properties and Oil Absorption of Whey-Protein-Coated Paper. J Food Sci 2001;66:294–9. https://doi.org/10.1111/J.1365-2621.2001.TB11335.X.
[65] Aloui H, Khwaldia K, Slama M Ben, Hamdi M. Effect of glycerol and coating weight on functional properties of biopolymer-coated paper. Carbohydr Polym 2011;86:1063–72. https://doi.org/10.1016/J.CARBPOL.2011.06.026.
[66] Rastogi VK, Samyn P. Bio-Based Coatings for Paper Applications 2015;5:887–930.

[67] Yang N, Deng Y. Paper Sizing Agents from Micelle-Like Aggregates of Polystyrene-Based Cationic Copolymers 2000. https://doi.org/10.1002/1097-4628.
[68] Sothornvit R. Effect of hydroxypropyl methylcellulose and lipid on mechanical properties and water vapor permeability of coated paper. Food Res Int 2009;42:307–11. https://doi.org/10.1016/J.FOODRES.2008.12.003.
[69] Yuvaraj D, Iyyappan J, Gnanasekaran R, Ishwarya G, Harshini RP, Dhithya V, et al. Advances in bio food packaging – An overview. Heliyon 2021;7:e07998. https://doi.org/10.1016/J.HELIYON.2021.E07998.
[70] Arfa A Ben, Chrakabandhu Y, Preziosi-Belloy L, Chalier P, Gontard N. Coating papers with soy protein isolates as inclusion matrix of carvacrol. Food Res Int 2007;40:22–32. https://doi.org/10.1016/J.FOODRES.2006.07.011.
[71] Vartiainen J, Motion R, Kulonen H, Rättö M, Skyttä E, Ahvenainen R. Chitosan-coated paper: Effects of nisin and different acids on the antimicrobial activity. J Appl Polym Sci 2004;94:986–93. https://doi.org/10.1002/APP.20701.
[72] Han JH, Aristippos G. Edible films and coatings: a review. Innov Food Packag 2005:239–62. https://doi.org/10.1016/B978-012311632-1/50047-4.
[73] Bi S, Pan H, Barinelli V, Eriksen B, Ruiz S, Sobkowicz MJ. Biodegradable polyester coated mulch paper for controlled release of fertilizer. J Clean Prod 2021;294:126348. https://doi.org/10.1016/j.jclepro.2021.126348.
[74] Schmid M, Dallmann K, Bugnicourt E, Cordoni D, Wild F, Lazzeri A, et al. Properties of whey-protein-coated films and laminates as novel recyclable food packaging materials with excellent barrier properties. Int J Polym Sci 2012;2012. https://doi.org/10.1155/2012/562381.
[75] Adeyeye OA, Sadiku ER, Babu Reddy A, Ndamase AS, Makgatho G, Sellamuthu PS, et al. The Use of Biopolymers in Food Packaging 2019:137–58. https://doi.org/10.1007/978-981-13-8063-1_6.
[76] Gastaldi E, Chalier P, Guillemin A, Gontard N. Microstructure of protein-coated paper as affected by physico-chemical properties of coating solutions. Colloids Surfaces A Physicochem Eng Asp 2007;301:301–10. https://doi.org/10.1016/J.COLSURFA.2006.12.079.
[77] Khwaldia K. WATER VAPOR BARRIER AND MECHANICAL PROPERTIES OF PAPER-SODIUM CASEINATE AND PAPER-SODIUM CASEINATE-PARAFFIN WAX FILMS. J Food Biochem 2010;34:998–1013. https://doi.org/10.1111/J.1745-4514.2010.00345.X.
[78] Khwaldia K, Linder M, Banon S, Desobry S. Effects of Mica, Carnauba Wax, Glycerol, and Sodium Caseinate Concentrations on Water Vapor Barrier and Mechanical Properties of Coated Paper. J Food Sci 2005;70:E192–7. https://doi.org/10.1111/J.1365-2621.2005.TB07135.X.
[79] Lin SY, Krochta JM. Plasticizer Effect on Grease Barrier and Color Properties of Whey-protein Coatings on Paperboard. J Food Sci 2003;68:229–33. https://doi.org/10.1111/J.1365-2621.2003.TB14144.X.
[80] Sabato SF, Ouattara B, Yu H, D'Aprano G, Le Tien G, Mateescu MA, et al. Mechanical and Barrier Properties of Cross-Linked Soy and Whey Protein Based Films. J Agric Food Chem 2001;49:1397–403. https://doi.org/10.1021/JF0005925.
[81] Rhim JW, Lee JH, Hong SI. Water resistance and mechanical properties of biopolymer (alginate and soy protein) coated paperboards. LWT - Food Sci Technol 2006;39:806–13. https://doi.org/10.1016/J.LWT.2005.05.008.
[82] Park HJ, Kim SH, Lim ST, Shin DH, Choi SY, Hwang KT. Grease resistance and mechanical properties of isolated soy protein-coated paper 2000;77:269–73. https://doi.org/10.1007/S11746-000-0044-2.

[83] Gällstedt M, Brottmon A, Hedenqvist MS. Packaging-related properties of protein- and chitosan-coated paper. Packag Technol Sci 2005;18:161–70. https://doi.org/10.1002/PTS.685.
[84] TREZZA TA, VERGANO PJ. Grease Resistance of Corn Zein Coated Paper. J Food Sci 1994;59:912–5. https://doi.org/10.1111/J.1365-2621.1994.TB08156.X.
[85] Parris N, Vergano PJ, Dickey LC, Cooke PH, Craig JC. Enzymatic Hydrolysis of Zein - Wax-Coated Paper. J Agric Food Chem 1998;46:4056–9. https://doi.org/10.1021/JF980406J/ASSET/IMAGES/LARGE/JF980406JF00004.JPEG.
[86] Mekonnen T, Misra M, Mohanty AK. Fermented Soymeals and Their Reactive Blends with Poly(butylene adipate-co-terephthalate) in Engineering Biodegradable Cast Films for Sustainable Packaging. ACS Sustain Chem Eng 2016;4:782–93. https://doi.org/10.1021/ACSSUSCHEMENG.5B00782/ASSET/IMAGES/LARGE/SC-2015-00782F_0010.JPEG.
[87] Mekonnen TH, Misra M, Mohanty AK. Processing, performance, and applications of plant and animal protein-based blends and their biocomposites. Biocomposites Des Mech Perform 2015:201–35. https://doi.org/10.1016/B978-1-78242-373-7.00017-2.
[88] Tadele DT, Shorey R, Mekonnen TH. Fatty acid modified zein films: Effect of fatty acid chain length on the processability and thermomechanical properties of modified zein films. Ind Crops Prod 2023;192:116028. https://doi.org/10.1016/J.INDCROP.2022.116028.
[89] Chen H, Wang J, Cheng Y, Wang C, Liu H, Bian H, et al. Application of protein-based films and coatings for food packaging: A review. Polymers (Basel) 2019;11:1–32. https://doi.org/10.3390/polym11122039.
[90] Wang J, Euring M, Ostendorf K, Zhang K. Biobased materials for food packaging. J Bioresour Bioprod 2022;7:1–13. https://doi.org/10.1016/J.JOBAB.2021.11.004.
[91] Mekonnen TH. Valorization of waste protein biomass for bio-based plastics , composites and adhesives development by Doctor of Philosophy in Bioresource and Food engineering 2014.
[92] Freitas F, Alves VD, Reis MA, Crespo JG, Coelhoso IM. Microbial polysaccharide-based membranes: Current and future applications. J Appl Polym Sci 2014;131:40047. https://doi.org/10.1002/APP.40047.
[93] Swain SK, Mohanty F. Polysaccharides-based bionanocomposites for food packaging applications. Bionanocomposites Packag Appl 2017:191–208. https://doi.org/10.1007/978-3-319-67319-6_10/TABLES/2.
[94] Bianco di, caruso M. Biodegradable packaging and edible coating for fresh-cut fruits and vegetables. Ital J Food Sci 2015;27:1–20. https://doi.org/10.14674/1120-1770/IJFS.V70.
[95] Du Y, Zang YH, Du J. Effects of starch on latex migration and on paper coating properties. Ind Eng Chem Res 2011;50:9781–6. https://doi.org/10.1021/IE200807W/ASSET/IMAGES/LARGE/IE-2011-00807W_0003.JPEG.
[96] Matsui KN, Larotonda FDS, Paes SS, Luiz DB, Pires ATN, Laurindo JB. Cassava bagasse-Kraft paper composites: analysis of influence of impregnation with starch acetate on tensile strength and water absorption properties. Carbohydr Polym 2004;55:237–43. https://doi.org/10.1016/J.CARBPOL.2003.07.007.
[97] Brodin FW, Gregersen ØW, Syverud K. Cellulose nanofibrils: Challenges and possibilities as a paper additive or coating material – A review. Nord Pulp Pap Res J 2014;29:156–66. https://doi.org/10.3183/NPPRJ-2014-29-01-P156-166.
[98] Teixeira-Costa BE, Andrade CT. Natural Polymers Used in Edible Food Packaging—History, Function and Application Trends as a Sustainable Alternative to Synthetic Plastic. Polysaccharides 2022, Vol 3, Pages 32-58 2021;3:32–58. https://doi.org/10.3390/POLYSACCHARIDES3010002.

[99] Kjellgren H, Gällstedt M, Engström G, Järnström L. Barrier and surface properties of chitosan-coated greaseproof paper. Carbohydr Polym 2006;65:453–60.
[100] Ham-Pichavant F, Sèbe G, Pardon P, Coma V. Fat resistance properties of chitosan-based paper packaging for food applications. Carbohydr Polym 2005;61:259–65. https://doi.org/10.1016/J.CARBPOL.2005.01.020.
[101] Despond S, Espuche E, Cartier N, Domard A. Barrier properties of paper–chitosan and paper–chitosan–carnauba wax films. J Appl Polym Sci 2005;98:704–10. https://doi.org/10.1002/APP.21754.
[102] Lavoine N, Bras J, Desloges I. Mechanical and barrier properties of cardboard and 3D packaging coated with microfibrillated cellulose. J Appl Polym Sci 2014;131:40106.
[103] Tyagi P, Hubbe MA, Lucia L, Pal L. High performance nanocellulose-based composite coatings for oil and grease resistance. Cellulose 2018;25:3377–91. https://doi.org/10.1007/S10570-018-1810-7/FIGURES/10.
[104] Tyagi P, Lucia LA, Hubbe MA, Pal L. Nanocellulose-based multilayer barrier coatings for gas, oil, and grease resistance. Carbohydr Polym 2019;206:281–8. https://doi.org/10.1016/J.CARBPOL.2018.10.114.
[105] Kumar V, Elfving A, Koivula H, Bousfield D, Toivakka M. Roll-to-Roll Processed Cellulose Nanofiber Coatings. Ind Eng Chem Res 2016;55:3603–13. https://doi.org/10.1021/ACS.IECR.6B00417/ASSET/IMAGES/LARGE/IE-2016-00417B_0014.JPEG.
[106] Mazhari Mousavi SM, Afra E, Tajvidi M, Bousfield DW, Dehghani-Firouzabadi M. Cellulose nanofiber/carboxymethyl cellulose blends as an efficient coating to improve the structure and barrier properties of paperboard. Cellulose 2017;24:3001–14. https://doi.org/10.1007/S10570-017-1299-5/FIGURES/10.
[107] Adibi A, Valdesueiro D, Simon L, Lenges CP, Mekonnen TH. High Barrier Sustainable Paper Coating Based on Engineered Polysaccharides and Natural Rubber. ACS Sustain Chem Eng 2022. https://doi.org/10.1021/ACSSUSCHEMENG.2C03466.
[108] Adibi A, Valdesueiro D, Mok J, Behabtu N, Lenges C, Simon L, et al. Sustainable barrier paper coating based on alpha-1,3 glucan and natural rubber latex. Carbohydr Polym 2022;282:119121. https://doi.org/10.1016/J.CARBPOL.2022.119121.
[109] Khwaldia K, Arab-Tehrany E, Desobry S. Biopolymer Coatings on Paper Packaging Materials. Compr Rev Food Sci Food Saf 2010;9:82–91. https://doi.org/10.1111/J.1541-4337.2009.00095.X.
[110] Rodríguez A, Batlle R, Nerín C. The use of natural essential oils as antimicrobial solutions in paper packaging. Part II. Prog Org Coatings 2007;60:33–8. https://doi.org/10.1016/J.PORGCOAT.2007.06.006.
[111] Gupta V, Biswas D, Roy S. A Comprehensive Review of Biodegradable Polymer-Based Films and Coatings and Their Food Packaging Applications. Mater 2022, Vol 15, Page 5899 2022;15:5899. https://doi.org/10.3390/MA15175899.
[112] Han J, Salmieri S, Le Tien C, Lacroix M. Improvement of water barrier property of paperboard by coating application with biodegradable polymers. J Agric Food Chem 2010;58:3125–31. https://doi.org/10.1021/JF904443N/ASSET/IMAGES/LARGE/JF-2009-04443N_0006.JPEG.
[113] Zhang W, Lu P, Qian L, Xiao H. Fabrication of superhydrophobic paper surface via wax mixture coating. Chem Eng J 2014;250:431–6. https://doi.org/10.1016/J.CEJ.2014.04.050.
[114] Trinh BM, Smith M, Mekonnen TH. A nanomaterial-stabilized starch-beeswax Pickering emulsion coating to extend produce shelf-life. Chem Eng J 2022;431:133905.

https://doi.org/10.1016/J.CEJ.2021.133905.
[115] Zhang W, Xiao H, Qian L. Enhanced water vapour barrier and grease resistance of paper bilayer-coated with chitosan and beeswax. Carbohydr Polym 2014;101:401–6. https://doi.org/10.1016/J.CARBPOL.2013.09.097.
[116] Fei T, Walker JA, Vickerman KL, Stanley LM, Jarboe D, Wang T. Synthesis and characterization of soybean oil-based waxes and their application as paraffin substitute for corrugated coating. J Ind Eng Chem 2018;58:113–22. https://doi.org/10.1016/J.JIEC.2017.09.015.
[117] Tambe C, Graiver D, Narayan R. Moisture resistance coating of packaging paper from biobased silylated soybean oil. Prog Org Coatings 2016;101:270–8. https://doi.org/10.1016/J.PORGCOAT.2016.08.016.
[118] Ren K, Fei T, Metzger K, Wang T. Coating performance and rheological characteristics of novel soybean oil-based wax emulsions. Ind Crops Prod 2019;140. https://doi.org/10.1016/J.INDCROP.2019.111654.
[119] Xiong SJ, Pang B, Zhou SJ, Li MK, Yang S, Wang YY, et al. Economically Competitive Biodegradable PBAT/Lignin Composites: Effect of Lignin Methylation and Compatibilizer. ACS Sustain Chem Eng 2020;8:5338–46. https://doi.org/10.1021/ACSSUSCHEMENG.0C00789/ASSET/IMAGES/LARGE/SC0C00789_0003.JPEG.
[120] Shorey R, Mekonnen TH. Sustainable paper coating with enhanced barrier properties based on esterified lignin and PBAT blend. Int J Biol Macromol 2022;209:472–84. https://doi.org/10.1016/J.IJBIOMAC.2022.04.037.
[121] Zhang Z, Terrasson V, Guénin E. Lignin nanoparticles and their nanocomposites. Nanomaterials 2021;11. https://doi.org/10.3390/nano11051336.
[122] Mujtaba M, Lipponen J, Ojanen M, Puttonen S, Vaittinen H. Trends and challenges in the development of bio-based barrier coating materials for paper/cardboard food packaging; a review. Sci Total Environ 2022;851:158328. https://doi.org/10.1016/j.scitotenv.2022.158328.
[123] Bucci DZ, Tavares LBB, Sell I. PHB packaging for the storage of food products. Polym Test 2005;24:564–71. https://doi.org/10.1016/J.POLYMERTESTING.2005.02.008.
[124] Kunam PK, Ramakanth D, Akhila K, Gaikwad KK. Bio-based materials for barrier coatings on paper packaging. Biomass Convers Biorefinery 2022. https://doi.org/10.1007/s13399-022-03241-2.
[125] Bang G, Kim SW. Biodegradable poly(lactic acid)-based hybrid coating materials for food packaging films with gas barrier properties. J Ind Eng Chem 2012;18:1063–8. https://doi.org/10.1016/J.JIEC.2011.12.004.
[126] Iotti M, Fabbri P, Messori M, Pilati F, Fava P. Organic-inorganic hybrid coatings for the modification of barrier properties of poly(lactic acid) films for food packaging applications. J Polym Environ 2009;17:10–9. https://doi.org/10.1007/S10924-009-0120-4/FIGURES/6.
[127] Bahari K, Mitomo H, Enjoji T, Yoshii F, Makuuchi K. Radiation crosslinked poly(butylene succinate) foam and its biodegradation. Polym Degrad Stab 1998;62:551–7. https://doi.org/10.1016/S0141-3910(98)00041-X.
[128] Duan H, Shao Z, Zhao M, Zhou Z. Preparation and properties of environmental-friendly coatings based on carboxymethyl cellulose nitrate ester & modified alkyd. Carbohydr Polym 2016;137:92–9. https://doi.org/10.1016/J.CARBPOL.2015.10.067.
[129] Belletti G, Buoso S, Ricci L, Guillem-Ortiz A, Aragón-Gutiérrez A, Bortolini O, et al. Preparations of poly(Lactic acid) dispersions in water for coating applications. Polymers (Basel) 2021;13:1–19. https://doi.org/10.3390/polym13162767.

[130] Choudalakis G, Gotsis AD, Wang J, Gardner DJ, Stark NM, Bousfield DW, et al. Moisture and Oxygen Barrier Properties of Cellulose Nanomaterial-Based Films. ACS Sustain Chem Eng 2018;6:49–70. https://doi.org/10.1021/acssuschemeng.7b03523.
[131] Choudalakis G, Gotsis AD. Permeability of polymer/clay nanocomposites: A review. Eur Polym J 2009;45:967–84. https://doi.org/10.1016/J.EURPOLYMJ.2009.01.027.
[132] Chen GQ, Scholes CA, Doherty CM, Hill AJ, Qiao GG, Kentish SE. Modeling of the sorption and transport properties of water vapor in polyimide membranes. J Memb Sci 2012;409–410:96–104. https://doi.org/10.1016/J.MEMSCI.2012.03.047.
[133] Comesaña-Gandara B, Ansaloni L, Lee YM, Lozano AE, De Angelis MG. Sorption, diffusion, and permeability of humid gases and aging of thermally rearranged (TR) polymer membranes from a novel ortho-hydroxypolyimide. J Memb Sci 2017;542:439–55. https://doi.org/10.1016/J.MEMSCI.2017.08.009.
[134] Zabihzadeh Khajavi M, Ebrahimi A, Yousefi M, Ahmadi S, Farhoodi M, Mirza Alizadeh A, et al. Strategies for Producing Improved Oxygen Barrier Materials Appropriate for the Food Packaging Sector. Food Eng Rev 2020 123 2020;12:346–63. https://doi.org/10.1007/S12393-020-09235-Y.
[135] Bertuzzi MA, Castro Vidaurre EF, Armada M, Gottifredi JC. Water vapor permeability of edible starch based films. J Food Eng 2007;80:972–8.
[136] Morillon V, Debeaufort F, Blond G, Capelle M, Voilley A. Factors affecting the moisture permeability of lipid-based edible films: a review. Crit Rev Food Sci Nutr 2002;42:67–89. https://doi.org/10.1080/10408690290825466.
[137] Catalano J, Myezwa T, De Angelis MG, Baschetti MG, Sarti GC. The effect of relative humidity on the gas permeability and swelling in PFSI membranes. Int J Hydrogen Energy 2012;37:6308–16. https://doi.org/10.1016/J.IJHYDENE.2011.07.047.
[138] Lasseuguette E, Malpass-Evans R, Carta M, McKeown NB, Ferrari MC. Temperature and Pressure Dependence of Gas Permeation in a Microporous Tröger's Base Polymer. Membranes (Basel) 2018;8. https://doi.org/10.3390/MEMBRANES8040132.
[139] Trinh BM, Chang BP, Mekonnen TH. The barrier properties of sustainable multiphase and multicomponent packaging materials: A review. Prog Mater Sci 2023;133:101071. https://doi.org/10.1016/J.PMATSCI.2023.101071.
[140] Aulin C, Ström G. Multilayered alkyd resin/nanocellulose coatings for use in renewable packaging solutions with a high level of moisture resistance. Ind Eng Chem Res 2013;52:2582–9. https://doi.org/10.1021/IE301785A/ASSET/IMAGES/IE-2012-01785A_M001.GIF.
[141] Choi JO, Jitsunari F, Asakawa F, Park HJ, Lee DS. Migration of surrogate contaminants in paper and paperboard into water through polyethylene coating layer. Http://DxDoiOrg/101080/02652030210151877 2010;19:1200–6. https://doi.org/10.1080/02652030210151877.
[142] Farhat W, Venditti R, Quick A, Taha M, Mignard N, Becquart F, et al. Hemicellulose extraction and characterization for applications in paper coatings and adhesives. Ind Crops Prod 2017;107:370–7. https://doi.org/10.1016/J.INDCROP.2017.05.055.
[143] Parreidt TS, Müller K, Schmid M. Alginate-Based Edible Films and Coatings for Food Packaging Applications. Foods (Basel, Switzerland) 2018;7:E170–E170. https://doi.org/10.3390/FOODS7100170.
[144] Li H, Qi Y, Zhao Y, Chi J, Cheng S. Starch and its derivatives for paper coatings: A review. Prog Org Coatings 2019;135:213–27. https://doi.org/10.1016/J.PORGCOAT.2019.05.015.
[145] Song Z, Xiao H, Zhao Y. Hydrophobic-modified nano-cellulose fiber/PLA biodegradable

composites for lowering water vapor transmission rate (WVTR) of paper. Carbohydr Polym 2014;111:442–8.
[146] Rhim JW, Lee JH, Hong SI. Increase in water resistance of paperboard by coating with poly(lactide). Packag Technol Sci 2007;20:393–402. https://doi.org/10.1002/PTS.767.
[147] Wang W, Qin C, Li W, Ge J, Feng C. Improving moisture barrier properties of paper sheets by cellulose stearoyl ester-based coatings. Carbohydr Polym 2020;235:115924. https://doi.org/10.1016/J.CARBPOL.2020.115924.
[148] Yook S, Park HH, Park HH, Lee SY, Kwon J, Youn HJ. Barrier coatings with various types of cellulose nanofibrils and their barrier properties. Cellulose 2020;27:4509–23. https://doi.org/10.1007/S10570-020-03061-5/FIGURES/10.
[149] Wang W, Gu F, Deng Z, Zhu Y, Zhu J, Guo T, et al. Multilayer surface construction for enhancing barrier properties of cellulose-based packaging. Carbohydr Polym 2021;255:117431. https://doi.org/10.1016/j.carbpol.2020.117431.
[150] Kansal D, Hamdani SS, Ping R, Sirinakbumrung N, Rabnawaz M. Food-Safe Chitosan-Zein Dual-Layer Coating for Water- And Oil-Repellent Paper Substrates. ACS Sustain Chem Eng 2020;8:6887–97. https://doi.org/10.1021/ACSSUSCHEMENG.0C02216/ASSET/IMAGES/LARGE/SC0C02216_0009.JPEG.
[151] Zhu R, Liu X, Song P, Wang M, Xu F, Jiang Y, et al. An approach for reinforcement of paper with high strength and barrier properties via coating regenerated cellulose. Carbohydr Polym 2018;200:100–5. https://doi.org/10.1016/j.carbpol.2018.07.069.
[152] Li Z, Rabnawaz M, Khan B. Response Surface Methodology Design for Biobased and Sustainable Coatings for Water- And Oil-Resistant Paper. ACS Appl Polym Mater 2020;2:1378–87. https://doi.org/10.1021/ACSAPM.9B01238/ASSET/IMAGES/LARGE/AP9B01238_0006.JPEG.
[153] Reis AB, Yoshida CMP, Reis APC, Franco TT. Application of chitosan emulsion as a coating on Kraft paper. Polym Int 2011;60:963–9. https://doi.org/10.1002/PI.3023.
[154] Khwaldia K. HPMC coating for paper. vol. 8. 2013.
[155] Parris N, Dickey LC, Wiles JL, Moreau RA, Cooke PH. Enzymatic hydrolysis, grease permeation, and water barrier properties of zein isolate coated paper. J Agric Food Chem 2000;48:890–4. https://doi.org/10.1021/JF991079Y/ASSET/IMAGES/LARGE/JF991079YF00007.JPEG.
[156] Rhim JW, Kim JH. No Title. J Food Sci 2009;74:E105–11. https://doi.org/10.1111/J.1750-3841.2009.01073.X.
[157] Cyras VP, Soledad CM, Analía V. Biocomposites based on renewable resource: Acetylated and non acetylated cellulose cardboard coated with polyhydroxybutyrate. Polymer (Guildf) 2009;50:6274–80. https://doi.org/10.1016/J.POLYMER.2009.10.065.
[158] He Y, Li H, Fei X, Peng L. Carboxymethyl cellulose/cellulose nanocrystals immobilized silver nanoparticles as an effective coating to improve barrier and antibacterial properties of paper for food packaging applications. Carbohydr Polym 2021;252:117156. https://doi.org/10.1016/J.CARBPOL.2020.117156.
[159] Lagaron JM, Catalá R, Gavara R. Structural characteristics defining high barrier properties in polymeric materials. Http://DxDoiOrg/101179/026708304225010442 2013;20:1–7. https://doi.org/10.1179/026708304225010442.
[160] Bonilla J, Atarés L, Vargas M, Chiralt A. Edible films and coatings to prevent the detrimental effect of oxygen on food quality: Possibilities and limitations. J Food Eng 2012;110:208–13.

https://doi.org/10.1016/J.JFOODENG.2011.05.034.
[161] Aulin C, Gällstedt M, Lindström T. Oxygen and oil barrier properties of microfibrillated cellulose films and coatings. Cellulose 2010;17:559–74.
[162] Herrera MA, Mathew AP, Oksman K. Barrier and mechanical properties of plasticized and cross-linked nanocellulose coatings for paper packaging applications. Cellulose 2017;24:3969–80.
[163] Song Y, Tzeng P, Grunlan JC. Super Oxygen and Improved Water Vapor Barrier of Polypropylene Film with Polyelectrolyte Multilayer Nanocoatings. Macromol Rapid Commun 2016;37:963–8. https://doi.org/10.1002/MARC.201600140.
[164] Felton LA. Characterization of coating systems. AAPS PharmSciTech 2007 84 2007;8:258–66. https://doi.org/10.1208/PT0804112.
[165] Adibi A, Kim J, Mok J, Lenges C, Simon L, Mekonnen TH. Enzymatic polymerization designed alpha-1,3 glucan particle morphology as reinforcing fillers of dipped and casted rubber films. Carbohydr Polym 2021;267:118234. https://doi.org/10.1016/J.CARBPOL.2021.118234.
[166] Guillaume C, Pinte J, Gontard N, Gastaldi E. Wheat gluten-coated papers for bio-based food packaging: Structure, surface and transfer properties. Food Res Int 2010;43:1395–401. https://doi.org/10.1016/J.FOODRES.2010.04.014.
[167] Hult EL, Iotti M, Lenes M. Efficient approach to high barrier packaging using microfibrillar cellulose and shellac. Cellulose 2010;17:575–86. https://doi.org/10.1007/S10570-010-9408-8/FIGURES/5.
[168] McGonigle EA, Liggat JJ, Pethrick RA, Jenkins SD, Daly JH, Hayward D. Permeability of N2, Ar, He, O2 and CO2 through biaxially oriented polyester films — dependence on free volume. Polymer (Guildf) 2001;42:2413–26. https://doi.org/10.1016/S0032-3861(00)00615-7.
[169] Li F, Biagioni P, Bollani M, Maccagnan A, Piergiovanni L. Multi-functional coating of cellulose nanocrystals for flexible packaging applications. Cellulose 2013;20:2491–504. https://doi.org/10.1007/s10570-013-0015-3.
[170] Kjellgren H. Barrier Properties of greaseproof paper 2005:1–94.
[171] Corte H. The Porous Structure of Paper. Fundam. Papermak. Fibres, Trans. Symp., British Paper and Board Maker's Association; 1958, p. 301–31.
[172] Chi K, Wang H, Catchmark JM. Sustainable starch-based barrier coatings for packaging applications. Food Hydrocoll 2020;103:105696. https://doi.org/10.1016/J.FOODHYD.2020.105696.
[173] Kopacic S, Walzl A, Zankel A, Leitner E, Bauer W. Alginate and Chitosan as a Functional Barrier for Paper-Based Packaging Materials. Coatings 2018, Vol 8, Page 235 2018;8:235. https://doi.org/10.3390/COATINGS8070235.
[174] Sheng J, Li J, Zhao L. Fabrication of grease resistant paper with non-fluorinated chemicals for food packaging. Cellulose 2019;26:6291–302. https://doi.org/10.1007/S10570-019-02504-Y/FIGURES/11.
[175] Tayeb AH, Tajvidi M, Bousfield D. Paper-based oil barrier packaging using lignin-containing cellulose nanofibrils. Molecules 2020;25. https://doi.org/10.3390/molecules25061344.
[176] Wang F, Wang L, Zhang X, Ma S. Improved Oil Resistance of Cellulose Packaging Paper by Coating with Natural Polymer Derived Materials Keywords: coated paper · oil resistance · air permeability · polarity n.d.
[177] Fein K, Bousfield DW, Gramlich WM. Thiol-norbornene reactions to improve natural rubber dispersion in cellulose nanofiber coatings. Carbohydr Polym 2020;250:117001. https://doi.org/10.1016/J.CARBPOL.2020.117001.

[178] de Freitas CAS, de Sousa PHM, Soares DJ, da Silva JYG, Benjamin SR, Guedes MIF. Carnauba wax uses in food – A review. Food Chem 2019;291:38–48. https://doi.org/10.1016/J.FOODCHEM.2019.03.133.
[179] Liu D, Duan Y, Wang S, Gong M, Dai H. Improvement of Oil and Water Barrier Properties of Food Packaging Paper by Coating with Microcrystalline Wax Emulsion. Polym 2022, Vol 14, Page 1786 2022;14:1786. https://doi.org/10.3390/POLYM14091786.
[180] Panchal P, Ogunsona E, Mekonnen T. Trends in Advanced Functional Material Applications of Nanocellulose. Process 2019, Vol 7, Page 10 2018;7:10. https://doi.org/10.3390/PR7010010.
[181] Dunlop-Jones N. Wet-strength chemistry. Pap Chem 1991:76–96. https://doi.org/10.1007/978-94-011-6474-0_6.
[182] Sun S, An Q, Li X, Qian L, He B, Xiao H. Synergistic effects of chitosan–guanidine complexes on enhancing antimicrobial activity and wet-strength of paper. Bioresour Technol 2010;101:5693–700. https://doi.org/10.1016/J.BIORTECH.2010.02.046.
[183] Arbatan T, Zhang L, Fang XY, Shen W. Cellulose nanofibers as binder for fabrication of superhydrophobic paper. Chem Eng J 2012;210:74–9. https://doi.org/10.1016/J.CEJ.2012.08.074.
[184] Khanjani P, King AWT, Partl GJ, Johansson LS, Kostiainen MA, Ras RHA. Superhydrophobic Paper from Nanostructured Fluorinated Cellulose Esters. ACS Appl Mater Interfaces 2018;10:11280–8. https://doi.org/10.1021/acsami.7b19310.
[185] Cheng HY, Yang YJ, Li SC, Hong JY, Jang GW. Modification and extrusion coating of polylactic acid films. J Appl Polym Sci 2015;132. https://doi.org/10.1002/APP.42472.
[186] El-Sadi H, Carreau P, Esmail N. Changes in the rheological and colloidal properties of paper coating liquids with paper-yellowing inhibition additives. J Colloid Interface Sci 2004;271:496–503. https://doi.org/10.1016/j.jcis.2003.07.019.
[187] Page A, Carreau PJ, Moan M, Heuzey MC. Rheological Behavior of Coating Colors: Influence of Thickener. Can J Chem Eng 2002;80:1181–8. https://doi.org/10.1002/CJCE.5450800620.
[188] Liang H, Long Z, Yang S, Dai L. Organic modification of bentonite and its effect on rheological properties of paper coating. Appl Clay Sci 2015;104:106–9. https://doi.org/10.1016/j.clay.2014.11.015.
[189] Liu C, Du H, Dong L, Wang X, Zhang Y, Yu G, et al. Properties of Nanocelluloses and Their Application as Rheology Modifier in Paper Coating. Ind Eng Chem Res 2017;56:8264–73.
[190] Vilela C, Kurek M, Hayouka Z, Röcker B, Yildirim S, Antunes MDC, et al. A concise guide to active agents for active food packaging. Trends Food Sci Technol 2018;80:212–22. https://doi.org/10.1016/J.TIFS.2018.08.006.
[191] OZDEMIR M, FLOROS JD. Active Food Packaging Technologies. Http://DxDoiOrg/101080/10408690490441578 2010;44:185–93. https://doi.org/10.1080/10408690490441578.
[192] Stoleru E, Vasile C, Irimia A, Brebu M. Towards a Bioactive Food Packaging: Poly(Lactic Acid) Surface Functionalized by Chitosan Coating Embedding Clove and Argan Oils. Mol 2021, Vol 26, Page 4500 2021;26:4500. https://doi.org/10.3390/MOLECULES26154500.
[193] Motelica L, Ficai D, Ficai A, Oprea OC, Kaya DA, Andronescu E. Biodegradable Antimicrobial Food Packaging: Trends and Perspectives. Foods 2020, Vol 9, Page 1438 2020;9:1438. https://doi.org/10.3390/FOODS9101438.
[194] Gaikwad KK, Singh S, Lee YS. Oxygen scavenging films in food packaging. Environ Chem Lett 2018;16:523–38. https://doi.org/10.1007/S10311-018-0705-Z/FIGURES/5.

[195] Gaikwad KK, Singh S, Ajji A. Moisture absorbers for food packaging applications. Environ Chem Lett 2019;17:609–28. https://doi.org/10.1007/S10311-018-0810-Z/TABLES/4.
[196] Taboada-Rodríguez A, García-García I, Cava-Roda R, López-Gómez A, Marín-Iniesta F. Hydrophobic properties of cardboard coated with polylactic acid and ethylene scavengers. J Coatings Technol Res 2013;10:749–55. https://doi.org/10.1007/S11998-013-9493-3/FIGURES/4.
[197] Ni X, Yu J, Shao P, Yu J, Chen H, Gao H. Preservation of Agaricus bisporus freshness with using innovative ethylene manipulating active packaging paper. Food Chem 2021;345:128757. https://doi.org/10.1016/J.FOODCHEM.2020.128757.
[198] Yildirim S, Röcker B, Pettersen MK, Nilsen-Nygaard J, Ayhan Z, Rutkaite R, et al. Active Packaging Applications for Food. Compr Rev Food Sci Food Saf 2018;17:165–99. https://doi.org/10.1111/1541-4337.12322.
[199] Ortega-Ramirez LA, Rodriguez-Garcia I, Leyva JM, Cruz-Valenzuela MR, Silva-Espinoza BA, Gonzalez-Aguilar GA, et al. Potential of Medicinal Plants as Antimicrobial and Antioxidant Agents in Food Industry: A Hypothesis. J Food Sci 2014;79:R129–37. https://doi.org/10.1111/1750-3841.12341.
[200] Ni S, Zhang H, Dai H, Xiao H. Starch-Based Flexible Coating for Food Packaging Paper with Exceptional Hydrophobicity and Antimicrobial Activity. Polym 2018, Vol 10, Page 1260 2018;10:1260. https://doi.org/10.3390/POLYM10111260.
[201] Bordenave N, Grelier S, Coma V. Hydrophobization and antimicrobial activity of chitosan and paper-based packaging material. Biomacromolecules 2010;11:88–96. https://doi.org/10.1021/BM9009528/SUPPL_FILE/BM9009528_SI_001.PDF.
[202] Wu YB, Yu SH, Mi FL, Wu CW, Shyu SS, Peng CK, et al. Preparation and characterization on mechanical and antibacterial properties of chitsoan/cellulose blends. Carbohydr Polym 2004;57:435–40. https://doi.org/10.1016/J.CARBPOL.2004.05.013.
[203] Yu Z, Ji Y, Bourg V, Bilgen M, Meredith JC. Chitin- and cellulose-based sustainable barrier materials: a review. Emergent Mater 2020;3:919–36. https://doi.org/10.1007/S42247-020-00147-5/TABLES/4.
[204] Razavi R, Tajik H, Moradi M, Molaei R, Ezati P. Antimicrobial, microscopic and spectroscopic properties of cellulose paper coated with chitosan sol-gel solution formulated by epsilon-poly-l-lysine and its application in active food packaging. Carbohydr Res 2020;489:107912. https://doi.org/10.1016/J.CARRES.2020.107912.
[205] Youssef AM, El-Sayed SM. Bionanocomposites materials for food packaging applications: Concepts and future outlook. Carbohydr Polym 2018;193:19–27. https://doi.org/10.1016/J.CARBPOL.2018.03.088.
[206] Jung J, Kasi G, Seo J. Development of functional antimicrobial papers using chitosan/starch-silver nanoparticles. Int J Biol Macromol 2018;112:530–6. https://doi.org/10.1016/J.IJBIOMAC.2018.01.155.
[207] Nieto G, Ros G, Castillo J. Antioxidant and Antimicrobial Properties of Rosemary (Rosmarinus officinalis, L.): A Review. Med 2018, Vol 5, Page 98 2018;5:98. https://doi.org/10.3390/MEDICINES5030098.
[208] Akhtar MJ, Jacquot M, Jamshidian M, Imran M, Arab-Tehrany E, Desobry S. Fabrication and physicochemical characterization of HPMC films with commercial plant extract: Influence of light and film composition. Food Hydrocoll 2013;31:420–7. https://doi.org/10.1016/J.FOODHYD.2012.10.008.
[209] Battisti R, Fronza N, Vargas Júnior Á, Silveira SM da, Damas MSP, Quadri MGN. Gelatin-coated paper with antimicrobial and antioxidant effect for beef packaging. Food Packag Shelf

Life 2017;11:115–24. https://doi.org/10.1016/J.FPSL.2017.01.009.
[210] Amor G, Sabbah M, Caputo L, Idbella M, De Feo V, Porta R, et al. Basil Essential Oil: Composition, Antimicrobial Properties, and Microencapsulation to Produce Active Chitosan Films for Food Packaging. Foods 2021, Vol 10, Page 121 2021;10:121. https://doi.org/10.3390/FOODS10010121.
[211] Mutlu-Ingok A, Devecioglu D, Dikmetas DN, Karbancioglu-Guler F, Capanoglu E. Antibacterial, Antifungal, Antimycotoxigenic, and Antioxidant Activities of Essential Oils: An Updated Review. Mol 2020, Vol 25, Page 4711 2020;25:4711. https://doi.org/10.3390/MOLECULES25204711.
[212] Li WC, Tse HF, Fok L. Plastic waste in the marine environment: A review of sources, occurrence and effects. Sci Total Environ 2016;566–567:333–49. https://doi.org/10.1016/J.SCITOTENV.2016.05.084.
[213] Roohi SP, Bano K, Zaheer MR, Kuddus M. Biodegradable smart biopolymers for food packaging: Sustainable approach toward green environment. Bio-Based Mater Food Packag Green Sustain Adv Packag Mater 2018:197–216. https://doi.org/10.1007/978-981-13-1909-9_9/TABLES/3.
[214] Avérous L, Pollet E. Biodegradable Polymers. Green Energy Technol 2012;50:13–39. https://doi.org/10.1007/978-1-4471-4108-2_2.
[215] Sander M. Biodegradation of Polymeric Mulch Films in Agricultural Soils: Concepts, Knowledge Gaps, and Future Research Directions. Environ Sci Technol 2019;53:2304–15. https://doi.org/10.1021/ACS.EST.8B05208/ASSET/IMAGES/LARGE/ES-2018-052088_0001.JPEG.
[216] Imam S, Glenn G, Chiou BS, Shey J, Narayan R, Orts W. Types, production and assessment of biobased food packaging materials. Environ Compat Food Packag 2008:29–62. https://doi.org/10.1533/9781845694784.1.29.
[217] Kechichian V, Ditchfield C, Veiga-Santos P, Tadini CC. Natural antimicrobial ingredients incorporated in biodegradable films based on cassava starch. LWT - Food Sci Technol 2010;43:1088–94. https://doi.org/10.1016/J.LWT.2010.02.014.
[218] Alvarez JVL, Larrucea MA, Bermúdez PA, Chicote BL. Biodegradation of paper waste under controlled composting conditions. Waste Manag 2009;29:1514–9. https://doi.org/10.1016/J.WASMAN.2008.11.025.
[219] Ni H, Zeng S, Wu J, Cheng X, Luo T, Wang W, et al. Cellulose nanowhiskers: Preparation, characterization and cytotoxicity evaluation. Biomed Mater Eng 2012;22:121–7. https://doi.org/10.3233/BME-2012-0697.
[220] Moustafa H, Guizani C, Dufresne A. Sustainable biodegradable coffee grounds filler and its effect on the hydrophobicity, mechanical and thermal properties of biodegradable PBAT composites. J Appl Polym Sci 2017;134:44498. https://doi.org/10.1002/APP.44498.
[221] Siracusa V, Rocculi P, Romani S, Rosa MD. Biodegradable polymers for food packaging: a review. Trends Food Sci Technol 2008;19:634–43. https://doi.org/10.1016/J.TIFS.2008.07.003.
[222] Mangaraj S, Yadav A, Lalit ·, Bal M, Dash · S K, Mahanti NK. Application of Biodegradable Polymers in Food Packaging Industry: A Comprehensive Review. J Packag Technol Res 2018 31 2018;3:77–96. https://doi.org/10.1007/S41783-018-0049-Y.
[223] McCall DW, Douglass DC, Blyler LL, Johnson GE, Jelinski LW, Bair HE. Solubility and Diffusion of Water in Low-Density Polyethylene. Macromolecules 1984;17:1644–9. https://doi.org/10.1021/MA00139A001/ASSET/MA00139A001.FP.PNG_V03.
[224] Dissanayake T, Peng Chang B, Mekonnen TH, Senaka Ranadheera C, Narvaez-Bravo C,

Bandara N. Reinforcing canola protein matrix with chemically tailored nanocrystalline cellulose improves the functionality of canola protein-based packaging materials. Food Chem 2022;383:132618. https://doi.org/10.1016/J.FOODCHEM.2022.132618.
[225] Dissanayake T, Trinh BM, Mekonnen TH, Sarkar P, Aluko RE, Bandara N. Improving properties of canola protein-based nanocomposite films by hydrophobically modified nanocrystalline cellulose. Food Packag Shelf Life 2023;35:101018. https://doi.org/10.1016/J.FPSL.2022.101018.
[226] Yu H, Yan C, Yao J. Fully biodegradable food packaging materials based on functionalized cellulose nanocrystals/poly(3-hydroxybutyrate-co-3-hydroxyvalerate) nanocomposites. RSC Adv 2014;4:59792–802. https://doi.org/10.1039/C4RA12691B.
[227] On NK, Rashid AA, Nazlan MMM, Hamdan H. Thermal and mechanical behavior of natural rubber latex-silica aerogel film. J Appl Polym Sci 2012;124:3108–16. https://doi.org/10.1002/app.35354.
[228] Joseph L, Joseph R. Study of the effect of polyethylene glycols and glycerol in filled natural rubber latex vulcanizates. Int J Polym Mater Polym Biomater 1995;27:189–208. https://doi.org/10.1080/00914039508009669.
[229] Lenges C, Behabtu N, Mok J, Sendijarevic I, Sendijarevic A. Engineered polysaccharide alpha-1,3 glucan as <scp>isocyanate-reactive</scp> component in viscoelastic polyurethane foams. J Appl Polym Sci 2021;138:49979. https://doi.org/10.1002/app.49979.
[230] Luing Nikalus Swee S, Guan Toh G, Wai Yip M, Chew Tai S. Systematic Innovation for Manufacturing Quality Improvement n.d. https://doi.org/10.1051/matecconf/201822102005.
[231] Kim DY, Park JW, Lee DY, Seo KH. Correlation between the crosslink characteristics and mechanical properties of natural rubber compound via accelerators and reinforcement. Polymers (Basel) 2020;12:1–14. https://doi.org/10.3390/polym12092020.
[232] Flory PJ, Rehner J. Statistical mechanics of cross-linked polymer networks I. Rubberlike elasticity. J. Chem. Phys., vol. 11, American Institute of PhysicsAIP; 1943, p. 512–20. https://doi.org/10.1063/1.1723791.
[233] Rhim JW, Mohanty KA, Singh SP, Ng PKW. Preparation and properties of biodegradable multilayer films based on soy protein isolate and poly(lactide). Ind Eng Chem Res 2006;45:3059–66. https://doi.org/10.1021/ie051207+.
[234] Downey, J.; Mekonnen, T.; Behabtu, N.; Lenges C. Rubber compositions comprising polysaccharides. WO/2018/081263, 2018.
[235] Raper S, Harris S, Corrigan D, Kim K, Lenges C. Engineered Polysaccharides: A Novel Biomaterial Additive with Multifunctional Properties. Am. Coatings Assoc., American Coatings Association; 2020, p. 13.
[236] Trinh B, Mekonnen T. Hydrophobic Esterification of Cellulose Nanocrystals for Epoxy Reinforcement. Polymer (Guildf) 2018. https://doi.org/10.1016/j.polymer.2018.08.076.
[237] Trinh BM, Mekonnen T. Hydrophobic esterification of cellulose nanocrystals for epoxy reinforcement. Polymer (Guildf) 2018;155:64–74. https://doi.org/10.1016/j.polymer.2018.08.076.
[238] Kumari S, Chauhan GS. New cellulose-lysine Schiff-base-based sensor-adsorbent for mercury ions. ACS Appl Mater Interfaces 2014;6:5908–17. https://doi.org/10.1021/am500820n.
[239] Aguayo MG, Pérez AF, Reyes G, Oviedo C, Gacitúa W, Gonzalez R, et al. Isolation and characterization of cellulose nanocrystals from rejected fibers originated in the Kraft Pulping process. Polymers (Basel) 2018;10. https://doi.org/10.3390/polym10101145.
[240] Carrillo I, Mendonça RT, Ago M, Rojas OJ. Comparative study of cellulosic components isolated from different Eucalyptus species. Cellulose 2018;25:1011–29.

https://doi.org/10.1007/s10570-018-1653-2.
[241] Kizil R, Irudayaraj J, And †, Seetharaman K. Characterization of Irradiated Starches by Using FT-Raman and FTIR Spectroscopy 2002. https://doi.org/10.1021/jf011652p.
[242] Sinclair A, Zhou X, Tangpong S, Bajwa DS, Quadir M, Jiang L. High-performance styrene-butadiene rubber nanocomposites reinforced by surface-modified cellulose nanofibers. ACS Omega 2019;4:13189–99. https://doi.org/10.1021/acsomega.9b01313.
[243] Norhazariah S, Azura AR, Sivakumar R, Azahari B. Effect of Different Preparation Methods on Crosslink density and Mechanical Properties of Carrageenan filled Natural Rubber (NR) Latex Films. Procedia Chem 2016;19:986–92. https://doi.org/10.1016/j.proche.2016.03.146.
[244] Ogunsona E, Hojabr S, Berry R, Mekonnen TH. Nanocellulose-triggered structural and property changes of acrylonitrile-butadiene rubber films. Int J Biol Macromol 2020;164:2038–50. https://doi.org/10.1016/j.ijbiomac.2020.07.202.
[245] Bokobza L. The reinforcement of elastomeric networks by fillers. Macromol Mater Eng 2004;289:607–21. https://doi.org/10.1002/mame.200400034.
[246] Afiq MM, Azura AR. Effect of sago starch loadings on soil decomposition of Natural Rubber Latex (NRL) composite films mechanical properties. Int Biodeterior Biodegrad 2013;85:139–49. https://doi.org/10.1016/j.ibiod.2013.06.016.
[247] Jardin JM, Zhang Z, Hu G, Tam KC, Mekonnen TH. Reinforcement of rubber nanocomposite thin sheets by percolation of pristine cellulose nanocrystals. Int J Biol Macromol 2020;152:428–36. https://doi.org/10.1016/j.ijbiomac.2020.02.303.
[248] Eslami H, Tzoganakis C, Mekonnen TH. Surface graft polymerization of lactic acid from the surface of cellulose nanocrystals and applications in chloroprene rubber film composites. Cellulose 2020;27:5267–84. https://doi.org/10.1007/s10570-020-03167-w.
[249] Eslami H, Tzoganakis C, Mekonnen TH. Constructing pristine and modified cellulose nanocrystals based cured polychloroprene nanocomposite films for dipped goods application. Compos Part C Open Access 2020;1:100009.
[250] Mekonnen THTH, Ah-Leung T, Hojabr S, Berry R. Investigation of the co-coagulation of natural rubber latex and cellulose nanocrystals aqueous dispersion. Colloids Surfaces A Physicochem Eng Asp 2019;583. https://doi.org/10.1016/j.colsurfa.2019.123949.
[251] Khalid M, Ismail AF, Ratnam CT, Faridah Y, Rashmi W, Al Khatib MF. Effect of radiation dose on the properties of natural rubber nanocomposite. Radiat Phys Chem 2010;79:1279–85. https://doi.org/10.1016/j.radphyschem.2010.07.002.
[252] Esmizadeh E, Chang BP, Jubinville D, Ojogbo E, Seto C, Tzoganakis C, et al. Can Medical-Grade Gloves Provide Protection after Repeated Disinfection? ACS Appl Polym Mater 2020:acsapm.0c01202. https://doi.org/10.1021/acsapm.0c01202.
[253] Zheng X, Jin Y, Chen J, Li B, Fu Q, He G. Mechanical properties and microstructure characterization of natural rubber reinforced by helical carbon nanofibers. J Mater Sci 2019;54:12962–71. https://doi.org/10.1007/s10853-019-03771-7.
[254] Jiang W, Gu J. Nanocrystalline cellulose isolated from different renewable sources to fabricate natural rubber composites with outstanding mechanical properties. Cellulose 2020;27:5801–13. https://doi.org/10.1007/s10570-020-03209-3.
[255] Visakh PM, Thomas S, Oksman K, Mathew AP. Crosslinked natural rubber nanocomposites reinforced with cellulose whiskers isolated from bamboo waste: Processing and mechanical/thermal properties. Compos Part A Appl Sci Manuf 2012;43:735–41. https://doi.org/10.1016/j.compositesa.2011.12.015.
[256] Zhang C, Dan Y, Peng J, Turng LS, Sabo R, Clemons C. Thermal and mechanical properties of natural rubber composites reinforced with cellulose nanocrystals from southern pine. Adv

Polym Technol 2014;33:E1–7. https://doi.org/10.1002/adv.21448.
[257] Das A, Costa FR, Wagenknecht U, Heinrich G. Nanocomposites based on chloroprene rubber: Effect of chemical nature and organic modification of nanoclay on the vulcanizate properties. Eur Polym J 2008;44:3456–65. https://doi.org/10.1016/j.eurpolymj.2008.08.025.
[258] Sadeghi Ghari H, Jalali-Arani A. Nanocomposites based on natural rubber, organoclay and nano-calcium carbonate: Study on the structure, cure behavior, static and dynamic-mechanical properties. Appl Clay Sci 2016;119:348–57. https://doi.org/10.1016/j.clay.2015.11.001.
[259] Abraham E, Thomas MS, John C, Pothen LA, Shoseyov O, Thomas S. Green nanocomposites of natural rubber/nanocellulose: Membrane transport, rheological and thermal degradation characterisations. Ind Crops Prod 2013;51:415–24. https://doi.org/10.1016/j.indcrop.2013.09.022.
[260] Vudjung C, Chaisuwan U, Pangan U, Chaipugdee N, Boonyod S, Santawitee O, et al. Effect of natural rubber contents on biodegradation and water absorption of Interpenetrating polymer network (IPN) hydrogel from natural rubber and cassava starch. Energy Procedia, vol. 56, Elsevier Ltd; 2014, p. 255–63. https://doi.org/10.1016/j.egypro.2014.07.156.
[261] Karkhanis SS, Stark NM, Sabo RC, Matuana LM. Water vapor and oxygen barrier properties of extrusion-blown poly(lactic acid)/cellulose nanocrystals nanocomposite films. Compos Part A Appl Sci Manuf 2018;114:204–11. https://doi.org/10.1016/j.compositesa.2018.08.025.
[262] Chen M, Wang Y, Yin S, Mo C, Yuan W, Lei W, et al. Effects of Temperature and Humidity on the Barrier Properties of Biaxially-oriented Polypropylene and Polyvinyl Alcohol Films. vol. 6. Wallace Center; 2014. https://doi.org/10.14448/japr.01.0004.
[263] Bras J, Hassan ML, Bruzesse C, Hassan EA, El-Wakil NA, Dufresne A. Mechanical, barrier, and biodegradability properties of bagasse cellulose whiskers reinforced natural rubber nanocomposites. Ind Crops Prod 2010;32:627–33.
[264] Jambeck JR, Geyer R, Wilcox C, Siegler TR, Perryman M, Andrady A, et al. Plastic waste inputs from land into the ocean. Science (80-) 2015;347:768 LP – 771.
[265] Miller SA. Sustainable polymers: Opportunities for the next decade. ACS Macro Lett 2013;2:550–4. https://doi.org/10.1021/mz400207g.
[266] Thompson RC, Moore CJ, Vom Saal FS, Swan SH. Plastics, the environment and human health: current consensus and future trends. Philos Trans R Soc B Biol Sci 2009;364:2153–66.
[267] Hauenstein O, Agarwal S, Greiner A. Bio-based polycarbonate as synthetic toolbox. Nat Commun 2016;7:11862.
[268] Divsalar E, Tajik H, Moradi M, Forough M, Lotfi M, Kuswandi B. Characterization of cellulosic paper coated with chitosan-zinc oxide nanocomposite containing nisin and its application in packaging of UF cheese. Int J Biol Macromol 2018;109:1311–8. https://doi.org/10.1016/j.ijbiomac.2017.11.145.
[269] Setajit C, Kongvarhodom C, Xiao H. Development of Grease Resistant Packaging Paper Using Cellulose Nanocrystals and Sodium Alginate. Sci Adv Mater 2019;12:212–9. https://doi.org/10.1166/sam.2020.3628.
[270] Vaezi K, Asadpour G, Sharifi SH. Effect of coating with novel bio nanocomposites of cationic starch/cellulose nanocrystals on the fundamental properties of the packaging paper. Polym Test 2019;80:106080. https://doi.org/10.1016/j.polymertesting.2019.106080.
[271] Bollström R, Preston J, Johannes Salminen P, Toivakka M. Barrier properties created by dispersion coating. Artic Tappi J 2013. https://doi.org/10.32964/TJ12.4.45.
[272] Farmahini-Farahani M, Xiao H, Zhao Y. Poly lactic acid nanocomposites containing modified nanoclay with synergistic barrier to water vapor for coated paper. J Appl Polym Sci 2014;131. https://doi.org/10.1002/APP.40952.

[273] Bota J, Kratofil Krehula L, Katančić Z, Brozović M, Hrnjak-Murgić Z. Surface characteristics and enhancement of water vapour properties of paperboard coated with polycaprolactone nanocomposites. Http://DxDoiOrg/101080/0169424320161218313 2016;31:466–86. https://doi.org/10.1080/01694243.2016.1218313.
[274] Conceição S, Santos NF, Velho J, Ferreira JMF. Properties of paper coated with kaolin: The influence of the rheological modifier. Appl Clay Sci 2005;30:165–73. https://doi.org/10.1016/J.CLAY.2005.03.010.
[275] Li Q, Wang S, Jin X, Huang C, Xiang Z. The Application of Polysaccharides and Their Derivatives in Pigment, Barrier, and Functional Paper Coatings. Polym 2020, Vol 12, Page 1837 2020;12:1837. https://doi.org/10.3390/POLYM12081837.
[276] Nelson K, Deng Y. Enhanced bondability between inorganic particles and a polysaccharide substrate by encapsulation with regenerated cellulose. J Appl Polym Sci 2008;107:2830–6. https://doi.org/10.1002/APP.27398.
[277] Al-Gharrawi M, Ollier R, Wang J, Bousfield DW. The influence of barrier pigments in waterborne barrier coatings on cellulose nanofiber layers. J Coatings Technol Res 2021:1–12. https://doi.org/10.1007/S11998-021-00482-0/FIGURES/13.
[278] Haghighat M, Zadhoush A, Nouri Khorasani S. Physicomechanical properties of α-cellulose-filled styrene-butadiene rubber composites. J Appl Polym Sci 2005;96:2203–11. https://doi.org/10.1002/app.21691.
[279] Ali Shah A, Hasan F, Shah Z, Kanwal N, Zeb S. Biodegradation of natural and synthetic rubbers: A review. Int Biodeterior Biodegrad 2013;83:145–57. https://doi.org/10.1016/j.ibiod.2013.05.004.
[280] Nechita P, Iana-Roman MR. Review on polysaccharides used in coatings for food packaging papers. Coatings 2020;10:566. https://doi.org/10.3390/COATINGS10060566.
[281] Gericke M, Tied A, Lenges C, Heinze T. α-1,3-Glucan benzoate – A novel polysaccharide derivative. Adv Ind Eng Polym Res 2020;3:71–6. https://doi.org/10.1016/j.aiepr.2020.01.003.
[282] Grüneberger F, Künniger T, Zimmermann T, Arnold M. Rheology of nanofibrillated cellulose/acrylate systems for coating applications. Cellulose 2014;21:1313–26.
[283] Mazhari Mousavi SM, Afra E, Tajvidi M, Bousfield DW, Dehghani-Firouzabadi M. Application of cellulose nanofibril (CNF) as coating on paperboard at moderate solids content and high coating speed using blade coater. Prog Org Coatings 2018;122:207–18.
[284] Hong SI, Lee JW, Son SM. Properties of polysaccharide-coated polypropylene films as affected by biopolymer and plasticizer types. Packag Technol Sci 2005;18:1–9. https://doi.org/10.1002/pts.667.
[285] Afra E, Mohammadnejad S, Saraeyan A. Cellulose nanofibils as coating material and its effects on paper properties. Prog Org Coatings 2016;101:455–60.
[286] Lavoine N, Desloges I, Khelifi B, Bras J. Impact of different coating processes of microfibrillated cellulose on the mechanical and barrier properties of paper. J Mater Sci 2014;49:2879–93. https://doi.org/10.1007/s10853-013-7995-0.
[287] Hashemi Najafi SM, Tajvidi M, Bousfield DW. Production and mechanical characterization of free-standing pigmented paper coating layers with latex and starch as binder. Prog Org Coatings 2018;123:138–45. https://doi.org/10.1016/J.PORGCOAT.2018.07.009.
[288] Wang S, Jing Y. Effects of a Chitosan Coating Layer on the Surface Properties and Barrier Properties of Kraft Paper. BioResources 2016;11. https://doi.org/10.15376/biores.11.1.1868-1881.
[289] Park HJ, Chinnan MS. Gas and water vapor barrier properties of edible films from protein and cellulosic materials. J Food Eng 1995;25:497–507. https://doi.org/10.1016/0260-

8774(94)00029-9.
[290] Christophliemk H, Johansson C, Ullsten H, Järnström L. Oxygen and water vapor transmission rates of starch-poly(vinyl alcohol) barrier coatings for flexible packaging paper. Prog Org Coatings 2017;113:218–24. https://doi.org/10.1016/j.porgcoat.2017.04.019.
[291] Andersson C. New ways to enhance the functionality of paperboard by surface treatment – a review. Packag Technol Sci 2008;21:339–73. https://doi.org/10.1002/PTS.823.
[292] Shen J, Fatehi P, Ni Y. Biopolymers for surface engineering of paper-based products. Cellul 2014 215 2014;21:3145–60. https://doi.org/10.1007/S10570-014-0380-6.
[293] Jendrossek D, Tomasi G, Kroppenstedt RM. Bacterial degradation of natural rubber: a privilege of actinomycetes? FEMS Microbiol Lett 1997;150:179–88. https://doi.org/10.1111/J.1574-6968.1997.TB10368.X.
[294] Misman MA, Azura AR. Overview on the Potential of Biodegradable Natural Rubber Latex Gloves for Commercialization. Adv Mater Res 2014;844:486–9. https://doi.org/10.4028/WWW.SCIENTIFIC.NET/AMR.844.486.
[295] Abraham E, Elbi PA, Deepa B, Jyotishkumar P, Pothen LA, Narine SS, et al. X-ray diffraction and biodegradation analysis of green composites of natural rubber/nanocellulose. Polym Degrad Stab 2012;97:2378–87. https://doi.org/10.1016/J.POLYMDEGRADSTAB.2012.07.028.
[296] Jayathilaka LPI, Ariyadasa TU, Egodage SM. Development of biodegradable natural rubber latex composites by employing corn derivative bio-fillers. J Appl Polym Sci 2020;137:49205. https://doi.org/10.1002/APP.49205.
[297] Riyajan SA. Robust and biodegradable polymer of cassava starch and modified natural rubber. Carbohydr Polym 2015;134:267–77. https://doi.org/10.1016/J.CARBPOL.2015.07.038.
[298] Nešić A, Cabrera-Barjas G, Dimitrijević-Branković S, Davidović S, Radovanović N, Delattre C. Prospect of Polysaccharide-Based Materials as Advanced Food Packaging. Mol 2020, Vol 25, Page 135 2019;25:135. https://doi.org/10.3390/MOLECULES25010135.
[299] Scaffaro R, Botta L, Lopresti F, Maio A, Sutera F. Polysaccharide nanocrystals as fillers for PLA based nanocomposites. Cellul 2016 242 2016;24:447–78. https://doi.org/10.1007/S10570-016-1143-3.
[300] Abdul Khalil HPS, Chong EWN, Owolabi FAT, Asniza M, Tye YY, Rizal S, et al. Enhancement of basic properties of polysaccharide-based composites with organic and inorganic fillers: A review. J Appl Polym Sci 2019;136:47251. https://doi.org/10.1002/APP.47251.
[301] Ganesarajan D, Simon L, Tamrakar S, Kiziltas A, Mielewski D, Behabtu N, et al. Hybrid composites with engineered polysaccharides for automotive lightweight. Compos Part C Open Access 2022;7:100222. https://doi.org/10.1016/J.JCOMC.2021.100222.
[302] Qiao C, Chen G, Zhang J, Yao J. Structure and rheological properties of cellulose nanocrystals suspension. Food Hydrocoll 2016;55:19–25. https://doi.org/10.1016/J.FOODHYD.2015.11.005.
[303] Shafiei-Sabet S, Martinez M, Olson J. Shear rheology of micro-fibrillar cellulose aqueous suspensions. Cellulose 2016;23:2943–53. https://doi.org/10.1007/S10570-016-1040-9/FIGURES/12.
[304] Li MC, Wu Q, Song K, Lee S, Qing Y, Wu Y. Cellulose Nanoparticles: Structure-Morphology-Rheology Relationships. ACS Sustain Chem Eng 2015;3:821–32. https://doi.org/10.1021/ACSSUSCHEMENG.5B00144/ASSET/IMAGES/ACSSUSCHEMENG.5B00144.SOCIAL.JPEG_V03.
[305] Nechyporchuk O, Belgacem MN, Pignon F. Current Progress in Rheology of Cellulose

Nanofibril Suspensions. Biomacromolecules 2016;17:2311–20. https://doi.org/10.1021/ACS.BIOMAC.6B00668/ASSET/IMAGES/ACS.BIOMAC.6B00668.SOCIAL.JPEG_V03.
[306] Shafiei-Sabet S, Hamad WY, Hatzikiriakos SG. Rheology of nanocrystalline cellulose aqueous suspensions. Langmuir 2012;28:17124–33. https://doi.org/10.1021/LA303380V/ASSET/IMAGES/LA303380V.SOCIAL.JPEG_V03.
[307] Walteros-León M, Álvarez-Láinez ML. Colloidal and rheological properties of natural rubber latex concentrated with hydroxyethyl cellulose and sodium dodecyl sulphate. J Appl Polym Sci 2022;139:52034. https://doi.org/10.1002/APP.52034.
[308] Jiang Y, Zhang Y, Ding L, Wang B, Chen Z, Zhong Y, et al. Sag control of waterborne acrylic latex with regenerated nanocellulose suspension. Prog Org Coatings 2018;123:146–52. https://doi.org/10.1016/J.PORGCOAT.2018.07.004.
[309] Pakdel AS, Niinivaara E, Cranston ED, Berry RM, Dubé MA. Cellulose Nanocrystal (CNC)–Latex Nanocomposites: Effect of CNC Hydrophilicity and Charge on Rheological, Mechanical, and Adhesive Properties. Macromol Rapid Commun 2021;42:2000448. https://doi.org/10.1002/MARC.202000448.
[310] Lim HM, Misni M. Colloidal and rheological properties of natural rubber latex concentrate. Appl Rheol 2016;26:25–34. https://doi.org/10.3933/APPLRHEOL-26-15659/MACHINEREADABLECITATION/RIS.
[311] Jiang Y, Liu L, Wang B, Yang X, Chen Z, Zhong Y, et al. Polysaccharide-based edible emulsion gel stabilized by regenerated cellulose. Food Hydrocoll 2019;91:232–7. https://doi.org/10.1016/J.FOODHYD.2019.01.028.
[312] Mabrouk A Ben, Dufresne A, Boufi S. Cellulose nanocrystal as ecofriendly stabilizer for emulsion polymerization and its application for waterborne adhesive. Carbohydr Polym 2020;229:115504. https://doi.org/10.1016/J.CARBPOL.2019.115504.
[313] Zakaria S, Chia CH, Wan Ahmad WH, Kaco H, Chook SW, Chan CH. Mechanical and antibacterial properties of paper coated with chitosan. Sains Malaysiana 2015;44:905–11. https://doi.org/10.17576/JSM-2015-4406-18.
[314] Türe H, Gällstedt M, Johansson E, Hedenqvist MS. Wheat-gluten/montmorillonite clay multilayer-coated paperboards with high barrier properties. Ind Crops Prod 2013;51:1–6. https://doi.org/10.1016/J.INDCROP.2013.08.054.
[315] Tanpichai S, Witayakran S, Wootthikanokkhan J, Srimarut Y, Woraprayote W, Malila Y. Mechanical and antibacterial properties of the chitosan coated cellulose paper for packaging applications: Effects of molecular weight types and concentrations of chitosan. Int J Biol Macromol 2020;155:1510–9. https://doi.org/10.1016/J.IJBIOMAC.2019.11.128.
[316] Koppolu R, Abitbol T, Kumar V, Jaiswal AK, Swerin A, Toivakka M. Continuous roll-to-roll coating of cellulose nanocrystals onto paperboard. Cellulose 2018;25:6055–69. https://doi.org/10.1007/S10570-018-1958-1/TABLES/7.
[317] Wilpiszewska K, Czech Z. Water-Soluble Pressure-Sensitive Adhesives Containing Carboxymethyl Starch with Improved Adhesion to Paper. J Polym Environ 2018;26:1453–8. https://doi.org/10.1007/S10924-017-1048-8/TABLES/3.
[318] Yousefi Shivyari N, Tajvidi M, Bousfield DW, Gardner DJ. Production and Characterization of Laminates of Paper and Cellulose Nanofibrils. ACS Appl Mater Interfaces 2016;8:25520–8. https://doi.org/10.1021/ACSAMI.6B07655/ASSET/IMAGES/ACSAMI.6B07655.SOCIAL.JPEG_V03.
[319] Gatto M, Ochi D, Yoshida CMP, da Silva CF. Study of chitosan with different degrees of acetylation as cardboard paper coating. Carbohydr Polym 2019;210:56–63.

https://doi.org/10.1016/J.CARBPOL.2019.01.053.
[320] Trinh BM, Chang CC, Mekonnen TH. Facile fabrication of thermoplastic starch/poly (lactic acid) multilayer films with superior gas and moisture barrier properties. Polymer (Guildf) 2021;223:123679. https://doi.org/10.1016/J.POLYMER.2021.123679.
[321] Olsson E, Menzel C, Johansson C, Andersson R, Koch K, Järnström L. The effect of pH on hydrolysis, cross-linking and barrier properties of starch barriers containing citric acid. Carbohydr Polym 2013;98:1505–13. https://doi.org/10.1016/J.CARBPOL.2013.07.040.
[322] George SC, Ninan KN, Thomas S. Permeation of nitrogen and oxygen gases through styrene–butadiene rubber, natural rubber and styrene–butadiene rubber/natural rubber blend membranes. Eur Polym J 2001;37:183–91. https://doi.org/10.1016/S0014-3057(00)00083-5.
[323] Ogunsona EO, Panchal P, Mekonnen TH. Surface grafting of acrylonitrile butadiene rubber onto cellulose nanocrystals for nanocomposite applications. Compos Sci Technol 2019;184:107884. https://doi.org/10.1016/j.compscitech.2019.107884.
[324] Riyajan SA, Chaiponban S, Tanbumrung K. Investigation of the preparation and physical properties of a novel semi-interpenetrating polymer network based on epoxised NR and PVA using maleic acid as the crosslinking agent. Chem Eng J 2009;153:199–205. https://doi.org/10.1016/J.CEJ.2009.05.043.
[325] Nontasorn P, Chavadej S, Rangsunvigit P, O'Haver JH, Chaisirimahamorakot S, Na-Ranong N. Admicellar polymerization modified silica via a continuous stirred-tank reactor system: Comparative properties of rubber compounding. Chem Eng J 2005;108:213–8. https://doi.org/10.1016/J.CEJ.2005.02.016.
[326] Kumagai A, Tajima N, Iwamoto S, Morimoto T, Nagatani A, Okazaki T, et al. Properties of natural rubber reinforced with cellulose nanofibers based on fiber diameter distribution as estimated by differential centrifugal sedimentation. Int J Biol Macromol 2019;121:989–95. https://doi.org/10.1016/J.IJBIOMAC.2018.10.090.
[327] Kazemi H, Mighri F, Park KW, Frikha S, Rodrigue D. EFFECT OF CELLULOSE FIBER SURFACE TREATMENT TO REPLACE CARBON BLACK IN NATURAL RUBBER HYBRID COMPOSITES. Rubber Chem Technol 2022;95:128–46. https://doi.org/10.5254/RCT.21.78988.
[328] Abraham E, Deepa B, Pothan LA, John M, Narine SS, Thomas S, et al. Physicomechanical properties of nanocomposites based on cellulose nanofibre and natural rubber latex. Cellulose 2013;20:417–27. https://doi.org/10.1007/S10570-012-9830-1/FIGURES/7.
[329] Roy K, Potiyaraj P. Development of high performance microcrystalline cellulose based natural rubber composites using maleated natural rubber as compatibilizer. Cellul 2017 252 2017;25:1077–87. https://doi.org/10.1007/S10570-017-1613-2.
[330] Yue Y, Zhang H, Zhang Z, Chen Y. Polymer–filler interaction of fumed silica filled polydimethylsiloxane investigated by bound rubber. Compos Sci Technol 2013;86:1–8. https://doi.org/10.1016/J.COMPSCITECH.2013.06.019.
[331] Xu T, Jia Z, Luo Y, Jia D, Peng Z. Interfacial interaction between the epoxidized natural rubber and silica in natural rubber/silica composites. Appl Surf Sci 2015;328:306–13. https://doi.org/10.1016/j.apsusc.2014.12.029.
[332] Soheilmoghaddam M, Wahit MU, Ibrahim Akos N. Regenerated cellulose/epoxidized natural rubber blend film. Mater Lett 2013;111:221–4. https://doi.org/10.1016/J.MATLET.2013.08.109.
[333] Arrigo R, Mascia L, Clarke J, Malucelli G. Structure evolution of epoxidized natural rubber (enr) in the melt state by time-resolved mechanical spectroscopy. Materials (Basel) 2020;13. https://doi.org/10.3390/ma13040946.

[334] Vu CM, Vu HT, Choi HJ. Fabrication of natural rubber/epoxidized natural rubber/nanosilica nanocomposites and their physical characteristics. Macromol Res 2015 233 2015;23:284–90. https://doi.org/10.1007/S13233-015-3040-2.
[335] Cao L, Fu X, Xu C, Yin S, Chen Y. High-performance natural rubber nanocomposites with marine biomass (tunicate cellulose). Cellulose 2017;24:2849–60. https://doi.org/10.1007/s10570-017-1293-y.
[336] Cao L, Huang J, Chen Y. Dual Cross-linked Epoxidized Natural Rubber Reinforced by Tunicate Cellulose Nanocrystals with Improved Strength and Extensibility. ACS Sustain Chem Eng 2018;6:14802–11. https://doi.org/10.1021/ACSSUSCHEMENG.8B03331/ASSET/IMAGES/LARGE/SC-2018-03331E_0010.JPEG.
[337] Ojogbo E, Tzoganakis C, Mekonnen TH. Batch Mixing for the in Situ Grafting of Epoxidized Rubber onto Cellulose Nanocrystals. ACS Sustain Chem Eng 2022;10:8743–53. https://doi.org/10.1021/ACSSUSCHEMENG.2C01054/ASSET/IMAGES/LARGE/SC2C01054_0008.JPEG.
[338] Somseemee O, Saeoui P, Schevenels FT, Siriwong C. Enhanced interfacial interaction between modified cellulose nanocrystals and epoxidized natural rubber via ultraviolet irradiation. Sci Reports 2022 121 2022;12:1–13. https://doi.org/10.1038/s41598-022-10558-5.
[339] Jiang C, He H, Yao X, Yu P, Zhou L, Jia D. In situ dispersion and compatibilization of lignin/epoxidized natural rubber composites: Reactivity, morphology and property. J Appl Polym Sci 2015;132:1–10. https://doi.org/10.1002/app.42044.
[340] Wang Z, Li Y, Song W, Wu X, Zhang L. Performance enhancement of bio-based rubber composites using epoxidized natural rubber for silica without carbon emissions and volatile organic compounds. J Appl Polym Sci 2022;139:1–13. https://doi.org/10.1002/app.52682.
[341] Xu C, Cui R, Fu L, Lin B. Recyclable and heat-healable epoxidized natural rubber/bentonite composites. Compos Sci Technol 2018;167:421–30. https://doi.org/10.1016/J.COMPSCITECH.2018.08.027.
[342] Tong H, Chen Y, Weng Y, Zhang S. Biodegradable-Renewable Vitrimer Fabrication by Epoxidized Natural Rubber and Oxidized Starch with Robust Ductility and Elastic Recovery. ACS Sustain Chem Eng 2022;10:7942–53. https://doi.org/10.1021/acssuschemeng.2c01163.
[343] Jantanasakulwong K, Leksawasdi N, Seesuriyachan P, Wongsuriyasak S, Techapun C, Ougizawa T. Reactive blending of thermoplastic starch, epoxidized natural rubber and chitosan. Eur Polym J 2016;84:292–9. https://doi.org/10.1016/j.eurpolymj.2016.09.035.
[344] Geitel K, Koschella A, Lenges C, Heinze T. Meltable fatty acid esters of α-1,3-glucan as potential thermoplastics. Adv Ind Eng Polym Res 2020;3:111–9. https://doi.org/10.1016/J.AIEPR.2020.07.004.
[345] Thevy Ratnam C, Nasir M, Baharin A, Zaman K. Electron beam irradiation of epoxidized natural rubber: FTIR studies n.d. https://doi.org/10.1002/1097-0126.
[346] Hamzah R, Bakar MA, Khairuddean M, Mohammed IA, Adnan R. A Structural Study of Epoxidized Natural Rubber (ENR-50) and Its Cyclic Dithiocarbonate Derivative Using NMR Spectroscopy Techniques. Mol 2012, Vol 17, Pages 10974-10993 2012;17:10974–93. https://doi.org/10.3390/MOLECULES170910974.
[347] Jubinville D, Tzoganakis C, Mekonnen TH. Recycled PLA – Wood flour based biocomposites: Effect of wood flour surface modification, PLA recycling, and maleation. Constr Build Mater 2022;352:129026. https://doi.org/10.1016/j.conbuildmat.2022.129026.
[348] Varghese S, Karger-Kocsis J, Gatos KG. Melt compounded epoxidized natural rubber/layered silicate nanocomposites: structure-properties relationships. Polymer (Guildf) 2003;44:3977–

83. https://doi.org/10.1016/S0032-3861(03)00358-6.
[349] Nie J, Mou W, Ding J, Chen Y. Bio-based epoxidized natural rubber/chitin nanocrystals composites: Self-healing and enhanced mechanical properties. Compos Part B Eng 2019;172:152–60. https://doi.org/10.1016/j.compositesb.2019.04.035.
[350] Bhakri S, Takenaka K, Boonmahitthisud A, Boondamnoen O. Effect of epoxidation levels on curing characteristic and mechanical properties of ENR/MFC composites. J Phys Conf Ser 2022;2175. https://doi.org/10.1088/1742-6596/2175/1/012020.
[351] Lan H, Venkatesh TA. On the relationships between hardness and the elastic and plastic properties of isotropic power-law hardening materials. Philos Mag 2014;94:35–55. https://doi.org/10.1080/14786435.2013.839889.
[352] Sun WJ, Kothari S, Sun CC. The relationship among tensile strength, Young's modulus, and indentation hardness of pharmaceutical compacts. Powder Technol 2018;331:1–6. https://doi.org/10.1016/J.POWTEC.2018.02.051.
[353] Trinh BM, Tadele DT, Mekonnen TH. Robust and high barrier thermoplastic starch - PLA blend films using starch-graft-poly(lactic acid) as a compatibilizer. Mater Adv 2022;3:6208–21. https://doi.org/10.1039/d2ma00501h.
[354] Setz LFG, Silva AC, Santos SC, Mello-Castanho SRH, Morelli MR. A viscoelastic approach from α-Al2O3 suspensions with high solids content. J Eur Ceram Soc 2013;33:3211–9. https://doi.org/10.1016/J.JEURCERAMSOC.2013.06.002.
[355] Mok KL, Eng AH. Characterisation of crosslinks in vulcanised rubbers: From simple to advanced techniques. Malaysian J Chem 2018;20:118–27.
[356] Masłowski M, Miedzianowska J, Strzelec K. Natural Rubber Composites Filled with Crop Residues as an Alternative to Vulcanizates with Common Fillers n.d. https://doi.org/10.3390/polym11060972.
[357] Magonov SN, Elings V, Whangbo MH. Phase imaging and stiffness in tapping-mode atomic force microscopy. Surf Sci 1997;375:L385–91. https://doi.org/10.1016/S0039-6028(96)01591-9.
[358] Azura AR, Leow SL. Effect of carbon black loading on mechanical, conductivity and ageing properties of Natural Rubber composites. Mater Today Proc 2019;17:1056–63. https://doi.org/10.1016/j.matpr.2019.06.512.
[359] Ismail H, Rusli A, Rashid AA. Maleated natural rubber as a coupling agent for paper sludge filled natural rubber composites. Polym Test 2005;24:856–62. https://doi.org/10.1016/J.POLYMERTESTING.2005.06.011.

Appendix A

Supporting Information from Chapter 4

Table A1. Composition of 12 solutions used in kit test.

Composition / Kit number	Castor oil (g)	Toluene (g)	Heptane (g)
1	969	0	0
2	872	50	50
3	775	100	100
4	678	150	150
5	581	200	200
6	484	250	250
7	388	300	300
8	2901	350	350
9	194	400	400
10	97	450	450
11	0	500	500
12	0	450	550

Table A2. Kit numbers of PE and NR/alpha-1,3 glucan coated films with 100 μm thickness

Coating composition	PE	NR-30wc (100 μm)	NR-100wc (100 μm)
Kit number	12	12	12

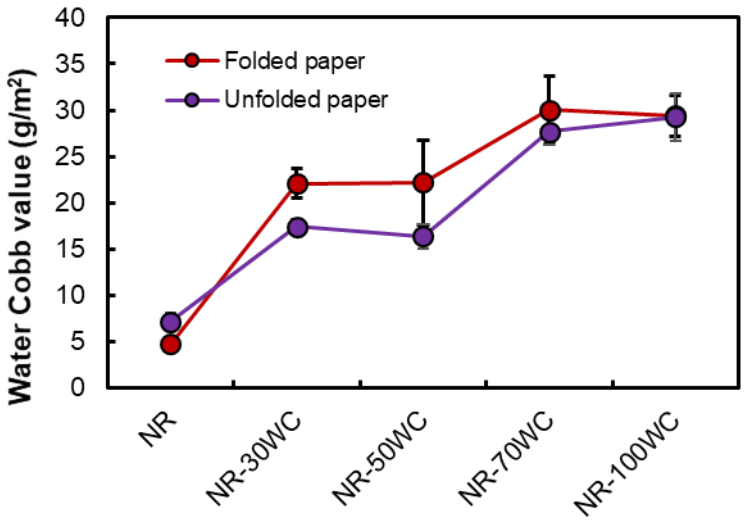

Figure A1. Water Cobb test of folded and unfolded of paper coatings.

Appendix B

Supporting Information from Chapter 5

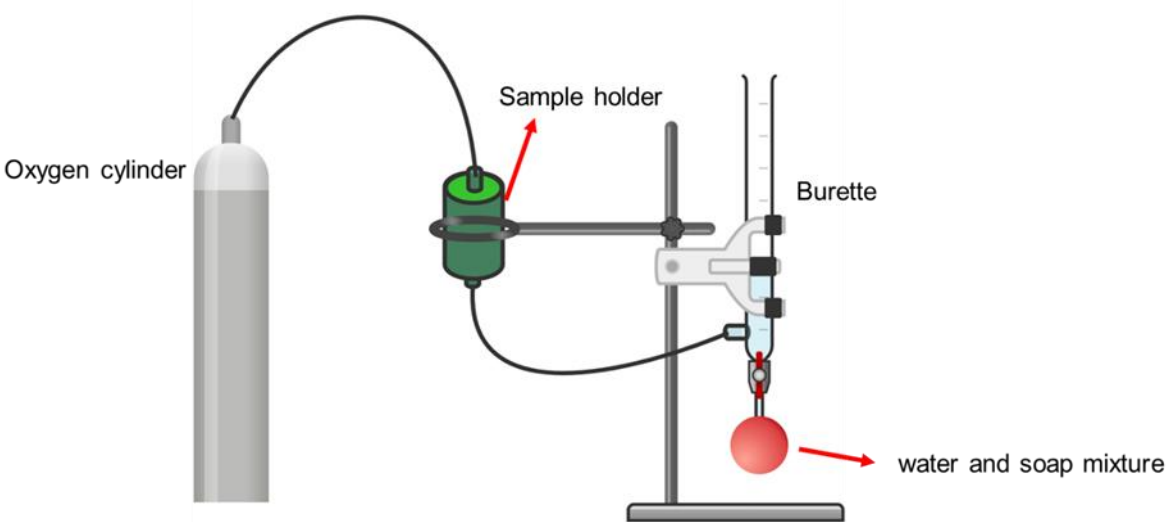

Scheme B1. Custom-made oxygen permeability measuring system

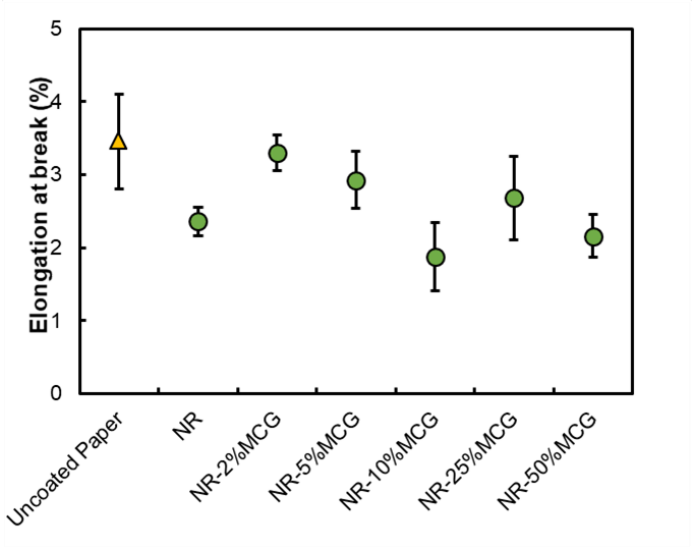

Figure B1. Elongation at break results of paper coatings.

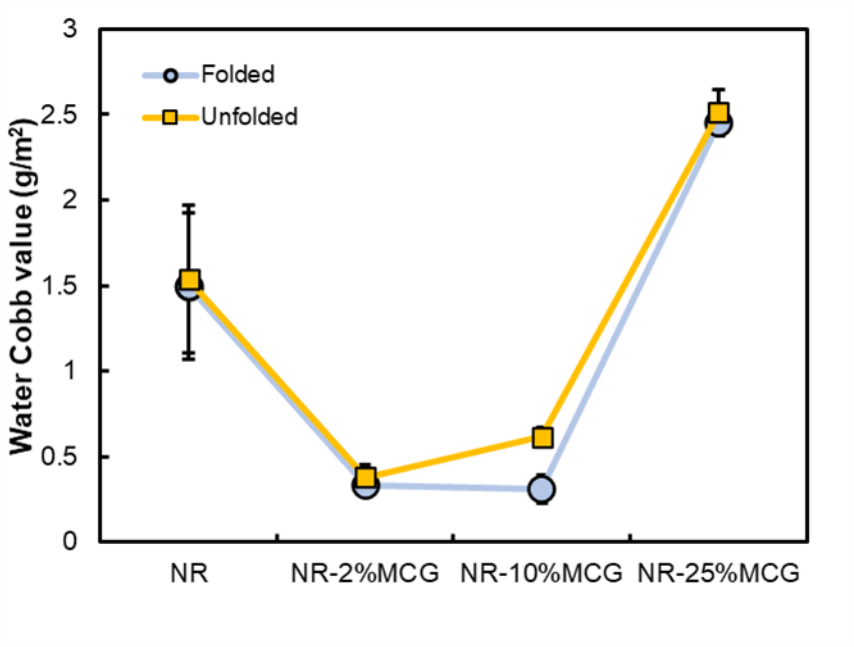

Figure B2. Water Cobb test of folded and unfolded of paper coatings.

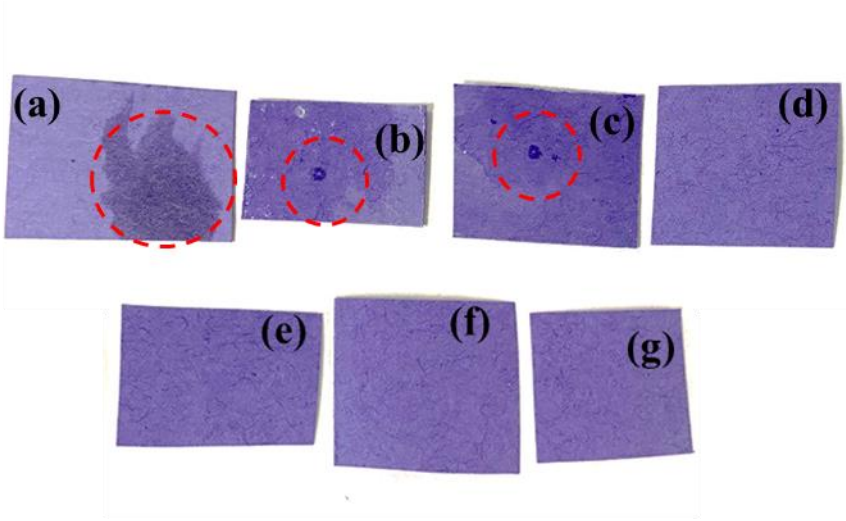

Figure B3. Kit test of a) uncoated sample at kit solution number 1, b) NR paper coating at kit solution number 5, c) NR-2%MCG paper coating at kit solution number 7, d) NR-5%MCG paper coating at kit solution number 12, e) NR-10%MCG paper coating at kit solution number 12, f) NR-25%MCG paper coating at kit solution number 12, g) NR-50%MCG paper coating at kit solution number 12.

Table B1. Statistical analysis of *OP* at higher relative humidity.

Relative Humidity / Paper coating Composition	OTR at 15% RH × 10^6 ($cm^3.m/m^2.Pa.day$)	OTR at 30% RH × 10^6 ($cm^3.m/m^2.Pa.day$)	OTR at 60% RH × 10^6 ($cm^3.m/m^2.Pa.day$)	OTR at 100% RH × 10^6 ($cm^3.m/m^2.Pa.day$)
NR-2%MCG	5.87 ± 0.29^{a}	2.770 ± 0.15^{d}	1.61 ± 0.42^{e}	1.18 ± 0.09^{f}
NR-10%MCG	3.11 ± 0.18^{b}	1.53 ± 0.13^{d}	1.34 ± 0.02^{e}	0.40 ± 0.00^{f}
NR-25%MCG	4.19 ± 0.40^{c}	1.16 ± 7.57^{d}	0.83 ± 0.47^{e}	0.27 ± 0.00^{f}

OP value = mean ± standard deviation (n = 5), means with the same superscript letters within a column are not significantly different at $P < 0.05$ level

Appendix C

Supporting Information from Chapter 6

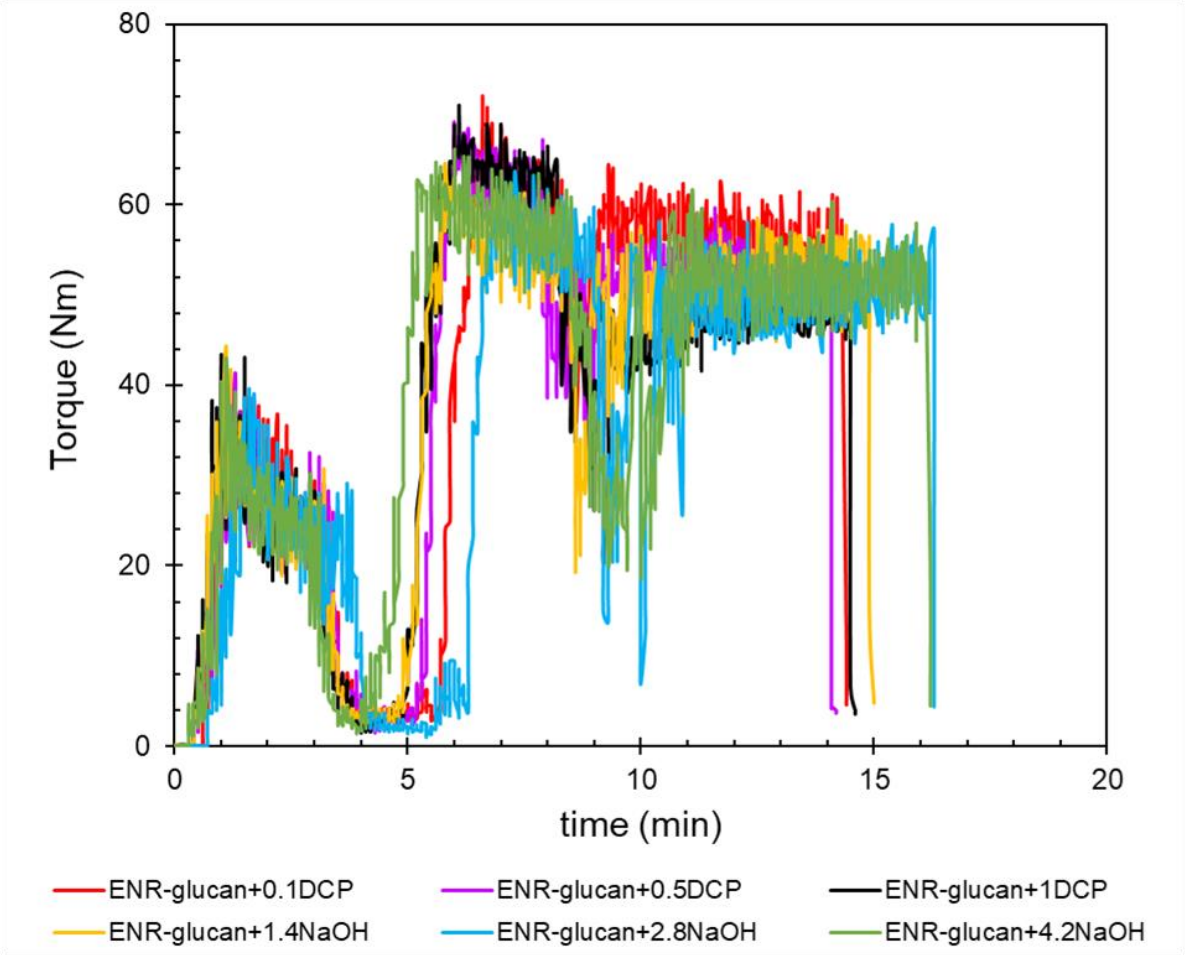

Figure C1. The torque graph of ENR-glucan blends with DCP/NaOH as catalyst.

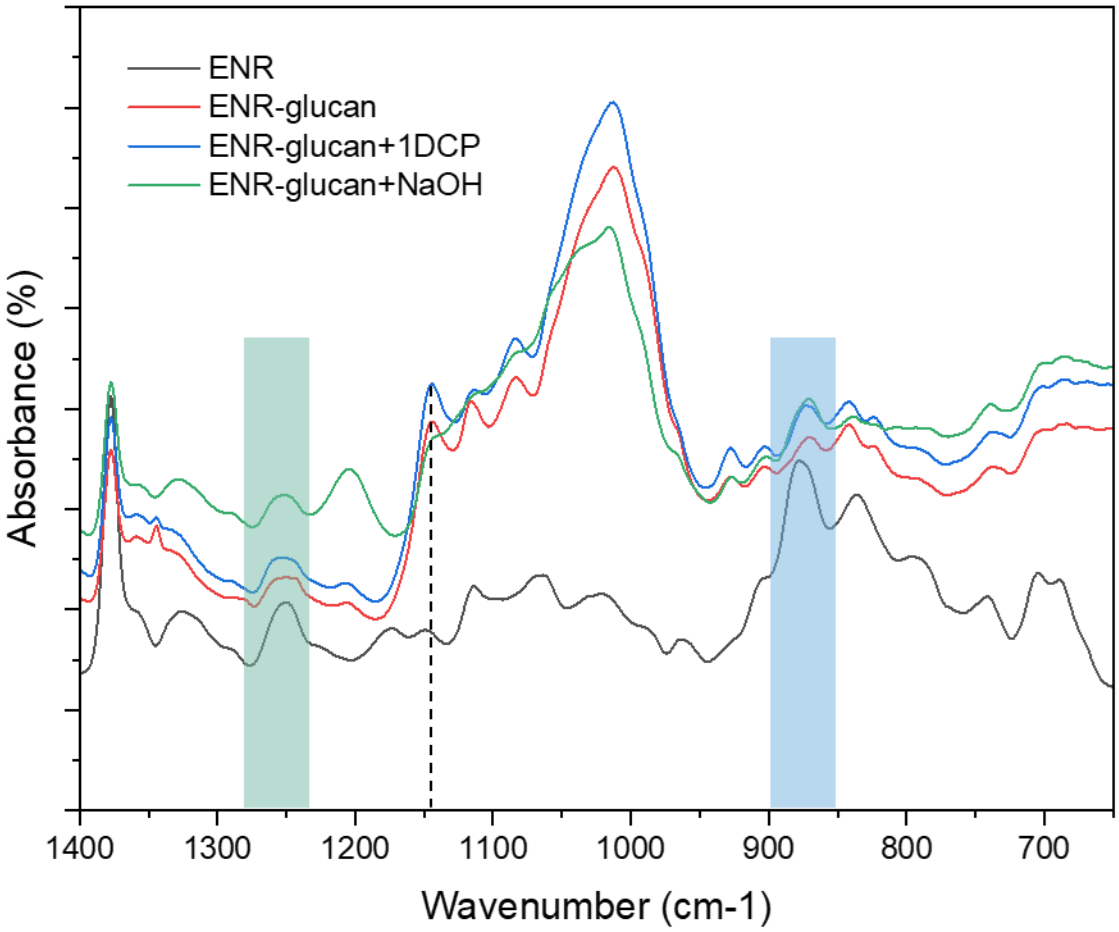

Figure C2. FTIR spectra of neat ENR and ENR-glucan composites in the wavenumber range of 600 to 1400 cm^{-1}.

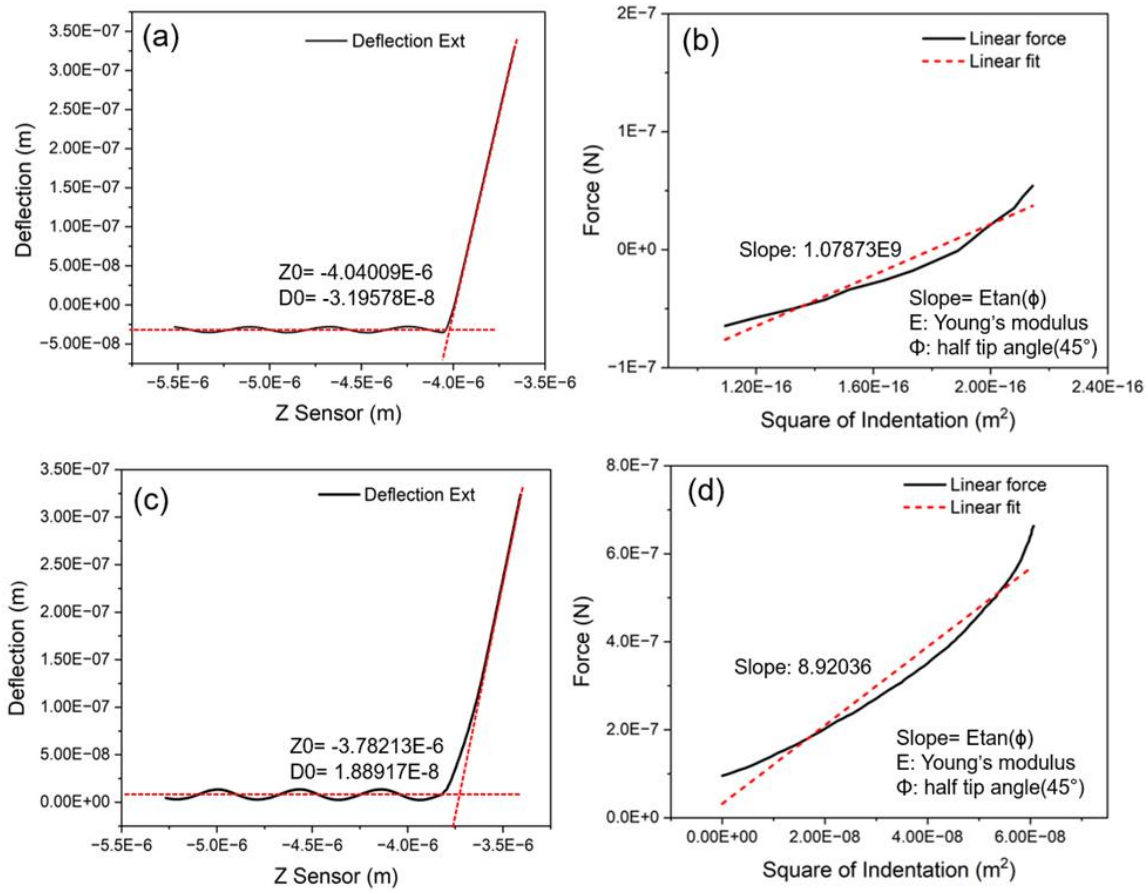

Figure C3. Force curves obtained from nanoindentation analysis of (a),(b) cellulose nanocrystal, and (c),(d) alpha-1,3 glucan.

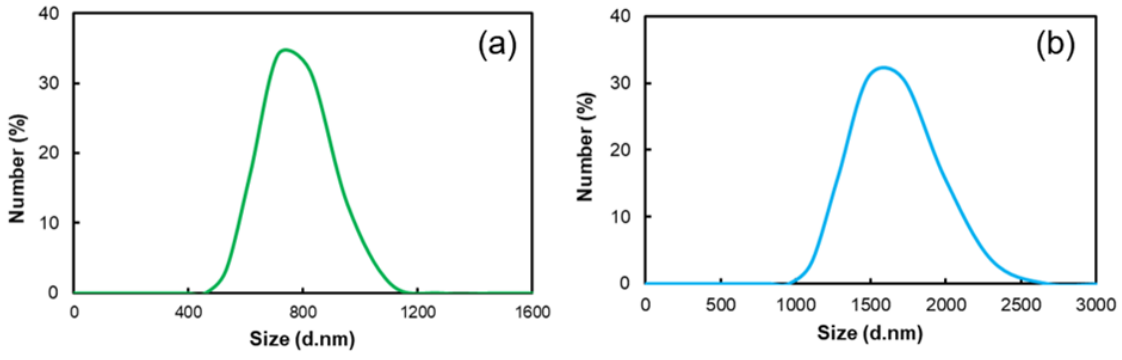

Figure S4. Particle size distribution of (a)silica and (b) calcium carbonate.